

Climate Dependencies and Deterministic Variability in Stratospheric Dynamics and Ozone

Dissertation
der Fakultät für Physik der
Ludwig-Maximilians-Universität München

vorgelegt von Rudolf Deckert
aus Wasserburg am Inn

München, 21. Dezember 2007

1. Gutachter: Prof. Dr. Martin Dameris, LMU München
 2. Gutachter: Prof. Dr. Olaf Krüger, LMU München
- Tag der mündlichen Prüfungen: 17. Juni 2008

Abstract

Estimates of the ozone layer future evolution must consider both climate dependencies and interannual variability. These considerations imply analyses of transient-scenario realisations with chemistry-climate models (CCM) under realistic boundary conditions. In this context, investigations of ozone variability usually involve multiple regression analysis (MRA), a statistically efficient albeit complicated tool. However, a careful use of advanced regression approaches may improve the variability assessment considerably. The present study addresses climate dependencies in ozone transport, and adopts an advanced regression approach to both quantify deterministic ozone variability and trace it back to the scenario boundary conditions; the investigations refer to transient output of the CCM E39/C.

Recent observations show a cooling of the tropical lower stratosphere, and CCMs suggest a spatial coincidence of the cooling with a stronger upward advection of ozone-poor tropospheric air. This advection increase appears to result from a currently unexplained strengthening of the planetary-wave driven mean meridional transport, arguably relating to the anthropogenic climate signal. The present study explores the strengthening by comparing realisations of two different scenarios. Both share the same boundary conditions including concentrations of ozone-depleting substances (ODS), but differ in their climate forcing via sea surface temperatures (SSTs) and well-mixed greenhouse gas concentrations (GHG). In the summer hemisphere tropics, higher SSTs for the warmer scenario amplify deep convection and hence the convective excitation of internal planetary waves. These waves travel upward through easterly winds while dissipating, but still carry enough of the signal into the lower stratosphere to intensify the mean meridional transport. The transport change in turn strengthens the input rate into the tropical lower stratosphere of ozone-poor tropospheric air, ultimately weakening lower-stratospheric ozone concentrations via higher tropical SSTs.

The ozone variability assessment relates to monthly-mean total columns from three independent realisations of a 60-year transient scenario with realistic boundary conditions. It focuses on three latitudinal bands: southern/northern mid-latitudes (SH/NH) and tropics. Common ozone MRAs are linear and iterate to account for auto-regression-induced nonlinearity. The present MRA is nonlinear and the first to demonstrate the validity of such iterations with respect to the least-squares surface: it detects only a weak distortion of the surface associated with autocorrelation, at least for the ozone time series examined. Also, the present MRA is among the few to demonstrate sufficient compliance with the regression requirements, particularly with that of independent residuals. Additionally, the new approach of response confidence bands permits a correct attribution

of individual anomalies to the scenario boundary conditions. As a consequence, the present MRA is the first to explain the year 1985 SH low-ozone event, here reproduced by E39/C. The MRA further captures, i.a., a similar anomaly for the year 1997, and verifies the total-ozone response to stratospheric-transport-modulating boundary conditions: tropical-SST anomalies (ENSO) affect the tropics and NH, but not the SH; or, the quasi-biennial oscillation (QBO) causes a seasonally synchronised ozone response at SH and more weakly at NH, but not in the tropics. While these features have already been reported for E39/C data, the present study establishes a firm statistical framework and discusses the physical background. Other responses refer to the 11-year solar cycle (SSC), to sulfate aerosols, and to ODS concentrations. The present nonlinear regression approach provides ample potential for further development. For instance, nonlinear deterministic regression terms may examine the existence of interactions between the NH ENSO response with long-term changes in the probability for northern polar heterogeneous ozone depletion. Last, accounting for moving-average regression parameters may improve the compliance with the inference requirements even further.

In conclusion, the E39/C boundary conditions modulate the ozone layer as well as stratospheric mean meridional mass transport on long and short time scales. In this respect, the most important result is the universal significance of tropical SSTs controlling stratospheric transport by governing the deep-convective production of internal and, probably, external planetary waves. An important future research task is whether increasing tropical SSTs can cause ENSO-like changes in wintertime mid- and polar-latitude stratospheric planetary-wave activity; such changes could disturb the northern polar vortex against the effect of radiatively induced stabilisation by higher GHG concentrations. E39/C and other CCMS have certain weaknesses, one of which is an unrealistically consistent QBO-related modulation of the northern polar vortex. Keeping these weaknesses in mind, MRA may represent a helpful tool as it improves the statistical efficiency.

Zusammenfassung

Voraussagen über die zukünftige Entwicklung der Ozonschicht müssen sowohl klimabedingte Änderungen als auch die interannuale Variabilität der Ozonschicht berücksichtigen. Hierfür sind Analysen von Realisierungen transienter Szenarien mittels Klima-Chemie Modellen (CCMs) unter realitätsnahen Randbedingungen notwendig. Untersuchungen der genannten Variabilität erfordern für gewöhnlich die Durchführung einer multiplen Regressionsanalyse (MRA), eines statistisch effizienten, aber auch anspruchsvollen Werkzeuges. Jedoch kann eine sorgfältige Anwendung fortschrittlicher Regressionsmethoden die Untersuchung der Variabilität entscheidend verbessern. Die vorliegende Studie untersucht klimabedingte Änderungen des Ozontransports. Außerdem verwendet sie eine fortschrittliche Regressionsmethode um die deterministische Variabilität der Ozonschicht zu quantifizieren, sowie auf die Randbedingungen der Modellszenarien zurückzuführen. Die Untersuchungen stützen sich auf transiente Ergebnisse des CCMs E39/C.

Neue Messergebnisse zeigen eine Abkühlung der unteren tropischen Stratosphäre. Entsprechende CCM-Ergebnisse deuten darauf hin, daß die gemessene Abkühlung örtlich mit einer verstärkten aufwärts-gerichteten Advektion ozonarmer troposphärischer Luftmassen zusammenfällt. Diese Verstärkung der Advektion scheint sich aus der Intensivierung des gemittelten wellenverursachten Meridionaltransports zu ergeben. Die Ursache für diese Intensivierung war bis jetzt jedoch ungeklärt. Die vorliegende Arbeit kann den Grund für diese Transportintensivierung nachweisen. Dies geschieht durch den Vergleich mehrerer Realisierungen zweier verschiedener transienter Modellszenarien. Diese Szenarien besitzen dieselben Randbedingungen, wie zum Beispiel Konzentrationen ozonzerstörender Substanzen (ODS). Sie unterscheiden sich jedoch in ihrem Klimaantrieb durch unterschiedliche Meeresoberflächentemperaturen (SSTs) und unterschiedliche Konzentrationen gut durchmischter Treibhausgase (GHG). In den Tropen der Sommerhemisphäre verstärken höhere SSTs im wärmeren Szenario die hochreichende Konvektion und folglich die konvektive Anregung interner planetarer Wellen. Diese Wellen steigen im Bereich der tropischen östlichen Winde auf und dissipieren dabei teilweise. Sie transportieren jedoch ein ausreichend starkes Signal bis in die untere Stratosphäre, um dort den gemittelten Massentransport zu verstärken. Dadurch intensiviert sich die Eintragsrate ozonarmer troposphärischer Luftmassen in die tropische untere Stratosphäre und verursacht dort eine Senkung der Ozonkonzentrationen, letztlich wegen klimabedingt höherer tropischer SSTs.

Die vorliegende Untersuchung der Variabilität stützt sich auf monatsgemittelte Gesamtozonsäulen dreier unabhängiger Realisierungen eines 60 Jahre umfassenden transienten Szenarios unter realitätsnahen Randbedingungen. Sie betrachtet drei verschiedene Breitenmittel: nördliche/südliche mittlere Breiten (SH/NH) und Tropen. Gebräuchliche MRAs des stratosphärischen Ozons sind linear und

müssen iterieren um der autoregressiv bedingten Nichtlinearität Rechnung zu tragen. Die vorliegende MRA ist nichtlinear und die erste MRA, welche die Anwendung solcher Iterationen hinsichtlich der Fläche der kleinsten Quadrate für gültig erklärt: sie findet nur eine schwache autoregressiv bedingte Verzerrung dieser Fläche, jedoch ist diese Aussage nur für die analysierten Ozonzeitreihen gültig. Darüber hinaus ist die vorliegende MRA eine der wenigen, welche eine ausreichende Einhaltung der Regressionsvoraussetzungen nachweist, vor allem der unabhängigen Residuen. Desweiteren erlaubt die Berechnung von Konfidenzbändern für Regressionslinien zum ersten Mal eine korrekte Zuordnung bestimmter Ozonanomalien zu einzelnen oder mehreren Randbedingungen. Die vorliegende MRA ist die erste, welche die Niedrigozonanomalie des Jahres 1985 in den SH erklärt, anhand der Daten von E39/C. Außerdem erklärt sie, unter anderem, eine entsprechende Anomalie des Jahres 1997 und verifiziert die Antwort von E39/C auf Randbedingungen, welche den stratosphärischen Ozontransport beeinflussen: tropische SST Anomalien (ENSO) wirken auf die Tropen und die NH, aber nicht auf die SH; die quasi-biannuale Oszillation (QBO) verursacht eine starke saisonal synchronisierte Ozonantwort in den SH und eine schwächere in den NH, jedoch fast keine in den Tropen. Während letztere Eigenschaften für E39/C schon bekannt sind, bietet die vorliegende Studie einen verbindlichen statistischen Rahmen und diskutiert die physikalischen Zusammenhänge. Außerdem quantifiziert die MRA andere schon bekannte Signale welche sich auf den 11-jährigen Sonnenfleckenzyklus (SSC), Sulfatoberflächen und ODS-Konzentrationen beziehen. Die verwendete Regressionsmethode bietet die Möglichkeit für Weiterentwicklungen. So könnten nichtlineare deterministische Terme in der Regressionsgleichung die Existenz von nichtlinearen Interaktionen überprüfen: die Ozonantwort auf starke ENSO-Ereignisse in den NH scheint desto intensiver auszufallen, je wahrscheinlicher eine arktische polare heterogene Ozonzerstörung durch langjährige Veränderungen wird. Sogenannte gleitende Mittel in der Regressionsgleichung könnten schließlich die Einhaltung der Regressionsvoraussetzungen weiter verbessern.

Festzuhalten ist: Die Randbedingungen der untersuchten Szenarien beeinflussen sowohl die Dicke der Ozonschicht, als auch den stratosphärischen gemittelten meridionalen Massentransport auf kurzen und langen Zeitskalen. Das in diesem Zusammenhang wichtigste Ergebnis ist die starke Stellung tropischer SSTs. Diese kontrollieren den stratosphärischen Transport, indem sie die konvektive Anregung interner, und wahrscheinlich auch externer, planetarer Wellen beeinflussen. Eine wichtige Aufgabe für zukünftige Arbeiten in diesem Zusammenhang ist folgende: herauszufinden, ob ansteigende tropische SSTs ENSO-ähnliche Veränderungen der Aktivität planetarer Wellen in der winterlichen Stratosphäre der mittleren und hohen Breiten verursachen können. Solche Veränderungen könnten den arktischen Polarwirbel schwächen, entgegengesetzt zu einer strahlungsbedingten Stabilisierung durch höherer GHG Konzentrationen. Das Modell E39/C und anderer Modelle haben gewisse Schwächen, zum Beispiel eine unrealistisch konsistente Beeinflussung des arktischen Polarwirbels durch die QBO. Unter Berücksichtigung dieser Schwächen jedoch, könnte die MRA durch ihre statistische Effizienz als nützliches Werkzeug dienen.

Contents

1	Introduction	2
2	Global warming and the ozone layer	5
2.0.1	Climate signal in modelled tropical ozone	6
2.0.2	Dynamical contribution to the ozone climate signal	9
2.0.3	Climate signal in tropical transport	10
2.0.4	Extratropical transport-induced ozone changes	11
2.0.5	Significance of dynamically induced ozone changes	12
2.0.6	Physical link connecting transport and boundary conditions	13
2.1	Aims and objectives	17
2.2	Background information about eddies and convective eddy generation	18
2.2.1	Eddy scale and generation	19
2.2.2	Eddy propagation	22
2.2.3	Eddy dissipation	23
2.2.4	Eliassen-Palm (EP) diagnostics	23
2.3	Data basis and plotting conventions	24
2.3.1	EP cross-sections	25
2.3.2	Transformed Eulerian mean (TEM) stream function	26
2.4	Validation of absolute model results	27
2.4.1	Temperature and zonal wind	27
2.4.2	EP diagnostics	29
2.4.3	TEM stream function	38

2.5	Response of the atmospheric background state	39
2.5.1	Latent-heat release	40
2.5.2	Zonal temperature gradient	44
2.5.3	Zonal wind	46
2.5.4	Land-sea temperature contrast	47
2.6	Statistical significance of the responses	47
2.6.1	Description of the statistical method	48
2.6.2	Temperature and zonal wind	48
2.6.3	EP flux, EP divergence, and latent-heat release	49
2.7	Response of wave-related dynamical quantities	50
2.7.1	July and August	51
2.7.2	December and January	54
2.8	Response of stratospheric transport	58
2.8.1	July and August	59
2.8.2	December and January	60
2.9	Summary and conclusion	61
2.9.1	Objective 1	61
2.9.2	Objective 2	62
2.9.3	Objective 3	64
2.9.4	Assessment of importance and recommendations for future work	67
3	Ozone column variability	70
3.0.1	Significance of modelled and observed interannual variability in total column ozone	74
3.0.2	Regression analysis and stratospheric ozone	75
3.0.3	Technical aspects of regression analysis	76
3.1	Aims and objectives	81
3.2	Regression algorithm description	83
3.2.1	Minimisation algorithm	83

3.2.2	Algorithms added to the minimisation algorithm	83
3.3	Regression model description	84
3.3.1	Combined regression model	84
3.3.2	Design of the ozone predictors	86
3.4	Description of the regression requirement diagnostics	89
3.4.1	Stationarity	90
3.4.2	Parsimony	90
3.4.3	Residual autocorrelation and distribution	91
3.5	Response confidence band validation	92
3.5.1	Independent residuals	94
3.5.2	Normal distribution	96
3.5.3	Asymptotic linearity	98
3.5.4	Validation of the Cochrane-Orcutt transformation	99
3.6	Interannual variability	100
3.6.1	Southern hemispheric mid-latitudes	101
3.6.2	Northern hemispheric mid-latitudes	105
3.6.3	Tropics	112
3.7	Summary and conclusion	116
3.7.1	Objective 1	116
3.7.2	Objective 2	116
3.7.3	Objective 3	118
3.7.4	Recommendations for future work	121
4	Wintertime northern polar stratospheric dynamics	123
4.1	Quasi-biennial oscillation (QBO) and 11-year solar cycle (SSC) . .	124
4.1.1	QBO-related modulation of the northern polar vortex . . .	124
4.1.2	SSC-related modulation of the stratosphere	125
4.1.3	QBO-SSC entangled impact on the northern polar vortex .	127
4.2	Model results	130
4.2.1	SSC-related influence and QBO-SSC entangled mechanism	130
4.2.2	QBO-related modulation without SSC influence	132
4.3	Summary and conclusion	134

5	Summary and conclusion	136
5.1	Objective 1	136
5.2	Objective 2	137
5.3	Objective 3	140
5.4	Conclusions and recommendations for future work	141
A	Model and scenario description	143
A.1	Model description	143
A.2	Scenario description	144
	References cited	146

List of Figures

2.1	Annual-mean SST and monthly mean CO ₂ concentrations for the model scenarios PAST, WARM, and COLD	7
2.2	Annual-mean anomaly of ozone concentrations, total ozone column, and TEM stream function	8
2.3	Annual-mean anomalous EP diagnostics	16
2.4	Absolute temperature and zonal wind velocity in the NH	28
2.5	JA absolute EP diagnostics for the stratosphere and the upper troposphere	31
2.6	Same as Figure 2.5, but for the troposphere	32
2.7	Same as Figure 2.5, but for DJ	33
2.8	Same as Figure 2.5, but for DJ and the troposphere	34
2.9	SST anomalies and modelled convective precipitation rates	41
2.10	Anomalous liquid-water content, temperature and zonal wind velocity	43
2.11	Absolute and anomalous TEM stream functions scaled to display the Hadley-Ferrel circulation	45
2.12	Same as Figure 2.3, but for JA and additionally the upper troposphere	52
2.13	Same as Figure 2.3, but for DJ	54
2.14	Absolute and anomalous TEM stream functions for the stratosphere	58
3.1	Scenario REF boundary conditions that serve as regression predictors for total column ozone	71
3.2	Deseasonalised monthly zonal-mean percental anomalies in total column ozone	73

3.3	Deseasonalised zonal-mean total column ozone for different latitude bands; corresponding 95% response confidence bands	93
3.4	SH mid-latitude residual autocorrelations; residuals as a function of time	95
3.5	NH mid-latitude and tropical residual autocorrelations; residuals as a function of time	97
3.6	Regression parameter confidence level as a function of the departure from the optimum parameter value	99
3.7	Response confidence bands for the SH mid-latitudes	103
3.8	Response confidence bands for the NH mid-latitudes	107
3.9	Response confidence bands for the tropics	114
4.1	Correlation coefficient between the 11-year solar cycle and January/February geopotential heights at 30 hPa	128
4.2	January/February mean 30 hPa geopotential height difference . .	133

List of Tables

3.1	Characteristics of the deterministic regression predictors and associated seasonal expansions that contribute to the regression analysis	94
A.1	E39/C scenario assumptions	145

Chapter 1

Introduction

During the 1980's, the stratospheric ozone layer had been attracting a lot of attention with regard to a human-induced thinning via emissions of ozone-depleting substances. This problem of ozone depletion was for the first time addressed by international policy in the year 1985 "Vienna Convention for the Protection of the Ozone Layer". However, the Vienna Convention did not adopt any measures regarding the production or consumption of ozone-depleting substances, but constituted a framework for measures to be implemented in its later protocol. In 1987, the "Montreal Protocol on Substances that Deplete the Ozone Layer" imposed specific measures, but these were not sufficient. It was the establishing scientific consensus about the causes of ozone depletion together with numerical projections as well as the development of alternative substances that led to the significant London Amendments to the Montreal Protocol in 1990. A tight compliance with these and with later amendments represents the basis for current measurements showing that the effective peak load of stratospheric ozone-depleting substances has been left behind and the burden has started to decrease. Nevertheless, even a continuing compliance implies a return to the pre-1980 burden only by the second half of this century.

The Montreal Protocol and its amendments represent a great success of international policy. Yet probably as essential for the success as a scientific consensus was the in-time development of alternative chemical compounds. The situation is different in case of mitigating human-induced climate change: the development of alternative energy sources is proceeding slowly, significant measures are likely to affect the present economy, and thus a relevant reduction of climate-modifying gas emissions is hard to accomplish. It is hence probable that climate change will be continuing to progress in the near future.

Climate change does not only alter the state of the troposphere, but also that of the stratosphere where the ozone layer resides. It both decelerates some of the ozone-destructing chemical reactions by stratospheric cooling and appears to

speed-up the stratospheric ozone transport from the equatorial source region polewards, accelerating ozone recovery particularly at mid-latitudes. Such beneficial effects may mislead certain parties to the Montreal Protocol to question the emission ban on ozone-depleting substances. Other parties might be tempted to deal with remaining stocks of banned chemical compounds less carefully. Note that the associated economic benefits are presumably small and at cost of retarding effects on ozone recovery, independently of climate-related modifications.

To counteract such tendencies it is important to clarify that, at the same time, climate change seems to have less beneficial consequences on the stratospheric ozone layer elsewhere from the mid-latitudes:

1. the associated acceleration of stratospheric ozone transport might affect the tropical ozone layer adversely. It could increase the rate of low-ozone tropospheric air masses penetrating into the tropical lower stratosphere; this would in turn mitigate or even over-compensate the effect of climate change causing a slow-down of certain ozone-destructing chemical reactions;
2. climate-change-induced stratospheric cooling makes those particular chemical reactions on polar stratospheric clouds more widespread that provoke the Antarctic ozone hole; the same may hold for the Arctic, but there the dynamical response to climate change adds additional complexity.

There is a lack of knowledge regarding item number 1. On the one hand, observations of the tropical stratosphere provide corresponding hints indeed, but are at present not suitable to ultimately verify a tropical transport enhancement and the associated ozone changes. On the other hand, state-of-the-art computer models yield both a climate-induced tropical transport enhancement and an according ozone response, but the physical mechanism for the transport enhancement is unclear. The present study tries to find that physical mechanism using the chemistry-climate model E39/C.

A general problem in detecting long-term changes is that the ozone layer exhibits a significant year-to-year variability. For all latitudes, but for the tropics in particular, that interannual variability complicates the detection of long-term modifications, particularly those relating to changing burdens of ozone-depleting substances or to climate change. Measured data show that, compared to its year 1980 reference thickness, the ozone layer has thinned down significantly; hence the notion of a future ozone recovery with regard to decreasing amounts of ozone-depleting substances in the stratosphere. In this respect, the tropical region represents an exception as there the data do not support a weaker ozone layer with regards to the year 1980 benchmark. The present study tries to both upgrade a statistical procedure used to remove the interannual variability, and to gain insight into the causal relationships that govern the variability. Again E39/C data are used.

Regarding item number 2 in the above list, current computer models have difficulties in calculating a correct behaviour of the northern polar stratospheric dynamics during winter and spring; this complicates estimates of the Arctic ozone layer future evolution and how it is affected by climate change. The present study tries to assess the dynamical characteristics in case of E39/C.

To summarise, the objectives of this study are to analyse E39/C output data and to

1. find the reason for climate change accelerating the upward transport across the tropical tropopause;
2. upgrade a statistical procedure used to account for the interannual variability of the ozone layer; gain insight into the causal relationships governing the interannual variability;
3. assess both general characteristics and climate-change-related modifications of the northern polar stratospheric dynamics during winter and spring.

Chapter 2 of the present study aims at finding the physical mechanism behind the enhanced tropical upwelling, Chapter 3 is devoted to the interannual variability of the ozone layer, Chapter 4 as well as parts of Chapter 2 assess the E39/C northern polar stratosphere during winter, Chapter 5 gives a summary and conclusions, and Appendix A provides a description of both E39/C and the model scenarios.

Chapter 2

Global warming and the ozone layer

Thompson and Solomon (2005) detect a recent annual-mean cooling of the tropical lower stratosphere in radiosonde data and speculate it might coincide with weaker ozone concentrations. The authors argue that their finding could result from enhanced upward mass transport across the tropical tropopause; the latter would intensify adiabatic cooling and more strongly advect ozone-poor tropospheric air into the lower stratosphere. Unfortunately, a verification is difficult to accomplish because satellite retrievals of total ozone column are rather insensitive to tropical lower-stratospheric ozone concentrations and the coverage by profile data is fragmentary (*Randel et al.*, 1999). Additionally, mass transport data for the lower stratosphere have large uncertainties, primarily because the observed heating rates needed in the computation are small (*Cordero and Kawa*, 2001; *Gettelman et al.*, 1997). Regarding observed time series of tropical total column ozone, it is worth noting that these display a large variability; the relevant studies detect a barely statistically significant decrease during the 1980s and parts of the 1990s, when concentrations of ozone-depleting substances (ODS) were strongly increasing (*WMO*, 2007).

Despite prospectively declining concentrations of ODS, however, most modelling studies predict that future ozone concentrations in the tropical lower stratosphere are not going to increase beyond the value modelled in 1980 significantly. Both, two-dimensional models (*Rosenfield and Schoeberl*, 2005; *Rosenfield et al.*, 2002), and three-dimensional models (*Fomichev et al.*, 2007; *Austin and Wilson*, 2006; *Shindell et al.*, 2006; *Rind et al.*, 2002) support this perspective, and some of the models even extend this finding to the tropical total ozone column.

The chemistry climate model (CCM) study by *Eyring et al.* (2007) analyses model runs of various CCMs and concludes that the future evolution in tropical total column ozone differs from that at middle latitudes which displays a positive

trend. Some of the models even predict that by the mid-century total tropical ozone values will not have increased, and for the year 2100 two out of three CCMs still do not indicate a thicker tropical ozone layer. This is an intriguing result, as the models account for both the above-mentioned future decline in ODS concentrations and the weakening rates of homogeneous ozone destruction. The latter weakening refers to increasing concentrations of well-mixed greenhouse gases (GHG) cooling the stratosphere (Section 2.0.2). *Eyring et al.* (2007) argue that the apparent lack of a tropical total column ozone increase might refer to a stronger tropical upwelling occurring as the climate warms. They emphasise the need to quantify future changes in the upwelling and how strongly it impacts on tropical ozone concentrations.

2.0.1 Climate signal in modelled tropical ozone

The study by *Dameris* (2007) uses a pioneering approach in that it addresses the above-mentioned questions using fully coupled three-dimensional CCMs and at the same time compares specific transient scenarios; the scenarios follow the same evolution of ODS according to the Ab scenario in *WMO* (2003), but are run with either increasing or constant concentrations of well-mixed greenhouse gases (GHG). For both scenarios compatible sea surface temperatures and sea ice coverage are prescribed; both quantities are hereafter summarized under the term “SST”.

By contrasting the realisations of both scenarios one can separate effects related to a warming climate from those related to decreasing ODS concentrations. Also, the use of three-dimensional models is important because planetary eddy dissipation reacts differently to a changing climate for two-dimensional compared to three-dimensional models. For two-dimensional models the eddies are parameterised and thus do likely not respond to all the relevant physical processes, while eddies in three-dimensional models are explicitly resolved (*Rosenfield et al.*, 2002). Finally, an appropriate computation of the polar regions necessitates the use of three-dimensional models (*WMO*, 2003).

All of the three models employed in *WMO* (2007) yield weaker ozone concentrations in the tropical lower stratosphere for the warm, compared to the cold scenario (not shown). E39/C represents one of these three models and the respective runs are analysed here in more detail. The warm scenario (WARM, see Appendix A.2) embraces the period 2000 to 2019 and follows the A1b evolution in *IPCC* (2001) of increasing GHG concentrations and of SSTs changing accordingly (Figure 2.1). The SSTs are taken from a transient model run with the HADGEM1 atmosphere ocean general circulation model (AOGCM) (*Stott et al.*, 2006; *Johns et al.*, 2006). The cold scenario (COLD, see Appendix A.1) covers the period 1980 to 2019, has the GHG concentrations fixed to their observed values of the year 1980, and uses decadal repetitive SSTs from observations

made during the 1970's (*Rayner et al.*, 2003) (Figure 2.1). The present Chapter considers the model period 2000 to 2019 in all of its Figures and, particularly, does not visualise shorter time spans.

Compared to COLD, the WARM scenario displays a region of small but significantly lower ozone concentrations (Figure 2.2a). The ozone decrease occurs at lower-stratospheric levels in the tropics and parts of the subtropics; maximises at a value of -0.1 ppmv close to the equator at a height of 30 hPa; reaches from the tropopause to the second highest model level centered at 20 hPa; and adversely affects the respective anomalous total column (Figure 2.2b). The corresponding percental ozone reduction maximises at a value of -7% , but occurs closer to the tropopause at 70 hPa (not shown), relating to the positive background vertical concentration gradient (*Dameris et al.*, 2005).

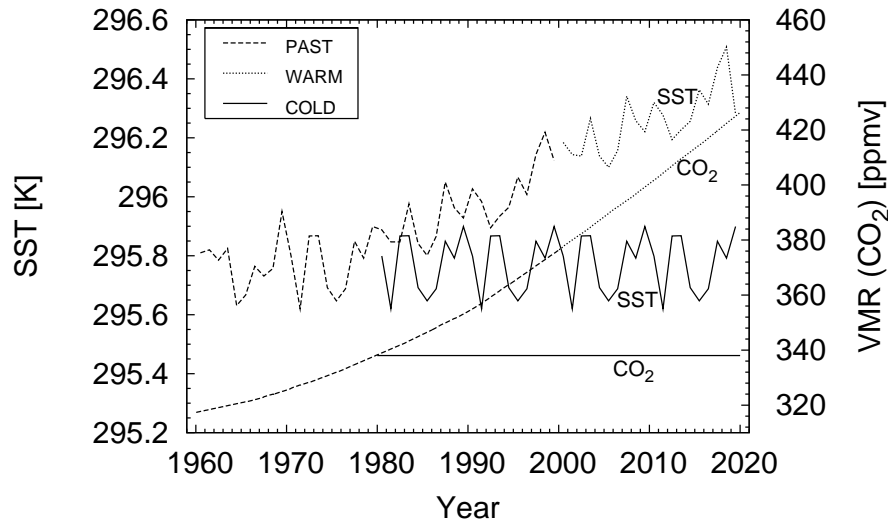
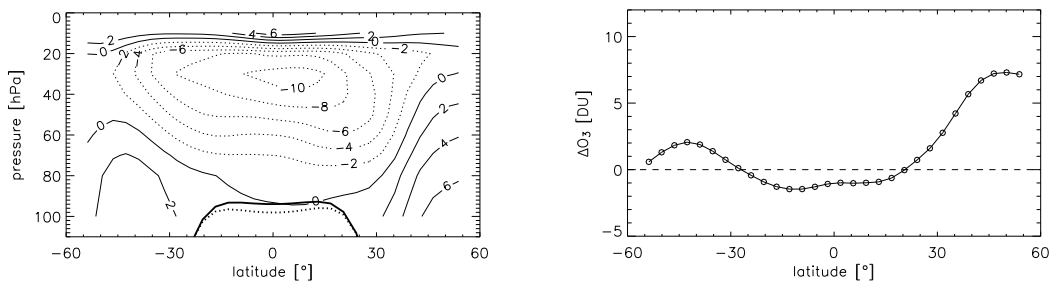


Figure 2.1: Annual-mean SST (near-global mean equatorward of any sea ice occurrence: 54°N to 54°S) and monthly mean CO_2 concentrations for the model scenarios PAST, WARM, and COLD. The mean SST is displayed for reasons of illustration. In fact, E39/C uses longitudinally/latitudinally distributed SSTs and sea ice coverage on a monthly basis.

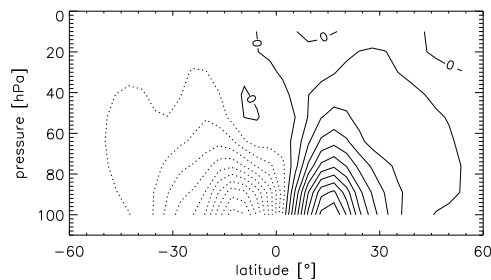
Because the two scenarios, WARM and COLD, respectively refer to modelled and observed SSTs, the negative tropical ozone anomaly might mirror a bias of the AOGCM run from which the WARM SSTs are taken. Yet the point of view changes when additionally considering transient E39/C model runs designed to reproduce the past period 1960 to 1999 and driven by observed SSTs (scenario PAST, Figure 2.1 and Appendix A.2). The runs reveal that the negative anomaly decadal develops from 1980 to 2009 (not shown) and thus is unlikely to represent an artefact of the year 2000 switch from observed to modelled SSTs.

A drawback of E39/C may be that it neglects ozone concentration changes above its 5 hPa upper lid. At these heights, changes in future ozone levels are well understood to be chemistry-dominated with the future increase occurring quicker in a warmer climate (*WMO, 2007; Shindell and Grewe, 2002*), and thus tending to compensate the transport-change-related effects below. The partial ozone column above 5 hPa only contributes about 10%, though, to tropical total ozone (*Russell et al., 1993*). Appropriately enough, its immediate contribution to the future evolution of total ozone may be small since even Middle-Atmosphere models with their higher upper lid do not predict increasing levels of tropical total column ozone for the future (*WMO, 2007; Eyring et al., 2007; Austin and Wilson, 2006*).



(a) Ozone concentration anomaly (in 10^{-8} ppmv). Thin straight contours denote a positive or zero anomaly, thin dotted contours a negative anomaly. The thick straight contour marks the position of the thermal tropopause for WARM, the thick dotted contour the position for COLD.

(b) Total ozone column anomaly (in DU).



(c) Anomalous TEM stream function (in integer multiples of $\pm 10^8$ kg/s). Straight contours denote positive values, dotted contours negative values. The mass transport is parallel to the iso-lines, clockwise around a stream function maximum, counter-clockwise around a minimum, and its strength proportional to the density of the iso-lines.

Figure 2.2: Annual-mean anomaly (WARM minus COLD) of ozone concentrations, total ozone column, and TEM stream function. The Figures do not contain the polar latitudes for reasons of illustration.

2.0.2 Dynamical contribution to the ozone climate signal

Both scenarios contributing to Figure 2.2 follow identical transient boundary conditions, except for GHG concentrations and SSTs. Therefore, only mechanisms that depend on the thermal structure of the atmosphere can yield a significant departure in stratospheric ozone concentrations among the two scenarios. The most important of the mechanisms are not only identified with mass transport, but also with ozone chemistry and atmospheric chemical composition.

Lower-stratospheric water vapour (*Eyring et al.*, 2007; *Stenke and Grewe*, 2005; *Shindell and Grewe*, 2002) and upper-stratospheric ozone concentrations (*Rosenfield and Schoeberl*, 2005; *Rind et al.*, 2002; *Rosenfield et al.*, 2002) are predicted to become more abundant in the warmer climate. As these adversely affect the future evolution of tropical lower-stratospheric ozone, intensified tropical upwelling does not represent the only mechanism potentially weakening tropical lower-stratospheric ozone concentrations as the climate warms; the other contributors thus deserve attention.

In case of E39/C, climate-related changes in atmospheric chemistry and water vapour abundance cause a net increase of lower-stratospheric ozone (see below), hence partly opposing the decrease associated with enhanced upwelling. The reason is that some important ozone-destructing homogeneous chemical reactions decelerate (not shown) because the stratosphere cools (Figures 2.10c and 2.10d), mainly through enhanced infrared emission from greater GHG concentrations (*WMO*, 2007). A similar deceleration is reported in the studies by *Rosenfield et al.* (2002); *Steil et al.* (1998). Polar heterogeneous ozone destruction, on the other hand, is indeed more likely the lower the temperature, but does not significantly impact on tropical ozone (*Rosenfield et al.*, 2002; *Chipperfield*, 1999).

At the same time calculations from E39/C show more abundant lower-stratospheric water vapour for the WARM than for the COLD scenario, by an amount of about 0.4–0.6 ppmv (not shown) and possibly for a variety of reasons (*Eyring et al.*, 2007). More abundant stratospheric water vapour accelerates the ozone-destructing HOx cycle (*Stenke and Grewe*, 2005). Results not shown here yet reveal that the stratospheric cooling mentioned above apparently dominates the overall net ozone production rate which strengthens in the warmer climate.

It follows that the slowed-down ozone loss cycles for WARM must also dominate over the effect of a radiation-induced weaker photochemical ozone net production rate. UV radiation penetrates less intensely down to lower-stratospheric levels as middle/upper-stratospheric ozone concentrations increase (*Fels et al.*, 1980); and the latter concentrations strengthen more quickly in the warmer climate since, as mentioned-above, important loss cycles slow down as the stratosphere cools *Rosenfield and Schoeberl* (2005); *Rind et al.* (2002); *Rosenfield et al.* (2002).

Figure 2.2a displays the latter ozone enhancement effect, but only at its uppermost model layer centered at 10 hPa. The reason is that E39/C neglects the middle stratosphere in part and the whole upper stratosphere due to its low upper lid. The model therefore probably neglects the impact of reduced UV radiation on lower-stratospheric photochemistry, and any results presented here thus should be seen as sensitivities largely without that effect.

Today, there is considerable uncertainty regarding the impact of reduced lower-stratospheric UV radiation on the future evolution of tropical total ozone (*Eyring et al.*, 2007). Two- and three-dimensional models differ in their response, though, hence providing evidence that the evolution might be dynamically dominated. On the one hand, most of the three-dimensional models presented in *Eyring et al.* (2007) and *Austin and Wilson* (2006) do contain the middle/upper stratosphere and display a lack of tropical lower-stratospheric ozone concentration increase for the warmer climate. On the other hand, two-dimensional models do not necessarily display a lack of increase (*Rosenfield et al.*, 2002). The reason for the discrepancy might well be dynamical since *Rosenfield et al.* (2002) report that planetary eddy dissipation in a warming climate significantly differs for the two types of models.

Here, the bottom line is that the total of any effects other than transport enhances tropical lower-stratospheric ozone concentrations in the warmer climate, and the negative anomaly apparent in Figure 2.2a thus results from transport changes.

2.0.3 Climate signal in tropical transport

Air parcels in the tropical lower stratosphere tend to travel upward and the time needed to arrive from the tropopause at a certain pressure level is in the range of months for E39/C, other models, and measurements (*Eyring et al.*, 2006). Ozone lifetime, on the other hand, is longer than a year below a level of roughly 60 hPa and decreases with altitude (*Brasseur and Solomon*, 1986). It follows that tropical lower-stratospheric ozone is dynamically controlled, but that the influence of chemistry gains importance with height. For the E39/C model, the minimum percental ozone anomaly occurs at 70 hPa (not shown), lower than the minimum concentration-anomaly (Figure 2.2a). Thus, the modelled tropical dynamical changes in the warmer climate have an upward direction.

Indeed, E39/C features for WARM a stronger upward mass transport across the tropical tropopause (Figure 2.2c), which must more intensely inject ozone-poor tropospheric air into the lower stratosphere. Due to the different chemistry, upper-tropospheric ozone concentrations are an order of magnitude weaker than their lower-stratospheric counterpart and in E39/C increase only slightly as the troposphere warms (Figure 2.2a). Hence, the negative ozone anomaly cannot be

due to changes in tropospheric ozone concentrations but must refer to intensified mass transport from the upper troposphere.

A quantification of how strongly the latter transport changes impact on tropical lower-stratospheric ozone is beyond the scope of this Chapter. Both, changes in tropical upwelling and in ozone concentrations tend to modify lower-stratospheric temperature, which again alters the net ozone production rate and possibly feeds back on the upwelling (*Austin and Wilson, 2006; Zhou et al., 2006; Rosenfield and Schoeberl, 2005*).

2.0.4 Extratropical transport-induced ozone changes

Poleward of the tropics, there is no simple way to qualitatively discern dynamically induced ozone changes from those due to slower homogenous ozone destruction. Both mechanisms act in the same direction because air parcels descending at stratospheric middle and higher latitudes have lost their specific low-ozone signature they had when entering the tropical stratosphere. These air parcels have been enriched with ozone while traveling across stratospheric regions where dynamically-induced ozone modulations are erased due to short ozone life times. As the ozone-rich air parcels descend, both surrounding pressure and ozone life time increase, causing ozone accumulation (*Salby and Callaghan, 2004a*). Additional complexity arises from polar springtime heterogeneous chemistry (*WMO, 2007*) and directional mass flux modifications (*Rind et al., 2002*).

Mass conservation implies that stronger tropical upwelling in the warmer climate must be balanced by enhanced downwelling at higher latitudes, thus forming an overturning circulation (*Eyring et al., 2007; Butchart et al., 2006*). Not only the overall increase of that circulation, but also the precise latitude height structure of the change is important when estimating the timing of total column ozone approaching its pre-1980 levels. For instance, such structural changes can alter the dynamical ozone accumulation mentioned above at any given latitude away from the tropics (*Rind et al., 2001*).

Also, the quicker removal of ODS concentrations in the warmer climate suggested by *Butchart and Scaife (2001)* necessitates amplified upwelling reaching into the middle stratosphere. There, UV radiation is intense enough to efficiently photolyse these chemical compounds. Still, some of the intensified tropical upwelling might be counterbalanced by a stronger and more downward vectored subtropical mass circulation (*Rind et al., 2002*), which is here apparent in Figure 2.2c. This would keep parts of the mass circulation increase within the lower stratosphere and thus delay the removal of ODS concentrations.

Springtime polar heterogeneous ozone destruction can sensitively react to temperature changes as destruction only occurs below a certain temperature threshold. The temperature within the stable Antarctic polar vortex is far below the

threshold nearly every winter season and dynamical changes are of minor importance. The Arctic polar vortex, on the other hand, is highly variable and temperature fluctuates around the threshold. Thus, there is a high potential for dynamical alterations to modify the Arctic total-column ozone recovery, and the modification can occur via changes in both adiabatic warming and mixing with lower latitudes (*WMO*, 2007).

2.0.5 Significance of dynamically induced ozone changes

In summary, climate-related dynamical changes are able to significantly modify the evolution of lower-stratospheric ozone concentrations. The modification is straightforward in the tropics where it counteracts the effect declining ODS concentrations have on future ozone increases. Measurements, this study, and other modelling studies show that effect. Away from the tropics, dynamically related ozone changes are more difficult to assess and so is their expected contribution to a possible ozone increase beyond the year 1980 values, in accordance with *WMO* (2007, Chapter 6). Arctic total column ozone might sensitively react to future dynamical changes, whereas Antarctic ozone recovery is expected to closely follow the future ODS decrease. And finally, dynamical changes could alter the rate of ODS removal from the stratosphere, but the alteration depends on changes in both strength and direction of stratospheric transport.

Today, there is a consensus among global climate modelers that the stratospheric annual mean tropical upwelling intensifies for the warmer scenarios (*Eyring et al.*, 2007; *Austin et al.*, 2007; *Butchart et al.*, 2006; *Rind et al.*, 2002; *Butchart and Scaife*, 2001). The definite reason for the stronger upwelling remains unknown (*Eyring et al.*, 2007; *Fomichev et al.*, 2007; *Austin and Li*, 2006; *Butchart et al.*, 2006; *Butchart and Scaife*, 2001), and the exact latitudinal distribution of the downwelling increase varies from model to model and from study to study (*Butchart et al.*, 2006; *Rind et al.*, 2002). Additionally, the sign of future dynamical changes in the mid-winter Arctic region is not clear as there are modelling studies which favour a warming due to enhanced dynamics (*Austin and Wilson*, 2006; *Schnadt et al.*, 2002; *Rind et al.*, 2001, 1998, 1990; *Mahfouf et al.*, 1994), studies which suggest a cooling due to an intensified infrared emission (*Shindell et al.*, 2006; *Pitari et al.*, 2002; *Shindell et al.*, 2001, 1998), and studies which are uncertain due to inter-model differences or low signal-to-noise ratios (*Austin et al.*, 2003; *Rind et al.*, 2002; *Rind et al.*, 2002). The problem of low signal-to-noise ratios in the mid-winter Arctic lower stratosphere is notorious; *Fomichev et al.* (2007); *Sigmond et al.* (2004); *Gillett et al.* (2003) report warmer Arctic mid-winter lower-stratospheric temperatures in connection with enhanced GHG concentrations and higher SSTs, but their Figures imply that the results are not statistically significant.

It follows that a better assessment of climate-related dynamical changes has

a potential to significantly improve projections of future stratospheric ozone concentrations. Such progress is especially important for the tropics where some kind of future dynamically induced ozone depletion cannot at present be excluded. In this context, *Geisler et al.* (1985), already, find in their GCM study that the tropical dynamical response to positive anomalies in tropical SSTs increases faster than linearly.

Current modelling studies do not predict a large dynamically induced depletion of tropical total ozone (*Eyring et al.*, 2007; *Austin and Wilson*, 2006), but some degree of uncertainty arises from the lack of knowledge about the cause of the enhanced tropical upwelling in a warmer climate. Finding the definite cause is identical with tracing the change in upwelling back to the boundary conditions of the respective model. Such attributions are relatively easily accomplished in case of two different model scenarios which only differ by their GHG concentrations and their respective SSTs, which represents the attempt employed here. In case of juxtaposing different time periods from a single scenario the situation is more complex because then various boundary conditions need to be considered simultaneously.

2.0.6 Physical link connecting transport and boundary conditions

Beyond mere statistical relationships, the attribution of stratospheric transport changes to the model boundary conditions requires an identification of the physical link. Modelling studies imply that climate-related stratospheric transport modifications are predominantly associated with changes in the above-mentioned stratospheric overturning mass circulation (*Butchart et al.*, 2006). This Brewer-Dobson (BD) circulation withdraws air masses from the tropical upper troposphere, transports them upward, then pushes them poleward and downward into the extratropical troposphere, with the transport maximising towards the winter pole (*Holton et al.*, 1995).

Eddy-driven BD circulation

There exist several potential pathways by which enhanced GHG concentrations and corresponding SSTs can alter the BD circulation. It is today accepted that eddies propel an eddy-driven contribution to the BD circulation by depositing momentum in the stratosphere via the process of dissipation. The dissipating eddies are mostly of planetary or of small-scale gravity scale (*Haynes et al.*, 1991; *Hines*, 1960). Here, the latter contribution is neglected because planetary eddies dominate lower-stratospheric eddy dissipation (*Salby and Callaghan*, 2006c,a) and gravity waves in global models represent a sub-grid parameterised feature that is

unlikely to realistically react to a warming climate (*Eyring et al.*, 2006; *Haynes*, 2005).

Butchart et al. (2006) analyse runs with several different mid-atmosphere models; show that the eddy-driven BD circulation roughly contributes 60% to the total BD circulation; and estimate a 60% contribution of eddy dissipation changes to the total BD circulation trend in a warming climate. They assume the remaining 40% to result from sub-grid scale momentum deposition even though other drive mechanisms that depend on the stratospheric concentrations of radiatively active gases might also contribute. Altered differential heating (*Rosenfield and Schoeberl*, 2005) and modified seasonal diabatic temperature changes (*Salby and Callaghan*, 2006c) represent likely candidates, but seem to have so far attracted only little attention in the context of a warming climate.

Since residual velocities (*Edmon et al.*, 1980) form the basis of the BD circulation difference displayed in Figure 2.2c, it does not only contain changes from eddy dissipation but from all known or unknown BD circulation driving engines the model supports. E39/C calculates a generally more intense total BD circulation for WARM than for COLD in both hemispheres, the increase maximising at lower-stratospheric tropical/subtropical latitudes. By contrasting the absolute BD circulations for WARM and COLD (not shown) it becomes apparent that enhanced upwelling occurs in the tropics and a stronger poleward mass transport in the subtropics. At the same time, for the WARM case, the subtropical flux has a more-downward orientation.

The respective anomalous eddy dissipation pattern in Figure 2.3a displays an annual-mean dissipation increase in the warmer climate, the maximum increase roughly occurring at 80 hPa and $\pm 20^\circ$ latitude. Note that a quantification of the anomalous eddy dissipation contribution (Figure 2.3a) to the total anomalous BD circulation (Figure 2.2c) involves the principle of downward-control, the implementation of which is beyond the scope of the present Chapter.

Downward-control principle

The physical principle of downward-control (*Haynes et al.*, 1991) links an eddy-driven BD circulation to a given eddy dissipation pattern and relies on near-steady zonal winds. It thus neglects the coupled aspect of zonal wind and eddy dissipation; but on a monthly basis the zonal wind is considered to be near steady and the coupling thus negligible, at least for practical purposes (*Newman et al.*, 2001).

Downward-control takes advantage of eddy dissipation locally exerting a poleward oriented force which connects downward along constant angular momentum surfaces, the latter, to a good approximation, being vertical outside the tropics

(*Plumb and Eluszkiewicz, 1999; Haynes et al., 1991*). In fact, the term “downward-control” usually only refers to the above-mentioned downward connection (*Haynes et al., 1991*), but is here used to denote the whole physical mechanism of eddy dissipation inducing an eddy-driven BD circulation.

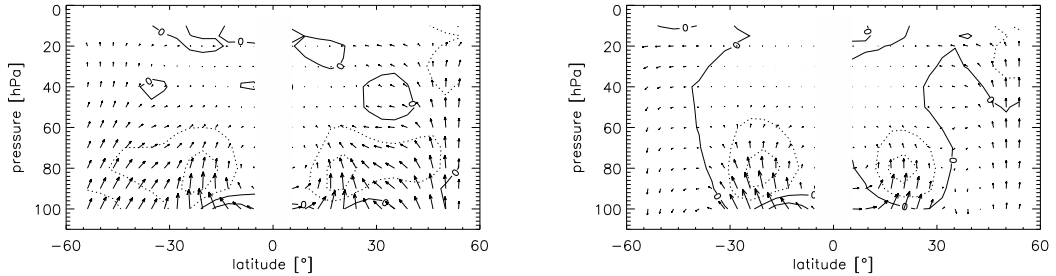
The principle of downward-control is invalid for low latitudes due to nonlinear effects, the latter being subject to current research (*Zhou et al., 2006; Haynes, 2005; McIntyre, 1998*). Closer to the equator the connection between eddy dissipation and poleward force becomes more nonlinear, and the constant angular momentum surfaces become more non-vertical and distorted. (*McIntyre, 1998; Holton et al., 1995*). In the analyses presented here, the modelled eddy dissipation increase peaks at roughly $\pm 20^\circ$ of latitude, thus challenges the concept of downward-control which may become unstable equatorward of $\pm 20^\circ$ (*McIntyre, 1998*).

This Chapter still refers to the principle of downward-control in order to demonstrate if a given modelled eddy dissipation pattern is likely to produce a significant contribution to the given modelled BD circulation. The decision is based on the two patterns qualitatively conforming to downward-control or not.

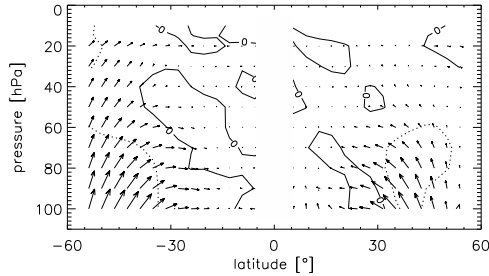
Quasi-stationary and transient eddies in E39/C

Together, the anomalous dissipation patterns in Figure 2.3a and 2.3b reveal that the tropical annual-mean dissipation change mainly results from a greater quasi-stationary eddy activity. The eddies responsible originate in the summer tropical upper troposphere, travel upward through the summer easterly winds while dissipating, and vanish far below the upper model lid (Section 2.4.2). Thus, the 5 hPa model lid is unlikely to represent a severe constraint regarding tropical/subtropical eddy activity changes in a warming climate. Instead, it enables E39/C to provide high vertical resolution around the tropical tropopause, a region of major importance here, while incorporating features such as a high horizontal resolution, a detailed fully coupled stratospheric ozone chemistry, the tropical quasi-biennial oscillation (QBO), and the 11-year solar cycle. Modelling the middle stratosphere necessitated a smaller dynamic time step, more different tracers, and thus would significantly increase the computing time (*Hein et al., 2001*).

Finally, a comparison of Figure 2.3b and Figure 2.3c shows that quasi-stationary and transient eddies fluxes do not similarly react to a warming climate; also, the two types of eddy fluxes differ in their seasonal behaviour (Section 2.4.2). Such features must be accounted for when referring eddy dissipation, and thus BD circulation changes, to the model boundary conditions of interest, being GHG concentrations and SSTs.



(a) Quasi-stationary plus transient contributions: $9.035 \times 10^{13} \rightarrow, 1.486 \times 10^{18} \uparrow$ (b) Quasi-stationary contribution only: $8.890 \times 10^{13} \rightarrow, 1.462 \times 10^{18} \uparrow$



(c) Transient contribution only: $7.469 \times 10^{13} \rightarrow, 1.228 \times 10^{18} \uparrow$

Figure 2.3: Annual-mean anomalous EP diagnostics (WARM minus COLD). A horizontal EP flux arrow of the same length as 10° of latitude on the diagram corresponds to the amount (in m^3) indicated by the first number. Similarly, a vertical EP flux arrow of the same length corresponds to the amount (in m^3kPa) indicated by the second number. The arrows depicted in the captions are not to scale, but meant to mark the above-mentioned numbers which give the horizontal and vertical scaling. The scaling follows the approach by *Edmon et al.* (1980) and makes the EP flux arrows correspond to their respective EP divergences, the latter denoted by the contours. Straight contours represent a positive or zero, dotted contours a negative EP divergence anomaly. The non-zero contours respectively denote values (in 10^{14} m^3) of $\pm 1.0 \pm 2.0 \pm 3.5 \pm 5.0 \pm 6.5 \pm 8.0 \pm 9.5 \pm 11.0 \pm 12.5 \pm 14.0 \pm 15.5 \pm 17.0 \pm 18.5 \pm 20.0 \pm 21.5 \pm 23.0 \pm 24.5 \pm 26.0$. The Figures do not contain the polar latitudes for reasons of illustration.

2.1 Aims and objectives

The majority of recent CCM studies, including the E39/C analysis presented here, suggest that the future evolution of lower-stratospheric ozone concentrations not only depends on the decline rate of stratospheric ODS concentrations and temperature-dependent reaction rates; it also relates to BD circulation changes. For the tropics, the studies agree with the future BD circulation intensifying and thereby affecting lower-stratospheric ozone, probably as a result of enhanced low-latitude eddy dissipation. The reason for the latter dissipation enhancement is unclear and this Chapter provides a new interpretation. Regarding higher latitudes, recent studies are uncertain about the sign of future eddy dissipation and BD circulation changes during the northern hemispheric polar winter and how these affect the polar vortex. There, heterogeneous ozone destruction and nonlinear dynamics add complexity.

This Chapter explores the above questions by deducing climate-related BD circulation responses from the relevant model boundary-conditions, via eddy dissipation responses and the principle of downward-control. The responses exclusively refer to the model boundary conditions of GHG concentrations and SSTs because realisations of two different but related scenarios are compared. The term “response” is meant to signify a particular result of one scenario subtracted from that of the other.

This Chapter examines a new hypothesis, namely that higher tropical SSTs strengthen the deep-convective production of tropical quasi-stationary eddies, the strengthened eddy activity propagating upward across the tropopause, where it dissipates and changes the BD circulation. Also, this Chapter aims at identifying and explaining extratropical eddy dissipation and BD circulation responses, in particular those in the mid-winter polar region.

The focus lies on the northern hemisphere (NH) because tropical NH and southern hemisphere (SH) responses look similar (Figures 2.2c, 2.3a) and follow the same physical mechanism, the NH response peaking during the northern summer, the SH response during the southern summer (not shown). In addition, it is today accepted that planetary eddies have a greater potential to modify the future evolution of the unstable NH polar vortex than that of its stable SH counterpart. Also, the focus is on July/August (JA) and December/January (DJ) averages because during these months E39/C yields the strongest and most robust tropical and higher-latitude dynamical NH response, respectively.

Regarding data quality, this Chapter benefits from the availability of several realisations for both of the two-decadal scenarios, improving the signal-to-noise ratio and facilitating the assessment if a response pattern is robust or not.

The objectives of this Chapter are:

1. to provide background information on planetary eddies, and to briefly review the literature on the mechanism of tropical deep-convective eddy forcing and related BD induction;
2. to consider the individual scenarios and
 - (a) validate these against observations;
 - (b) check these for tropical deep-convective eddy forcing;
 - (c) check eddy divergence and BD circulation patterns for downward-control;
3. to find robust tropical and extratropical response patterns of
 - (a) latent-heat release, temperature, zonal wind, and relate these to the model boundary conditions;
 - (b) net eddy activity flux, net eddy dissipation, and relate these to the robust responses under (a), thus to the model boundary conditions;
 - (c) BD circulation and relate these, qualitatively considering downward-control, to the robust eddy divergence responses under (b), thus also to the model boundary conditions.

2.2 Background information about eddies and convective eddy generation

The life cycle of large-scale eddies involves the processes of generation, propagation, and dissipation which may all depend on the model boundary conditions, especially on the concentration of GHG and on the SSTs. In addition to the stratosphere, the troposphere is also of interest because most of the stratospheric eddy activity originates in the troposphere and travels upward across the tropopause (*Son et al.*, 2007; *Koshyk and Hamilton*, 2001; *Newman and Nash*, 2000; *Randel*, 1987).

An estimation of how the modelled stratospheric wave activity develops in a warmer climate consequently requires an assessment of how both, local stratospheric and remote tropospheric eddies respond to the model boundary conditions. It is thus important to summarise what sorts of eddies are involved, which physical mechanisms govern the life cycles in the stratosphere and the troposphere, and to introduce the necessary diagnostic tools. Such information also explains a large portion of the processes governing stratospheric transport because eddy dissipation contributes to the stratospheric BD circulation (Sections 2.0.6 and 2.2.4).

2.2.1 Eddy scale and generation

Mid-latitude forced quasi-stationary eddies occur at the planetary-scale, i.e. 1-3 troughs fit around a latitudinal circle (*Dutton, 1976*). The Rossby-wave formula for planetary eddies (*Dutton, 1976*) relates number of troughs, phase speed, and zonal-mean wind velocity, and implies that extratropical quasi-stationary eddy modes are usually of planetary-scale as well. Extra-tropical transient eddies, generally encompassing 1-8 troughs, can be both planetary or synoptic, but the planetary-scale dominates the total temporal variance of geopotential height at winter extratropical latitudes in the middle troposphere (*Blackmon and White, 1982*).

Forced eddies

Mid-latitude forced quasi-stationary eddies need to constantly be maintained by geographically-fixed excitation mechanisms of given wavenumber. The mechanisms are commonly identified with flow across large mountain ridges such as the Himalaya (*Charney and Eliassen, 1949*) and with continent ocean temperature contrasts (*Smagorinsky, 1953*). The forced quasi-stationary eddy activity maximises during winter and minimises during summer, probably due to seasonal variations in low-level zonal-mean zonal wind velocity (*WMO, 2007*), or in position and velocity of the subtropical jetstream (*Nigam and Lindzen, 1989*). Finally, forced quasi-stationary eddies can exhibit zonally travelling nodal surfaces when the forcing mechanism travels zonally (*Andrews et al., 1987*).

Eddy generation by atmospheric instability

In contrast to the forced quasi-stationary eddies, other quasi-stationary eddies are spontaneously generated by hydrodynamic instability (*Charney and Drazin, 1961*). In the extratropics, the latter quasi-stationary eddies display a weaker seasonal cycle than forced quasi-stationary eddies and generally correspond to eigen-modes of the atmosphere that need to be excited, but not necessarily constantly maintained (*Andrews et al., 1987*). The excitation mechanisms comprise barotropic instability associated with the subtropical jetstream and its horizontal wind shear (*Blackmon et al., 1987; Branstator, 1985; Simmons et al., 1983*), baroclinic instability associated with vertical wind shear in general (*Rind et al., 2005a,b, 2002; Koshyk and Hamilton, 2001; Singh, 1982*), and the nonlinear upscale evolution of synoptic-scale eddies (*Haynes, 2005; Koshyk and Hamilton, 2001; Plumb, 1985; Itoh, 1985*). According to the modelling study by *Scinocca and Haynes (1998)* the latter process maximises at near-tropopause levels. In the following, the term “quasi-stationary” will refer to both, forced and spontaneously generated quasi-stationary characteristics.

From a physical perspective, a strict discrepancy does not exist between spontaneously generated quasi-stationary eddies and transient eddies, as the distinction artificially follows from the procedure of monthly averaging. Finally, synoptic eddies are superimposed on the planetary quasi-stationary eddies, featuring extra-tropical low-level baroclinic development modulated by vertical stability (*Hoskins et al.*, 1983; *Dutton*, 1976; *Saltzman*, 1970).

Convective eddy forcing

With regards to lower-stratospheric quasi-stationary planetary eddy activity, tropical latent-heat release represents a less widely known excitation mechanism, hereafter referred to as “convective production”, “convective forcing”, or “convective excitation”. That mechanism has extensively been studied, often in the context of planetary quasi-stationary eddies excited by convection causing dry conditions elsewhere on the planet. There are analytical studies, for instance *Salby and Garcia* (1987); *Gill* (1980); numerical studies, for instance *Black and Sutton* (2007); *Lu and Delworth* (2005); *Feldstein* (2003); *Giannini et al.* (2003); *Horinouchi et al.* (2003); *Inatsu et al.* (2002); *Chen* (2001); *Ricciardulli and Garcia* (2000); *Rodwell and Hoskins* (1996); *Rowell et al.* (1995); *Garcia and Salby* (1987); *Blackmon et al.* (1987); *Geisler et al.* (1985); and there are observational studies, for instance *Feldstein* (2006); *Rowell et al.* (1995); *White* (1982).

There is observational and theoretical evidence that tropical latent-heat release associated with deep convection contributes to mid-latitude planetary eddy activity (*Inatsu et al.*, 2002; *Blackmon et al.*, 1987). However, it particularly and robustly excites low latitude upper-tropospheric quasi-stationary planetary eddies. The seasonal cycle of the eddies is tied to that of tropical deep convection, a summer activity maximum opposing a winter minimum (*Wang and Ting*, 1999). The wave phases tend to oppose as well, with rapid transitions during spring and autumn (*Chen*, 2001; *White*, 1982). Surface precipitation is a useful indicator of the tropical quasi-stationary eddy forcing (*Horinouchi et al.*, 2003) because it measures the vertically integrated latent-heat release and deep convection constitutes the major trigger of tropical precipitation (*Barsugli et al.*, 2006; *Anderson et al.*, 2004)

In their model study, *Garcia and Salby* (1987) describe that slowly evolving latent heating excites a narrow Hough spectrum (*Longuet-Higgins*, 1968) of both, equatorially symmetric Kelvin and asymmetric Rossby internal modes; these propagate vertically, as opposed to external modes. During solstice, when the latent heating is the most asymmetric with respect to the equator, the asymmetric Rossby modes dominate the low-latitude planetary eddy activity. Then, total tropical eddy activity peaks and reaches farthest into the summer subtropics.

Vertically, the activity extends into the lower stratosphere where it dissipates. Yet it is unclear if the dissipation is to be associated with the summer easterly

stratospheric winds, or integral to the excitation mechanism, independently of the winds. *Garcia and Salby* (1987) rely on a single heat source and on given time-independent distributions of zonal-mean zonal winds, but the low-latitude summertime easterlies and planetary eddy activity may actually form a coupled system (*Chen and Yen, 1993*).

Based on modelling and observational results, *Chen et al.* (2001); *Chen* (2001) suggest that the summertime subtropical eddy activity may result from a quasi-stationary zonally asymmetric distribution of latent heating, mainly associated with the east Asian monsoon and the western-Pacific rain band. The heating forces quasi-stationary planetary waves which vertically propagate across the tropopause into the lower stratosphere where the summer easterly winds make the eddies dissipate. There is evidence that both, east Asian monsoon and western Pacific rain band are sensitive to positive and negative anomalies of tropical SSTs, mainly associated with the Indian Ocean and the western Pacific (*Chen and Yen, 1993*). As a result, the tropical convectively forced eddies could react to the changes in convection induced by the SST anomalies. However, there does probably not exist any study which infers future increases in tropical quasi-stationary eddy activity from an enhanced convective production related to higher tropical SSTs, the eddy activity propagating upward across the tropical tropopause.

It seems that only the modelling study by *Boehm and Lee* (2003) directly relates the existence of a low latitude lower-stratospheric BD cell to convectively excited tropical eddies. In their study, an axisymmetric global circulation model is driven by observed fields of eddy momentum convergence associated with Rossby-waves; the waves propagate horizontally away, both southwards and northwards, from their convective source. The convergence is consequently restricted to those tropospheric heights where the latent-heat release occurs, but the model still calculates a low-latitude lower-stratospheric BD cell, in discordance with the principle of downward control. In the tropics, nevertheless, a weak horizontal Coriolis force and weak horizontal gradients of angular momentum may allow for both, upward- and downward-control (*Boehm and Lee, 2003; Plumb and Eluszkiewicz, 1999*).

In their double-CO₂ modelling studies, *Fomichev et al.* (2007); *Rind et al.* (2002) prescribe SST patterns adjusted to the given atmospheric CO₂ concentrations. They yield both a tropical lower-stratospheric eddy dissipation enhancement and a consequent anomalous BD cell in the warmer climate, but do not infer a strengthened convective eddy production.

It is likely that there do not exist any studies relating the structure of the summertime low-latitude lower-stratospheric BD circulation to convectively forced eddies propagating upward across the tropical tropopause. In particular, there is none which considers the full causal chain of higher tropical SSTs changing the lower-stratospheric BD circulation via enhanced deep-convective eddy forcing.

2.2.2 Eddy propagation

The study by *Charney and Drazin* (1961) provides a criterion if non-interacting linear Rossby-waves can propagate vertically. On the one hand, the eddies cannot penetrate critical surfaces where their phase speed is equal to or more westerly than the zonal-mean zonal wind. Consequently, forced quasi-stationary eddies cannot enter regions of zero or easterly winds, while forced transient eddies travelling at eastward phase speeds can.

On the other hand, the zonal-mean wind must not be too strong, depending on the wavenumber; and the smaller the wavenumber, the broader is the window for vertical propagation is. Typical wind velocities given, the criterium qualitatively explains why only planetary eddies can usually enter the stratosphere, more efficiently in winter than summertime. However, the criterion relies on a laterally uniform zonal-mean wind field.

For arbitrary wind fields the above criterion is modified by the concept of a wavenumber-dependent refractive index for horizontal and vertical eddy propagation and attenuation (*Nathan and Cordero*, 2007; *Andrews et al.*, 1987). In principle, the concept is restricted to forced quasi-stationary Rossby waves, but it satisfactorily works for forced transient Rossby waves as well (*Chen and Robinson*, 1992). The eddies tend to both refract towards and easier propagate within larger positive squared index values. In a constant wind field the eddies thus travel not only vertically, but also equatorward because the index depends on latitude.

It is stressed that the refractive index only describes the propagation properties of a given non-interacting linear forced Rossby-wave. The propagation characteristics of atmospheric external modes, for instance, are different due to their preference for horizontal propagation (*Andrews et al.*, 1987; *Longuet-Higgins*, 1968). Nevertheless, observational and theoretical studies show that the refractive index approach still yields satisfactory results (*Andrews et al.*, 1987).

The concept of a refractive index comprises the above window for vertical eddy propagation, but additionally includes horizontal propagation and modified window edges. The latter modification is particularly important for regions of large vertical wind shear and of large buoyancy frequency vertical gradients, commonly associated with the subtropical jet and the tropopause (*Li et al.*, 2007; *Hu and Tung*, 2002; *Chen and Robinson*, 1992).

For the former, recent studies conclude that a more positive vertical wind shear facilitates vertical eddy propagation against the impeding strong winds (*Li et al.*, 2007; *Hu and Tung*, 2002). For the latter, a smaller buoyancy gradient can act likewise (*Chen and Robinson*, 1992). Also, positive vertical shear within the base of the polar night jet favors upward eddy penetration (*Hu and Tung*, 2002). Finally, the lower-stratospheric polar night jet mainly represents a vertical feature

and as such forms a horizontal barrier for eddy propagation, separating the polar and the equatorial eddy guides from each other (*Matsuno, 1970; Dickinson, 1968*).

On the one hand, the wintertime middle and high latitude tropopause might constitute a valve for tropospheric planetary eddies entering the stratosphere, thus controlling stratospheric planetary eddy activity (*Chen and Robinson, 1992*). On the other hand, for intermediate tropospheric forcing the winter stratosphere may still arrange its eddy activity distribution (*Gray et al., 2003*). This would leave room for a possible influence from stratospheric characteristics represented by, i.a., the stratospheric concentration of radiatively active gases (*Hu and Tung, 2002*).

2.2.3 Eddy dissipation

Most of the stratospheric planetary eddies are not reflected back into the troposphere (*Hitchman and Huesmann, 2007; Perlwitz and Harnik, 2003*) and consequently must vanish somewhere above the tropopause. Linear planetary Rossby-waves approaching a critical surface can vanish due to the process of breaking, similarly to ocean waves approaching a beach. Away from critical surfaces, planetary eddies tend to break when their amplitude becomes too large which usually happens in case of upward travelling eddies since, due to momentum conservation, their amplitude increases with height. Also, diabatic processes and Rayleigh friction can attenuate stratospheric planetary eddy activity.

Finally, zonal-mean flow and eddy activity form an entangled system. Breaking Rossby waves decelerate the westerly flow in turn changing their propagation and breaking conditions. The coupling is especially prominent for the wintertime polar vortex and associated sudden warmings (*Baldwin and Dunkerton, 1999*).

2.2.4 Eliassen-Palm (EP) diagnostics

The concept of zonal-mean Eliassen-Palm (EP) flux and EP divergence constitutes a powerful tool to diagnose large-scale eddy activity and how the latter modifies the zonal-mean zonal wind (*Andrews and McIntyre, 1978, 1976; Eliassen and Palm, 1961*). Yet a meaningful interpretation of EP fluxes and EP divergences necessitates some information on the theory of atmospheric eddies and how these interact with the atmospheric background state.

The EP flux represents a measure of the net rate of eddy activity transfer from one latitude and height to another. According to the theory of atmospheric large-scale motion, the horizontal component of the EP flux is proportional to the northward eddy flux of zonal momentum, the vertical component proportional to the northward eddy flux of heat. The interpretation in terms of net eddy activity transfer does not depend on the validity of quasi-geostrophy and holds for

any Rossby-wave-like disturbances on a positive northward gradient of potential vorticity. Note that, in contrast to turbulent disturbances, every kind of atmospheric eddy has its particular restoring mechanism, for Rossby waves being the latitudinally dependent horizontal Coriolis parameter.

The EP flux remains a useful concept in case of instantaneous strongly nonlinear flows, albeit in a more qualitative manner, such flows typically occurring during wintertime/spring polar sudden warmings (*Gray et al.*, 2003). In case of linear eddies weakly interacting with the background state, for nonlinear eddies more qualitatively, wave packet theory states that the EP flux is proportional to the group velocity and features of geometric optics apply, such as a refractive index for eddy propagation (*Lighthill*, 1978)

Patterns of EP divergence are identified with a spatially divergent EP flux, mostly resulting from changes in local eddy activity being usually associated with eddy breaking processes or eddy dissipation due to diabatic, frictional, or nonlinear effects. In combination with EP divergence these effects form a conservation law for local eddy activity which is valid for any wave-like disturbance and does not depend on the appropriateness of quasi-geostrophy. This conservation law can potentially help to clarify which particular mechanisms induce a given pattern of EP flux or EP divergence; but the law is not unique and individual mechanisms can cancel each other (*Edmon et al.*, 1980).

EP divergence represents an important diagnostic tool to quantify the impact of eddies on the mean state because it relates to the westward eddy forcing of the zonal-mean wind (*Held*, 1985); also, it represents the only such forcing if quasi-geostrophic theory holds, independently of the eddy forcing being wave-like or turbulent. Dissipating Rossby waves always impose a westward and not an eastward force, due to their inherent chirality with regards to the sense of the planetary rotation; chirality represents an attribute in analogy to right-handed or left-handed molecules, for instance. The westward forcing on the zonal-mean flow induces a form of gyroscopic pumping driving air packets in a poleward direction across surfaces of constant angular momentum, a consequence of the horizontal Coriolis effect. That pumping is identical with the poleward force mentioned in Section 2.0.6 which induces the dynamically driven BD circulation.

In the following, a discrimination between the processes of eddy breaking and dissipation is not made, and the terms “dissipation” and “negative EP divergence” are interchangeably used, when appropriate.

2.3 Data basis and plotting conventions

All of the modelled data depicted are averaged to form annual means, or the two-monthly averages of July/August (JA) and December/January (DJ). The focus

lies on the JA and DJ averages because during these months E39/C yields the strongest and most robust tropical and higher-latitude dynamical NH response, respectively (not shown). Then, the 20 individual averages of the model period 2000 to 2019 are averaged to obtain 20-year inter-annual means, either “absolute” means representing one of the two scenarios, or “anomalous” means representing the difference of the scenarios, WARM-COLD. The term “response” is identified with “anomalous”. Finally, the three WARM realisations result in 60, the two COLD realisations in 40 samples per absolute inter-annual mean.

2.3.1 EP cross-sections

The modelled EP fluxes and EP divergences shown (Figure 2.3, for instance) are calculated from 12-hourly fields of instantaneous model data and then averaged as described above. Here, calculation method and scaling of the modelled EP flux are adopted from *Edmon et al.* (1980), the EP flux arrow patterns thus visually correspond to their respective divergence, times a plot-specific scaling factor, referred to as eddy activity scaling. Acceleration scaling better accounts for wave mean-flow interaction, especially in case of polar stratospheric warmings (*Gray et al.*, 2003), but does not properly consider the eddy conservation properties being of interest here. In the cross-sections depicted, thin iso-lines quantify the respective EP divergence patterns, thick iso-lines demonstrate the position of the zero-wind line.

Eddy attenuation causes the EP flux to strongly drop off with height and only a small fraction of the flux, mostly of planetary-scale, actually enters the stratosphere (*Andrews et al.*, 1987). To overcome this visualisation problem many studies apply a logarithmic ordinate and scale the EP flux by the inverse of density, thereby neglecting the eddy conservation properties mentioned above. Here, the EP cross-sections are separately generated for three different scale heights each of which obeying eddy activity scaling, but with respectively different scaling factors for the lower stratosphere (100 – 10 hPa), the uppermost troposphere lowermost stratosphere (UTLS) (300 – 100 hPa), and the troposphere (1000 – 400 hPa). To improve the visual traceability of eddy activity ascending across the tropopause, EP flux arrows at 100 hPa are plotted twice using the respective scaling factor, once in the stratospheric and once in the UTLS cross-sections.

A-geostrophic corrections are not applied to the modelled EP diagnostics and as such the latter is probably unreliable close to the equator where the weak horizontal Coriolis force cannot maintain a sufficiently tight geostrophic balance (*Andrews et al.*, 1987). According to *Edmon et al.* (1980), however, the horizontal component of the EP flux may still specify horizontal Rossby-like flow across the equator. Also, the instantaneous EP flux represents a more qualitative measure of eddy activity propagation through the northern polar region during winter/springtime when sudden warmings cause considerable transience (*Gray*

et al., 2003), albeit yearly or two-monthly averaging should cope with this problem (*Newman et al.*, 2001). Finally, the EP flux better describes stratospheric than tropospheric eddy activity because eddies tend to be more Rossby-like above the tropopause then below (*Son et al.*, 2007).

The net eddy-related northward transport of heat and momentum across a latitudinal circle consists of two components, a quasi-stationary part due to the time mean departure from the zonal-mean and a transient part due to the zonal-mean departure from the time mean (*Lee*, 1999, for instance). As an example, Figures 2.3b and 2.3c depict such quasi-stationary and transient EP flux contributions.

The monthly mean chosen here represents a filter in the sense that those internal atmospheric wave modes can contribute to the quasi-stationary part whose constant-phase surfaces travel sufficiently slowly in a longitudinal direction and whose amplitudes vary slowly enough (*Toth*, 1992). This spontaneously-generated quasi-stationary contribution physically differs from that due to forced quasi-stationary eddies showing, on the averaging time scale, geographically near-fixed phase surfaces and amplitudes. The transient eddy-related transport is thought to be mainly made up of travelling or standing oscillating eddies but can also contain other time-dependent mechanisms, such as changes in the mean state during polar warmings or breaking planetary eddies (*Andrews et al.*, 1987). Because the life cycles of quasi-stationary and transient eddies tend to differ, a separate consideration helps to more profoundly validate the modelled EP diagnostics, and identify causal relationships connecting both modelled anomalous EP diagnostics and model boundary conditions.

2.3.2 Transformed Eulerian mean (TEM) stream function

Transformed Eulerian mean (TEM) residual velocities define the residual circulation which well represents Lagrangian mass transport, the latter differing from the Eulerian velocity field via the Stokes drift (*Dunkerton*, 1978); in the stratosphere that residual circulation is commonly identified with the BD circulation, even though the latter is specifically calculated from observed atmospheric fields of chemical trace species and temperature because stratospheric vertical velocity is weak and cannot be measured (*Andrews et al.*, 1987). Here, the terms “residual” and “Brewer-Dobson” circulation are used interchangeably.

The computation of TEM residual velocities involves modelled values of Eulerian meridional and vertical velocities, the northward eddy flux of heat, and the vertical buoyancy-gradient. A TEM stream function can then be obtained which has the advantage over residual velocities in that it simultaneously provides information on strength and latitude height structure of the residual circulation. Here, the calculation of the TEM stream functions follows the approach by *Edmon et al.* (1980) and is accomplished on a 12-hourly basis of instantaneous model

data. The residual circulation (Figure 2.2c, for instance) is parallel to the TEM stream function iso-lines, clockwise around a stream function maximum, counter-clockwise around a minimum, and its strength is proportional to the density of the iso-lines.

2.4 Validation of absolute model results

A validation of the absolute model results against observations is important because it facilitates and improves both, interpretation and relevance assessment of anomalies associated with anomalous boundary conditions (*WMO, 2007; IPCC, 2007*). Only robust modelled quantities should be evaluated which, as Section 2.6 shows, applies to all of the absolute quantities hereafter considered.

The validation comprises the modelled EP and TEM diagnostics, as well as temperature and zonal wind because the latter quantities affect the life cycle of planetary eddies. In this context, a thorough validation of the absolute tropical liquid-water contents and convective rain rates is also important, but beyond the scope of this Chapter. Section 2.5.1 still addresses latitude longitude distributions of absolute convective surface precipitation briefly. Finally, this Section 2.4 assesses whether the modelled tropical eddy activity pattern is likely to refer to deep-convective eddy production, and whether the modelled EP diagnostics qualitatively conform with the principle of downward-control.

2.4.1 Temperature and zonal wind

In the atmosphere, zonal temperature gradients and vertical wind shear are connected via the thermal wind relationship, which implies that validating one of the two variables is also of significance to the other. *Chen et al. (2001)* present a 40-year mean cross-section of July zonal-mean winds, based on NCEP/NCAR re-analysis data (*Kalnay et al., 1996*), *Pawson et al. (2000)* present a similar cross-section for January using an updated version of NMC analyses (*Randel, 1992*).

Adequate two-monthly means, JA and DJ, of observational temperature and zonal-wind data are above reach, and thus the modelled one-monthly cross-sections for July and January validated instead (not shown). Yet the modelled zonal-mean zonal wind fields during July and August resemble except for the core of the tropopause jet being more intense during August, and the middle to polar winds above 40 hPa being easterly during July, but westerly in August. The modelled December and January cross-sections noticeable differ only in their intensity of the tropopause jet core, being stronger in January.

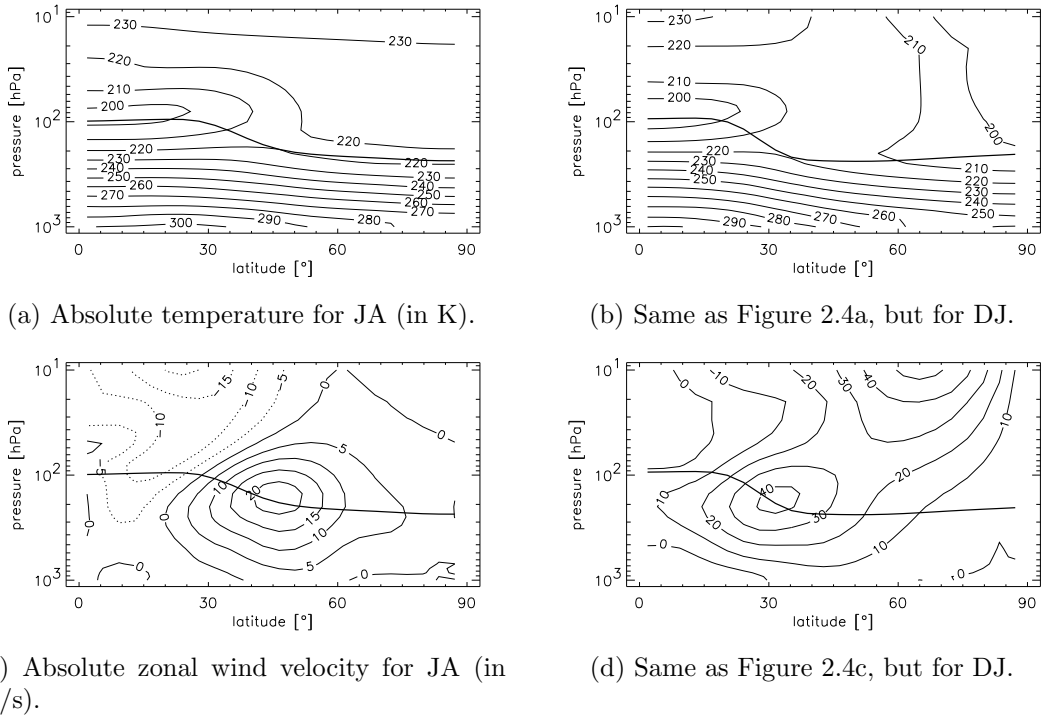


Figure 2.4: Absolute (WARM) temperature and zonal wind velocity in the NH. The differences between WARM and COLD (Figure 2.10), WARM and PAST (not shown), as well as COLD and PAST (not shown), are by an order of magnitude weaker than the respective absolute values, facilitating validations against observations of WARM and COLD absolute temperature and zonal wind velocity. Straight contours denote positive values of temperature and velocity, dotted contours negative values of velocity. Thick lines mark the position of the thermal tropopause (mean of WARM and COLD).

Modeled (Figure 2.4) and observational wind fields during July agree well; nevertheless, the mid and polar latitude easterly wind regime does not descend deeply enough into the lower stratosphere, down to 40 hPa at a latitude of 60°N for the model compared to 60 hPa for the observations. Also, the model produces a too weak tropical stratospheric easterly jet, by about 5 m/s, and the tropopause westerly jet slightly extends too far southwards. The model well reproduces the January wind pattern and even catches the spatial separation of the tropopause and polar night jets, albeit the modelled jets appear less clearly distinct since the middle and high latitude winds are too strong.

The above findings agree with those in *Dameris et al.* (2005) who validate a E39/C reference transient simulation and show additionally that the model has a slightly reduced inter-annual variability in zonal-mean temperature and zonal wind at polar latitudes in early winter, associated with rarer-than-observed major stratospheric warmings.

The rare occurrence probably results from the cold-pole problem, lower than observed polar temperatures. The cold-pole problem represents a common bias among most CCMs and is partly associated with an in-complete gravity wave drag parameterisation and a too dissipative advection scheme (*Stenke et al.*, 2007; *Eyring et al.*, 2006; *Stenke and Grewe*, 2005; *Austin et al.*, 2003). For E39/C during both summer and wintertime, the 60°N-to-pole average at heights between 30 and 90 hPa differs from observations by less than $\pm 2\text{K}$, but by a significantly larger amount right above the tropopause. There is also a large bias above 30 hPa during wintertime (*Eyring et al.*, 2006). Sufficiently far below the model upper lid, the strong numerical dissipation dominates the temperature bias in that it advects too large amounts of vapour concentrations, thus causes excessive long-wave cooling (*Stenke and Grewe*, 2005).

Despite the more-stable-than-observed mid-winter polar vortex, though, modelled stratospheric DJ eddy activity is more intense than that observed (not shown) and should counteract the bias-related vortex stabilisation (*Newman et al.*, 2001). Section 2.7.2 covers a similar seeming contradiction, not in the context of too high water vapour, but of enhanced GHG concentrations.

2.4.2 EP diagnostics

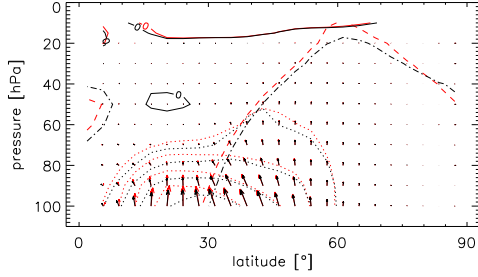
The study by *Edmon et al.* (1980) still appears to represent the most comprehensive survey in terms of displaying and discussing observed tropospheric EP fluxes and EP divergences, separately for summer/wintertime and for quasi-stationary/transient flux contributions. They analyse the three-monthly means of June-August and December-February and do not well resolve the lower stratosphere. Also, the arrow-scaling tends to disregard the tropopause region and thus the tropical upper troposphere, and the data base is short.

It seems that significant observed EP cross-sections for the summertime tropical/subtropical UTLS have not yet been published. Cross-sections are available of eddy geopotential and temperature amplitudes, phases, and zonal standard deviations. For instance, *Malone et al.* (1984) display cross-sections of zonal standard deviations up to a height of 100 hPa for July. *White* (1982) displays the same quantity up to a height of 100 hPa northwards of 20°N for the July-September mean, based on 12 years of operational NMC data from 1966 to 1977. *van Loon et al.* (1973) display amplitudes and phases up to 30 km northwards of 20°N for July and rely on data by *Labitzke* (1972); *Crutcher and Meserve* (1970).

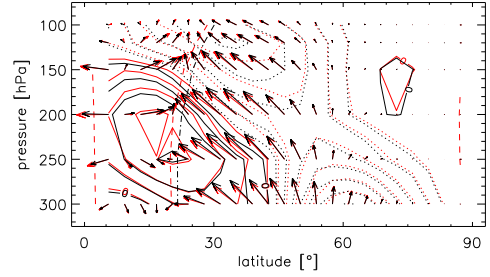
The wintertime extratropical latitudes are better documented; *Chen et al.* (2003) present density-scaled EP cross-sections of the quasi-stationary wavenumbers 1-3 for the wintertime stratosphere at heights up to 10 hPa. Their data base comprises the three-monthly December-February mean of the 40 winters from 1958 to 1998 of NCEP/NCAR reanalysis data.

There is better than order-of-magnitude agreement between the modelled (Figures 2.5, 2.6, 2.7, 2.8) and the corresponding observed values (*Edmon et al.*, 1980) of both EP divergence and the length of the EP flux arrows. A more precise comparison required identical scaling, of the arrows in particular, and is beyond the scope of this Chapter. Thus, this Section 2.4.2 primarily validates modelled EP flux arrow directions and their length relative to that of arrows at other latitudes and heights associated with the same plot. Regarding EP divergence, this Section primarily validates the position of positive and negative EP divergence patterns, and the position of their extremes.

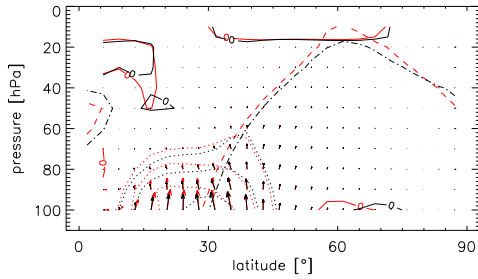
Since the modelled EP flux and EP divergence patterns qualitatively depend on latitude, altitude, and season, the following regions are separately validated: extratropical troposphere, summertime UTLS, and wintertime stratosphere.



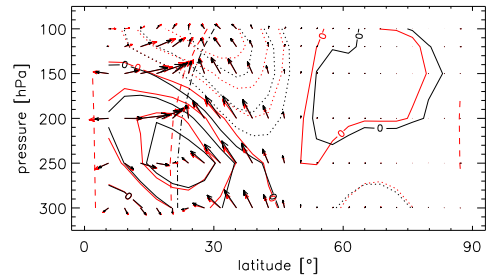
(a) Quasi-stationary plus transient contributions: $9.581 \times 10^{14} \rightarrow 2.462 \times 10^{19} \uparrow$



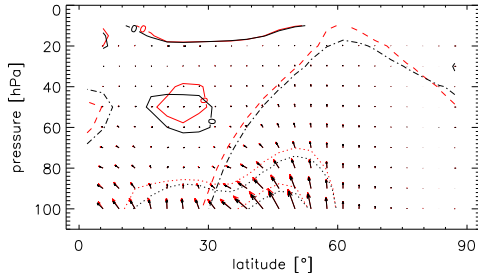
(b) Quasi-stationary plus transient contributions: $6.617 \times 10^{14} \rightarrow 8.781 \times 10^{19} \uparrow$



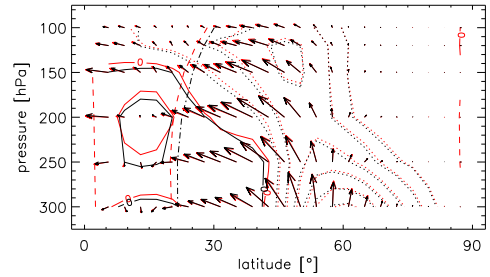
(c) Quasi-stationary contribution only: $7.323 \times 10^{14} \rightarrow 1.882 \times 10^{19} \uparrow$



(d) Quasi-stationary contribution only: $5.515 \times 10^{14} \rightarrow 7.320 \times 10^{19} \uparrow$

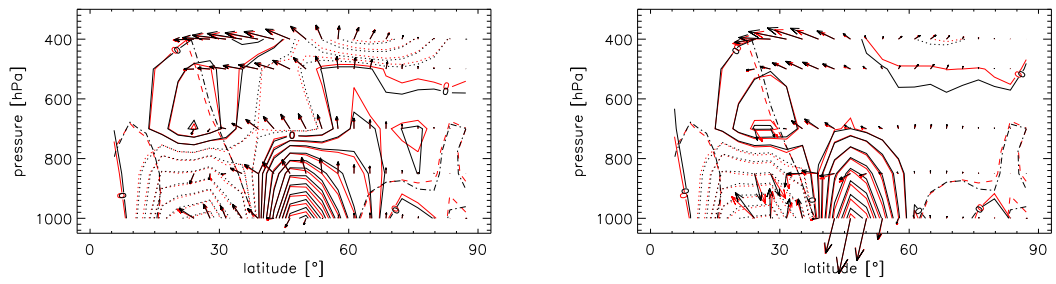


(e) Transient contribution only: $4.296 \times 10^{14} \rightarrow 1.104 \times 10^{19} \uparrow$



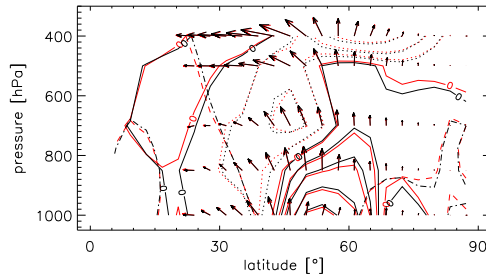
(f) Transient contribution only: $4.437 \times 10^{14} \rightarrow 5.889 \times 10^{19} \uparrow$

Figure 2.5: JA absolute EP diagnostics (red: WARM, black: COLD) for the stratosphere and the upper troposphere. The EP flux scaling analogously follows the approach in Figure 2.3. Thin contours denote positive/negative EP divergence similarly to Figure 2.3, but the contour interval is wider by one order of magnitude (in 10^{15} m^3). The thick dashed contour marks the position of the zero-zonal-wind line for WARM, the thick dashed-dotted contour does so for COLD. The zonal wind at low latitudes is easterly.



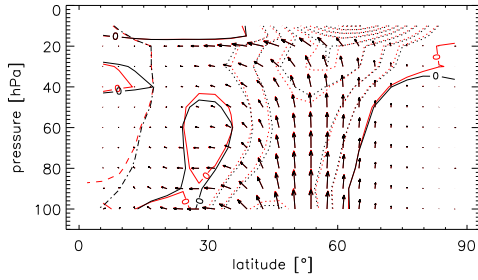
(a) Quasi-stationary plus transient contributions: $2.452 \times 10^{14} \rightarrow 2.929 \times 10^{20} \uparrow$

(b) Quasi-stationary contribution only: $9.142 \times 10^{13} \rightarrow 1.092 \times 10^{20} \uparrow$

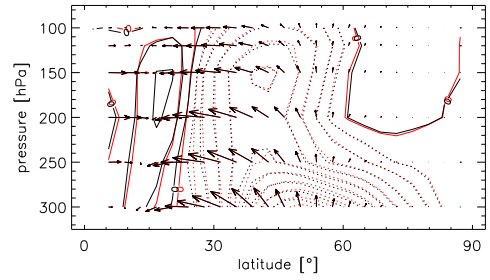


(c) Transient contribution only: $1.721 \times 10^{14} \rightarrow 2.055 \times 10^{20} \uparrow$

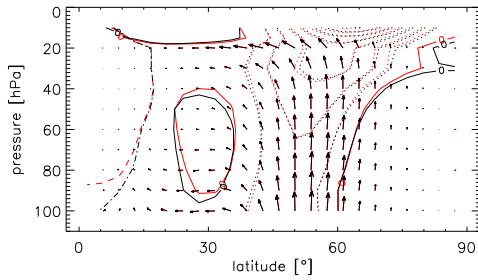
Figure 2.6: Same as Figure 2.5, but for the troposphere. The zonal wind is easterly at low latitudes.



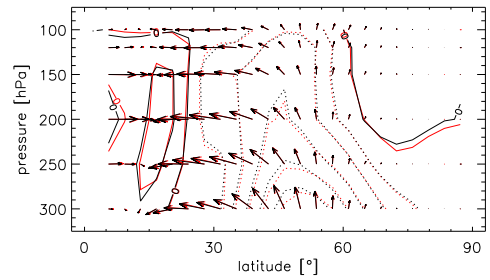
(a) Quasi-stationary plus transient contributions: $2.220 \times 10^{15} \rightarrow 5.704 \times 10^{19} \uparrow$



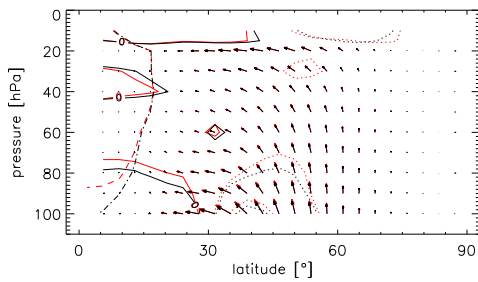
(b) Quasi-stationary plus transient contributions: $1.928 \times 10^{15} \rightarrow 2.559 \times 10^{20} \uparrow$



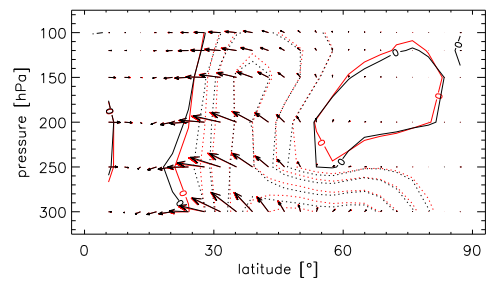
(c) Quasi-stationary contribution only: $1.690 \times 10^{15} \rightarrow 4.343 \times 10^{19} \uparrow$



(d) Quasi-stationary contribution only: $1.011 \times 10^{15} \rightarrow 1.341 \times 10^{20} \uparrow$

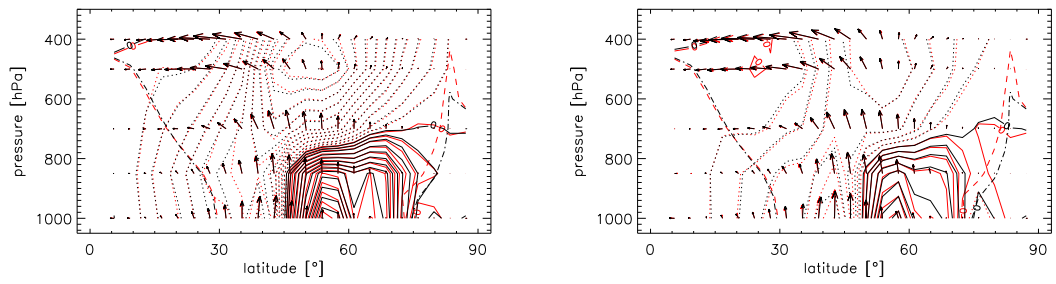


(e) Transient contribution only: $8.290 \times 10^{14} \rightarrow 2.130 \times 10^{19} \uparrow$



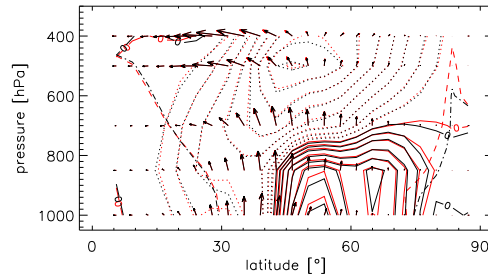
(f) Transient contribution only: $1.069 \times 10^{15} \rightarrow 1.420 \times 10^{20} \uparrow$

Figure 2.7: Same as Figure 2.5, but for DJ. The zonal wind is mostly westerly.



(a) Quasi-stationary plus transient contributions: $1.078 \times 10^{15} \rightarrow 1.288 \times 10^{21} \uparrow$

(b) Quasi-stationary contribution only: $4.343 \times 10^{14} \rightarrow 5.188 \times 10^{20} \uparrow$



(c) Transient contribution only: $6.456 \times 10^{14} \rightarrow 7.712 \times 10^{20} \uparrow$

Figure 2.8: Same as Figure 2.5, but for DJ and the troposphere. The zonal wind is mostly westerly.

Extratropical troposphere

In the troposphere, EP divergence and EP flux are not solely governed by eddy activity. Other influential factors are identified, i.a., with diabatic heating, near-surface baroclinic processes, and low latitude weak or negative northward gradients of potential vorticity. In the observations, these factors act to produce and position the regions of positive EP divergence relatively to those of negative EP divergence (*Edmon et al.*, 1980). E39/C reproduces the position of the positive and negative EP divergence patterns, suggesting that the model realistically incorporates the above-mentioned physical processes. A thorough validation of the individual processes, though, is beyond the scope of this Chapter. Finally, *Edmon et al.* (1980) are not confident of their summertime total and quasi-stationary EP divergence values and in those two cases the similarity above 900 hPa is worse.

The modelled and observed (*Edmon et al.*, 1980) EP fluxes agree in the following characteristics: during both seasons and for both flux contributions the upper-tropospheric arrows tilt equatorward, probably due to the latitude-dependent refractive index (Section 2.2.2). Stronger transient eddy activity occurs in winter than in summertime, but the tropospheric patterns look broadly similar. In the lower troposphere, the upward component maximises at roughly 40° in wintertime, but at about 50° in summertime. The generation of forced quasi-stationary eddies strongly depends on the season (Section 2.2.1) and so does the quasi-stationary flux. Wintertime quasi-stationary and transient patterns look alike, but there is not any summertime surface source for quasi-stationary eddies. These develop higher-up in the troposphere, maybe due to convection, maybe due to nonlinear interaction with the transient eddies (Section 2.2.1). A different explanation is that the transient flux may become more quasi-stationary as the background flow intensifies with height (Section 2.3.1).

Summertime extratropical UTLS

Convective heating and baroclinic processes are largely absent in the stratosphere facilitating the interpretation of EP fluxes and EP divergences there. Processes relating to stratospheric eddy-induced ozone heating (*Nathan and Cordero*, 2007) and weak potential vorticity gradients (*Haynes*, 2005; *Edmon et al.*, 1980) can still modify both quantities, apart from eddy dissipation associated with eddy breaking and adiabatic relaxation.

Figure 2.5f shows that the modelled transient flux cannot enter the summertime tropical easterly jet. Only a minor portion crosses the zero-wind line or originates inside the jet until dissipating while ascending (Figures 2.5f and 2.5e). Poleward of the zero-wind line, the transient flux causes significant divergence in the lowermost stratosphere, with the largest vertical reach of about 70 hPa occurring at mid-latitudes (see Figure 2.5e).

The situation is different for the summertime quasi-stationary flux contribution. The zero-wind line apparently defines two distinct regimes of equatorward directed and poleward directed EP fluxes (see Figure 2.5d). The extratropical regime is discussed in the subsection above and the associated EP flux attenuates at the zero-wind line, in compliance with the theory presented in Section 2.2.3.

Summertime tropical UTLS: convective forcing

The tropical regime possesses EP fluxes of comparable magnitude to the extratropical regime (see Figures 2.5c and 2.5d); the fluxes originate in the uppermost tropical troposphere and travel across the tropical tropopause while bending equatorward and dissipating (see Figure 2.5c). Consequently, the eddies are likely excited by deep-convective latent heating (Section 2.2.1) which maximises at 10° latitude, 300 – 400 hPa altitude, and extends to a height of about 150 hPa (deduced from modelled absolute liquid-water contents, not shown) matching the vertical reach of the positive EP divergence pattern (Figure 2.5c). Below 150 hPa, latent heating seems to produce southward and northward horizontally propagating eddy activity creating positive EP divergence, in accordance with the modelling results by *Boehm and Lee* (2003). Note that the the modelled EP flux displayed here is not a-geostrophically corrected and its vertical component equatorward of 10° latitude may thus not be reliable.

Malone et al. (1984); *White* (1982); *van Loon et al.* (1973) interpret their observed low-latitude quasi-stationary eddy amplitude patterns in terms of a response to convective eddy forcing. The modelled quasi-stationary EP flux and EP divergence patterns shown here are latitudinally and altitudinally consistent with these observations, and hence may also relate to convective forcing.

The latitudinal position of the distinct EP flux maximum at 100 hPa (see Figure 2.5c) corresponds to that of the eddy amplitude maximum in *Malone et al.* (1984); *White* (1982); *van Loon et al.* (1973). Note that now both of the above-mentioned modelled quasi-stationary regimes are considered, namely the low-latitude convective and the extratropical jet-affected regime.

The modelled EP flux extends to slightly lower latitudes, but this could result from the inconsistency of comparing EP fluxes with eddy amplitudes; the vertical component of the former is actually proportional to the latter squared, at least for an individual eddy (*Newman et al.*, 2001). ERA40 re-analysis data (*Uppala et al.*, 2005), on the other hand, reveal a robust tropical poleward heat flux maximum at 100 hPa and lower latitudes (not shown).

The modelled tropical EP flux regime maximises in the UTLS and weakens towards the middle troposphere, its divergence being confined to levels below of about 70 hPa (see Figure 2.5c). These are altitudinally dependent characteristics that correspond with observations: *Malone et al.* (1984); *White* (1982); *van Loon*

et al. (1973) observe eddy amplitude maxima both in the UTLS and close to the surface, with a minimum in-between associated with a phase reversal; and a cross-section in *van Loon et al.* (1973), which capture the region above 100 hPa, shows that only small eddy amplitudes occur above a height of 70 hPa.

Wintertime stratosphere

In contrast to the summertime easterlies, the wintertime stratospheric westerlies favour the upward propagation of planetary eddies (Section 2.2.2). *Edmon et al.* (1980) argue that middle and high latitudes quasi-stationary eddies penetrate into the wintertime stratosphere, whereas the respective transients do not. The scaling in *Edmon et al.* (1980) might hide such transient contributions to stratospheric eddy activity, and E39/C calculates significant transient eddy activity ascending across the tropopause and reaching the model upper lid (Figures 2.7e and 2.7f).

The modelled transient and quasi-stationary EP flux patterns differ from each other. While the former displays rather uniformly distributed propagation, the latter splits into two branches. The upper-tropospheric branch is equatorward vectored, the stratospheric branch mostly upward (Figures 2.7c, 2.7d, and 2.8b). *Chen et al.* (2003) obtain a similar split in case of quasi-stationary EP flux calculated from re-analyses data (Section 2.4.2). Their Figure 1 shows that the split mainly results from the flux being forced at a range of latitudes and from flux contributions of different wavenumbers propagating in a different way.

The stratospheric patterns of modelled and re-analysed (*Chen et al.*, 2003) quasi-stationary EP divergence resemble. For both cases, divergence associated with the stratospheric branch intensifies above 60 hPa, very likely due to eddy dissipation. Poleward from that divergent region there is an area of convergence. Another convergent area is apparent in the subtropics, although situated more equatorward for the model. Both convergent regions could result from weak or negative latitudinal potential vorticity gradients or eddy-induced ozone heating or cooling.

For the model, mid- to high-latitude divergence above 60 hPa covers a broader latitudinal range, making high-latitude convergence less widespread than for the re-analyses. The discrepancy does not result from the wavenumber 1-3 filtering *Chen et al.* (2003) apply, as quasi-stationary wavenumbers greater than number 3 are largely absent from the stratosphere (Section 2.2.2). The discrepancy is not a consequence of the different averaging periods, being December-January for the model, but December-February for the re-analysis (not shown). The averaging procedure might yet introduce a bias. Here, monthly mean fluxes are separately calculated for each month and then averaged, while *Chen et al.* (2003) average before.

The model upper sponge obviously enhances EP divergence above 20 hPa.

The sponge spans the two uppermost model layers and involves amplified horizontal diffusion (*Hein et al.*, 2001) applied to each Fourier component of the model except for the zero order. That diffusion is designed to not greatly violate energy or angular momentum conservation (*Grewe*, 2007); it is hence tempting to assume that the intense upper-level EP divergence should drive a poleward Lagrangian flux that favors the upper model layers and is un-realistically strong.

It remains unclear if the broader latitudinal range of EP divergence further down, between 20 and 60 hPa, immediately results from the upper sponge as well. Other potential mechanisms such as the cold-pole problem (*Dameris et al.*, 2005) come into consideration.

2.4.3 TEM stream function

The modelled absolute TEM stream function pattern during JA represents a shallower circulation than the DJ pattern (Figures 2.14a and 2.14b), in accordance with observations (*Andrews et al.*, 1987). Appropriate scaling and averaging reveal that the stratospheric northern hemispheric residual circulation during January (not shown) well conforms with the respective NCEP2 standard stream function depicted in *Jiang et al.* (2007); in particular, the high-latitude disparity at 50 hPa *Austin et al.* (2003) mention in case of E39/C time slice model runs is absent. A similar standard stream function for northern hemispheric summertime conditions is out of reach.

Downward-control

According to the theory by *Haynes et al.* (1991) being valid poleward of some finite distance away from the equator, about $\pm 20^\circ$ of latitude (*McIntyre*, 1998), eddy dissipation exerts a local poleward force which connects vertically downward at the speed of sound; the individual northward forces and downward connections of a given eddy dissipation pattern superpose and thereby yield the eddy-driven BD circulation.

Even though eddy dissipation does not constitute the sole BD circulation driving force (Section 2.0.6) it still exerts a significant stimulation. This becomes apparent when comparing stratospheric EP fluxes and divergences (Figures 2.5a, 2.7a) and corresponding TEM stream function cross-sections (Figures 2.14a, 2.14b); the relevant indicator is defined by the cross-sections qualitatively matching the above specified theory or not.

The Figures 2.5a and 2.7a show that the total modelled negative EP divergence generally occurs at lower levels during JA than during DJ, in accord with the respective TEM stream function cross-sections. The total JA negative EP

divergence is more intense and occurs at lower levels equatorward of the zero-wind line than it does poleward of the line, roughly matching both spatial reach and intensity distribution of the clockwise northward stream function branch. Note that total EP divergence is associated with the sum of quasi-stationary and transient contributions.

As a consequence, the mechanism of upward-control (*Boehm and Lee, 2003; Plumb and Eluszkiewicz, 1999*) is not essential to explain the modelled low-latitude lower-stratospheric residual circulation during summer; and downward-control seems to apply at latitudes lower than the critical boundary at 20°N , at least qualitatively. The modelled anti-clockwise southward stream function branch does not fit to the dissipation pattern displayed. It is affected by BD circulation driving forces in the southern hemisphere and occurs next to the equator where downward-control may not be valid (*Zhou et al., 2006*, and references therein).

During DJ, total negative EP divergence generally maximises at mid-latitudes, intensifies towards the model upper lid, and the residual circulation responds accordingly. The pattern of weakly positive divergence in the subtropics may cause the slightly slower subtropical residual circulation at heights between 80 and 40 hPa, compared to the transport at heights above and below.

Compared to the NCEP2 data, the modelled stream function iso-lines during January do not crowd at upper model levels; rather, they appear to be truncated by the model upper lid, indicating that the sponge-induced artificially strong upper-level EP divergence does not induce a corresponding stream function. *Grewe (2006)*, on the other hand, reports a too fast mass transport for the E39/C upper layers, but applies a different and more concise method which does not rely on the TEM equations and takes into account the annual cycle.

2.5 Response of the atmospheric background state

Section 2.4 shows that E39/C generally produces valid zonal-mean patterns of atmospheric temperature and zonal wind, EP flux, EP divergence and residual circulation; that the JA tropical eddy activity regime is in accordance with the mechanism of convective eddy forcing; that the EP diagnostics roughly accord with the principle of downward-control. Thus, the corresponding anomalous patterns may now be investigated for their dependence on the respective scenario, being rising SSTs and GHG concentrations (WARM) on the one hand, and constant climate forcing (COLD) on the other.

Since the life cycle of planetary eddies depends on the rate of tropical latent-heat release and on the atmospheric background state (Section 2.2), it is important to discuss how the latter respond to the respective scenario and it is also

important to refer the differences detected to the model boundary conditions. Also, this Section 2.5 briefly touches the issue of continent ocean temperature contrasts since altered contrasts may affect the production of forced planetary eddies (*WMO*, 2007).

This Section exclusively refers to robust responses, but the issue of statistical significance is important and extensively covered in Section 2.6

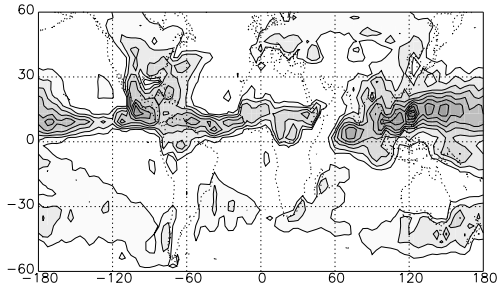
2.5.1 Latent-heat release

In general, a higher tropical SST tends to increase the local rainfall, largely because it strengthens the amount of precipitation associated with deep convection (*IPCC*, 2007). Deep convection is here defined as any convection reaching higher than the 500 hPa level. In the extratropics, the response to extratropical SST anomalies is weaker, shallower, and more complicated, since it involves baroclinicity (*Kushnir et al.*, 2002; *Hall et al.*, 2001a,b).

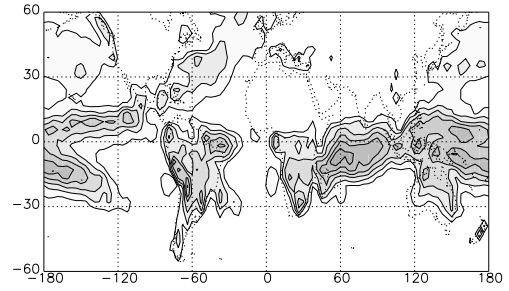
In the tropics and the NH, the anomalous SST patterns for JA and DJ look similar (Figures 2.9e and 2.9f). Yet a major part of the sea surface is warmer for WARM than for COLD, except for a cooler belt situated at roughly 30-40°N which represents a systematic cold bias of the AOGCM HADGEM1 (*Stott et al.*, 2006), arguably resulting from excessive surface wind stresses (*Johns et al.*, 2006)

Obviously, the convection scheme in E39/C (*Tiedtke*, 1989) captures the tropical precipitation increase associated with the tropical higher SSTs. In JA, the tropical anomalous SST broadly maximises in the northern, in DJ in the southern hemisphere, with maximum values of about 1 K in both seasons. The modelled anomalous convective precipitation (Figures 2.9c and 2.9d) has a pattern of increase which mirrors that of the anomalous SST, with the JA maximum occurring in the northern, the DJ maximum in the southern tropics.

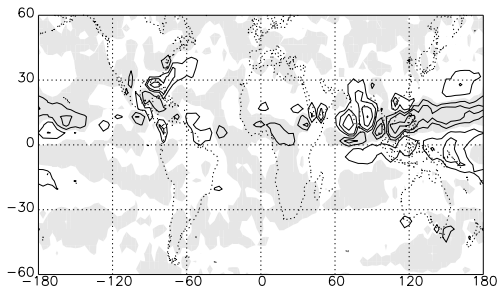
The modelled absolute convective precipitation (Figures 2.9a and 2.9b) exhibits the typical tropical rain bands (*Horinouchi et al.*, 2003). *Chen and Roeckner* (1997) validate total cloud covers and total cloud liquid water paths from ECHAM4 model runs and find a reasonable agreement with observations. Regarding anomalous precipitation, comparing Figures 2.9c and 2.9d with Figures 2.9a and 2.9b reveals that the higher SST tends to enhance tropical precipitation within the rain bands. Thus, the mechanisms governing the rain bands (*Barsugli et al.*, 2005, and references therein) also tend to modify the modelled precipitation response to a higher SST. The gravest precipitation enhancement occurs in the range of the western-Pacific warm pool during JA, as reported in the model study by *Barsugli et al.* (2006).



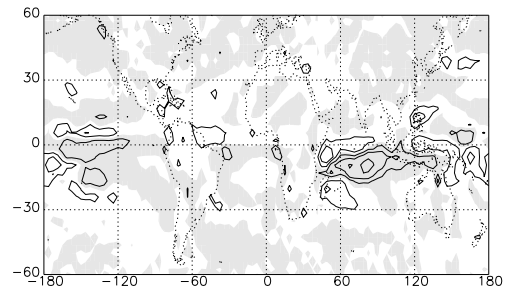
(a) Rate of absolute WARM surface convective precipitation during JA. The contours are quadratically scaled and denote values (in 10^{-8} m/s) of 1.0, 4.0, 9.0, 16.0,



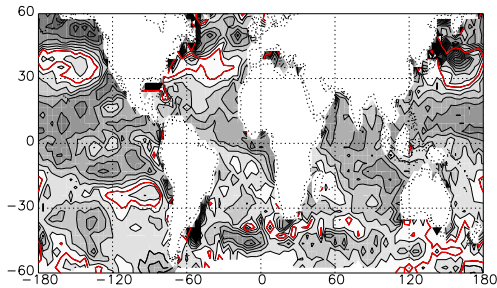
(b) Same as Figure 2.9a, but for DJ.



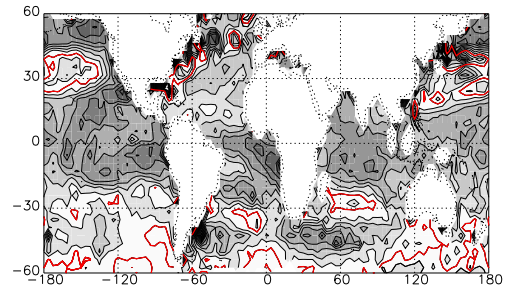
(c) Same as Figure 2.9a, but for the anomaly WARM minus COLD, and the contours half an order-of-magnitude more tightly scaled denoting values (in 2×10^{-9} m/s) of ± 1.0 , ± 4.0 , ± 9.0 , ± 16.0 , Shading marks positive anomalies, white negative anomalies.



(d) Same as Figure 2.9c, but for DJ.



(e) SST anomaly WARM minus COLD for JA. The red contour denotes the position of the zero SST anomaly, black contours denote non-zero SST anomalies (in integer multiples of ± 0.2 K). The SST anomalies are mostly positive.



(f) Same as Figure 2.9e, but for DJ.

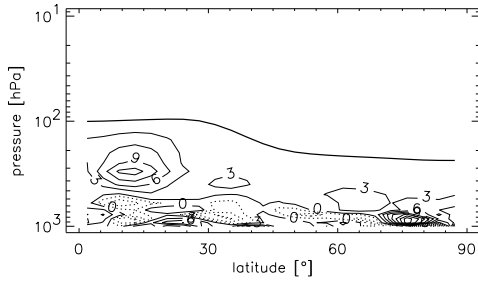
Figure 2.9: SST anomalies and modelled convective precipitation rates. The Figures do not contain the polar latitudes for reasons of illustration.

Figure 2.9c shows that E39/C yields a weaker Indian-monsoon precipitation for the warmer climate, which could result from stronger tropical quasi-stationary planetary eddies, intensified by the enhanced Pacific Warm pool convection. These eddies may strengthen atmospheric downward motion over India via a stronger anti-cyclonic activity and thus induce the dry conditions. The mechanism would resemble that in *Black and Sutton (2007)*; *Giannini et al. (2003)*; *Rodwell and Hoskins (1996)* for the Sahara during northern summer, and for the year 2003 European warm anomaly. It is interesting that the AOGCM HADGEM1 from which the warming climate SSTs are taken also has a too weak Indian monsoon, compared to observations (*Johns et al., 2006*).

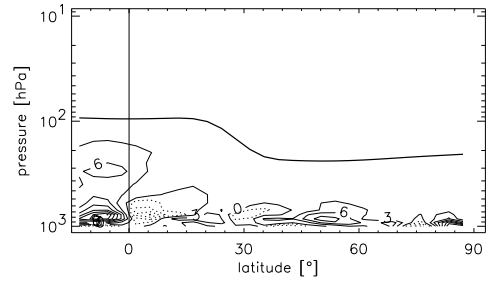
In contrast to E39/C, most of the current models with an interactive ocean (AOGCMs) yield a stronger Indian monsoon precipitation in a warmer climate (*IPCC, 2007*). Also, *Dowville (2005)* perform model runs with and without interactive ocean and demonstrate that only the interactive runs yield an appropriate South Asian monsoon response. On the other hand, the high resolution non-interactive model in *May (2004b,a)* yet predicts a stronger Indian monsoon precipitation for the warmer climate. Finally, *Timbal et al. (1997)* find that general circulation models (GCMs) driven by AOGCM SST-output tend to reproduce hydrological characteristics of the respective AOGCM, but they exclusively inspect zonal-mean quantities.

The E39/C response patterns in convective precipitation emerge in the zonal-mean vertical distribution of modelled latent heating (Figures 2.10a and 2.10b). In fact, scenario WARM and COLD values of latent heating are not available, but the liquid-water content above 500 hPa well measures latent-heat release since the E39/C deep convection scheme is set to a high precipitation efficiency (*Tiedtke, 1989*).

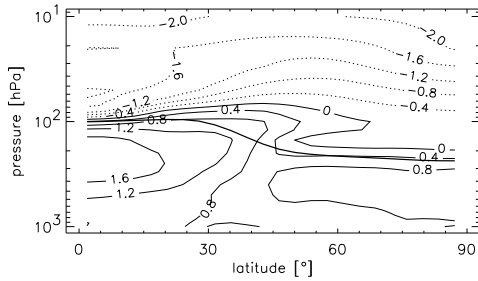
In both seasons there is stronger zonal-mean deep-convective release in the warmer climate. The enhancement occurs at roughly the same latitudes as the convective precipitation increase presented, during JA in the northern and, more weakly, during DJ in the southern hemisphere tropics. The enhanced Western Pacific release obviously dominates the JA zonal-mean against the reduced Indian monsoon precipitation.



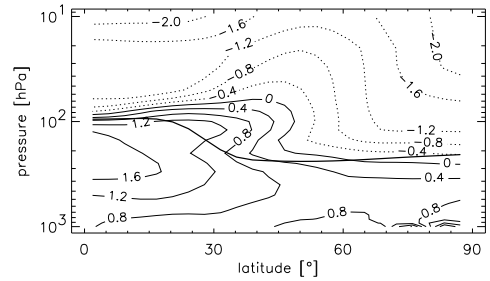
(a) Anomalous liquid-water content for JA (in 7×10^{-6} kg/kg).



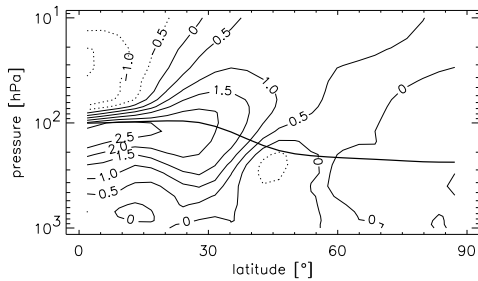
(b) Same as Figure 2.10a, but for DJ.



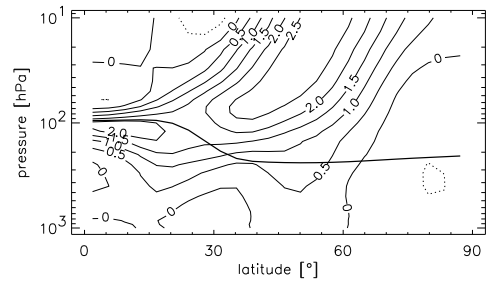
(c) Anomalous temperature for JA (in K).



(d) Same as Figure 2.10c, but for DJ.



(e) Anomalous zonal wind velocity for JA (in m/s).



(f) Same as Figure 2.10e, but for DJ.

Figure 2.10: Anomalous (WARM minus COLD) liquid-water content, temperature and zonal wind velocity. Straight contours denote positive anomalies, dotted contours negative anomalies. Thick lines respectively mark the position of the thermal tropopause (mean of WARM and COLD).

2.5.2 Zonal temperature gradient

The Figures 2.10c and 2.10d display the typical bipolar climate change pattern with a warmer troposphere opposing a generally cooler stratosphere (*IPCC*, 2007; *WMO*, 2007). Here, the changes in the latitudinal temperature gradient are of primary interest because these modify the zonal wind, affecting the life cycle of planetary eddies.

Troposphere

In the warmer climate, enhanced deep convection warms the tropical upper troposphere both during summer (JA) and winter (DJ). The Figures 2.10c and 2.10d show that the upper-tropospheric warming patterns during the two seasons roughly resemble, but that mid-tropospheric warmer air penetrates to higher latitudes in case of DJ.

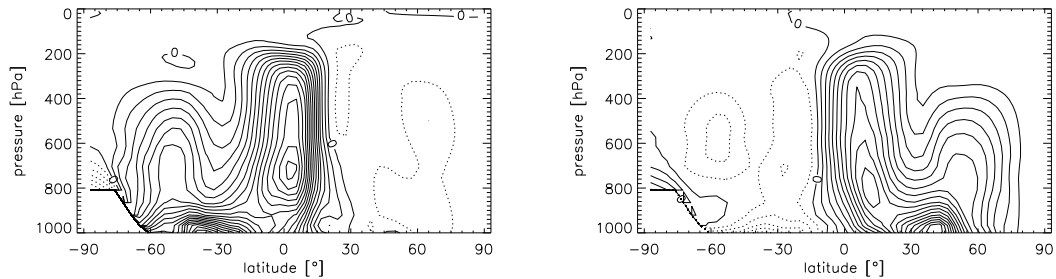
In fact, the latent-heat release during DJ (Figure 2.10b) mostly intensifies south of the equator, away from the upper- and mid-tropospheric warming in Figure 2.10d. The additional heat must thus somehow be transported towards the north, which is by the wintertime Hadley-Ferrel circulation, as Figure 2.11b suggests. Also, the DJ mid-tropospheric warming mentioned cannot result from a faster transport since the extratropical Hadley-Ferrel circulation weakens in the warmer climate (Figure 2.11c).

In contrast, the JA latent-heat release mainly strengthens north of the equator (Figure 2.10a). But the additional heat cannot propagate further northwards because the JA Hadley circulation is opposite (Figure 2.11a). Finally, it is important to be aware that the heat is transported and not the latent-heat release, the latter exciting the tropical quasi-stationary eddies.

A variety of global warming experiments show that changes in the latitudinal SST distribution merely affect the lower-tropospheric horizontal temperature gradient. For instance, a weaker low-altitude temperature gradient is usually associated with a polar surface warming amplification induced by melting sea ice. At higher levels, on the contrary, the gradient strengthens, mainly due to the enhanced tropical convective heating (*Rind et al.*, 2005a,b, 2002; *Timbal et al.*, 1997).

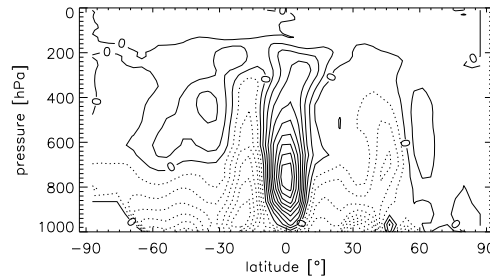
Here, that finding appears to be valid for the modelled wintertime northern hemisphere (Figure 2.10d) where the Hadley-Ferrel circulation acts to transport the additional tropical heat poleward. The summertime temperature enhancement, though, exhibits a minimum at mid-latitudes and parts of the subtropics; the minimum becomes extreme at a latitude of 30-40°N close to the surface, indicated by the 0.4 K contour just about visible (Figure 2.10c). The minimum is

hence likely to result from the JA zonal belt of negative anomalous SST at 30-45°N (Figure 2.9e), even though the exact latitudinal position of the minimum is not robust. The local maximum latent heating at 400 hPa and 35°N (Figure 2.10a) appears to be unimportant.



(a) Same as Figure 2.11b, but for JA. The mass transport is clockwise around a stream function minimum, counter-clockwise around a maximum (exception, for this Figure 2.11a only).

(b) Same as Figure 2.2c, but for DJ and two times two orders-of-magnitude wider contours (in integer multiples of $\pm 2 \times 10^{10}$ kg/s).



(c) Same as Figure 2.11b, but for the anomaly WARM minus COLD during DJ, and one order-of-magnitude tighter contours (in integer multiples of $\pm 2 \times 10^9$ kg/s).

Figure 2.11: Absolute and anomalous TEM stream functions scaled to display the Hadley-Ferrel circulation.

Stratosphere

In the warmer climate, the stratosphere primarily cools via enhanced long-wave emission by larger concentrations of GHG. Other effects modify that latitude-independent cooling response, here indicated by latitude-dependent temperature changes above the tropopause (Figures 2.10c and 2.10d).

As E39/C lacks an upper stratosphere, altered short-wave irradiance at lower levels is not an issue (Section 2.0.2). Short-wave heating primarily depends on ozone concentrations; on the one hand, weaker tropical ozone-concentrations via

enhanced annual-mean upwelling (Section 2.0.3) may add to the tropical long-wave cooling; on the other hand, stronger ozone concentrations due to enhanced annual-mean downwelling and slower ozone-destructing chemical reactions (Sections 2.0.1, 2.0.2, and 2.0.6) may warm the subtropical lowermost stratosphere (Figures 2.10c and 2.10d).

It is important to be aware that ozone concentrations in the lower stratosphere at a particular place and point in time do rather depend on the preceding mass transport history than on its instantaneous characteristics (*Brasseur and Solomon, 1986*). In this context, considering the annual-mean residual circulation is thus more meaningful than looking at JA or DJ two-monthly means. Finally, adiabatic temperature changes could intensify the above-mentioned ozone-induced temperature response, but rather depend on the instantaneous anomalous residual circulation.

Polar stratospheric temperature decreases more strongly than that at mid-latitudes, intensifying the temperature gradient associated with these two regions, and the gradient strengthens more vigorously in case of DJ than JA. A possible explanation for the gradient changes involves modified differential heating. *Sigmond et al. (2004)* compare GCM runs with and without altered SSTs, tropospheric and stratospheric GHG concentrations. Their Figure 10a) shows that an exclusive enhancement of stratospheric GHG concentrations strengthens the above-mentioned temperature gradient. Note that stratospheric eddy activity changes are also important, Section 2.7.2 discussing that effect more deeply. *Hu and Tung (2002)* analyse NCEP/NCAR re-analysis data (*Kalnay et al., 1996*) and infer that enhanced radiative cooling is producing the recent negative trend in mid-winter polar lower-stratospheric temperature.

The effect of altered stratospheric differential heating is thought to act as follows (*Fomichev et al., 2007; Gillett et al., 2003; Hartmann et al., 2000; Forster and Shine, 1999; Kodera and Yamazaki, 1994*). For constant uniform ozone concentrations, stratospheric short-wave irradiance and hence short-wave heating decrease polewards of the tropics, especially during DJ when the polar region lies in constant shade. As long-wave cooling does not directly depend on short-wave solar irradiance, the radiative equilibrium temperature towards higher latitudes both decreases and more sensitively reacts to GHG concentration changes. Therefore, higher GHG and ozone concentrations tend to enhance the DJ meridional temperature contrast between middle and polar latitudes. In case of E39/C, part of the effect consequently directly relates to the model boundary condition of GHG concentrations.

2.5.3 Zonal wind

For zonal averages in pressure coordinates the thermal wind relationship implies that temperature and zonal wind are concisely connected. A positive equator-

to-pole local temperature gradient accompanies a stronger zonal wind aloft, a negative gradient a weaker wind. The relationship is not valid equatorward of a critical boundary situated in the tropics; also, the flow must not be too turbulent and exhibit only weak acceleration (*Dutton, 1976*). The zonal wind changes in Figures 2.10e and 2.10f mostly correspond to the respective temperature changes in Figures 2.10c and 2.10d and the changes in zonal-mean temperature and wind result hence largely from identical causes.

Troposphere

The enhanced tropical convective warming strengthens the tropical/subtropical zonal tropospheric wind during both seasons, with a maximum increase right below the tropopause. In contrast, the mid-latitude negative SST anomaly during JA weakens the summertime tropospheric jet.

Stratosphere

During both seasons, weaker winds in the tropical/subtropical middle stratosphere are likely to result from the combined effect of smaller ozone concentrations and enhanced upwelling. Stronger winds in the subtropical lower stratosphere during JA may be due to enhanced ozone concentrations and dynamical changes (Section 2.5.2). The same occurs during DJ, but the winds not only intensify in the subtropics but strengthen throughout the mid-latitude and parts of the polar stratosphere, the high-latitude change signifying a more intense polar vortex. These changes likely follow from the intensified differential heating associated with enhanced GHG and mid-latitude ozone concentrations (Section 2.5.2).

2.5.4 Land-sea temperature contrast

In the warmer climate, the zonal-mean continent-ocean temperature contrast changes. It reduces by about 0.5 K (5%) at subtropical- and mid-latitudes during JA and strengthens by roughly the same amount during DJ.

2.6 Statistical significance of the responses

Prior to a discussion of the modelled anomalous EP fluxes and EP divergences the topic of statistical reliability deserves some closer attention. *Haynes (2005)*;

Butchart et al. (2000); *Steil et al. (1998)* emphasise the necessity of long-term integrations or ensembles of integrations to achieve an acceptable signal-to-noise ratio, particularly at wintertime polar latitudes where sudden warmings cause large inter-annual variability. For instance, *Fomichev et al. (2007)* analyse December-February (DJF) 30-year mean anomalous stratospheric temperature taken from model runs which differ in their underlying SSTs and concentrations of GHGs. They find robust results only away from the northern hemispheric polar region and argue that a standard statistical T test should not be used since its requirements are not met, being independence and normal distribution.

Standard statistical Monte Carlo methods are more useful in the presence of non-normality but also demand independent samples (*von Storch and Zwiers, 1999*; *Salby and Shea, 1991*). Here, the individual DJ samples of a single realisation are not independent since significant low-frequency variability is present in the time series, for example due to the QBO or a trend. On the other hand, the entire realisations are considered to be independent from each other because different initialisation values were specified.

2.6.1 Description of the statistical method

To arrive at a qualitative measure of robustness or stability, anomalous cross-sections are obtained from each possible combination of a COLD realisation subtracted from a WARM realisation. Three independent WARM and two independent COLD realisations yield six partially dependent anomalous cross-sections and only if all of them qualitatively show identical patterns a result is regarded as robust. The same procedure applies to the anomaly plots of temperature, wind, precipitation, et cetera. While the simple method employed works well for clearly robust or clearly noise-dominated results it does less so for intermediate signal-to-noise ratios; in these cases an appropriate Monte Carlo method could help, with adjusted degrees of freedom, to take account of auto-correlation, or, additional realisations to improve the signal-to-noise ratio.

Here, a compromise is made between the number of DJ and JA samples averaged per realisation and the distance from the reference year 1980; while the former governs the noise the latter governs the signal, since the boundary conditions of the two scenarios diverge with time. The model data given, reducing the noise is more delicate than maximising the signal and therefore the individual time-averaged ensemble members comprise the full 20-year period 2000 to 2019 of the WARM scenario and the same period in case of COLD.

2.6.2 Temperature and zonal wind

In case of the absolute modelled stratospheric patterns of temperature and zonal wind (Figures 2.4a, 2.4b, 2.4c, and 2.4d) stability is not a problem during JA

and DJ. The stratospheric anomalous temperatures and zonal winds (Figures 2.10c, 2.10d, 2.10e, and 2.10f) are also stable during both seasons, except for the JA weak temperature response in the lowermost stratosphere poleward of about 50°N ; the latter involves, via the thermal wind relation, unstable anomalous polar winds below 30 hPa. The corresponding polar response during DJ vacillates but may be real.

The tropospheric temperature and zonal wind responses during JA and DJ are clearly robust in the tropics and the subtropics, possibly due to the stable anomalous latent-heat release. At higher latitudes the situation is more complex. The summertime tropospheric mid-latitude response vacillates more intensely than that at lower latitudes, but still appears to be stable, in contrast to the unstable summertime polar response. Finally, tropospheric mid-latitude and polar responses during wintertime are not robust.

2.6.3 EP flux, EP divergence, and latent-heat release

Similarly to temperature and wind, the modelled absolute EP fluxes and EP divergences (Figures 2.5, 2.6, 2.7, and 2.8) are stable for JA and DJ, whereas the anomalous cross-sections (Figures 2.12 and 2.13) are characterised by one order-of-magnitude weaker values and vary considerably more strongly.

Nevertheless, the JA anomalous cross-sections shown are mostly robust and the JA low-latitude quasi-stationary pattern in Figure 2.12c is even extremely stable. The relatively strongest vacillations occur for the total anomalous flux divergence pattern at mid-latitudes in the stratosphere (Figure 2.12a). There is a robust patch of total negative EP divergence at about 45°N latitude and 80 hPa altitude associated with the transient anomalous component, separated from the tropical stable regime by a tongue of instability where quasi-stationary and transient anomalous components compete (Figures 2.12c and 2.12e).

The anomalous convective precipitation rates and liquid-water contents shown are also robust during both seasons, especially in the tropics, indicating that these quantities are closely tied to the thermal lower boundary condition being represented by the SSTs. The robustness suggests that the higher tropical SSTs immediately excite, via enhanced deep convection, the prominent JA low-latitude pattern of enhanced quasi-stationary eddy activity because the latter is also very stable. The low-latitude eddy activity enhancement would be less robust if it was due to mid-latitude eddies more efficiently refracting into the tropics. In this hypothetical case, considerably less stable extratropical eddy generation and propagation responses were involved.

The anomalous flux directions during DJ are generally less robust than those during JA; the stability depends on altitude and latitude, differs for quasi-stationary and transient anomalous fluxes, and deteriorates when separately inves-

tigating the two months of December and January. The quasi-stationary anomalous flux directions are robust throughout the stratospheric cross-section (Figure 2.13b), in the UTLS only above 200 hPa poleward of the subtropics; further down the noise dominates. The transient anomalous flux directions vary more strongly but are still robust at 100 hPa and above except for the polar region (Figure 2.13c). The whole domain below 100 hPa vacillates strongly. The sum of quasi-stationary and transient anomalous directions appears to be robust all over the stratospheric cross-section (Figure 2.13a).

The DJ anomalous divergence patterns generally vacillate more strongly than the respective anomalous flux directions. Nevertheless, the total of quasi-stationary and transient anomalous divergences depicted in Figure 2.13a is still robust above 60 hPa equatorward of 60°N and below 60 hPa equatorward of 30°N. The quasi-stationary component also displays robustness in these regions, but additionally in the region beyond 60 hPa poleward of 60°N (Figure 2.13c). There is a stable transient pattern below 60 hPa equatorward of 60°N (Figure 2.13b) though the transient part generally vacillates more strongly than the quasi-stationary anomalous divergence.

2.7 Response of wave-related dynamical quantities

Section 2.4 discusses and validates the modelled absolute EP diagnostics and shows that model results and observations share important characteristics. When more closely examining the model results in Figures 2.5, 2.6, 2.7, and 2.8, it becomes obvious that in some regions black (constant climate: COLD) and red arrows (changing climate: WARM) differ and hence the two scenarios disagree in their properties of net eddy activity fluxes.

This Section 2.7 discusses such disagreements and aims at relating these to the model boundary conditions. The attribution is attempted via a comparison with the respective anomalous patterns of temperature, zonal wind, and latent-heat release. These variables themselves depend on the model boundary conditions (Section 2.5) and consequently provide a pathway for the boundary conditions modulating the life cycle of atmospheric planetary and synoptic eddies.

It is, i.a., shown that WARM yields a more intense dissipation of tropical lower-stratospheric quasi-stationary eddy activity than COLD and that the increase results from an enhanced convective eddy triggering, the latter ultimately induced by the prescribed tropical SSTs, being higher in case of WARM. This link into the lower stratosphere of anomalous eddy dissipation very likely represents a novel finding in the field of atmospheric science.

The representation of absolute EP fluxes (Section 2.4.2), simultaneous for WARM and COLD, provides coexistent information on length and direction of the anomalous EP flux; small but still important anomalies may be hard to see that way. Such anomalies are more easily detected in the Figures 2.12 and 2.13 which depict anomalous cross-sections of EP flux and EP divergence, WARM minus COLD. Information is lost that way since subtracting two vectors from each other mixes information about length and direction. As a consequence, it is important to consider both absolute and anomalous cross-sections at the same time. All of the patterns discussed are robust and Section 2.6.3 more deeply refers to statistical reliability.

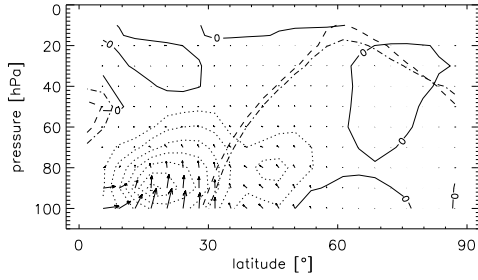
2.7.1 July and August

A comparison of the anomalous stratospheric cross-sections in Figure 2.12 with their absolute counterparts in Figure 2.5 shows that lower-stratospheric eddy activity and dissipation strengthen in the warmer climate.

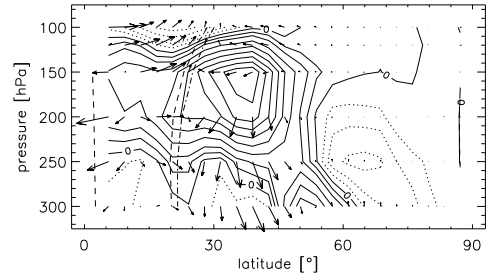
Quasi-stationary and transient components in the lower stratosphere

Both, stratospheric quasi-stationary and transient EP flux contributions intensify for WARM, the quasi-stationary component within the low-latitude easterly wind regime, and more than the transient EP flux which mainly strengthens at mid-latitudes, less so at low-latitudes. A weakening of the quasi-stationary component arises at mid-latitudes in the westerly wind regime. Compared to mid-atmospheric models, the mid-latitude increase in the lower-stratospheric transient contribution (Figure 2.12d) might spread out to higher levels, as E39/C underestimates the summertime descent of the mid-latitude lower-stratospheric easterly winds.

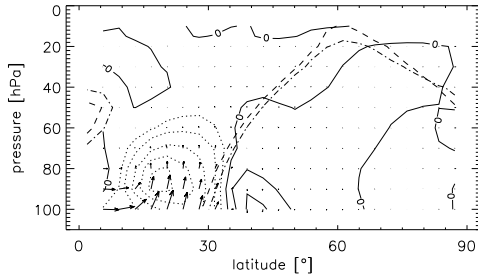
For both the quasi-stationary and transient EP flux contributions shown in Figures 2.12c and 2.12e, the longest anomalous vectors emerge at 100 hPa, shorten with increasing altitude until becoming negligibly small at about 50 hPa. Consequently, the main reason for the stratospheric anomalous pattern lies below 100 hPa in the UTLS and the troposphere. Below 400 hPa both, quasi-stationary and transient anomalous vectors, mostly point downward (not shown), signifying that the stronger upward flux in the summertime stratosphere probably results from changes at heights between 100 and 400 hPa. Yet altered near-surface small-scale eddy activity could obscure near-surface production changes of planetary eddies; at least in case of the transient eddies which display a significant near-surface source (Figure 2.6c), in contrast to the quasi-stationary eddies during JA (Figure 2.6b).



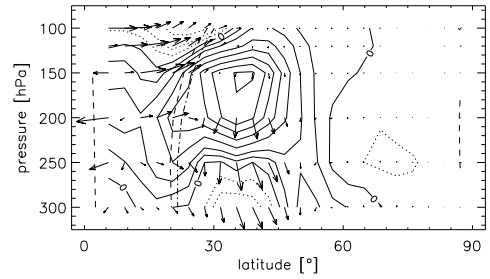
(a) Quasi-stationary plus transient contributions: $2.093 \times 10^{14} \rightarrow 5.378 \times 10^{18} \uparrow$



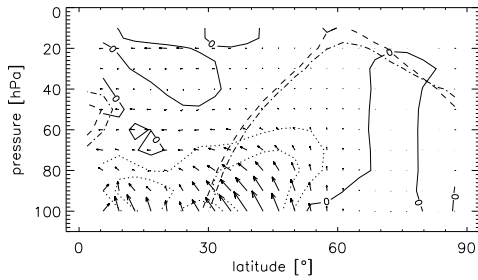
(b) Quasi-stationary plus transient contributions: $1.139 \times 10^{14} \rightarrow 1.511 \times 10^{19} \uparrow$



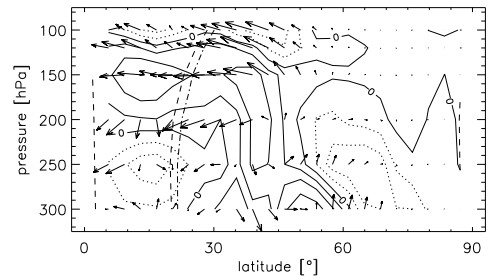
(c) Quasi-stationary contribution only: $1.820 \times 10^{14} \rightarrow 4.676 \times 10^{18} \uparrow$



(d) Quasi-stationary contribution only: $1.015 \times 10^{14} \rightarrow 1.348 \times 10^{19} \uparrow$



(e) Transient contribution only: $6.846 \times 10^{13} \rightarrow 1.759 \times 10^{18} \uparrow$



(f) Transient contribution only: $3.311 \times 10^{13} \rightarrow 4.394 \times 10^{18} \uparrow$

Figure 2.12: Same as Figure 2.3, but for JA and additionally the upper troposphere.

Quasi-stationary component in UTLS and upper troposphere: convective forcing

For the upper troposphere, a comparison of the quasi-stationary cross-sections in Figure 2.12 with those in Figure 2.5 shows that the two regimes of summertime quasi-stationary eddies (Section 2.4.2) differ in their response.

Throughout the region of low-latitude easterly winds the anomalous and absolute arrow orientations resemble, and the anomalous and absolute EP divergence patterns show a roughly similar positioning of negative/positive patterns. The whole low-latitude regime hence intensifies in the warmer climate, signifying that the enhanced latent heating due to higher tropical SSTs (Section 2.5.1) produces additional low-latitude quasi-stationary eddy activity that crosses the tropical tropopause. It is emphasised that there probably does not exist any scientific study which relates future increases in tropical quasi-stationary eddy activity crossing the tropical tropopause to an enhanced convective eddy triggering by higher tropical SSTs.

The extratropical quasi-stationary regime weakens for WARM, being indicated by the downward oriented anomalous vectors opposing the absolute vectors. The weakening probably occurs in connection with the slow-down of the westerly jet below the tropopause and thus presumably relates to the cool anomalous subtropical- and mid-latitude SSTs which themselves represent a model artefact (Section 2.5.1). The processes involved in the weakening could implicate less intense large-scale barotropic or baroclinic instability associated with the slower tropopause jet (Section 2.5.3). Or it could relate to the less efficiently upward travelling transients below the tropopause, being evident in Figures 2.12f and 2.5f. The latter effect would imply wave-wave interaction or a weakened quasi-stationary part in the phase velocity spectrum, simply because the amplitude of the total spectrum decreases.

Transient component in UTLS and upper troposphere

The Figures 2.12f and 2.5f demonstrate that the transient response intensifies above 200 hPa outside the polar region, as anomalous and absolute vectors parallel each other there. The tropical part of this intensification, to speculate, could result from a more strongly fluctuating latent heating caused by the higher tropical SSTs.

In the subtropics, there is a bipolar pattern of more intense eddy activity above the tropopause contrasting more downward orientation underneath. It could relate to the latitudinal temperature gradient and hence to changes in the thermal wind. In the lowermost subtropical stratosphere the temperature gradient increases, as a result of the inclined tropopause separating a warmer troposphere

from a cooler stratosphere. the effect is modulated by the dynamically-induced warming of the lowermost stratosphere (Section 2.5.2). The gradient decreases below the tropopause due to the negative anomalous mid-latitude SSTs.

The weaker temperature gradient underneath the tropopause could hamper eddy production and upward propagation, the stronger gradient above could strengthen the local production of planetary transient eddies which generally more strongly react to large-scale temperature contrast changes than small-scale eddies (*Rind et al.*, 2005b). The strengthening might also occur via a more efficient nonlinear upscale evolution of the type described by *Scinocca and Haynes* (1998), or via a stronger barotropic or baroclinic instability (Section 2.2.1).

2.7.2 December and January

The modelled wintertime stratospheric reaction contrasts the summertime response; EP flux and EP divergence changes deeply reach into the stratospheric westerlies, with the greatest changes emerging at mid-latitudes (Figure 2.13).

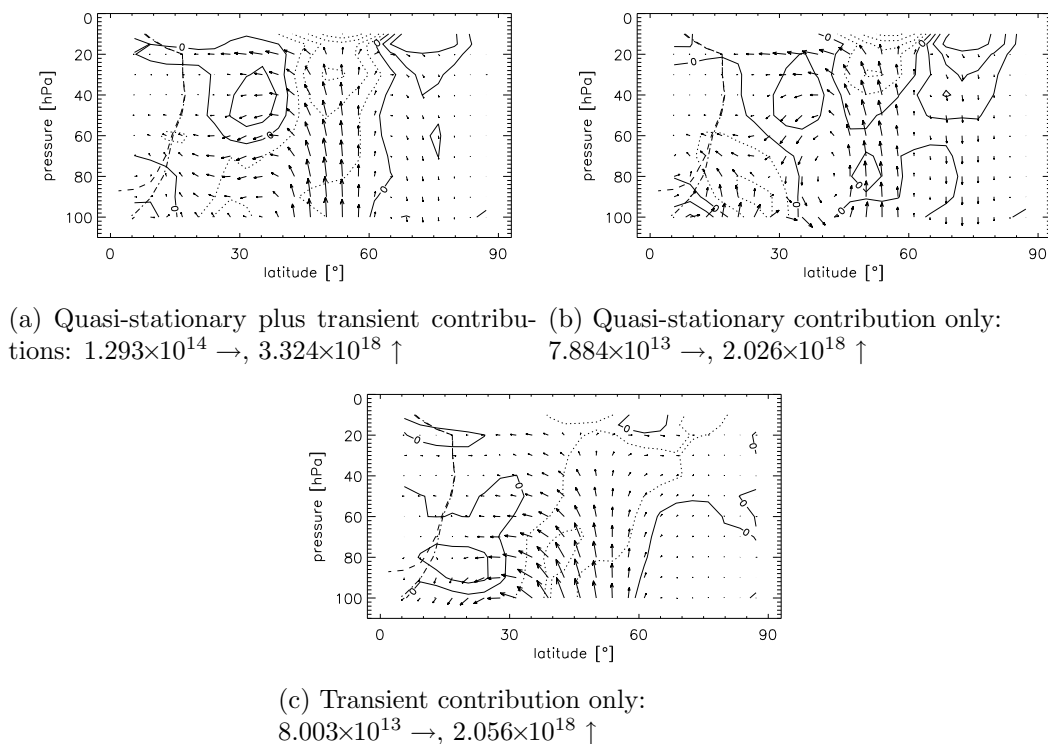


Figure 2.13: Same as Figure 2.3, but for DJ.

Extratropics

A comparison of the Figures 2.13 and 2.7 for their respective mid-latitude arrow orientations shows that both contributions intensify in the warmer climate, the transient component within a broader latitudinal band extending into the subtropics and bending more equatorward than the quasi-stationary part. The latter feature likely relates to the respective absolute arrow orientations which point more equatorward in the transient case (Figures 2.7e and 2.7c). In contrast to its mid-latitudinal intensification, the polar quasi-stationary contribution weakens in the warmer climate, and the polar transient response is not robust among the individual ensemble members.

For both, quasi-stationary and transient anomalous contributions, the flux input into the stratosphere at 100 hPa from underneath comparably strongly intensifies at mid-latitudes for the warmer climate (Figure 2.13); but the relative increase is considerably more intense in the transient case as evident in the corresponding cross-sections of Figure 2.13 and 2.7. The upper model lid affects the transient response less strongly than the quasi-stationary response, as the transient anomalous EP flux dissipates at lower heights than its quasi-stationary counterpart; the latter anomalous EP flux, in contrast, the most extremely dissipates next to the upper lid where the sponge artificially intensifies horizontal diffusion.

Even though eddy dissipation imposes a decelerating westerly force, the modelled stratospheric eddy activity strengthens within a region of enhanced zonal westerly winds (Figure 2.10f), identified, i.a., with a stronger polar vortex. In other words, enhanced eddy activity and higher stratospheric GHG concentrations oppositely affect zonal wind velocity, but radiative effects due to the concentration increase obviously dominate. To assess the model behaviour, those mechanisms are going to be reviewed that are reported to affect the mid-winter extratropical lower stratosphere.

It is today accepted that only the largest planetary eddies can usually enter the stratosphere (Section 2.2.2). Hence altered planetary eddy life cycles must govern the modelled stratospheric eddy activity changes. Extra-tropical planetary eddy generation, propagation, and dissipation depend on the mean state of both, the atmosphere and the lower boundary; this mean state in turn depends on the model boundary conditions directly (Section 2.5). As a result of the eddy-induced westerly force can planetary eddies that are generated in the troposphere modify the stratospheric mean state; the force consequently produces nonlinear entangled effects.

Which processes then control the extratropical wintertime stratosphere depends on the time scale considered. In case of the polar vortex, extratropical planetary eddy activity and stratospheric wave mean-flow interaction appear to dominate on shorter-than-monthly time scales (*Baldwin et al., 2003; Newman*

et al., 2001; *Fusco and Salby*, 1999). Wave mean-flow interaction tends to create downward propagating disturbances that usually start at mid-stratospheric levels (*Baldwin and Dunkerton*, 2001, 1999) beyond the E39/C upper lid, and might hence not be adequately represented here.

The situation is different for decadal time scales. The study by *Hu and Tung* (2002) provides plausible observational evidence that neither nonlinear wave mean-flow interactive processes dominate the long-term changes in mid-winter vortex strength, nor a long-term correlation exists between changes in stratospheric planetary-eddy activity and NH polar-vortex strength. Also, *Hu and Tung* (2002) demonstrate that altered zonal winds in a warmer climate are unlikely to dynamically strengthen the polar vortex by diffracting planetary eddies equatorward away from the vortex. The studies by *Hartmann et al.* (2000); *Limpasuvan and Hartmann* (2000); *Hartmann et al.* (2000); *Rind* (1998); *Shindell et al.* (1998); *Perlwitz and Graf* (1995) follow a different argumentation, but *Hu and Tung* (2002) uncover in these studies severe methodical deficiencies which also apply to the studies by *Rind et al.* (2005b); *Austin et al.* (2003).

Finally, *Hu and Tung* (2002) highlight the dominant role of stratospheric cooling by enhanced concentrations of radiatively active gases against a warming by intensified eddy dissipation, as a consequence supporting the results presented here. In contrast, arctic lower-stratospheric temperature warms as a result of enhanced GHG concentrations and higher SSTs in the model studies by *Fomichev et al.* (2007); *Sigmond et al.* (2004); *Gillett et al.* (2003), but their respectively shown Figures reveal that the warming is not statistically significant. This Chapter benefits from a large data basis which produces robust mid-winter polar responses verifiably.

There are basically two main mechanisms capable of provoking the modelled extratropical eddy activity response evident in Figure 2.13. Changes to both, the mean state of the stratosphere and the tropopause, are thought to mainly modify upward propagation and dissipation. Changes to the mean state of both the troposphere and the lower boundary additionally alter tropospheric planetary eddy generation; this in turn affects stratospheric planetary eddy activity (*Butchart et al.*, 2000).

The question if the stratosphere, the UTLS, the troposphere, or all the three govern the stratospheric extratropical eddy activity response cannot be properly resolved here. Such attribution first of all required separating the modelled EP flux into its spectral components, because in the DJ troposphere small-scale contributions could mask robust near-surface source changes for planetary-scale eddies; the former might account for the strong inter-annual noise in the troposphere (Section 2.6.3).

There is evidence that the modified vertical wind shear associated with the UTLS and the lower stratosphere (Figure 2.10f) may control the stratospheric

eddy activity response. At mid-latitudes, where the vertical wind shear intensifies, stronger upward propagation occurs for both quasi-stationary and transient flux components (Figure 2.13). Anomalous EP fluxes and vertical wind shear hence conform with the mechanism proposed by *Hu and Tung (2002)*, namely that enhanced vertical wind shear in the UTLS and the lower stratosphere intensifies the upward propagation of planetary eddies that are generated in the troposphere (Section 2.2.2). From a strict perspective, the mechanism is only valid in case of quasi-stationary eddies. If the mechanism actually dominated the model results, then the model boundary condition of stratospheric GHG concentrations would not only control mid-winter extratropical stratospheric temperature and wind but also eddy activity on a decadal-scale. Further backup to this theory comes from the respective absolute wave activity propagating more intensely upward into the lower-stratosphere than observed. The reason may be found in the lower-stratospheric cold-pole problem which artificially enhances the zonal westerly winds due to artificially high water vapour concentrations causing excessive latitudinal differential heating (Section 2.4.1).

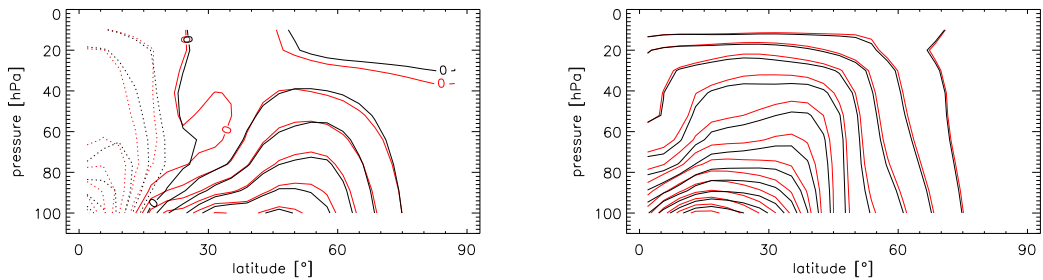
Tropics

The quasi-stationary EP flux possesses a secondary amplification pattern at low latitudes (Figure 2.13b) which resembles the corresponding summertime pattern albeit being less intense and robust and involving a considerable directional change towards more upward propagation (Figure 2.7c). Despite the latter discrepancies, intensified latent-heat release might cause the wintertime secondary amplification pattern similarly to the summertime pattern, and could refer to the tropical anomalous SSTs: Figure 2.10b shows that enhanced upper-tropospheric latent-heat release during DJ maximises in the southern tropics, but slightly extends across the equator possibly more intensely exciting quasi-stationary eddies in the tropical NH.

The amplification pattern less prominently emerges in the total anomalous cross-section (Figure 2.13a) because the transient anomalous contribution is more downward (Figure 2.13c) and opposes the quasi-stationary component. Section 2.7.1 speculates that the tropical transient component might also respond to convective heating and should rather intensify than weaken. But the precise response to anomalous convective heating might differ among transient and quasi-stationary components. To speculate, the former could rather relate to the fluctuation amplitudes than to the time-averaged intensity of deep convection, and both convection characteristics might differ for JA and DJ. Also, unknown mechanisms could counteract an enhancement of the tropical transient component. Conspicuously, Figure 2.7e shows that the absolute transient tropical EP divergence is positive, which could relate to a small or negative northward gradient of potential vorticity (*Edmon et al., 1980*), for some reason not affecting the quasi-stationary eddies.

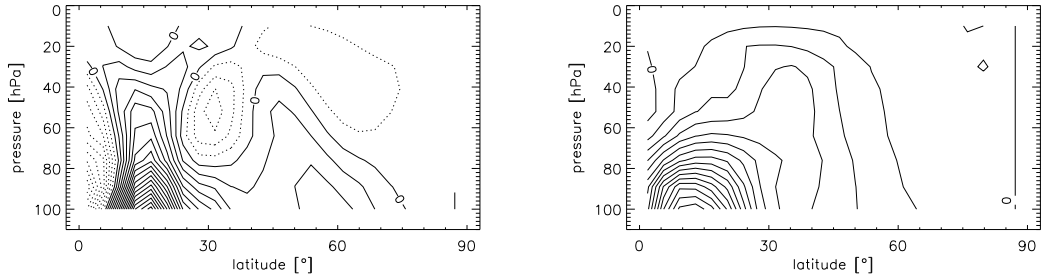
2.8 Response of stratospheric transport

It is fundamental to keep in mind that the absolute and anomalous TEM cross-sections depicted comprise all of the BD circulation inducing processes the model E39/C supports, and not only eddy dissipation (Section 2.0.6). Still the absolute eddy dissipation does not only produce a significant dynamically-induced contribution to the absolute BD circulation (Section 2.4.3); but also, as is shown here, the anomalous eddy dissipation patterns presented in Section 2.7 significantly contribute to the BD circulation response via the principle of downward-control, similarly to the absolute case.



(a) Same as Figure 2.2c, but for JA, the absolute stream functions, and one order-of-magnitude wider contours (in integer multiples of 10^9 kg/s).

(b) Same as Figure 2.14a, but for DJ.



(c) Same as Figure 2.2c (anomaly), but for JA.

(d) Same as Figure 2.14c, but for DJ.

Figure 2.14: Absolute (red: WARM, black: COLD) and anomalous (WARM minus COLD) TEM stream functions for the stratosphere.

In order to demonstrate the qualitative relationship between anomalous BD circulation and eddy dissipation the same reasoning by analogy is adopted as for the absolute case in Section 2.4.3. At the same time does the mere existence of such connections help to relate the modelled BD circulation changes to the model boundary conditions. The reason is that the modelled anomalous EP divergences tend to refer to the the model boundary conditions of GHG concentrations and SSTs, primarily via responses of latent-heat release, temperature and zonal wind (Section 2.7).

Regarding tropical convective eddy forcing it is shown that its SST-induced enhancement intensifies the tropical lower-stratospheric eddy dissipation, and strengthens the low-latitude part of the BD circulation. This important pathway communicating anomalous SSTs to the BD circulation has probably not yet been established in the field of atmospheric science.

2.8.1 July and August

The low-latitude convective dissipation enhancement during JA spatially coincides with a strong BD circulation response (Figure 2.14c); the latter is characterised by both, an intensification and a directional change towards more poleward transport, manifesting itself when juxtaposing the absolute stream functions (Figure 2.14a). Equatorward of about 15°N an intensified upwelling occurs in the warmer climate, but further poleward the more poleward-directed transport signifies a leakier summer hemispheric tropical pipe.

A similar response also arises in the double-CO₂ modelling studies by *Fomichev et al. (2007)*; *Rind et al. (2001)* who prescribe SST patterns adjusted to the given atmospheric CO₂ concentrations, but do not relate the tropical eddy dissipation increase to an intensified tropical convective eddy production. Here, Section 2.7.1 establishes the latter connection, hence linking the modelled tropical anomalous BD circulation to the anomalous tropical SSTs via a strengthened convective latent-heat release. In E39/C, this new pathway seems to represent a major contribution to the amplified tropical lower-stratospheric BD circulation. A further result is that, from a qualitative perspective, the downward-control mechanism seems to apply at latitudes lower than the 20°N critical border *McIntyre (1998)* suggest.

The subtropical feature of negative anomalous stream function values (Figure 2.14c) probably results from the convective dissipation intensification being height-restricted. Below a height of about 60 hPa reinforced dissipation locally coincides with a more poleward-directed residual circulation (Figure 2.12a and 2.14a), whereas above that height both dissipation enhancement and more poleward justification of the residual circulation cease at the same time.

Figure 2.14c displays for the tropics above 30 hPa a weak feature of counter-clockwise anomalous circulation, in opposition to the region below which has a clockwise sense of rotation. The feature spatially coincides with a patch of positive anomalous eddy dissipation (Figure 2.12a) and probably does not relate to the sponge layer because the latter barely affects the absolute residual circulation (Section 2.4.3).

The modelled anomalous BD circulation during JA (Figure 2.14c) is robust throughout the cross-section, except for the pattern of positive iso-lines poleward of 35°N. The dominating EP divergence feature for the latter region is readily

identified with the tongue of unstable total anomalous eddy dissipation, which separates the stable regimes of robust tropical and robust mid-latitude negative EP divergence (Section 2.6.3). The tongue of unstable dissipation changes sign among the six possible anomalous combinations of the scenario realisations (Section 2.6.1) and the BD circulation response co-varies (not shown). As a consequence, the downward-control principle connecting eddy dissipation and residual circulation still applies even though anomalous eddy dissipation is not robust.

2.8.2 December and January

During DJ, robust anomalous BD circulation patterns exclusively emerge equatorward of 45°N and basically refer to two features: to the relatively strong low-latitude cell below 60 hPa (Figure 2.14d), and to the bulge of comparably weak enhancement between 30 – 60 hPa at 35°N . Above these features the response is not robust. The bulge clearly coincides with a robust pattern (Section 2.7) of positive anomalous eddy dissipation (Figure 2.13a).

A comparison of the absolute stream functions in Figure 2.14b reveals that the low-latitude cell is associated with both, intensification and directional change of the residual circulation, similarly to the respective summertime pattern. For DJ and WARM, compared to COLD, the upwelling intensifies equatorward of 10°N , but the subsequent directional change now results in a more downward oriented stream function, accordingly in a tighter wintertime tropical pipe.

Comparing the DJ responses of BD circulation (Figure 2.14d) and total EP divergence (Figure 2.13a) reveals that the spatial coincidence for the low-latitude cell is not very definite; the respective JA low-latitude coincidence, on the contrary, is significantly more obvious because the low-latitude dissipation enhancement is much stronger there (Section 2.7.1).

Within the region occupied by the DJ low-latitude cell there is better spatial coincidence with the quasi-stationary response (Figure 2.13b) than with the total dissipation response, because the transient part is positive and hence opposes the quasi-stationary part (Figure 2.13c). Also, the BD circulation response better co-varies with the six individual quasi-stationary patterns than with the respective total anomalous dissipation patterns (not shown), implying that a relationship after *Haynes et al.* (1991) applies to the quasi-stationary but much less to the transient dissipation response. Nevertheless, the anomalous BD cell and the tropical quasi-stationary eddy dissipation response spatially coincide, suggesting a link to the anomalous tropical SSTs via enhanced convection, similarly to the JA result.

It is not clear why the relationship for the low-latitude transient component is so weak, but it could be due to the transient EP flux or the background state

somehow not fulfilling necessary requirements to the relevant theory. Conspicuously, Figure 2.7e shows that the absolute transient EP divergence in the region of interest is positive, which could relate to a small or negative northward gradient of potential vorticity (*Edmon et al.*, 1980).

It is intriguing that the mid-latitude eddy dissipation enhancement (Figure 2.13a), despite its robustness above a height of 60 hPa (Section 2.6.3), does not produce a stable mid-latitude BD circulation response. Yet Formula 2.5 in *Haynes et al.* (1991) shows that the effectiveness of a given eddy dissipation pattern inducing a residual circulation inversely depends on the zonal gradient of angular momentum if the latter is latitudinally constant. Since the gradient usually maximises and weakly zonally varies at mid-latitudes (*Haynes et al.*, 1991), the response to eddy dissipation there may be weaker than that at lower or higher latitudes and consequently be obscured by the strong mid-latitude inter-annual variability. The response to eddy dissipation may also be obscured by the residual circulation reacting to changes in other driving mechanisms, for instance to altered differential heating (*Rosenfield and Schoeberl*, 2005) or seasonal transience (*Salby and Callaghan*, 2006c) which themselves depend on the concentration of radiatively active gases.

2.9 Summary and conclusion

This Section recapitulates the results obtained for each objective (Section 2.1), assesses the importance of the results, and gives recommendations for future work.

2.9.1 Objective 1

The life cycle of planetary eddies involves the processes of eddy generation, propagation, and dissipation, which to a first approximation depend on the atmospheric background state of temperature and wind, but also on the convective release of latent heat.

There is both observational and theoretical evidence of tropical deep convection robustly producing planetary quasi-stationary waves that propagate into the tropical lower stratosphere vertically and dissipate there; in case of a single convective heat source the waves forced seem to belong to internal modes of the Hough spectrum. The seasonal cycle of the deep-convective forcing is tied to that of the deep convection, with a maximum in the summer hemispheric tropics. Tropical surface precipitation represents a useful indicator of the eddy forcing and appears to be sensitive to tropical SST anomalies.

There does probably not exist any scientific study which designates higher tropical SSTs and the associated reinforcement of convective eddy production as

the cause for future increases in tropical quasi-stationary eddy activity; in this context, the corresponding eddies are required to propagate upward across the tropical tropopause.

The idealised GCM study by *Boehm and Lee* (2003) relates the existence of a low-latitude lower-stratospheric BD cell to convective eddy forcing, but the mechanism does involve horizontal and not vertical propagation of the forced eddies. In their double-CO₂ modelling studies *Fomichev et al.* (2007); *Rind et al.* (2001) prescribe SST patterns adjusted to the given atmospheric CO₂ concentrations. They yield both a tropical lower-stratospheric eddy dissipation enhancement and a consequent anomalous BD cell in the warmer climate, but do not infer a strengthened convective eddy production.

It is likely that there do not exist any studies relating the structure of the summertime low-latitude lower-stratospheric BD circulation to convectively forced eddies propagating upward across the tropical tropopause. In particular, there is none which considers the full causal chain of higher tropical SSTs changing the lower-stratospheric BD circulation via enhanced deep-convective eddy forcing.

2.9.2 Objective 2

(a)

For both WARM and COLD, the fields of zonal-mean temperature and zonal wind agree well with observations. Such comparisons are feasible as the differences with respect to absolute values are small for WARM and COLD compared with each other, as well as for WARM and COLD compared with the PAST scenario. Note that the JA lower stratosphere for WARM and COLD displays middle and high latitude easterly winds that do not extend down to sufficiently low levels of altitude. Also, the JA lower-stratospheric easterly jet is weaker than observed, and in the troposphere the westerly tropopause jet slightly extends to too low latitudes. Due to the cold-pole problem the DJ stratospheric winds at middle and polar latitudes are too strong, despite a higher eddy activity acting to decelerate these winds. As in reality, the tropical convective rain is organised in rain bands, but a thorough validation of the tropical deep-convective latent-heat release is beyond the scope of this Chapter. Yet *Chen and Roeckner* (1997) show that ECHAM4 modelled cloud covers and liquid water paths agree with observations reasonably well.

A rough comparison shows that the strength of the modelled EP fluxes and EP divergences agrees to better than order-of-magnitude with observations. EP flux directions and relative lengths of EP flux vectors, as well as the position of positive/negative EP divergence patterns, are well reproduced in both the troposphere and the stratosphere. E39/C hence captures the most important

mechanisms that govern the EP diagnostics, and as a consequence the whole eddy life cycles. The low-height positioning of the sponge layer is irrelevant for JA, but during DJ produces artificially intense EP divergence next to the upper model lid at middle and polar latitudes. Despite the latter drawback, the DJ TEM stream function well conforms with published re-analysis data, even considering the uppermost model domain. Appropriate published JA observations are not found.

(b)

At JA low-latitudes, deep-convective forcing very likely dominates the modelled EP flux and EP divergence patterns, the patterns mainly associated with quasi-stationary eddies. In particular, the pattern cannot result from quasi-stationary eddy activity generated at mid-latitudes and then travelling equatorward because the quasi-stationary EP flux directions at mid- and low-latitudes do not support this. Also, the low-latitude easterly winds keep away the mid-latitude quasi-stationary wave activity.

The modelled tropical liquid-water content above 500 hPa, a measure of deep-convective latent-heat release, matches the altitudinal reach of the tropical positive EP divergence pattern, positive divergence here associated with eddy production. Additionally, the altitudinal reach of positive EP divergence is consistent with that in the study by *Boehm and Lee* (2003) and mainly refers to divergence in the horizontal EP flux component. That is also the case for the study by *Boehm and Lee* (2003), but they do in fact not account for the vertical component and hence neglect vertical eddy propagation.

Finally, both latitudinal and altitudinal extent of the modelled low-latitude EP flux are consistent with that in observations of eddy amplitudes; and the latter observed eddy amplitudes reportedly result from low-latitude deep-convective forcing. At heights above the low-latitude pattern of positive EP divergence the modelled EP flux orientation changes with increasing altitude from horizontal into vertical, while displaying negative EP divergence due to dissipation; the EP flux still reaches into the lower stratosphere and continues to dissipate until it vanishes at a height of about 70 hPa.

(c)

Spatial reach, direction, and intensity distribution of the modelled JA and DJ TEM stream functions are generally consistent with the respective modelled EP divergences via the principle of downward-control. During JA, the principle even applies qualitatively at latitudes equatorward of the 20°N critical border where its validity may not be guaranteed from a theoretical perspective.

Consequently, the modelled EP divergence represents a significant BD circulation driver and, particularly, convective forcing contributes to the JA low-latitude northward circulation branch. Since the model calculates convectively forced eddies propagating upward into the lower-stratosphere and dissipating, the mechanism of upward-control by *Boehm and Lee (2003)* is not essential to explain the structure of the low-latitude BD circulation. Finally, it is interesting that the DJ sponge-induced EP divergence at mid and polar latitudes does not produce an appropriate stream function.

2.9.3 Objective 3

(a)

Compared to COLD, the tropical SSTs for WARM are higher by up to 1 K and the model convection scheme enhances the JA tropical convective rain primarily within the Pacific warm-pool rain band, but weakens that associated with the Indian monsoon. In the JA zonal mean, the deep-convective latent-heat release intensifies. During DJ, the zonal-mean intensification mainly happens in the Southern tropics, but slightly extends across the equator.

As a result of the enhanced latent-heat release, the latitudinal gradient of temperature increases in the NH tropical/subtropical upper troposphere, causing stronger zonal winds; the increase is similar for DJ and JA because the Hadley-Ferrel circulation transports the convectively released heat northwards during DJ, but not during JA. Also, the latitudinal temperature gradient increases on a hemispheric scale in both the upper troposphere and the UTLS. The reason is that the temperature increase is most intense and of greatest vertical reach in the tropics, separated via a latitudinally sloped tropopause from a stratosphere that cools via higher GHG concentrations. In contrast to the observed SSTs used in case of COLD, the SSTs for WARM are taken from an AOGCM model run which exhibits a cool bias in its mid-latitude SSTs. For E39/C, that mid-latitude negative SST anomaly decreases the mid-latitude latitudinal temperature gradient during JA and weakens the tropospheric part of the tropopause jet.

In the DJ stratosphere, stronger westerly winds at middle and polar latitudes are likely to follow from enhanced differential heating caused by the higher GHG concentrations. The associated stronger winds significantly increase the vertical wind shear at mid-latitudes. In this context, the effect of enhanced differential heating is weaker during JA, probably because of a stronger short-wave heating. It is emphasised that the results at wintertime high latitudes are robust, which is in other modelling studies often not the case.

Despite higher GHG concentrations, the subtropical lowermost stratosphere warms for both JA and DJ, intensifying the subtropical lower-stratospheric westerly winds. The warming is likely to result from higher ozone concentrations

owing to slower ozone-destructing reactions and more downward-oriented transport. The former is associated with stronger GHG concentrations, the latter very likely associated with intensified tropical convection, hence with higher tropical SSTs. Finally, the stronger downward component must also amplify the subtropical adiabatic warming.

(b)

The low-latitude JA quasi-stationary EP flux/divergence pattern very robustly intensifies in the troposphere and the lower stratosphere; the tropospheric intensification spatially coincides with the very robustly enhanced latent-heat release and is confined to the region of easterly winds. Additionally, the low-latitude quasi-stationary EP flux direction and EP divergence patterns resemble their absolute counterparts. This indicates that the whole tropical convective quasi-stationary eddy regime intensifies, and that deep convection plays the dominant role in forcing low-latitude quasi-stationary eddies. Finally, eddies generated in the extratropics are unlikely to cause the tropical intensification because the former regime responds significantly less robustly.

The JA quasi-stationary component weakens within the regime of the mid-latitude westerlies, probably due to the weaker tropospheric part of the tropopause jet and thus relating to the cool bias in mid-latitude SSTs. As surface production for these eddies is negligible, the processes involved in the weakening might comprise baroclinic or barotropic instability.

The transient component intensifies in the lower stratosphere at tropical, subtropical and mid-latitudes, but the reason is unclear. To speculate, the tropical enhancement could result from more strongly fluctuating convective heating and thus relate to the higher tropical SSTs. To speculate further, the sub-tropical and mid-latitude enhancement right above the tropopause might refer to the intensified westerly winds in the same region, thus to a combined influence of GHG concentrations and SSTs via altered instability or nonlinear eddy upscale evolution. The JA transient component weakens below the mid-latitude and subtropical tropopause, probably due to the SST-related slowing down of the tropospheric part of the tropopause jet.

In the JA stratosphere, anomalous EP flux is closely associated with anomalous EP divergence because the absolute zonal winds are weak, probably making the eddies break. During DJ, the absolute zonal winds are strongly westerly and anomalous EP divergence is less robust than the associated anomalous EP flux directions.

At mid-latitudes during DJ, both quasi-stationary and transient EP flux contributions robustly intensify above the tropopause up to the model upper lid; the response is not stable below. However, the intensification above the tropopause

could still result from a stronger surface source of planetary eddies as synoptic-scale tropospheric eddy contributions can disguise the planetary scale, but are more rapidly damped with height than the planetary contribution. In the particular case presented here, such a surface intensification would have to be weak enough to not over-compensate the GHG-induced stratospheric cooling. In this context, the low lid of E39/C could act to underestimate the polar adiabatic warming as air parcels cannot descend through the upper stratosphere and parts of the mid-stratosphere.

An alternative explanation is that the enhanced stratospheric vertical wind shear could favour the upward propagation of planetary eddies across the tropopause and within the stratosphere against the stronger westerly winds. Thus, the GHG-induced enhancement of stratospheric differential heating could not only modulate the mid- and high-latitude stratospheric zonal winds but also the respective EP fluxes and EP divergences on a decadal scale. It is interesting that E39/C provides such patterns of stronger zonal winds and enhanced EP fluxes not only in case of the responses, but also in case of the individual scenarios compared to observations. The reason might be that the model has too high concentrations of water vapour in the lower stratosphere which artificially strengthen the differential heating, in a similar way enhanced GHG concentrations do.

Similarly to the JA intensification, the DJ low-latitude quasi-stationary regime strengthens and causes enhanced eddy dissipation in the low-latitude lower stratosphere. However, the strengthening during DJ is less intense and less robust than that during JA and involves an upward directional change, probably because both, DJ absolute NH latent-heat release and its intensification, are much weaker. Finally, the DJ transient anomalous component opposes the low-latitude quasi-stationary intensification as it is downward oriented and involves positive EP divergence, but the reason is not clear.

(c)

For JA, E39/C calculates a lower-stratospheric anomalous TEM stream function cell associated with anomalous tropical up and subtropical downwelling. For the absolute WARM scenario compared to the COLD scenario, the cell corresponds to an intensification of the tropical upwelling and to a leakier subtropical transport barrier. The corresponding anomalous EP divergence and stream function patterns qualitatively conform with the principle of downward-control. Consequently, the anomalous cell mainly relates to the higher tropical SSTs, the SSTs enhancing the convective forcing of eddies that propagate vertically into the low-latitude lower stratosphere and dissipate. A further justification is that each response representing an element of the chain of reasoning is extremely robust: deep-convective latent-heat release, upward EP flux, low-latitude lower-stratospheric EP divergence, and the corresponding stream function cell.

The JA mid-latitude stream function response is not robust, probably owing to the hardly stable EP divergence response at mid-latitudes. The instability arises from competing quasi-stationary and transient EP divergence responses, ultimately following from the former being weakened by the negative anomalous mid-latitude SSTs, but the latter being intensified by the enhanced zonal winds in the lowermost stratosphere. Still, strength and direction of the mid-latitude anomalous stream function co-vary with the above-mentioned unstable EP divergence, indicating the validity of downward-control even in case of a non-robust anomalous EP divergence.

During DJ, a similar low-latitude anomalous stream function cell occurs, albeit it is weaker and less robust than its JA counterpart. Again, it is associated with intensified tropical upwelling, but in contrast tightens the subtropical transport barrier. For any reason, the anomalous cell better co-varies with the low-latitude quasi-stationary than the transient anomalous EP divergence, and seems to refer to SST-induced intensified tropical convective eddy forcing.

The DJ stream function response poleward of about 45°N is not robust, despite of a stable EP divergence pattern at mid-latitudes above 60 hPa. The reason is not clear, but it might presumably refer to a strong northward gradient of angular momentum at mid-latitudes. It might also relate to other processes which contribute to the residual circulation and depend on the concentration of radiatively-active gases.

2.9.4 Assessment of importance and recommendations for future work

For the present research, the major finding is that a SST-induced enhancement of tropical convective eddy forcing strengthens tropical lower-stratospheric eddy dissipation, in turn inducing an anomalous mass transport cell; the cell is confined to the lower stratosphere, enhances the tropical upward mass transport and orientates the subtropical transport more downward. Higher tropical SSTs hence tend to oppose the beneficial effects on tropical column ozone of decreasing ODS concentrations and of a GHG-induced deceleration of homogeneous ozone destruction in the stratosphere. Another consequence is that the removal of ODS from the stratosphere will probably not occur as quickly as has been suggested. Last, clear-sky tropical surface UV radiation may react sensitively, as the UV radiative-transfer through the atmosphere appears to be the more susceptible to lower stratospheric ozone concentrations the smaller the solar zenith angle is (*WMO, 2007; Krzyscin et al., 2004*).

The above finding is hence of importance for not only to the scientific community, but also for the policy makers involved in the United Nations framework

convention on climate change, and in the Vienna framework convention for the protection of the ozone layer.

A convincing quantification of the above effect is hard to accomplish because nonlinearity needs to be considered and convection in global atmospheric models represents a highly parameterised process that deserves to be improved (*WMO*, 2007; *IPCC*, 2007). Also, future CCMs should incorporate the atmosphere ocean feedback to more realistically estimate the deep-convective response to enhanced GHG concentrations (*Baldwin et al.*, 2007); as a start, a slab ocean could be considered.

Note that E39/C is already well set up as it provides high vertical resolution in the UTLS, and its upper lid does not interfere with the tropical dynamical response. Yet the model may be overoptimistic about the trend in tropical lower-stratospheric ozone concentrations as it does not include the upper-stratospheric ozone increase.

Convectively-induced tropical eddy dissipation in the lower stratosphere not only occurs in the NH, but also in the SH and there maximises during the northern winter. Convective eddy forcing might consequently contribute to the annual-mean upwelling in the tropics, the existence of which has not yet been sufficiently well explained (*Zhou et al.*, 2006).

Regarding the mid-winter middle and polar latitude stratosphere, E39/C suggests that future increases in stratospheric GHG concentrations may strengthen the polar vortex as well as intensify the extratropical stratospheric planetary wave activity. The model hence supports the view that in the future enhanced GHG concentrations might over-compensate the effect of intensified eddy activity. In this context, the implication of the low lid for the modelled wintertime stratospheric dynamics needs to be more thoroughly addressed. Convectively forced external modes can travel poleward and contribute to the wintertime mid- and high-latitude planetary wave activity (*Inatsu et al.*, 2002; *Blackmon et al.*, 1987); future work might also aim at quantifying that contribution. Finally, tropical SST interannual variability appears to modulate planetary wave activity in a similar way (Chapter 3).

Future work may additionally account for:

- a latitudinally and longitudinally dependent analysis of quasi-stationary eddy amplitudes and phases to further investigate the association with convective forcing;
- a wavenumber-dependent analysis to clarify the relative importance for stratospheric eddy activity of eddy propagation characteristics and eddy surface sources;
- a-geostrophic corrections to the EP diagnostics;

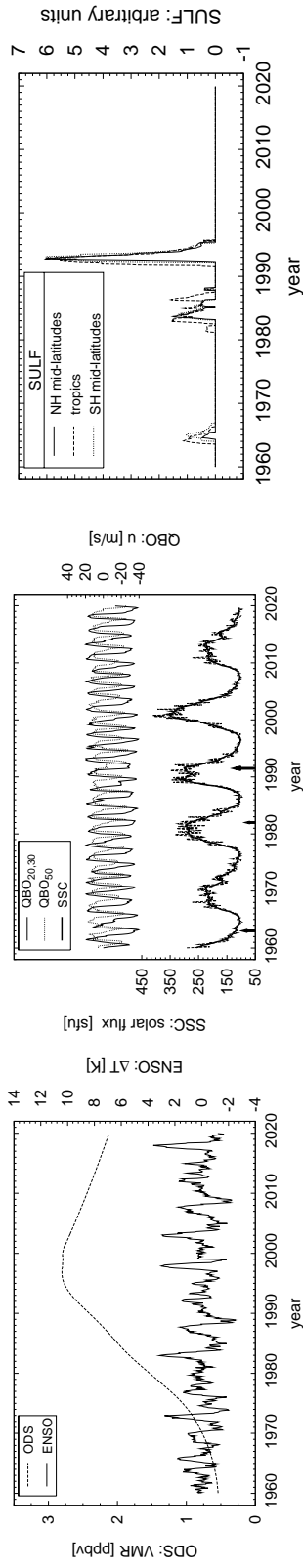
- an analysis of convection properties comprising mean strength and variability;
- an improved statistical analysis using an appropriate Monte Carlo method with corrected degrees of freedom;
- an analysis of how the mid-latitude response changes in case of positive mid-latitude anomalous SSTs.

Chapter 3

Ozone column variability

Recent studies conclude that a prescription of realistic transient boundary conditions forces the chemistry climate model (CCM) E39/C to reproduce the observed time evolution of total column ozone (*Bodeker et al.*, 2007; *Dameris et al.*, 2006; *Steinbrecht et al.*, 2006b; *Dameris et al.*, 2005). The model not only reproduces the observed decadal variability acceptably, but also much of the year-to-year vacillations, indicating that the model boundary conditions at these time scales effectuate a significant deterministic signal. In this context, the most relevant boundary conditions are identified with the tropical quasi-biennial oscillation (QBO), the 11-year solar cycle (SSC), anomalies in tropical sea surface temperatures associated with the El Niño-southern oscillation (ENSO), and volcanic eruptions. The multi-decadal evolution mainly relates to the concentrations of ozone-depleting substances (ODS), the concentrations of well mixed greenhouse gases (GHG), sea surface temperatures, and sea ice coverage; the latter two quantities are hereafter summarised under the term “SST”.

It is important to be aware that, except for *Dameris et al.* (2006), the studies mentioned above base on a single realisation of the PAST scenario, whereas the current Chapter considers threefold ensemble means of the scenario realisations PAST (1960–1999) and WARM (2000–2019) (see Appendix A.2 and Figure 3.1) *Dameris et al.* (2006) show that the year 1999/2000 switch from observed (PAST) to projected boundary conditions (WARM) only produces a small bias in total column ozone, which is not considered here. Therefore, the term “REF” is chosen to refer to both scenarios stuck together at their ends.



(a) Predictors of ozone variations via chemical destruction by ozone-depleting substances (ODS), and due to tropical SST variability related to the El Niño-southern oscillation (ENSO). ODS is defined by global mean monthly-mean zonal wind velocity (QBO_{50}), fate aerosol surfaces at 50 hPa averaged for deseasonalised and detrended monthly mean SST averaged between 215.625° – 256.875° longitude, and 3.715° N– 3.715° S latitude. (b) Predictors of ozone variations owing to the quasi-biennial oscillation (QBO), and to heterogeneous destruction on volcanic sulfate aerosol surfaces (SULF). The predictability related to the 11-year solar cycle (SSC). QBO is defined by the 50 hPa tropical (10° N– 10° S) zonal wind velocity (QBO_{50}), fate aerosol surfaces at 50 hPa averaged for deseasonalised and detrended monthly mean SST averaged between 215.625° – 256.875° longitude, and 3.715° N– 3.715° S latitude. (c) Predictors of ozone variations owing to the quasi-biennial oscillation (QBO), and to heterogeneous destruction on volcanic sulfate aerosol surfaces (SULF). The predictability related to the 11-year solar cycle (SSC). QBO is defined by the 50 hPa tropical (10° N– 10° S) zonal wind velocity (QBO_{50}), fate aerosol surfaces at 50 hPa averaged for deseasonalised and detrended monthly mean SST averaged between 215.625° – 256.875° longitude, and 3.715° N– 3.715° S latitude. (d) Predictors of ozone variations owing to the quasi-biennial oscillation (QBO), and to heterogeneous destruction on volcanic sulfate aerosol surfaces (SULF). The predictability related to the 11-year solar cycle (SSC). QBO is defined by the 50 hPa tropical (10° N– 10° S) zonal wind velocity (QBO_{50}), fate aerosol surfaces at 50 hPa averaged for deseasonalised and detrended monthly mean SST averaged between 215.625° – 256.875° longitude, and 3.715° N– 3.715° S latitude. (e) Predictors of ozone variations owing to the quasi-biennial oscillation (QBO), and to heterogeneous destruction on volcanic sulfate aerosol surfaces (SULF). The predictability related to the 11-year solar cycle (SSC). QBO is defined by the 50 hPa tropical (10° N– 10° S) zonal wind velocity (QBO_{50}), fate aerosol surfaces at 50 hPa averaged for deseasonalised and detrended monthly mean SST averaged between 215.625° – 256.875° longitude, and 3.715° N– 3.715° S latitude.

eruptions associated with the tropical stratosphere (volcanos Agung, El Chichon, and Pinatubo). The arrow lengths give the relative eruptive strengths (relative peak load of global-mean sulfate aerosol surfaces at 50 hPa). Figure 3.1c displays the ozone predictors that relate to the volcanic eruptions.

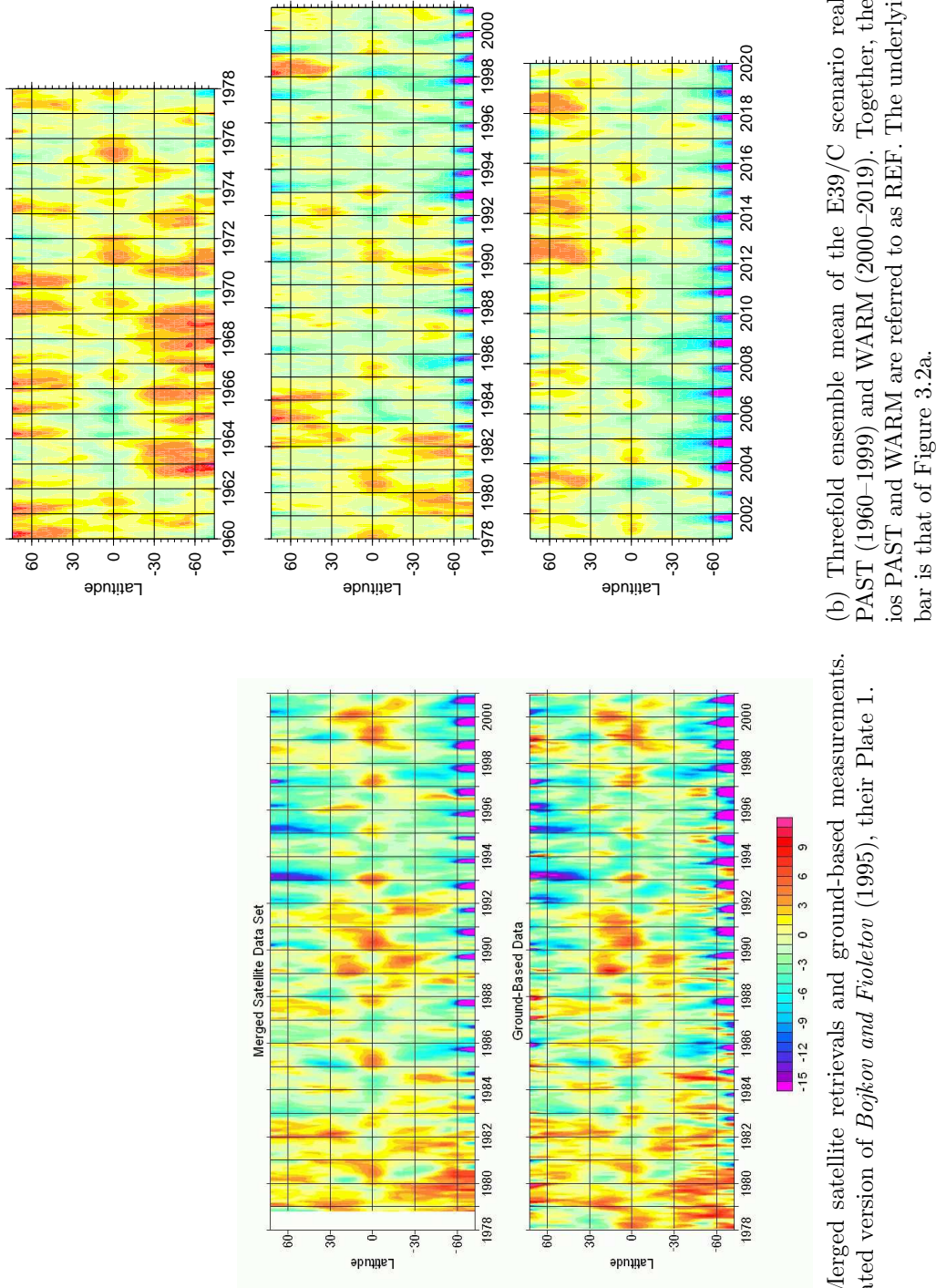
eruptions associated with the tropical stratosphere (volcanos Agung, El Chichon, and Pinatubo). The arrow lengths give the relative eruptive strengths (relative peak load of global-mean sulfate aerosol surfaces at 50 hPa). Figure 3.1c displays the ozone predictors that relate to the volcanic eruptions.

Figure 3.1: Scenario REF boundary conditions that serve as regression predictors for total column ozone. Sections 3.3.2 and 3 provide further information.

The percental anomalies in zonal-mean total column ozone for both, observations and the REF threefold ensemble average show apparent features of covarying interannual variability (Figures 3.2a and 3.2b). There are features which arise in the observed as well as the modelled data: for instance a synchronous quasi-biennial alteration of the tropical anomalies, and pronounced negative departures at southern mid-latitudes during 1985 and 1997. The studies by *Bodeker et al. (2007)*; *Cordero and Nathan (2002)*; *Fioletov et al. (2002)*; *Connor et al. (1999)*; *Bodeker et al. (1998)*; *Bojkov (1987)*, for example, investigate the latter two anomalous years. In E39/C, these features are unlikely to occur by chance as each of the three independent REF realisations qualitatively displays the same anomaly pattern. The individual realisations are not shown here, but *Dameris et al. (2005, Figure 4)* illustrate one of the PAST realisations, equivalently to the REF ensemble average shown in Figure 3.2b. The study by *Dameris et al. (2006)* analyses deseasonalised time series of globally averaged total column ozone, and compares five different observational data sets with the bandwidth spanned by the REF ensemble; the Figure shows that model results and observations tend to covary, QBO, SSC, and volcanic eruptions contributing to the synchronous interannual variability. Spotting ENSO-induced covarying variability is less straightforward as intense ENSO events occur irregularly.

The well documented covariance between E39/C modelling results and observations suggests that the model captures the most important mechanisms governing interannual variability in zonal-mean total column ozone. That is not self-evident because E39/C does not generate the QBO internally and its SSTs are offline; the model hence neglects some of the atmospheric internal modes and the entire atmosphere ocean coupling (*Baldwin et al., 2007*), and might even produce some of the realistic variability via unrealistic feedbacks. Yet a simultaneous consideration of online chemistry, of online oceanic characteristics, and of an internally-generated QBO, is at present too expensive. Also, an entirely free running model would complicate the comparison between modelling results and observations. The 1985 southern mid-latitude negative ozone anomaly, for instance, occurred at a particular level of stratospheric ODS concentrations. A free transient model scenario would possibly have to be realised several times until, at 1985 ODS concentrations, the model finally adopts the observed QBO phase by chance.

The covariance between E39/C model results and observations mentioned above indicates that the low upper model lid does not severely impact on the interannual variability of total column ozone. Further evidence in this respect comes from the study by *Steinbrecht et al. (2006b)*. It shows that the interannual variability of a PAST realisation with the middle atmosphere version of the ECHAM model does not differ principally from that with E39/C. The interannual variability of the polar vortex in the northern hemisphere (NH) represents an exception, as Chapter 4 of the present study suggests the vortex might not react realistically to the QBO and SSC phases.



(a) Merged satellite retrievals and ground-based measurements. Updated version of *Bojkov and Fioletov* (1995), their Plate 1.

(b) Threefold ensemble mean of the E39/C scenario realisations PAST (1960–1999) and WARM (2000–2019). Together, the scenarios PAST and WARM are referred to as REF. The underlying color bar is that of Figure 3.2a.

Figure 3.2: Deseasonalised monthly zonal-mean percentual anomalies in total column ozone. Both deseasonalisation and anomaly calculation base on the time span from 1964 until 1980. Only the region south of 60°S during August–November is deseasonalised with respect to the reference period 1979–1987.

The anomalous amplitudes mentioned above in the tropics and the southern mid-latitudes (Figure 3.2b) are noticeably weaker than their observed counterparts (Figure 3.2a); partly due to the high signal-to-noise ratio of the ensemble average as the individual realisations tend to display stronger amplitudes (not shown); but also owing to an excessively strong modelled impact of the volcanic eruptions (*Dameris et al.*, 2005). Likewise, numerical diffusion may blur the amplitudes.

3.0.1 Significance of modelled and observed interannual variability in total column ozone

In summary, E39/C reproduces the observed interannual variability in zonal-mean total column ozone very well despite the limitations described above. An analysis of the model output may thus help to unravel which factors govern the observed variability how strongly. The reason is, for instance, that model data are complete and the signal-to-noise ratio of ensemble means is higher than that of observations; furthermore, the latter suffer from inconsistencies because of an assimilation of data from varying measuring devices (i.a. *Lee and Smith*, 2003). Finally, an assessment of the discrepancies between modelled and observed variability might contribute to a progress in both, modelling procedures and the knowledge about ozone-modulating processes in general (*Dameris and Deckert*, 2008).

Estimating the interannual variability of total ozone is important because it significantly influences the surface ultraviolet (UV) radiation. UV radiation affects human health, ecosystems and man made materials such as plastic (i.a. *Norval et al.*, 2007; *Aucamp*, 2007). For example, both QBO and long-term trend appear to play a major role in the 1997 observed low-ozone anomaly at SH mid-latitudes (*Cordero and Nathan*, 2002; *Connor et al.*, 1999), being associated with a 40% increase in monthly mean DNA-damaging UV radiation, relative to the 1994–1996 period. The QBO alone seems to explain the year-to-year 1996–1997 difference in UV radiation nearly completely (*Connor et al.*, 1999).

CCMs are typically used for future ozone projections (i.a. *Eyring et al.*, 2007; *Austin et al.*, 2003, and references in both studies), and a quantification of the modelled interannual variability may generally improve the ability to detect the stages of ozone recovery in observational data (*WMO*, 2007, Section 6.2.2.). The study by *Dameris et al.* (2006) represents a good example as it relates the rising global average levels in total ozone around the turn of the millennium to the SSC, and not to decreasing concentrations of ODS.

Currently, the noise in measured data often prevents a statistically significant detection of an ODS-related turnaround in total ozone levels (*WMO*, 2007). The latter assessment states that “the detection of (ozone) recovery milestones is

essentially a signal-to-noise ratio problem ...”. The noise mainly results from transport variability owing to, i.a., the QBO and ENSO, from the SSC, and from volcanic eruptions. Multiple regression analysis represents an important tool to remove the noise and detect changes in multi-annual trends (*WMO*, 2007).

3.0.2 Regression analysis and stratospheric ozone

Multiple regression analysis (MRA) is a powerful and popular statistical tool in ozone research. Its application aims at relating short-term fluctuations and long-term deviations of a given ozone response time series to a set of given parameter functions; the latter are often associated with a trend and with ozone predictor time series for, i.a., the QBO, SSC, and ENSO (*Wohltmann et al.*, 2007). MRA has been used in a variety of studies devoted to both measured and modelled data (i.a. *Fleming et al.*, 2007; *Mäder et al.*, 2007; *Vyushin et al.*, 2007; *Wohltmann et al.*, 2007; *Dhomse et al.*, 2006; *Soukharev and Hood*, 2006; *Steinbrecht et al.*, 2006b; *Lee and Smith*, 2003; *Newchurch et al.*, 2003; *Fioletov et al.*, 2002; *Connor et al.*, 1999; *Bodeker et al.*, 1998; *SPARC*, 1998, and references in these studies).

There are drawbacks in the above-specified application of MRA to stratospheric ozone data. It assumes that simple proxies of QBO, ENSO, and so on, sufficiently characterise complex atmospheric processes, but not all of the associated effects may be completely accounted for this way (i.a. *Steinbrecht et al.*, 2003). Most of the MRA studies apply linear deterministic regression models that cannot handle nonlinear processes; among these are nonlinear interactions of the individual ozone predictors. Nonlinear deterministic regression models can incorporate nonlinear effects, but are more difficult to handle. It seems that only the study by *Krzyścin* (1994) applies a nonlinear deterministic regression model to stratospheric ozone data. Also, linear deterministic regression models assume that the predictors are independent from each other, not collinear, a requirement that may not strictly apply to all of the proxies; for instance, the QBO may contain SSC, ENSO, and volcanic signals (*Salby and Callaghan*, 2006b; *Soukharev and Hood*, 2006).

Interannual variability of ozone

Most of the MRA studies available focus on the analysis of trends and mean responses to the given ozone predictors; only a few aim at the explanation of individual events such as the 1985 and 1997 SH mid-latitude low-ozone anomalies.

As already mentioned, *Connor et al.* (1999) relate a major portion of the 1997 anomaly to the QBO. The authors apply a multiple linear regression approach wherein the QBO response predictor accounts for seasonal synchronisation (see Section 4.2e); but their estimation fails to explain the 1985 anomaly. *Fioletov*

et al. (2002) use multiple linear regression without seasonal synchronisation and miss both, a large part of the 1997 anomaly and a major portion of the 1985 anomaly. It seems that none of the regression analyses published can explain the 1985 negative deviation.

Using analysis approaches other than regression, *Bodeker et al.* (2007); *Bojkov* (1987) show that the 1985 event mainly follows from the QBO, and, to a weaker extent, from the SSC. The former study in particular emphasises the importance of the QBO phasing relative to the annual cycle. Hence, to explain the event, a statistical model should include a seasonally synchronised QBO response predictor. On the other hand, *Connor et al.* (1999) account for a seasonally synchronised QBO in their statistical model and still cannot explain the event. *Bojkov* (1987) suggest that the prominence of the 1985 event, with respect to other QBO-induced low-ozone anomalies, maybe on account of a temporal coincidence of both a QBO-related deviation and the ODS-related trend during the 1980's.

The physical mechanisms behind the QBO-induced modulation of mid-latitude total column ozone include a QBO-related modulation of the mean meridional circulation via a nonlinear latitudinal extension of the QBO secondary circulation, as well as a QBO-caused modulation of planetary-wave-induced diffusion. The Holton-Tan (H-T) mechanism of QBO-dependent planetary wave guides (Section 4.1.1) seems to be of secondary importance at low- and mid-latitudes (*Garny et al.*, 2007; *Bodeker et al.*, 2007; *Kinnersley and Tung*, 1999, 1998).

3.0.3 Technical aspects of regression analysis

Equation 3.1 defines the statistical model that is behind many of the multiple linear regression studies in ozone research. Y_t represents a given ozone time series of length T (“dependent variable”), $\beta_{k,t}$ denotes a given set of K time series (“ozone predictors” or “predictors”), x_k stands for the K unknown parameters, and a_t represents the residuals. The estimated regression line is also called “response”. The estimation procedure usually involves least squares, meaning that the values for the unknown parameters x_k are chosen to globally minimise the sum of squared residuals $\sum_{t=1,T} a_t^2$.

$$Y_t = x_1\beta_{1,t} + x_2\beta_{2,t} + \dots + x_K\beta_{K,t} + a_t \quad (3.1)$$

Confidence band for the response

With regards to a given set of ozone predictors, the attribution and quantification of deterministic interannual variability in the dependent ozone time series involves

the concept of a confidence band for the response. The confidence band for the response is defined as that region around the estimated regression line that has a given chance, typically 95%, of containing the true unknown regression line (i.a. *Dolan et al.*, 2007). A confidence band can be chosen to specify the combined response to each of the estimators in a given regression equation, or the response to any arbitrary estimator subset (*Naiman*, 1987). Finally, prediction bands (i.a. *Dolan et al.*, 2007) have not been adopted.

Many of the regression studies in stratospheric ozone research report parameter confidence intervals, usually in terms of the decision making process if a particular ozone predictor is appropriate and should enter the statistical model. A confidence band for the response is not identical with adding up the respective parameter confidence intervals, though, and needs to be computed separately (i.a. *Bates and Watts*, 1988, Formula 1.37 on page 59). It seems that confidence bands for the response have probably not yet been applied in stratospheric ozone research.

Regression assumptions

A meaningful application of both, confidence bands for the response and parameter confidence intervals, requires a tight compliance with the regression assumptions. Also, the F and t significance tests are not robust with regard to violations of the assumptions. Therefore, the statistical model must be parsimonious (see below) (i.a. *Vyushin et al.*, 2007; *von Storch and Zwiers*, 1999), and the residuals a_t must represent white noise, hence follow a normal independent distribution with zero mean and time-independent variance σ_a^2 , $a_t \sim \text{NID}(0, \sigma_a^2)$ (i.a. *Draper and Smith*, 1998).

The term “parsimonious” signifies that each regressor reduces the residual sum of squares (RSS) significantly, that all regressors are independent from each other, and that the statistical model is not too complicated for the given data. The simpler the model and the fewer regressors are needed to make a_t obey $a_t \sim \text{NID}(0, \sigma_a^2)$, the better.

With regards to the statistical model defined by Formula 3.1, observed and modelled total column ozone data can violate the $a_t \sim \text{NID}(0, \sigma_a^2)$ requirement in a variety of ways. The variance σ_a^2 is usually seasonally dependent, especially at mid and higher latitudes where planetary waves disturb the stratosphere more intensely in wintertime than during the summer. The usage of iteratively weighted regression, a special case of feasible generalised least squares, represents a widely accepted remedy (i.a. *Bodeker et al.*, 1998; *SPARC*, 1998; *Reinsel et al.*, 1994; *Bojkov et al.*, 1990; *Reinsel et al.*, 1987); *Carroll and Ruppert* (1988, pages 13, 16), for instance, describe the procedure extensively.

The residuals a_t are usually not independent from each other. The main reason in case of monthly mean data is that the ozone predictors insufficiently

well represent or miss important ozone-modulating processes (i.a. *Dhomse et al.*, 2006; *Tiao et al.*, 1990). For instance, if the SSC modulation of total column ozone is not accounted for, the residuals will be autocorrelated with a time lag of about eleven years. QBO-related autocorrelation is more complex as it involves various different time lags; these are represented by the main QBO frequency and its harmonics with respect to the annual cycle. It is difficult to establish a QBO estimator that represents nearly all of the QBO-induced ozone variability (*Newchurch et al.*, 2003).

Spatially and temporally averaging acts like a filter on ozone variability, consequently filters the response to ozone-modulating mechanisms. Generally, the averaging increases the signal-to-noise ratio by removing reversible components of ozone variability that are usually associated with a conservative ozone redistribution. The redistribution mainly follows from rapid zonally asymmetric tropopause height fluctuations due to synoptic eddies (*Wohlmann et al.*, 2007; *Stahelin et al.*, 2002). On monthly and longer time scales, the latitudinally and vertically dependent photochemistry tends to make the ozone fluctuations irreversible, and the averages may contain a component that relates to the tropopause height (*WMO*, 2007; *Hood and Soukharev*, 2005; *Steinbrecht et al.*, 1998). But the dominant portion of irreversible dynamically-induced ozone variability still appears to refer to the mean meridional circulation and irreversible mixing (*Bodeker et al.*, 2007; *Fusco and Salby*, 1999; *Kinnersley and Tung*, 1999; *Solomon*, 1999; *Kinnersley and Tung*, 1998; *Randel*, 1993). Finally, zonally averaging enhances the signal-to-noise ratio indeed, but also amplifies the serial correlation of monthly mean total column ozone data (*Vyushin et al.*, 2007).

There are basically two different approaches to remove the residual autocorrelation. One possibility is to improve the existing predictors or to add additional ones; but the capacity to reduce the autocorrelation that way is limited as it is hard to optimise the predictors: not all of the ozone-modulating processes are known, and the principle of parsimony needs to be considered.

Another reason for the unsuitability of this approach is that the present Chapter focuses on the causality and quantification of E39/C modelled ozone interannual variations, and therefore exclusively adopts model boundary conditions as ozone predictors. An inclusion into the regression equation of ozone-modulating internal variables, such as planetary wave activity, would indeed reduce the residual autocorrelation and the residual sum of squares (RSS) significantly (*Mäder et al.*, 2007; *Dhomse et al.*, 2006; *Reinsel et al.*, 2005). The problem is that internal variables do usually not add to the attribution of causality since the associated variability is often not well explained physically, and because internal variables can themselves respond to the model boundary conditions as well as react on the calculated ozone concentrations (*Vyushin et al.*, 2007; *Wohlmann et al.*, 2007). In reality, of course, QBO and ENSO represent internal modes of the climate system, in contrast to external variables such as the SSC, volcanic eruptions, or

ODS concentrations. But what discerns the former from other internal variables is their narrow and well defined power spectrum. The latter permits an estimation of their contribution to future ozone level variability, and of their potential to hide the onset of ozone recovery (*Vyushin et al., 2007; Naiman, 1987*).

An alternative approach to remove the residual autocorrelation is to associate the latter with stochastic processes, and hence to treat autocorrelation as a nuisance of which the physical and causal background is not of interest (i.a. *Vyushin et al., 2007; Thejll and Schmith, 2005; von Storch and Zwiers, 1999; Pandit and Wu, 1983*).

Stochastic processes

The most widely employed stochastic process in atmospheric research is probably the first order auto-regressive process, AR(1), which represents a memory that decreases exponentially with time (*Milionis and Davies, 1994*). The popularity of the AR(1) process stems from its straightforward applicability via the Cochrane-Orcutt transformation in connection with any given linear deterministic regression model (*Dhomse et al., 2006; Thejll and Schmith, 2005; Bodeker et al., 1998; Tiao et al., 1990; Cochrane and Orcutt, 1949*), for instance in connection with the model given by Equation 3.1.

Note that, the residual autocorrelation in stratospheric ozone data not necessarily obeys an exponential law. Analysing near-surface tropospheric ozone data, *Kim and Kumar (2005)* show that their residuals display a daily periodic autocorrelation that cannot be removed by AR(n) processes of any given order n . Monthly mean stratospheric data might contain an equivalent yearly periodic autocorrelation. Other sources for residual autocorrelation may include remaining traces of, i.a., the QBO, or a seasonally dependent trend.

The ARMA(n, m) process of order n, m extends the pure AR(n) process by a moving average component, MA(m) (*Box et al., 1994; Pandit and Wu, 1983*). Equation 3.2 defines and illustrates the ARMA(n, m) model. There, the term a_t is associated with a given time series, for example with the residuals of the deterministic model in Formula 3.1. The set of factors Φ and Θ represents the unknown parameters that are determined by minimisation, similarly to the unknown parameters x_k in Formula 3.1. The final residual time series ϵ_t is desired to represent white noise.

$$a_t = \epsilon_t + \underbrace{+\Phi_1 a_{t-1} + \Phi_2 a_{t-2} + \dots + \Phi_n a_{t-n}}_{\text{AR}(n)} - \underbrace{\Theta_1 \epsilon_{t-1} - \Theta_2 \epsilon_{t-2} - \dots - \Theta_m \epsilon_{t-m}}_{\text{MA}(m)}$$

$$\underbrace{\hspace{15em}}_{\text{ARMA}(n, m)}$$
(3.2)

It is accepted that an ARMA(n, m) stochastic model can approximate every bounded stationary stochastic system (*Box et al.*, 1994; *Pandit and Wu*, 1983). Even the low-order ARMA(2, 1) model can, depending on the values for the parameters Φ_1 , Φ_2 , and Θ_1 , represent an exponentially decreasing memory similarly to the AR(1) model, or represent a sinusoidally oscillating memory with arbitrary period and degree of damping (*Pandit and Wu*, 1983).

Thus, the application of an ARMA(n, m) stochastic model on the residuals a_t of a deterministic statistical model has, compared to the usage of an AR(n) process, the potential to remove a significantly larger portion of the residual autocorrelation (*Milionis and Davies*, 1994; *Pandit and Wu*, 1983). The current Chapter uses the modelling approach by *Pandit and Wu* (1983) where nonlinear least-squares minimisation yields the unknown parameters of the combined deterministic/stochastic model.

Kim and Kumar (2005) present a different methodology to cope with periodically autocorrelated residuals, but the method is probably inappropriate in case of the more complex QBO-induced residual components in total column ozone. Finally, monthly zonal mean time series of total column ozone may contain long-range memory power law components that ARMA(n, m) stochastic models cannot handle (*Vyushin et al.*, 2007).

Nonlinear error surface curvature

Equation 3.3 gives the deterministic/stochastic model that follows from the combination of the linear deterministic model in Equation 3.1 (here for $K = 2$), and the AR(1) stochastic model. Without loss of generality, Equation 3.3 shows that any linear deterministic model combined with an ARMA(1, 0) or higher order stochastic part displays products of unknown parameters, as a consequence features nonlinearity (*Bates and Watts*, 1988, for instance).

$$Y_t - \Phi_1 Y_{t-1} = x_1 \beta_{1,t} - \underbrace{\Phi_1 x_1}_{\text{parameter product}} \beta_{1,t-1} + x_2 \beta_{2,t} - \underbrace{\Phi_1 x_2}_{\text{parameter product}} \beta_{2,t-1} + \epsilon_t \quad (3.3)$$

It is a characteristic of nonlinear regression models that these usually are more difficult to deal with than linear models. Nonlinear models implicate both the use of nonlinear minimisation routines and, in case of multiple minima, an accurate specification of initial values; in contrast, linear models have analytical solutions.

For any given nonlinear model that consists of a linear deterministic part and an AR(1) component, the Cochrane-Orcutt transformation mentioned above permits the iterative use of linear least-squares minimisation routines that yield asymptotic linear confidence bands and intervals. *Thejll and Schmith* (2005), for instance, explain the method in more detail.

The problem with the Cochrane-Orcutt transformation is that nonlinear regression problems may not always obey asymptotic linearity. Studies in economics and other science fields show that the outcome can be a marked underestimation of the width of confidence bands and intervals, as well as the invalidity of common significance tests (*Dolan et al.*, 2007; *Benabbas et al.*, 2005; *Canjels and Watson*, 1997; *Bates and Watts*, 1988; *Aschheim and Tavlas*, 1987; *Dufour et al.*, 1983). A property of the associated inconsistency is that it appears to be the more pronounced the more nonlinear the regression model is, thus the stronger the autocorrelation turns out to be; small sample sizes, too, intensify the inconsistency (*Benabbas et al.*, 2005).

It seems that the validity of asymptotic linearity has not yet been verified in case of regression models for stratospheric ozone time series. For a first assessment in case of the E39/C scenario REF data, a profiling method for individual parameters by *Bates and Watts* (1988, pages 200-216 and 302-303) is used.

3.1 Aims and objectives

The interannual variability of total column ozone is important. It goes hand in hand with a significant modulation of the harmful UV radiation, and complicates the detection of the ozone recovery stages. MRA studies are helpful to quantify the ozone interannual variability and have contributed to detect first signs of the slowing-of-decline ozone recovery stage in the upper stratosphere. Also, MRA investigations of the modelled ozone interannual variability contribute to an improvement of the present CCMs and have the potential to identify starting points for future research about stratospheric-ozone modulating processes, about dynamical processes in particular.

The benefits associated with MRA of total column ozone have not yet been fully exploited and the fulfillment of the regression assumptions has rarely been assessed. Compared to linear MRA, nonlinear MRA has got a greater potential to fulfill the regression assumptions and to maximise the deterministic response of ozone interannual variability; in this context, nonlinear MRA might unravel deterministic nonlinear interactions among ozone-modulating processes. Future MRA studies may even give the probability of occurrence for low-ozone events, via the well known spectrum of ozone-modulating mechanisms such as the QBO and ENSO.

The current approach is unique in that 3D CCM transient total column ozone data are analysed that reproduce the observed interannual variability as well as the temporal occurrence of individual anomalous events. In comparison with the study by *Steinbrecht et al.* (2006b), longer and less noisy time series are investigated. Also, the current study is among the rare ones to focus on a quantification and causal attribution of both, interannual variability and individual anomalous

events away from the polar regions. Recent MRA studies have been unable to explain the observed 1985 southern mid-latitude ozone anomaly, and this MRA study tries to recover it from the CCM data.

Additionally, this Chapter introduces a novel MRA approach into stratospheric ozone research; it applies regression line confidence bands for statistical inference, adopts a nonlinear ARMA stochastic model to remove residual autocorrelation, and investigates the validity of the Cochrane-Orcutt transformation in terms of asymptotic linearity with respect to the E39/C data.

The present Chapter focuses on zonal and monthly means of E39/C total column ozone data for the three latitude bands SH mid-latitudes (35-60°S), NH mid-latitudes (35-60°N), and tropics (15°N-15°S), and consequently leaves the polar regions to future investigations. Commercial statistical software is expensive, and both, commercial and free programme packages are probably not flexible enough to meet the profile of application, the latter defined by the data analysed and by the questions addressed.

The current profile of application implies the use of iteratively weighted regression in combination with nonlinear deterministic/stochastic models, the calculation of response confidence bands as well as an investigation of asymptotic linearity. As a consequence, a robust nonlinear minimisation routine needs to be selected and adapted in order to comply with the specifications. Such an adapted routine may promote the future use of nonlinear MRA in the field of stratospheric ozone research, an approach pioneered by *Krzyścin* (1994).

The objectives of this Chapter are to

1. select an adequate nonlinear least-squares minimisation routine and provide it with the required capabilities;
2. regress monthly zonal means of E39/C scenario REF total column ozone data and
 - (a) assess whether the regressions conform with the requirements for statistical inference;
 - (b) assess whether asymptotic linearity, a prerequisite for the Cochrane-Orcutt transformation, is appropriate;
3. discuss the regression results for the latitude bands
 - (a) SH mid-latitudes;
 - (b) NH mid-latitudes;
 - (c) and tropics.

3.2 Regression algorithm description

This section briefly introduces the nonlinear least-squares minimisation software package, and outlines the algorithms added to the package in order to meet the requirements of the present Chapter.

3.2.1 Minimisation algorithm

MINPACK-1 (*Garbow et al.*, 1980; *Moré et al.*, 1980) represents a robust and intensively tested software package for solving nonlinear least squares problems. It uses an implementation of the Levenberg-Marquardt minimisation algorithm. Basically, the algorithm is designed to find a local minimum in a sum of squares surface, while being able to cope with near-singular surface slopes in a numerically stable way (more detailed information available in *Bates and Watts*, 1988, for instance). The provision of accurate initial values for the regression parameters can be crucial as nonlinear sum of squares surfaces may display multiple minima, but only the global minimum is usually of interest. Inaccurate initial values may cause the algorithm to converge at a local, and not at the global sum of squares minimum.

3.2.2 Algorithms added to the minimisation algorithm

The MINPACK-1 package is upgraded by the following algorithms. An iterative weighting procedure (*Carroll and Ruppert*, 1988, pages 13, 16) estimates the twelve monthly variances directly from the given E39/C total ozone time series. Each of the three series comprises 720 modelled months, a length considered to be sufficient for reliable estimates of monthly variances (*Carroll and Ruppert*, 1988). The latter study recommends the use of weighted regression in case the standard deviation differs by more than 3:1 between the noisiest and the least noisiest month, and argue against the use of weighting if the standard deviation differs by less than 1.5:1. The authors reason that the neglect of weighting in the former case can cause both inflated confidence bands and intervals, and violate the requirement of constant residual variance.

Another procedure combines any deterministic model of the type defined by Formula 3.1 with an ARMA(n, m) stochastic model of any desired order n, m . The authors of *Pandit and Wu* (1983, Appendix III) provide a routine that gives initial values for the stochastic part, but the implementation turned out to be beyond the scope of this study. Low-order AR(n) stochastic models are still adopted, as in this case the provision of accurate initial values is less complicated.

A further procedure calculates asymptotic linear confidence bands for the regression lines (*Bates and Watts*, 1988, Formula 1.37 on page 59) from the final

output of the minimisation routine when it has converged at a sum of squares minimum. To recapitulate, nonlinearity may invalidate asymptotic linear confidence bands and intervals for both the regression lines and the parameters. Also, the validity of asymptotic linearity represents a prerequisite for the Cochrane-Orcutt transformation.

Finally, a procedure is implemented that detects departures from asymptotic linearity and gives parameter confidence intervals which consider nonlinear effects (*Bates and Watts*, 1988, pages 200-216, 302-303). Starting from a minimum (RSS_{min}) in the sum of squares surface, the procedure takes a single parameter x_k , moves it away from its RSS-minimising value by a finite amount Δl , and fixes it there. Then, a conditional minimisation over all other parameters results in a new, higher $RSS_{x_k}(\Delta l)$. The procedure is done at both sides of the minimum for stepwise increases in $|\Delta l|$. If the shape of the square-root profile trace function, $\sqrt{t_{x_k}(\Delta l)} = \sqrt{RSS_{x_k}(\Delta l) - RSS_{min}}$, differs from a straight line, then the regression problem is nonlinear with respect to the parameter x_k . A straightforward modification of the square-root profile trace function gives the confidence level for x_k as a function of Δl . Similarly to $\sqrt{t_{x_k}(\Delta l)}$, the confidence level for x_k plotted against Δl indicates the degree of nonlinearity with respect to x_k , but additionally yields the nonlinear parameter confidence interval at any desired confidence level (Figure 3.6). Beyond graphical approximation, the numerically exact confidence interval is specified by interval nesting.

A related profiling procedure also exists for the regression line confidence bands, but has not been implemented. Yet the asymptotic linear confidence band is valid if the method explained above signifies linearity for each of the parameters x_k contributing to the band (*Bates and Watts*, 1988). Of course, the regression requirements of parsimony and residual white noise must be met as well (Section 3.0.3).

3.3 Regression model description

Section 3.0.3 provides background information about MRA in general, and introduces the class of deterministic and stochastic regression models used. More detailed information is necessary in order to accurately interpret the MRA results. To provide the information, this section discusses the combined deterministic/-stochastic regression model more deeply, and explains important characteristics of the ozone predictors.

3.3.1 Combined regression model

Together, Equations 3.1, 3.2, and 3.4 define the combined regression model. The dependent variable Y_t represents zonal monthly mean total-column ozone in Dob-

son Units, given by a threefold ensemble mean of independent REF realisations. The three Y_t time series of interest (Figure 3.3) represent the following latitudinal means: SH mid-latitudes (35-60°S), NH mid-latitudes (35-60°N), and tropics (15°N-15°S). In fact, the MRA involves the full non-deseasonalised ozone data, but, with regards to interannual variability, graphing deseasonalised values is more informative. Finally, separate sets of ozone predictors apply to each of the three latitude bands (Table 3.1), but the associated MRAs refer to the same regression model mentioned above.

Seasonal expansion of the ozone predictors

The ozone predictors $\beta_{k,t}$ (Figure 3.1) represent typical ozone-modulating boundary conditions of the REF scenario, such as the QBO and ENSO. An expansion of the deterministic regression parameters x_k (Equation 3.1) with sinusoidal terms (Equation 3.4) allows the relationship between ozone and any of the predictors to depend on the seasonal cycle; for instance, the impact of the QBO on mid-latitude total ozone has a large seasonal component (Section 3.0.2).

Which and how many of the sinusoidal terms in Equation 3.4 contribute to the regression equation depends on both the dependent variable Y_t , as well as on the individual ozone predictors $\beta_{k,t}$. It is decided on the basis of several diagnostics (Section 3.4.2). It can happen that an individual ozone predictor is chosen to contain, for instance, the semi-annual term, but not the lower-frequency annual oscillation. Finally, owing to aliasing effects, the monthly mean approach largely precludes sinusoidal terms of higher than quarterly order.

$$\begin{aligned}
 x_k = & x_{k,0} + \underbrace{x_{k,1} \cos\left(\frac{2\pi}{12} t + x_{k,2}\right)}_{\text{annual}} + \underbrace{x_{k,3} \cos\left(\frac{2\pi}{6} t + x_{k,4}\right)}_{\text{semi-annual}} \\
 & + \underbrace{x_{k,5} \cos\left(\frac{2\pi}{4} t + x_{k,6}\right)}_{\text{four-monthly}} + \underbrace{x_{k,7} \cos\left(\frac{2\pi}{3} t + x_{k,8}\right)}_{\text{quarterly}}
 \end{aligned} \tag{3.4}$$

The particular method of sinusoidal expansion (Equation 3.4) conforms with the regression approach by *Pandit and Wu* (1983), and is nonlinear as it contains products of regression parameters. More common in stratospheric ozone research is a linear sinusoidal expansion of the form

$$x_k = x_{k,0} + x_{k,1} \cos\left(\frac{2\pi}{12}\right) + x_{k,2} \sin\left(\frac{2\pi}{12}\right) + \dots \tag{3.5}$$

but the two different approaches have both their respective advantage and drawback. The nonlinear approach is more parsimonious as it displays a weaker

collinearity (not shown), probably because for each sinusoidal term the first parameter is devoted exclusively to the amplitude and the second parameter to the phase. The linear expansion is easier to handle.

Regression initial values

Following *Pandit and Wu* (1983), initial parameter values for the nonlinear combined model (Equations 3.1, 3.4, and 3.2) are obtained from separate fits, first of the deterministic model (Equations 3.1 and 3.4) and then of the stochastic model (Equation 3.2) using the respective deterministic residuals.

Without considering the stochastic parts, the deterministic model contains nonlinear seasonal terms (Equation 3.4) that need to be initialised. Picking optimum initialisation values is accomplished by choosing the minimum RSS from several model fits with a range of different initialisation values for the seasonal parameters. However, it is convenient that the deterministic model is not very sensitive to initialisation (not shown). In contrast to the deterministic model mentioned above, an ARMA($n, 0$) stochastic model without a moving average part is linear and does not need to be initialised. *Pandit and Wu* (1983) provide a routine that yields initial parameters for a full ARMA(n, m) nonlinear model, but the implementation is beyond the scope of this study and ARMA(n, m) models are ignored.

3.3.2 Design of the ozone predictors

To clarify and quantify causal relationships of total column ozone variability, the MRA adopts as ozone predictors the most important ozone-modulating boundary conditions of the E39/C scenario REF (Section 3). In order to increase the MRA deterministic response, for each ozone predictor a particular design is chosen (Figure 3.1). This section provides information how the choice is made, and briefly covers the issue of time lags.

QBO

Compared to other predictors such as ODS, ENSO, or SULF, the design of QBO response predictors is more complex because the QBO involves the tropical wind profile throughout a range of lower-stratospheric levels. For each of the three latitude bands of interest, a single time-lagged QBO response predictor is used, and, following *Bodeker et al.* (1998), accounts for the QBO seasonal synchronisation by a seasonal expansion (Equation 3.4). The MRA adopts a nonlinear expansion and, in this respect, adopts an approach which differs from *Bodeker et al.* (1998).

The choice of a particular time series as QBO response predictor is not straightforward and there exist different approaches. Most of the studies either incorporate a single time-lagged QBO response predictor (i.a. *Weatherhead et al.*, 2000; *Connor et al.*, 1999; *Logan*, 1994), or two QBO proxies without time lag (i.a. *Fleming et al.*, 2007; *Mäder et al.*, 2007; *Ziemke et al.*, 1997; *Randel and Wu*, 1996).

Depending on the study, a single lagged QBO time series may refer to the QBO-dominated tropical zonal wind velocity at a particular height level or refer to a composite of several levels; similar to the single time series, the two unlagged time series may each also refer to a single level or a level composite. The latter approach without time lags takes into account that there are two QBO ozone response patterns in the real stratosphere which are out of phase at tropical latitudes. One of the response patterns maximises in the lower stratosphere, the other one maximises in the middle stratosphere (*Randel and Wu*, 1996); the out-of-phase behaviour is not important in case of E39/C modelled ozone data because the CCM neglects parts of the middle stratosphere. Also, the unlagged approach facilitates the implementation of automatic stepwise regression (*Mäder et al.*, 2007), but goes hand in hand with a stronger collinearity (not shown). For both of the approaches mentioned above, methods akin to empirical orthogonal decomposition (EOD) may yield a QBO response predictor in form of a linear composite of several height levels that is more effective in capturing the ozone QBO than a less sophisticated predictor (*Randel and Wu*, 1996). The present analysis does not apply EOD, but a more subjective approach instead. The MRA is done for all QBO heights and some linear height combinations, finally using the most effective QBO response predictor.

A difficulty is that the optimum QBO response predictor varies with the latitude at which the ozone response is considered (*Yang and Tung*, 1995), and the ozone response at a given latitude is probably not purely linearly proportional to a linear composite of equatorial zonal wind velocity (*Lee and Smith*, 2003). Hence, the mentioned QBO proxies are unlikely to remove the whole ozone QBO signal, particularly in case of latitudinal averages.

Finally, *Steinbrecht et al.* (2004); *Newchurch et al.* (2003) apply a range of sinusoidal terms without zonal wind velocity to remove the QBO signal in stratospheric ozone concentrations, thus treat the QBO signal as a nuisance parameter since the approach is likely to impede a causal attribution. The method does well if the focus is on trend detection, but is obviously unsuitable if the causal attribution of interannual variability itself is of interest.

ODS

It is common practice among MRA studies of total column ozone to adopt as ozone trend predictor the evolution of equivalent effective stratospheric chlorine, a

weighted integral over all ozone-depleting substances in the stratosphere (*WMO*, 2007). E39/C does not account for the second most important ozone-depleting element bromine (Appendix A.1); Global chlorine concentrations therefore represent a suitable predictor for ODS-related trends.

SSC

Figure 3.1b shows that the SSC time series displays a significant monthly variability, compared to the amplitude of the 11-year oscillation. Every linear or nonlinear MRA involves the time derivative of the ozone predictors and, hence, the monthly SSC variability tends to unwontedly bias the 11-year response towards the monthly fluctuations, resulting in a too weak 11-year response (not shown). To overcome this bias, a yearly running mean SSC response predictor is implemented (Figure 3.1b).

E39/C accounts for the ozone chemistry above its model domain by the prescription of NO_y contents in the two uppermost model layers (see Appendix A.2). The NO_y time series contains a SSC signal, but using NO_y concentrations as SSC response predictor does not reduce the RSS more strongly than using the solar-flux-based predictor in Figure 3.1b (not shown).

ENSO

The ENSO response predictor is based on the mean SST associated with those twenty model boxes that cover the area defined by the longitude section 215.625° - 256.875° and the latitude section 3.715°N - 3.715°S . In this part of the tropical Pacific, the SST interannual variability is dominated by ENSO (i.a. *Rayner et al.*, 2003) and hence gives a suitable ENSO response predictor. To avoid correlations with the time series of both ODS and annual cycle, the ENSO time series is detrended and deseasonalised. Finally, the resulting monthly mean ENSO response predictor is superior to multi-monthly running means (not shown).

SULF

Sulfate aerosol surfaces exclusively cause heterogeneous ozone destruction in the presence of significant ODS concentrations (i.a. *Dameris et al.*, 2005). ODS weighted SULF response predictors (Figure 3.1c) are taken since these more strongly reduce the RSS than the pure SULF response predictors without weighting (not shown). In addition to incorporating sulfate aerosol surfaces, the REF scenario prescribes eruption-induced heating rates (*Dameris et al.*, 2005; *Kirchner et al.*, 1999), but these are not considered here.

Annual cycle

Many of the published MRA studies, that explicitly account for the annual cycle in monthly mean ozone data, apply a range of sinusoidal terms in the regression equation to remove the annual cycle (i.a. *Fleming et al.*, 2007; *Vyushin et al.*, 2007; *Brunner et al.*, 2006; *Newchurch et al.*, 2003; *Fioletov et al.*, 2002; *SPARC*, 1998). Here, however, this approach results in an excessively high yearly residual autocorrelation of the deterministic model (not shown), signifying that sinusoidal terms do not fit the annual cycle well.

To overcome the yearly autocorrelation, this Chapter adopts an approach similar to that in *Soukharev and Hood* (2006). A long-term mean annual cycle is determined from the E39/C ozone data prior to the MRA, using the full data set length of 60 years. Then, the resulting annual cycle is implemented into the regression equation in terms of an ordinary ozone predictor without the sinusoidal expansion given by Equation 3.4. In case of the SH mid-latitudes, which display a robust trend, the annual cycle is calculated from detrended data.

Time lags

Time lags not only apply in case of the QBO, but also in case of the other monthly varying predictors ENSO and SULF. Following the approach by, i.a., *Bodeker et al.* (1998), optimum time lags (Table 3.1) are determined by fitting the full combined regression model for a range of monthly lags up to 24 months, finally adopting the lag which is associated with a minimum RSS. The remaining ozone predictors, ODS and SSC, vary on the scale of several years or more slowly and in this case time lags only negligibly reduce the RSS.

3.4 Description of the regression requirement diagnostics

As for any MRA studies, applying MRA with the present regression model necessitates the usage of certain diagnostics that are crucial to come to some important decisions: if iterative weighting applies, if a particular deterministic ozone predictor should enter the regression equation, which order n of the statistical model $AR(n)$ is appropriate, and if the regression requirements of parsimony and independent normally distributed residuals are met. This section assesses if weighted regression is necessary, introduces parsimony tests, discusses the associated results, and finally defines the diagnostics of residual autocorrelation and distribution. It is important to recall that the regression requirements must hold in order to get valid confidence bands and intervals.

3.4.1 Stationarity

The iteratively weighted MRA results in significantly thinner confidence bands than the equivalent MRA without weighting (not shown), which is a typical effect (*Carroll and Ruppert*, 1988). For the three latitude bands, the standard deviation ratio of the noisiest and the least noisiest month of the year has a value of around 3.0, 2.8 (January:July) for the tropics, 3.2 (February:September) for the NH mid-latitudes, and 3.2 (September:February) for the SH mid-latitudes. Thus, according to *Carroll and Ruppert* (1988), the use of weighted least squares is necessary. For the tropics and NH mid-latitudes, the iterative weighting routine converges quickly after a few iterations, but more slowly for the SH mid-latitudes where the monthly standard deviations begin to stabilise only after about ten iterations. In case of suboptimal ozone predictors, the routine may not converge at all.

3.4.2 Parsimony

Under certain circumstances, individual MRA statistical diagnostic tools can mislead, particularly in case of nonlinear MRA. Therefore, when examining parsimony, several diagnostics should be consulted that rely on different characteristics of a particular MRA result (*Draper and Smith*, 1998; *Milionis and Davies*, 1994).

Here, the approach by *Pandit and Wu* (1983) as well as the following tests are applied. The statistical significance of a regression parameter reducing the RSS is tested via the F-statistics at the 95% probability level. Also, deterministic as well as stochastic parameter confidence intervals should not include zero, except for the sinusoidal phase parameters (Equation 3.4) whose cyclic response does not change sign at zero parameter value. Each of the deterministic and stochastic parameters contributing to the regression equations (Table 3.1) are chosen to meet these criteria.

There is a range of other tests which are not used (i.a. *Draper and Smith*, 1998; *Ryan*, 1997). *Bates and Watts* (1988), for instance, provide a t-test which involves the statistical significance of the ratio parameter estimate divided by the parameter confidence interval width.

Beyond the approach by *Pandit and Wu* (1983), the pairwise parameter correlation associated with the approximate correlation matrix is assessed. *Bates and Watts* (1988) argue that the pairwise parameter correlation coefficients of a nonlinear regression model should definitely not exceed the absolute value of 0.99, indicating detrimental overparameterisation. The present MRA considers a higher amount of data points than the data sets which *Bates and Watts* (1988) typically analyse, and the nonlinearity for most of the parameters is not great (Section 3.5.3); hence, some critical value markedly lower than 0.99 is probably more appropriate. The combined regression model of this Chapter appears

to meet this 0.99 requirement: the pairwise correlation coefficients are weaker than 0.01 for the three latitude bands, except for the ODS trend terms at SH mid-latitudes which display a peak pairwise correlation of about 0.18.

Both multicollinearity of several parameters and pairwise collinearity tend to inflate the widths of confidence intervals and bands, and violate the principle of parsimony (i.a. *Ryan, 1997*). Awareness is hence important of the correlation matrix helping detect pairwise collinearity, but not multicollinearity. The statistical diagnostic of variance inflation factors helping to detect multicollinearity (i.a. *Ryan, 1997*) is beyond the scope of this Chapter, but a useful performance of the test in terms of nonlinear regression is not granted anyways. Using orthogonalised ozone predictors would indeed circumvene the problem of collinearity, but would also complicate the physical interpretation of the individual predictors (i.a. *Draper and Smith, 1998*).

3.4.3 Residual autocorrelation and distribution

In order to validate the regression assumptions of independent and normally distributed residuals, checks of the residual autocorrelation and distribution apply. According to *Pandit and Wu (1983)*, the null hypothesis of independent residuals at any given lag is rejected at the 95% (99%) probability level if the residual autocorrelation for the lag lies outside the confidence limit $\pm 1.96/\sqrt{T}$ ($\pm 2.32/\sqrt{T}$), where T is the number of data points; in this context, the residual autocorrelation function is commonly plotted out to a lag of roughly $T/5$.

The above approach does not account for autocorrelations at successive lags tending to depend on each other. Hence, the large-lag standard error of the autocorrelation function (i.a. *Box et al., 1994*) gives a more appropriate confidence limit (Figures 3.4a, 3.5a, and 3.5b). If the autocorrelation function at any lag lower than $T/5$ exceeds the limit clearly, the regression model should have a more suitable deterministic part, or a higher order stochastic component. Following straightforward considerations there is a 5% (1%) chance of the autocorrelation at any lag exceeding the 95% (99%) confidence limit even if the null hypothesis holds. It is therefore a good idea to seek physical causes behind statistically significant autocorrelation.

In order to give a rough indication of the residual distribution, of the existence of outliers in particular, residuals plots are provided together with levels of standard deviation as a function of time. Outliers are usually defined as those residuals which are at least three to four standard deviations away from zero (i.a. *Ryan, 1997*). Distribution plots are not shown, though these have been made and do not reveal severe departures from normality such as double peaks or strong skewness, but tend to indicate a more heavily than normal tailed residual distribution.

3.5 Response confidence band validation

This Section assesses if the response confidence bands are valid for the given predictors, being the case if the MRA fulfills the regression assumptions (see Sections 3.0.3, 3.2.2, and 3.4). The Sections 3.4.1 and 3.4.2 already demonstrate the validity of stationarity and parsimony, respectively, and leave to the following passage the assessment of independence, normal distribution, and asymptotic linearity.

The total response confidence bands (Figure 3.3) account for the combined ozone response to all of the ozone predictors listed in Table 3.1, except for the seasonal cycle. Note that the seasonal cycle confidence bands each display a reasonable width (not shown), but their inclusion into the total response complicates the interpretation of interannual variability.

It is important to recall that a given set of predictors determines the regression line; but any given predictor is unlikely to account for the associated ozone-modulating physical process entirely (Section 3.0.3). For instance, even in case a given deterministic regression model may contain a QBO response predictor, the model will most likely not remove the entire ozone QBO signature (Section 3.3.2). A stochastic model is then needed to eliminate the corresponding residual autocorrelation.

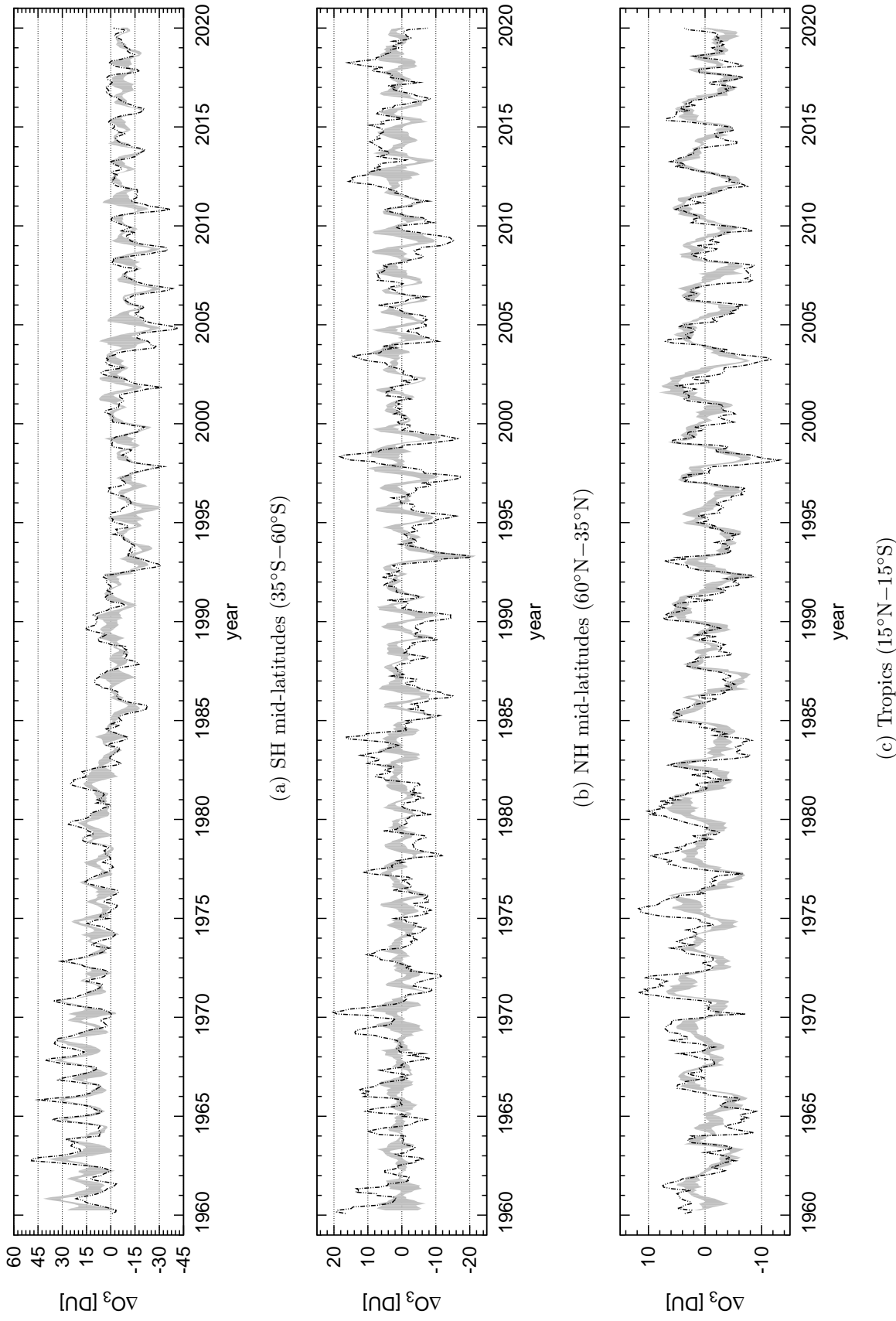


Figure 3.3: Deseasonalised threefold ensemble means (E39/C scenario REF) of monthly-zonal mean total column ozone for different latitude bands (black dashed-dotted lines), and the corresponding 95% response confidence bands for all regression parameters except for the seasonal cycles (grey shadings). Both deseasonalisations and respective regression seasonal cycles consider the same period 1960 to 2019.

Table 3.1: Characteristics of the deterministic regression predictors and associated seasonal expansions that contribute to the MRA. Figure 3.1 depicts the underlying predictor times series, which refer to boundary conditions of the E39/C scenario REF. The Table does not list the annual cycle predictors being of minor importance to the present Chapter. The last column refers to the orders n and parameter values of the stochastic AR(n) model parts.

	<i>QBO</i>	<i>ENSO</i>	<i>SULF</i>	<i>SSC</i>	<i>ODS</i>	AR(n)
<i>SH mid-lat.</i> ¹						
<i>periods [yrs]:</i>	$c + \frac{1}{1}$	–	c	c	$c + \frac{1}{1} + \frac{1}{2} + \frac{1}{3} + \frac{1}{4}$	$n = 2$
<i>lag [mths]:</i>	10	–	8	–	–	–
<i>level [hPa]:</i>	50	–	50	–	10	–
<i>lat. band:</i>	–	–	35°S–60°S	–	90°N–90°S	–
<i>comments:</i>	–	–	ODS-	–	–	$\Phi_1 = 1.22$
	–	–	-weighted	–	–	$\Phi_2 = -0.33$
<i>NH mid-lat.</i> ²						
<i>periods [yrs]:</i>	$c + \frac{1}{1}$	$c + \frac{1}{1}$	c	–	$\frac{1}{1}$	$n = 2$
<i>lag [mths]:</i>	0	8	15	–	–	–
<i>level [hPa]:</i>	20, 30	–	50	–	10	–
<i>lat. band:</i>	–	–	60°N–35°N	–	90°N–90°S	–
<i>comments:</i>	–	–	ODS-	–	–	$\Phi_1 = 1.01$
	–	–	-weighted	–	–	$\Phi_2 = -0.17$
<i>tropics</i> ³						
<i>periods [yrs]:</i>	$c + \frac{1}{1}$	$c + \frac{1}{1}$	c	c	–	$n = 2$
<i>lag [mths]:</i>	0	1	–	–	–	–
<i>level [hPa]:</i>	20, 30	–	50	–	–	–
<i>lat. band:</i>	–	–	15°N–15°S	–	–	–
<i>comments:</i>	–	–	ODS-	–	–	$\Phi_1 = 0.95$
	–	–	-weighted	–	–	$\Phi_2 = -0.08$

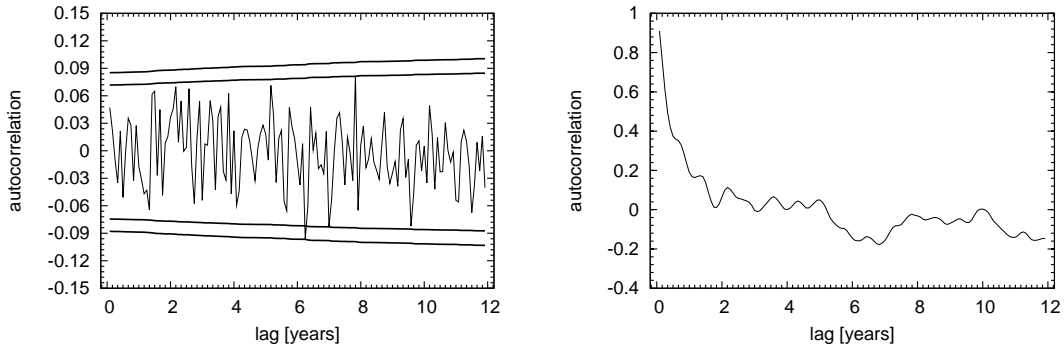
¹35°S–60°S, ²60°N–35°N, ³15°N–15°S.

3.5.1 Independent residuals

The importance of the AR(2) stochastic part (Table 3.1) is evident in a drastic reduction of residual autocorrelation when going from the pure deterministic model (Figure 3.4b) to the deterministic/stochastic combined model (Figure 3.4), particularly at lags shorter than about two years. Obviously, the stochastic component removes much of the ozone variability not being covered by the deterministic model alone; Section 3.0.3 briefly outlines some of the physical processes which can cause residual ozone persistence that needs to be removed by a stochastic

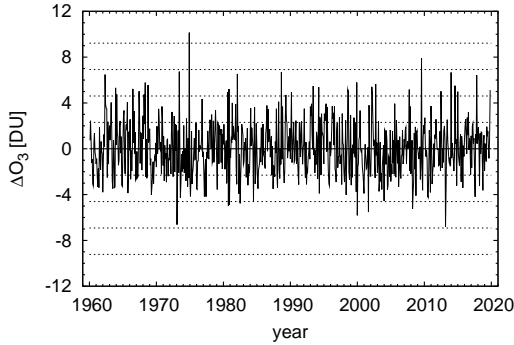
model part. The AR(2) stochastic component has a similar effect in case of both the NH mid-latitudes and the tropics (not shown).

The series of SH mid-latitude residual autocorrelations (Figure 3.4a) does not display an obvious structure, and the individual values lie mostly inside the 0.95% confidence limit, indicating that the null hypothesis of zero autocorrelation is not to be rejected for most of the lags; only the lag at 6.25 years reaches the 99% level. Though the high significance might be accidental, since for Figure 3.4a the expected number of lags reaching the 99% level is 1.44, even in case the null hypothesis holds. Thus, there are no indications against the null hypothesis from a pure statistical perspective. The expected number of 1.44 refers to each of the 144 individual monthly autocorrelations depicted having a chance of 0.01 to reach the 99% level in case the null hypothesis is true.

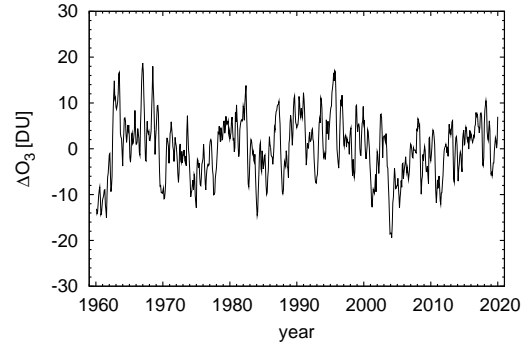


(a) Combined model: residual autocorrelations

(b) Deterministic model: residual autocorrelations



(c) Combined model: residuals and associated sigma intervals



(d) Deterministic model: residuals

Figure 3.4: SH mid-latitude residual autocorrelations with confidence limits at 95% (inner lines) and 99% (outer lines) probability; residuals as a function of time and associated sigma intervals.

The attribution of physical causes behind the highly significant 6.25 year lag is ambiguous; for instance, straightforward considerations suggest that the beat

frequencies of the QBO with respect to the annual cycle result in various autocorrelation peaks at scales of several months (*Steinbrecht et al.*, 2004; *Newchurch et al.*, 2003) but also at several years (not shown). The AR(2) stochastic part may then remove the monthly-, but maybe not the yearly-scale autocorrelations, and therefore leave the 6.5 year peak.

As for the SH mid-latitudes, the series of NH mid-latitude residual autocorrelations (Figure 3.5a) does not reveal an obvious structure either. None of the individual autocorrelations reaches the 99% level, but a total number of seven autocorrelations hits the 95% confidence limit; the number still falls within the expected number of 7.2 individual autocorrelations (144 monthly autocorrelations each with a chance of 0.05 to reach the 95% level). To speculate, the three significant peaks at yearly and shorter lags could refer to residual QBO- or ENSO-related variability, and so mirror physically plausible autocorrelations requiring an improvement of the respective deterministic predictors. A stochastically-based removal probably involved a full ARMA(n, m) approach, the order (n, m) of which to be determined by partial autocorrelation functions (*Box et al.*, 1994).

The tropics (Figure 3.5b) clearly violate the null hypothesis of zero autocorrelations, since the number of five autocorrelations reaching the 99% limit is significantly larger than the expected number of 1.44, and the autocorrelations tend to favour positively significant values. The peak at six months may be associated with the QBO or ENSO, and hence require better suitable deterministic predictors; alternatively, a full ARMA(n, m) stochastic model could apply.

In conclusion, the residual autocorrelations are likely to not affect the validity of the SH mid-latitude response confidence bands, but indicate a minor degree of caution for the NH mid-latitudes, and some scepticism for the tropics.

3.5.2 Normal distribution

It is obvious that the AR(2) stochastic part of the combined model both dampens the amplitudes and modifies the distribution towards a more important contribution by small amplitudes, consequently makes the distribution more normal (Figures 3.4d and 3.4c); the AR(2) stochastic contribution exerts a similar effect on the NH mid-latitudes and the tropics (not shown). The following discussions exclusively refer to the deterministic/stochastic combined models.

For all of the three latitude bands, distribution plots (not shown) suggest that the residuals of smaller than $\pm 2\sigma$ amplitude follow the shape of a normal distribution well. In order to validate the residuals distribution beyond the $\pm 2\sigma$ limit, simple characteristics of the normal distribution are used; note that parametric distribution tests have not been done. A normal distribution with 720 degrees of freedom, the number of monthly data for this Chapter, has an expected number

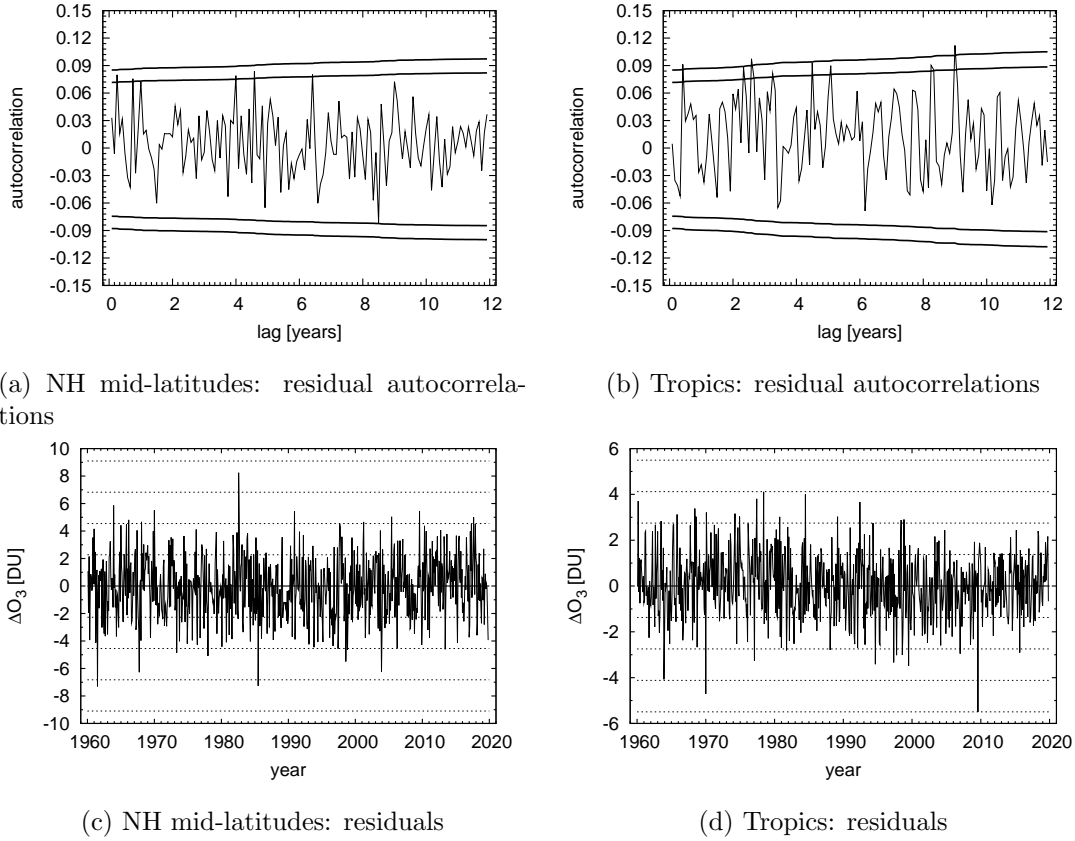


Figure 3.5: NH mid-latitude and tropical residual autocorrelations with confidence limits at 95% (inner lines) and 99% (outer lines) probability; residuals as a function of time and associated sigma intervals.

of 33 samples beyond the $\pm 2\sigma$ limit, 2 samples beyond the $\pm 3\sigma$ limit, and 0.05 samples beyond $\pm 4\sigma$ limit.

Hence, the negative tail of the SH mid-latitude distribution (Figure 3.4c) does not indicate a severe departure from normality, whereas the positive tail is heavier than normal. For the NH mid-latitudes (Figure 3.5c), on the other hand, there are no clear indications against a normality assumption. Also, the tropics (Figure 3.5d) do not violate a normality assumption when considering the whole time span 1960 to 1999. Considering shorter time spans, the positive tail seems to be heavier than normal prior to the year 2000, but lighter than normal afterwards, indicating decadal instationarity that may either result from a decadal trend in the boundary conditions or reflect the year 2000 step in boundary conditions: the REF scenario (1960–2019) investigated here consists of the two different scenarios PAST (1960–1999) and WARM (2000–1999) (Section 3). The latter two scenarios differ, for instance, in their prescribed SSTs, since they use observed SSTs for PAST but AOGCM modelled SSTs for WARM.

In summary, the respective residuals distributions do probably not affect the

validity of the NH mid-latitude response confidence bands, but some precaution is required in case of both the SH mid-latitudes and the tropics.

3.5.3 Asymptotic linearity

The profile trace functions for both the SH mid-latitudes and the tropics (Figures 3.6a and 3.6c) display a weak curvature, and accordingly a weak degree of nonlinearity. Usually, nonlinearity can cause asymmetric parameter confidence intervals, meaning that the two sides of a particular nonlinear interval may not be equally long (*Bates and Watts*, 1988). The resulting percental departures refer to interval nesting (Section 3.0.3), and apply to both deterministic and stochastic regression parameters.

At SH mid-latitudes, the interval nesting shows that nonlinearity stretches the lengths of the 95% one-sided parameter confidence intervals by less than 3.5%, compared to the linear approximation. Some of the one-sided lengths even shorten by a small amount. In case of the tropics, the broadening is smaller than 4.7%, except for the QBO response phase parameter which displays a 7.5% length increase of the positive interval side. Interestingly, nonlinearity narrows the other QBO-associated one-sided intervals by an amount of up to 9.5%.

Similarly to the SH mid-latitudes and the tropics, the NH mid-latitude curvature (Figure 3.6b) is weak, and nonlinearity stretches the one-sided intervals by less than 4.3%. The positive interval side of the ENSO response sinusoidal phase parameter (Table 3.1) represents a noticeable exception. Due to its prominent kink visible in Figure 3.6b, the interval length formally increases by 164%; but a statistics literature survey for this awkward situation has remained inconclusive. Only *Uusipaikka* (1996) appears to touch the issue of monotonous profile trace functions. But there does probably not exist literature which covers the nonlinearity of autoregressive models with nonlinear seasonal parameters. It is nevertheless tempting to assume that the cyclicity of sinusoidal phase parameters might allow for a linear extrapolation, simply neglecting the kink.

For all of the three latitudinal means, in conclusion, nonlinearity broadens the linearly approximated parameter confidence intervals by less than 7.5%, and even narrows some of the confidence intervals. The usage of nonlinear response confidence bands is consequently not necessary (Section 3.0.3) for the present ozone data analysed and the present regression model used. That is an important and not self-evident result because it is very unlikely that MRA studies in ozone research are aware of the nonlinear-curvature problem at all. Note that this result is not necessarily transferable to other studies since the degree of nonlinear curvature is likely to depend, i.a., on the data set length (see Section below).

Prominent nonlinear behaviour only arises in case of the NH mid-latitudes, and is associated with the ENSO response sinusoidal phase parameter. Last,

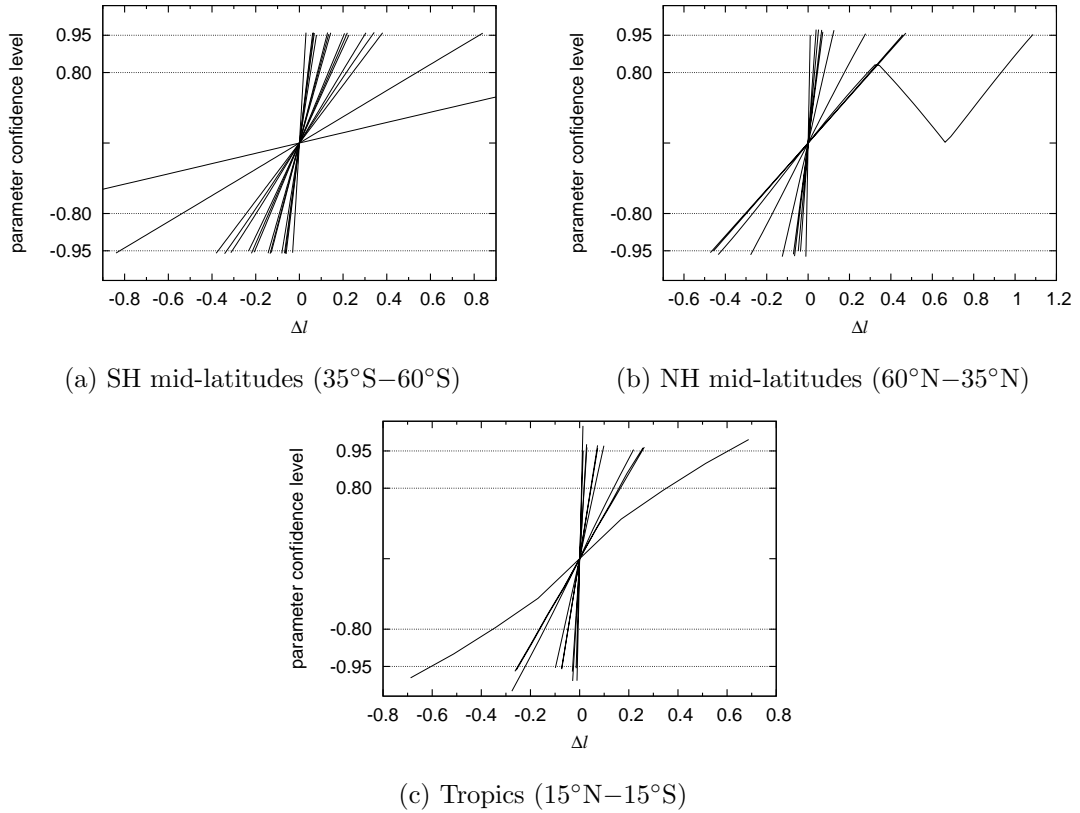


Figure 3.6: Regression parameter confidence level as a function of the departure Δl from the optimum parameter value (Section 3.2.2). Each square-root profile trace function (solid lines) refers to one of the regression parameters listed in Table 3.1, and for each of the parameters in Table 3.1 the trace function is depicted. The 95% confidence interval, for instance, for any particular regression parameter is given by the abscissa projection of the intersection between the function and the $\pm 95\%$ parameter confidence levels. Departures of any particular function from a straight line denote nonlinearity of the regression model with respect to this particular regression parameter. The stronger the departure from a straight line, the stronger the degree of nonlinearity is.

for all of the three latitudinal means the degree of nonlinearity for the nonlinear deterministic seasonal parameters (Equation 3.4) is greater than that for the other deterministic parameters, whose nonlinearity exclusively relates to the stochastic model (Equation 3.3).

3.5.4 Validation of the Cochrane-Orcutt transformation

According to the above Section 3.5.3, the degree of nonlinear curvature is weak for the given deterministic/stochastic regression models. These combined regression

models are of the stochastic order AR(2) (Table 3.1), for which the Cochrane-Orcutt transformation is not applicable in a strict sense; it is applicable in case of AR(1) (Cochrane and Orcutt, 1949). However, for the same deterministic regression models mentioned above, but with an AR(1) stochastic part instead of AR(2), the degree of nonlinearity does not change much (not shown). The Cochrane-Orcutt transformation is hence approximately valid and iterative linear regression may be used without the cost of producing severe errors in the estimated confidence intervals and bands for both responses and parameters. Also, the kink in the NH mid-latitude phase parameter does not represent a constraint with regards to the validity of the transformation, as the kink mainly refers to the particular nonlinear representation of the seasonal expansion (Equation 3.4), and vanishes in case of a linear representation (Equation 3.5) (not shown).

It is fortunate that the present analysis demonstrates a weak degree of nonlinearity associated with autoregression. Note that a more disadvantageous result would have cast into doubt most of the regression analyses in stratospheric ozone research published/done so far, since autocorrelation is a fundamental property of stratospheric ozone time series. Still, checks of least-squares surface contortion need to be carried out whenever nonlinearity arises from deterministic or moving-average regression parameters.

Also, it is important to keep in mind that the degree of nonlinearity depends on the type of the regression model as well as on the data investigated (Bates and Watts, 1988); shorter ozone time series, that is weaker amounts of degrees of freedom, might well display a stronger nonlinear curvature of the least-squares surface (Benabbas *et al.*, 2005). Besides, iterative linear regression does not permit the use of nonlinear seasonal expansions, which appear to be more parsimonious than linear expansions (Section 3.3.1). Last, linear regression is simply unusable in case of ARMA(n, m) ($n, m > 0$) stochastic models, or, in case of nonlinear interactions among deterministic predictors (Section 3.6.2).

3.6 Interannual variability

The above Section 3.5 defines the total response confidence bands (Figure 3.3), and shows that the characteristics of both the regression residuals and the sum of squares surfaces do probably not affect the validity of the bands severely. A certain degree of irregularity seems to necessitate some caution about the exact band widths; yet the band widths are assumed to be correct.

Table 3.1 lists the predictors which contribute to the total bands. The inclusion of additional predictors shown in Figure 3.1 but not listed by the Table is insignificant and tends to violate the regression assumptions (not shown). The present Section discusses the individual response confidence bands that refer to the listed predictors, hence attributes and quantifies interannual variability,

and investigates individual events such as the 1985 SH mid-latitude low-ozone anomaly. It is emphasised, in this context, that the confidence bands reflect the unique characteristics of the given set of predictors (Figure 3.1), and change when using other predictor time series. Also, it must be born in mind that, because of graphical representation, the confidence band widths appear thicker the more parallel to the abscissa the bands run, and appear narrower the less parallel to the abscissa the bands are oriented.

3.6.1 Southern hemispheric mid-latitudes

For the SH mid-latitude data, the QBO, SSC, SULF, and ODS response predictors (Table 3.1) are both statistically significant and improve the compliance with the regression assumptions (not shown). With regards to ENSO, the MRA does not verify a statistically significant response, in contrast to the NH mid-latitude and tropical time series which display a distinct ENSO signal. Last, the QBO-related amplitudes maximise in case of the SH mid-latitudes.

QBO

Obviously, the constant QBO term causes an interannual variability of about ± 5 DU (Figure 3.7a) that covaries with the 50 hPa QBO time series (Figure 3.1b). The seasonal expansion induces an additional departure which displays peaks of up to $-5/+3$ DU beyond the constant term. The departure does not occur every year because the impact of the QBO is seasonally synchronised: a particular phase of the QBO time series needs to coincide with a particular phase of the yearly seasonal expansion. Section 3.0.2 provides the respective physical background.

Together, the constant and seasonally expanded QBO predictors cause a maximum deviation of about $-11/+6$ DU. In this respect, the year 1985 is exceptional in that it displays a strong seasonally synchronised negative departure, but, at the same time, seasonal synchronisation does not magnify the adjacent QBO-related ozone minima during 1983 and 1988. Last, the departures mentioned above refer to the outer margins of the confidence bands, and, by definition, the whole bandwidths should be considered.

It ought to be noted here that the QBO seasonal synchronisation at SH and NH extratropical latitudes complicates a direct comparison of the QBO response to results from other studies. The reason is that many studies do not account for the seasonal synchronisation (i.a. *Fleming et al.*, 2007; *Fioletov et al.*, 2002), use other approaches to consider the synchronisation (i.a. *Steinbrecht et al.*, 2006b; *Newchurch et al.*, 2003), analyse individual zonal means without averaging latitudinally (i.a. *Randel and Wu*, 1996; *Yang and Tung*, 1994), or apply an approach

related to this Chapter but do not average longitudinally or altitudinally (i.a. *Bodeker et al.*, 1998). Finally, it is worth noting that the regression model captures a large fraction of the seasonally synchronised QBO-related ozone modulation (Figure 3.3a), adopting an approach criticised by *Newchurch et al.* (2003).

SSC

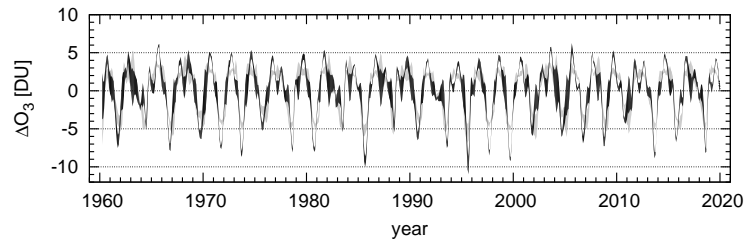
Depending on the intensity of a particular SSC predictor maximum (Figure 3.1b), the amplitude of SSC-induced ozone modulations ranges from about 4 DU for the weakest cycle to about 7 DU for the strongest cycle (Figure 3.7b); in this context, the year 1985 coincides with a SSC minimum. The amplitude range mentioned above is in basic agreement with that in the MRA study by *Steinbrecht et al.* (2006b, Figure 13), who analyse, i.a., a subset of E39/C scenario REF data and TOMS satellite observations for the months December to February.

The SSC confidence band width depends on the season, being broadest during late southern summer, and narrowest during late southern winter. This seasonal cycle refers to the iterative weighting and reflects the seasonally-dependent variance of SH mid-latitude ozone, which probably refers to dynamic features (Figure 9 in *Dameris et al.*, 2005; *Fusco and Salby*, 1999); in the absence of weighting the confidence band broadens, becoming nearly seasonally independent (not shown), which is not realistic.

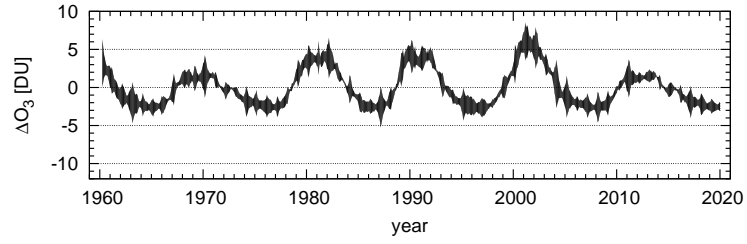
SULF

Similarly, a seasonally dependent confidence band width also arises in case of the SULF predictor (Figures 3.1c and 3.1b). The SULF confidence band (Figure 3.7c) is obviously more susceptible to both the seasonally dependent variance and the regression residuals (Figure 3.4c). The reason is probably that the small number of three volcanic eruptions results in a weak effective amount of degrees of freedom. Nevertheless, the eruption of Pinatubo is associated with a peak negative departure of -5 to -10 DU, the eruption of El Chichon with a small negative departure in 1983 and 1984, but also in 1985 via a barely visible displacement of the confidence band. The eruption of Agung, too, causes a slight confidence band displacement. Note that the small impact of the El Chichon and Agung eruptions, relatively to that of Pinatubo, both refers to the weaker eruptive scale and to the weaker ODS-concentrations (Figure 3.1).

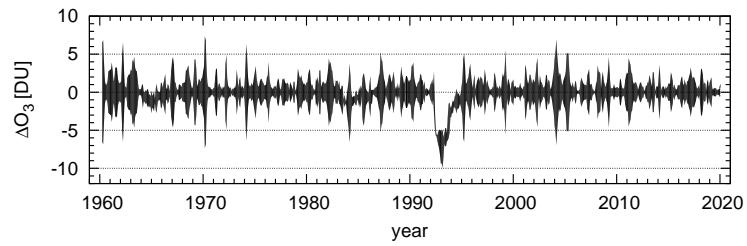
The Pinatubo-related peak departure is associated with a -1.2 to -2.2% deviation relative to the 1960–2019 SH mid-latitude mean annual cycle. A direct comparison to published Pinatubo response has not been done, as most of the publications seem to give percental deviations relative to various different base



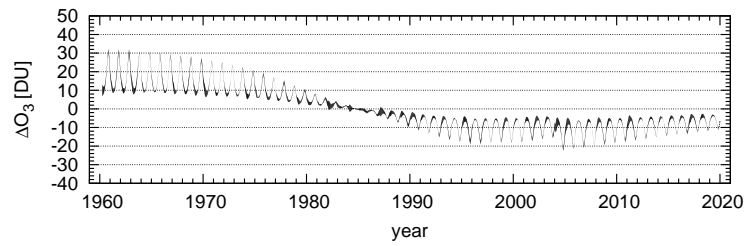
(a) QBO constant term only (gray), QBO constant term plus yearly expansion (black)



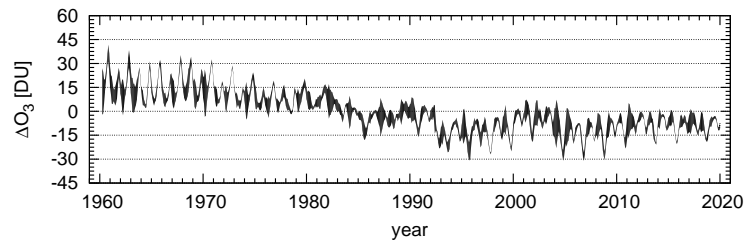
(b) SSC



(c) SULF



(d) ODS



(e) Total response of QBO, SSC, SULF, and ODS

Figure 3.7: Response confidence bands at the 95% probability level for the SH mid-latitudes (35°S – 60°S).

periods. Yet the deviations are in at least order-of-magnitude accord with those presented in, i.a., *Kirchner et al.* (1999); *McCormick et al.* (1995); *Randel et al.* (1995); *Zerefos et al.* (1994).

ODS

Due to the seasonal expansion (Table 3.1), the ODS-related trend (Figure 3.7d) is seasonally dependent; the strongest trend occurs during the southern early summer, likely associated with heterogeneously ozone-depleted air advected from polar latitudes after the wintertime polar vortex has broken down (*Fioletov and Shepherd*, 2005; *Chipperfield*, 2003). The weakest trend arises during the southern winter, when transport dominates column ozone and the effect of the heterogeneously ozone-depleted air is largely erased (*Salby and Callaghan*, 2004b). Around the year 2000, compared to the 1960's, the ODS response is associated with an ozone decrease of about 50 DU during the southern early summer, and of about 15 DU during the southern winter.

Apparently, the seasonality of the ODS response minimises around the year 1985 (Figure 3.7d); in this case, the seasonality is accounted for by that particular predictor which represents the average ozone annual cycle (not shown) over the full period 1960 to 1999 (Section 3.3.2). A different view is that the seasonally dependent ODS response is identical with a time evolution of the column ozone annual cycle.

Total ozone response and 1985 negative ozone anomaly

The total confidence band in Figure 3.7e comprises the combined response to all of the predictors mentioned above, except for the ozone average annual cycle. Obviously, ODS-related trend, SSC-induced decadal variations, and the SULF-related negative departure in 1992/1993, cause a decadally stepwise ozone decrease; the latter is clearly identifiable in *Dameris et al.* (2006, Figure 1) for both measured and modelled deseasonalised globally averaged total column ozone, and in *Lee and Smith* (2003) for satellite data.

For the year 1985, the total response confidence band (Figure 3.7e) yields a negative anomaly with a maximum departure in August of about -18 DU (lower band margin) to -7 DU (upper band margin). The margins of the band are below -10 DU (lower margin) and -7 DU (upper margin) during the period August to December, and both margins remain below zero during the period February 1985 to February 1986. As a consequence, there is good temporal consistence with the annual evolution mentioned in *Bodeker et al.* (2007) and shown in *WMO* (2007, Figures 3-3, 3-5, and 3-11).

The 1984 and 1987 adjacent negative peaks of the lower band margin are accompanied by positive peaks of the upper band margin, and differ in this respect from the peak during 1985 which displays negative departures for both margins. The 1984 and 1987 peaks do hence not reflect a robust response to a deterministic predictor, but largely result from the uncertainty accounted for by the stochastic model part.

In conclusion, the MRA shows that the SH mid-latitude 1985 negative ozone anomaly of the REF scenario (Figure 3.7e) is mainly associated with a negative departure by the seasonally synchronised QBO (Figure 3.7a), as well as with the ODS-related trend (Figure 3.7d). The latter makes the 1985 QBO response stand out of the preceding QBO-related negative peaks (Figure 3.7a). This finding is in accordance with the study by *Bojkov* (1987) for observed ozone data, but is for the first time here verified and quantified using MRA. SSC-related variability (Figure 3.7b) strengthens the REF 1985 anomaly further, and the volcanic eruption of El Chichon may also contribute (Figure 3.7c), but only very little.

It should be mentioned that *Bodeker et al.* (2007) focus on the physical aspects of QBO-related ozone interannual variability (Section 3.0.2), and do not agree on the importance of the ODS-related trend with regard to the 1985 event. The reason may be that *Bodeker et al.* (2007) do not account for ODS-related decadal changes in their analysis. Yet a similar low-ozone event during the year 1997 has been attracting research effort; the present analysis demonstrates that the most relevant stimulation is owing to the QBO and the 11-year solar cycle (Figure 3.7). This finding is in accordance with that by *Bodeker et al.* (2007) for the same year, since trend-like changes during the mid-1990's are weaker than those during the mid-1980's (Figure 3.7d). Finally, the MRA yields for all QBO definition heights (10 to 60 hPa) “year 1985” negative responses similar to that in Figure 3.7e (not shown), but the adoption of the QBO winds at 50 hPa effectuates the most extreme negative deviation.

A comparison of the actual deseasonalised E39/C model output with the total response confidence band (Figure 3.3a) reveals, that the E39/C model data in 1985 lie beyond the lower confidence band margin by a value of up to -4 DU during the period August to October, and by a weaker absolute amount during nearly the whole year 1985. It is thus likely that at least one of the deterministic regression predictors does not fully capture the associated physical process (Section 3.3.2), or that a significant predictor is missing. Nevertheless, the MRA still captures a major portion of the 1985 anomaly.

3.6.2 Northern hemispheric mid-latitudes

As for the SH mid-latitudes, the MRA for the NH mid-latitudes demonstrates statistical significance for the response predictors QBO, SULF, and ODS (Table

3.1). For any reason, the MRA does not verify a SSC-related ozone modulation; instead, there is a statistically significant ENSO-related component which the MRA does not imply for the SH mid-latitudes.

A comparison of the Figures 3.3a and 3.3b suggests that the MRA explains the deseasonalised E39/C model output for the NH mid-latitudes less tightly than that for the SH mid-latitudes. It seems, though, that part of the poorer description refers to the visualisation, being due to both the larger ordinate scaling and the weaker ODS-related trend in case of the NH mid-latitudes.

QBO

There is a significant QBO-related ozone response (Table 3.1), but the magnitude is only about half of the SH midlatitude QBO response (Figures 3.8a and 3.7a), and the seasonally synchronised peaks point in a positive direction, whereas these point in a negative direction for the SH mid-latitudes. The reason for the dissimilar pointing directions is unclear, but the fraction of time during which the QBO causes enhanced ozone levels seems to be greater for the SH mid-latitudes than for the NH mid-latitudes. Last, the QBO₅₀-response predictor is used for the SH mid-latitudes, but the QBO_{20,30}-response predictor for the NH mid-latitudes (Figure 3.1b), making a direct comparison questionable. Yet the general picture does not change much in case of adopting the QBO₅₀-response predictor for the NH mid-latitudes (not shown).

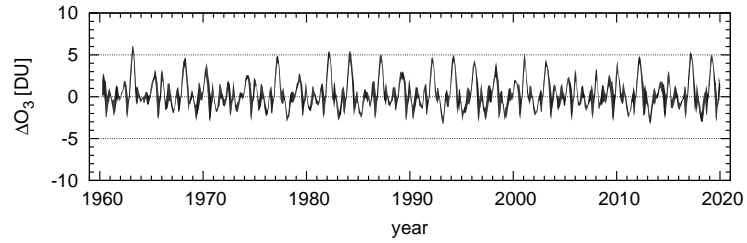
SULF

The impact of the Pinatubo eruption (Figure 3.8b) in DU is comparably intense to that for the SH mid-latitudes (Figure 3.7c), but displays a slightly larger percental deviation of -2 to -2.5% , relatively to the 1960–2019 NH mid-latitude mean annual cycle. In general, modelling studies of the Pinatubo ozone response tend to agree in that the NH and SH mid-latitude responses are of about the same quantitative extent. In observations, however, interannual variability seems to mask a possible SH Pinatubo-related ozone deviation (*WMO*, 2007).

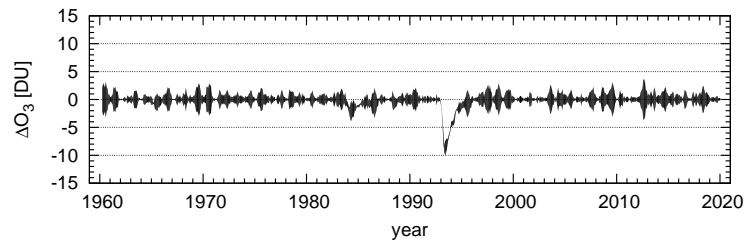
In relation to the SH mid-latitudes, the NH mid-latitude response to the El Chichon eruption displays a weaker noise level, and the eruption of Agung is barely visible (Figure 3.8b), a result of the weak NH mid-latitude SULF predictor during the period 1963 to 1966 (see Section 3.6.1: “SULF” and Figure 3.1).

SSC

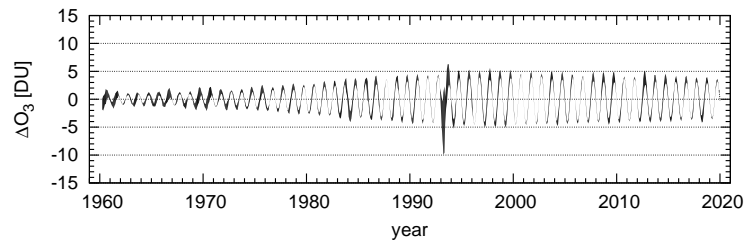
As mentioned above, this MRA does not support a statistically significant modulation by the SSC in case of the NH mid-latitudes. In contrast, *Dhomse et al.*



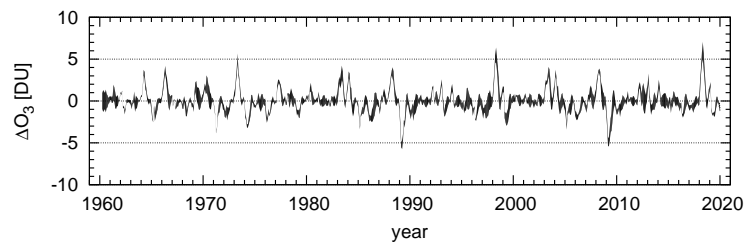
(a) QBO



(b) SULF



(c) ODS



(d) ENSO

Figure 3.8: Response confidence bands at the 95% probability level for the NH mid-latitudes (60°N – 35°N).

(2006) infer a SSC-related total column ozone variation of about 1 to 1.5 DU at NH mid-latitudes in their MRA analysis of zonally averaged SBUV satellite data of the period 1979 to 2004. Also, *Steinbrecht et al.* (2006b) show a statistically significant SSC modulation of zonal-mean total ozone during December-February in case of a E39/C scenario REF subset, as well as in case of other modelled data and satellite measurements. The weak amount of degrees of freedom of the REF subset might feign a statistically significant result as the authors do not validate the residuals distribution (Section 4.2.1).

ODS

In contrast to the SH mid-latitude long-term evolution, the NH mid-latitude ODS-related trend only includes a yearly seasonal expansion, and not a trend constant (Table 3.1). The trend constant is clearly insignificant and even increases the residual sum of squares; its exclusion is hence plausible, signifying that the trend does not contain an annual-mean component. The inclusion of the ODS seasonal expansion is at the border of statistical significance, but, on the other hand, its parameter confidence intervals are small compared to the parameter estimates (Section 3.4.2). Also, the ODS seasonal expansion definitely removes a clear pattern of yearly residual autocorrelation, and reduces the overall degree of residual autocorrelation (not shown). The ODS seasonal expansion is therefore judged to realistically represent a trend in NH mid-latitude total column ozone of the REF scenario.

The ODS-related trend at NH mid-latitudes during northern autumn is positive, in accordance with Figure 5d in *Dameris et al.* (2005) which displays total column ozone decadal differences, 1990's minus 1960's, for one of the three PAST realisations. Figure 6b in *Dameris et al.* (2005) shows that this positive trend in their Figure 5d results from the combination of a statistically significant increase of tropospheric ozone concentrations, and of a statistically insignificant increase of lower-stratospheric ozone concentrations. Results not shown here confirm these findings by *Dameris et al.* (2005) and reveal that the lower-stratospheric increase in their Figure 6b refers to a remaining QBO signal: *Dameris et al.* (2005) utilise one of the tree PAST realisations, but redoing their Figure 6b using the three-fold PAST ensemble average does not change much; only when one of the time series, 1960's or 1990's, is shifted by one year back or forth the positive stratospheric signal vanishes; the reason is that then the mean QBO phase in the respective 10-year average changes. Additional results not shown here demonstrate a considerable increase of NH mid-latitude lower stratospheric ozone concentrations for the 1990's of the past scenario compared with the 2000's and 2010's of the WARM scenario. It is likely that this statistically significant increase (not shown) represents the main feature detected by the ODS predictor for total column ozone during northern autumn (Figure 3.8c). Nevertheless, tropospheric positive ozone concentration trends may also contribute.

Above the lower stratospheric increase during northern autumn lies a robust feature of weakening ozone concentrations (not shown). To speculate, the lower stratospheric concentration increase could therefore result from BD circulation changes, similarly to the double-CO₂-induced BD circulation changes in *Jiang et al.* (2007), and refer to the tropical SSTs modulating planetary waves (next Section: “ENSO”). The lower stratospheric increase would either represent an artefact of the year 2000 switch from observed to modelled SSTs, or represent a realistic effect of the considerable mean-SST difference for the 1990’s compared with the 2000’s (Figure 2.1). On the other hand, an accompanying dynamically induced depression of tropical column ozone is not found, but the signal may be disguised by changes in other ozone-modulating mechanisms (Section 3.6.3). Last, in view of the results for northern autumn mentioned above, predictors are probably more appropriate that do not refer to ODS concentrations solely.

The ODS-associated trend during northern spring is negative, presumably in connection with a stronger polar heterogeneous ozone depletion covarying with increasing ODS-concentrations, part of the ozone-depleted air parcels being advected to NH mid-latitudes after the final warming (*Fusco and Salby, 1999*). It should be noted that not only ODS concentrations govern polar heterogeneous ozone depletion, but also climate-dependent properties that affect the polar vortex such as latitudinal differential heating and the characteristics of stratospheric planetary-wave activity (Section 2.7.2). It is hence likely, again, that an ODS response predictor adjusted for climate effects may be more efficient than the pure ODS shape shown in Figure 3.1a. Alternatively, the regression could incorporate two different trend parameters, one of which referring to the ODS shape, the other one to a global warming proxy. In future studies, such refinements to the NH mid-latitude trend assessment may even permit a quantification of those trend contributions that do not relate to stratospheric ODS concentrations. In case of the two-parameter approach the findings by *Phillips (2007)* deserve close attention, as multiple slowly varying predictors usually display a large degree of collinearity.

When comparing the period around the year 2000 with the 1960’s, the trend amplitude of -4 DU in total column ozone during northern spring is by about an order of magnitude weaker than its SH mid-latitude counterpart during southern early summer. The main reason is possibly that the northern polar vortex is more disturbed and warmer than the southern polar vortex, and the contribution to the trend by changes in heterogeneous ozone depletion is less important for the NH than the SH mid-latitudes (*Dameris et al., 2005; Fioletov and Shepherd, 2005; Chipperfield, 2003*).

ENSO

The ENSO-response contributes to the interannual variability significantly (Figure 3.8d), and associated peaks display maximum amplitudes of about ± 5 DU. Because strong ENSO events are rare (Figure 3.1a), intense ENSO-related ozone peaks occur less often than the seasonally synchronised QBO-related peaks. Both, positive and negative ENSO-related peaks mainly appear during northern spring, in accordance with indications by, i.a., *Clarke and Kim (2005)* that ENSO modulates the NH mid-latitude stratospheric planetary-wave activity, the modulation maximising during winter and spring when tropospheric planetary waves can cross the tropopause and propel the dynamically driven Brewer-Dobson circulation via dissipation in the stratosphere (Section 2.0.6).

It ought to be noted that there is a conceptual similarity in the mechanisms of planetary-wave activity modulation, by, on the one hand, ENSO-related tropical SST vacillations and associated convective latent-heat release variability, and, on the other hand, enhanced tropical latent-heat release due to warmer SSTs in a warmer climate (Section 2.2.1). Both mechanisms impact on the convective excitation of tropical internal planetary waves, whose small group and phase velocities together with the low-latitude easterly winds restrict the vertical propagation to the lower stratosphere, where the waves tend to dissipate strongly (*García-Herrera et al., 2006*). This is the mechanism, which, as Chapter 2 discovers, changes the tropical/subtropical lower-stratospheric Brewer-Dobson circulation in a warmer climate.

Also, both ENSO-related tropical SST variability and climate-dependent tropical SST changes appear to modulate the low-latitude convective excitation of external planetary waves that travel poleward within the troposphere, finally entering the stratosphere during winter and spring at mid and higher latitudes (*Calvo Fernández et al., 2004; Sassi et al., 2004; Inatsu et al., 2002; Diaz et al., 2001; Hall and Derome, 2000; Baldwin and O’Sullivan, 1995; Randel and Cobb, 1994; Blackmon et al., 1987; Garcia and Salby, 1987; Salby and Garcia, 1987*). That is the mechanism in *Clarke and Kim (2005)* mentioned above, by which ENSO appears to impact on the mid and higher latitude Brewer-Dobson circulation, and thus on total column ozone. Similarly, it is well possible that the contrast between observed (1960–1999) and modelled SSTs (2000–2019) (Figures 2.9 and 2.1) causes the positive trend in NH mid-latitude total column ozone during northern autumn (Figure 3.8c and Section above: “ODS”), when planetary waves begin to enter the extratropical stratosphere (*Dameris et al., 2005, Figure 9b*).

Finally, even though the ENSO-related variability of zonal mean diabatic heating is strongly asymmetric (*Gettelman et al., 2001*), ENSO still alters the tropospheric zonal-mean latitudinal temperature gradients (*Clarke and Kim, 2005*), thereby changing the Hadley circulation and the propagation characteristics for

planetary waves (*Seager et al.*, 2003).

It is today accepted that high ENSO events coincide with elevated levels of total ozone at NH mid-latitudes, with a time lag of a few months (*Brönnimann et al.*, 2006; *García-Herrera et al.*, 2006; *Manzini et al.*, 2006). Furthermore, it is tempting to assume that ENSO may impact on the northern polar vortex, and therefore possibly on the effect polar heterogeneous ozone depletion may have on NH mid-latitude ozone levels.

Nevertheless, *Manzini et al.* (2006) remain inconclusive about the impact of low ENSO events on NH mid-latitude planetary-wave activity. This implies an asymmetric ENSO-response, as already noted by *Hall and Derome* (2000); and *Zerefos et al.* (1992) argue that warm ENSO events, for instance that during 1982/1983, are associated with low total-ozone values at NH mid-latitudes, contradicting the findings mentioned above. It is worth noting that E39/C does not yield a large positive peak during 1982/1983 either (Figure 3.3b), possibly because the negative QBO-response during the same period opposes (Figure 3.8a).

Also, it must be considered that the occurrence of ENSO-related high and low tropical SST anomalies is locked to the annual cycle: intense ENSO events mostly occur during northern winter. The locking of the ENSO-related SST anomalies seems to result from an interaction of ocean Rossby waves with the seasonal variation of the tropical convergence zone (*Krishnamurti and Chakraborty*, 2005; *Sheinbaum*, 2003; *An and Wang*, 2001). The clustering to the northern winter of the ENSO-related NH mid-latitude ozone response might therefore partly be associated with the locking, and not only with the annual cycle of stratospheric planetary-wave activity.

Additionally, the locking of ENSO-related tropical SST anomalies to the northern winter is possibly the reason why the SH mid-latitude ENSO-related ozone signal is weaker than that for the NH mid-latitudes, and in the present study statistically insignificant: during the northern winter, the SH mid-latitude tropospheric planetary-wave activity cannot cross the tropopause, and so cannot carry an ENSO signal into the stratosphere (*García-Herrera et al.*, 2006).

E39/C shows a clear and strongly positive ozone response to the extreme warm ENSO events of the years 1997/1998, 2002/2003, and 2017/2018 (Figure 3.1a and Figure 3.3b), but the MRA underestimates these events. Part of this underestimation probably relates to an antagonism associated with the positive ENSO responses (Figure 3.8d) and the negative ODS amplitudes (Figure 3.8c); as mentioned above, both occur during the northern spring. It is possible that there is a nonlinear interaction between the two predictors which is not included into the present regression model. Presumably, ENSO may both modulate the mid-latitude Brewer-Dobson circulation and polar heterogeneous ozone depletion, amplifying the NH mid-latitude ENSO-related total ozone response the higher the ODS concentration levels are. In this context, the deseasonalised evolution of

total column ozone in Figure 3.2b suggests an influence of ENSO on the NH polar vortex: for the extremely warm ENSO events mentioned above, 1997/1998, 2002/2003, and 2017/2018, the northern polar vortex is weaker than normal. Note that high-ozone anomalies at NH polar latitudes during boreal spring signify an anomalously weak polar heterogeneous ozone depletion owing to a disturbed vortex.

Additionally, the impact of planetary waves themselves, and hence of ENSO, on the NH polar vortex might display a significant degree of nonlinearity, since wave-induced NH polar stratospheric warmings are associated with large modifications of the background flow; this flow modification may affect the latitudinal position of the planetary wave guides (Sections 2.7.2 and 4.1.1), and therefore possibly alter the NH mid-latitude Brewer-Dobson circulation in a nonlinear fashion.

Finally, some caution is appropriate with regards to the ENSO-response confidence band (Figure 3.8d), as the phase parameter of the ENSO yearly seasonal expansion displays a severe nonlinear kink (Figure 3.6b). It is unclear at present what the consequences are with respect to the interpretation of the confidence band (Section 3.5.3), but, to speculate, the kink might concern the above-mentioned nonlinearity in the E39/C ozone response to ENSO.

3.6.3 Tropics

The tropics display statistically significant contributions by the response predictors QBO, SSC, SULF, and ENSO (Table 3.1). In contrast to the SH and NH mid-latitudes, the MRA does not support an ODS-related trend for the tropics, which is a plausible result: in observational as well as CCM data the long-term ozone decline has a minimum in the tropics and increases towards the poles, with larger values in the SH than the NH mid-latitudes. In this context, polar heterogeneous ozone loss appears to account for the stronger decline in the extratropics substantially (*Eyring et al.*, 2006; *Fioletov and Shepherd*, 2005; *Chipperfield*, 2003).

Lack of multi-decadal trend

A close inspection of Figure 3.3c and Figure 3.2b reveals that the REF tropical column ozone during the 1960's is weaker than that during the 1970's, but subsequently appears to decrease near-monotonously. The low values of total-column ozone during the 1960's may consequently prevent the regression model to detect a tropical ODS-related trend, because the total-ozone time series differs from an inverse-ODS shape (see Figure 3.1a) too strongly. Similarly to the NH mid-latitude long-term evolution (Section 3.6.2: "ODS"), a different trend predictor might perform more efficiently.

Results that account for the QBO-related response, but are not shown, proof that the low total-column ozone values during the 1960's mainly refer to weak ozone concentrations in the tropical lower stratosphere; recall that the latter is dynamically controlled. Hence, to speculate, the tropical low-ozone anomaly during the 1960's may result from the tropical SSTs affecting stratospheric transport, following the mechanism presented in Chapter 2. Yet it is important to make clear that climate-change-induced lower ozone destruction rates do not play a role for the low-ozone anomaly investigated here. The effect of transport-induced weaker ozone concentrations on total column ozone during the 1960's may consequently be more obvious than that reported in Chapter 2.

The annual mean near-global SSTs shown in Figure 2.1 are indeed relatively low from 1964 to 1968, which could explain the tropical low-ozone anomaly in these years. Note that near-global mean SSTs contain a large tropical-SST signal (*Rayner et al.*, 2003) and that the 1960's do not display intense ENSO events (Figure 3.1a), which hence cannot interfere much.

From 1963 to 1966, ozone depletion associated with the eruption of Mount Agung (Figure 3.1c) may also contribute; its stratospheric impact occurs at lower-stratospheric levels (*Dameris et al.*, 2005) where the low-ozone anomaly resides. In this context, the regression model might underestimate the eruption-induced ozone perturbation as the regression accounts for the eruption-induced elevated levels of sulfate aerosol surfaces, but not for the associated temperature disturbance (Appendix A.2). The temperature disturbance might be relatively important, since ODS levels during the 1960's are weak and hence the sulfate surfaces are unlikely to trigger a strong tropical heterogeneous ozone depletion.

Last, *Dameris et al.* (2005) stress the importance of the SSC, together with the Agung eruption, for the unexplained tropical low-ozone anomaly during the 1960's. The present MRA does not support this interpretation as it accounts for the SCC-related response, and the SSC itself is known to hardly impact on ozone concentrations in the tropical lower stratosphere (Chapter 4). The ozone anomaly, though, mainly relates to the tropical lower stratosphere (see above).

QBO

The tropical QBO-related ozone response amplitude of about 8 DU (Figure 3.9a) is in excellent accordance with the amplitude in *Fleming et al.* (2007, Figure 10), who conduct a MRA of TOMS/SBUV merged satellite data. It is important to make clear that there is only a minor contribution by seasonal synchronisation in the tropics, which facilitates a comparison with the study cited above. Also, the findings presented here confirm that in E39/C the QBO-related ozone response causes the main portion of tropical total ozone interannual variability (Figures 3.9a and 3.3b), a well established result for both observational and CCM data

(WMO, 2007). Last, tropical and SH mid-latitude QBO-related response peaks clearly oppose (Figures 3.9a and 3.7a), which is in accordance with the physical mechanism given in Section 3.0.2. Interestingly, the opposition is less clear for the tropics and the NH mid-latitudes (Figures 3.9a and 3.8a).

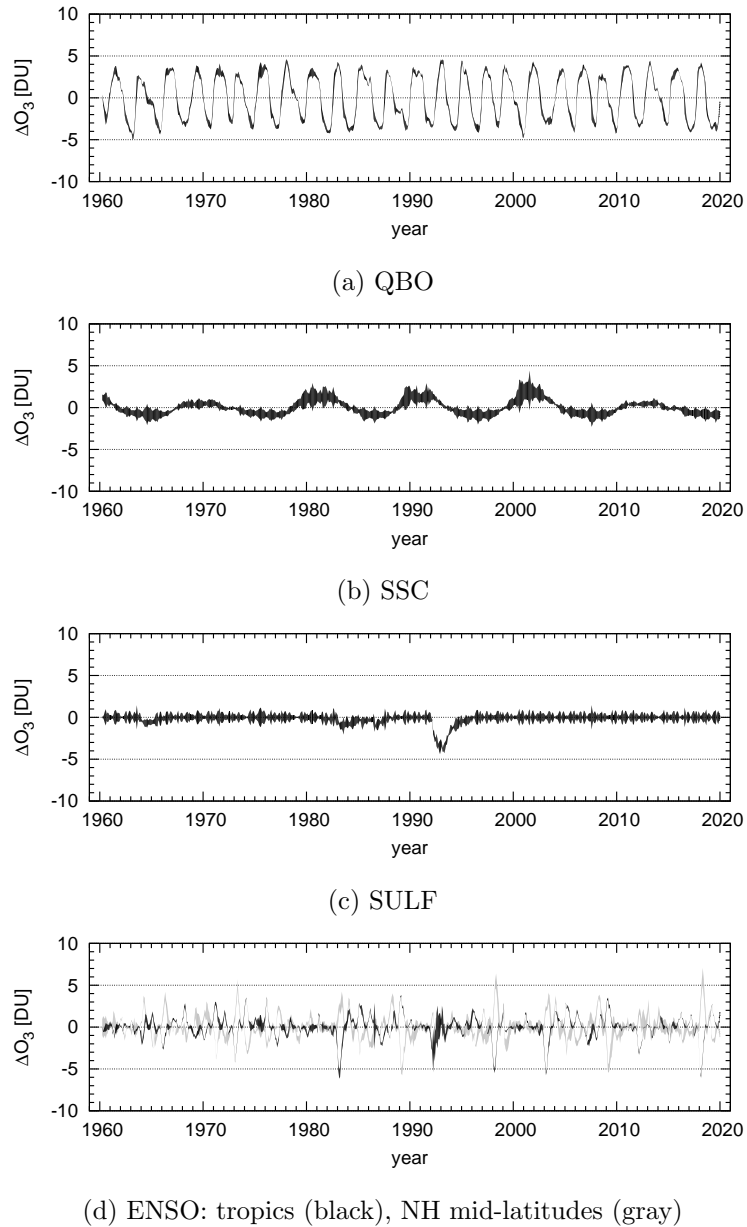


Figure 3.9: Response confidence bands at the 95% probability level for the tropics (15°N–15°S).

SSC

The tropical SSC-related ozone response displays an amplitude of about 3 DU for the most intense cycle during the 2000's, and amplitudes of about 2 DU for the weaker cycles (Figure 3.9b), in agreement with *WMO* (2007) and *SPARC* (1998).

It is interesting that the tropical SSC-related response is significantly weaker than that for the SH mid-latitudes (Figure 3.7b), even though the impact of the associated 11-year UV variability on ozone production maximises in the tropics (Section 4.1.2). Other studies confirm this result for both measurements and CCM data (i.a. *Steinbrecht et al.*, 2006b, 2003; *Fioletov et al.*, 2002). Supposedly, the Brewer-Dobson circulation transports the tropical SSC signal via SSC-modulated ozone concentrations to the SH mid-latitudes, where the air parcels accumulate, magnifying the SSC-associated signal (*Steinbrecht et al.*, 2006b; *Tourpali et al.*, 2005, 2003). Additionally, dynamical mechanism may contribute (*WMO*, 2007). An alternative explanation for E39/C is that the SSC-signal-containing NO_y upper boundary condition of the REF scenario (Section 4.2e) might exert a greater effect for the SH mid-latitudes than for the tropics.

SULF

In case of the Pinatubo eruption, the SULF-related ozone response displays a peak amplitude of about -3 to -4 DU (Figure 3.9c), corresponding to a -1 to -1.5% percental deviation relative to the 1960–2019 tropical mean annual cycle. Consequently, the tropics reveal a weaker peak response than the NH and SH mid-latitudes, which is realistic (*Randel et al.*, 1995; *Zerefos et al.*, 1994).

ENSO

Figure 3.9d shows that the tropical ENSO-related ozone predictor is associated with negative peaks of up to -5 DU, and with weaker positive peaks of roughly 3 DU. The negative peaks refer to intense warm ENSO events (Figure 3.1a), and oppose the NH mid-latitude response, where intense warm ENSO events correspond to positive ozone peaks (Figure 3.9d). This opposing ENSO-related ozone response is noted by *Brönnimann et al.* (2006). It corresponds with the finding by *Fusco and Salby* (1999) that the ozone variability in the tropics and the mid-latitudes during boreal winter tends to be reverse, as a result of hemispheric-scale interannual variability in the Brewer-Dobson circulation.

The opposing behaviour in Figure 3.9d hence supports the theory that the ENSO-related ozone response refers to an ENSO-related modification of the Brewer-Dobson circulation (Section 3.6.2). An enhancement of the Brewer-Dobson circulation is known to weaken the tropical total column ozone. The reason

is that ozone-poor tropospheric air enters the lower stratosphere more efficiently, but strengthens the mid-latitude total column ozone since the advection of ozone-rich air from lower latitudes increases (Sections 2.0.3 and 2.0.4). The MRA yields different optimum lags for the ENSO predictors (Table 3.1, Section 3.3.2), adopts a one-month delay in case of tropics, but an eight-month delay for the NH mid-latitudes. One might expect to find different lags, as the tropical ozone signal to a change in the Brewer-Dobson circulation establishes more quickly than the mid-latitude signal. The latter, compared to the former, is associated with a greater transport distance and a time-integral compressive accumulation of ozone-rich air (Section 2.0.4).

3.7 Summary and conclusion

This Section recapitulates the results obtained for each objective (Section 3.1) and gives recommendations for future work.

3.7.1 Objective 1

The MINPACK-1 software package for solving nonlinear least-squares problems has been successfully upgraded by routines that permit an efficient use of nonlinear seasonal deterministic/stochastic combined regression models in connection with iterative weighting and a validity assessment of asymptotic linearity. It is this particular combination of characteristics that has probably not yet been used in stratospheric ozone research, and to which the statistics literature seems to not pay much attention. Additional routines permit a calculation of both linearly approximated response confidence bands and nonlinear parameter confidence intervals. The use of these statistical inference features, too, appears to be new to stratospheric ozone research. It is unfortunate that a lack of resources prevented an implementation of initial value algorithms for autoregressive moving-average stochastic models, at present restricting the stochastic analysis to autoregressive decomposition. Nevertheless, the exceptional MRA results (see below) show that the current stage of development already represents a significant advancement.

3.7.2 Objective 2

(a)

Beyond pure curve fitting, a strength of multiple regression analysis is that it permits an empirical detection and quantification of multiple time-dependent quantities simultaneously, reducing the individual effect sizes needed to verify a

relationship. With this aim, the regression needs to obey implicit assumptions in order to yield trustworthy results. In this Chapter, the use of several different tools and diagnostics aims at preventing detrimental violations of the regression assumptions, the latter assumptions associated with parsimony of the regression predictors and stationary independent normally distributed regression residuals.

It is important to survey the characteristics of both, regression predictors and residuals distribution, as these represent antagonists in the compliance with the regression requirements. A too large number of predictors, for instance, may improve the residuals distribution but tends to violate the principle of parsimony, and vice versa. Additionally, an inspection of the residuals distribution indicates whether a stochastic model part is required and which order it should have.

Beyond common tests of parsimony and beyond the usage of weighted regression to account for instationarity, the degree of pairwise predictor collinearity is verified, and the residuals are checked for autocorrelation and departures from normality. In this respect, the present regression analysis is shown to violate the regression assumptions only weakly, but some caution is still required about the exact confidence band and interval widths. A tighter compliance with the assumptions may involve better suitable sets of deterministic predictors and the use of moving-average stochastic components; also, the usage of more sophisticated compliance checks would make sense. Last, nonlinear seasonal expansions seem to cause a weaker degree of pairwise collinearity than linear seasonal expansions.

(b)

In general, the degree of nonlinear curvature is weak for this regression analysis, validating the usage of linearly approximated confidence bands and intervals. The NH mid-latitude ENSO phase parameter represents an exception in that it displays a distinct nonlinear kink which refers to the nonlinear seasonal expansion. Yet the statistics literature does not appear to cover the associated implications for statistical inference.

It is fortunate that the present analysis demonstrates a weak degree of nonlinearity associated with autoregression. Note that a more disadvantageous result would have cast into doubt most of the regression analyses in stratospheric ozone research published/done so far, since autocorrelation is a fundamental property of stratospheric ozone time series. Still, checks of least-squares surface contortion need to be carried out whenever nonlinearity arises from deterministic or moving-average regression parameters.

The weak degree of nonlinear curvature encourages the use of iterative linear regression in connection with the Cochrane-Orcutt transformation. Nevertheless, this conclusion is not generally valid for stratospheric ozone research, as the degree of nonlinearity may depend on the type of the regression model as well as

on the properties of the respective ozone data basis. Also, the Cochrane-Orcutt transformation implies a restriction to first-order autoregressive processes, which might not always meet the data-dependent requirements. Additionally, linear regression itself breaks down for both autoregressive moving-average decomposition and nonlinear interactions among deterministic predictors.

3.7.3 Objective 3

The present regression analysis is successful in detecting and quantifying column ozone interannual variability that relates to the scenario REF model boundary conditions; for instance, it is the first to explain a large fraction of the year 1985 SH mid-latitude ozone anomaly.

Yet beyond pure attribution and quantification, this regression analysis sheds light on the physical processes behind column ozone long- and short-term variability, and suggests starting points for future research. In particular, a starting point is identified with modulations of stratospheric transport by ENSO- and GHG-related tropical SST changes. Another starting point concerns nonlinear interactions among the model boundary conditions on stratospheric ozone, and nonlinear ozone responses in general.

In principle, these results confirm those by *Steinbrecht et al.* (2006b); yet the latter rely on a substantially weaker amount of E39/C data and do neither consider the effect of autocorrelation nor check the regression assumptions compliance thoroughly. Their error bounds and statistical tests are hence not reliable; indeed, their regression results regarding a SSC-related modulation of wintertime Arctic temperature are wrong. Also, because of their three-monthly resolution they might underestimate or even miss responses that vary with the annual cycle. Such deficiencies are not crucial for *Steinbrecht et al.* (2006b) as they rather focus on an inter-comparison of E39/C and other data sources than on a thorough quantification of interannual variability. In this context, *Steinbrecht et al.* (2006b, 2003) do not suggest a physical explanation for the ENSO-related stratospheric signal occurring in the northern mid-latitudes but not in the southern mid-latitudes.

(a) SH mid-latitudes

There are statistically significant effects by the ozone response predictors for QBO, SSC, SULF, and ODS, but an ENSO-related signature is not detectable, in contrast to the other latitude bands. Note that the SH mid-latitude QBO-related ozone response is the strongest among the three latitude bands and displays a large seasonally synchronised component.

With regards to a regression-based attribution of the year 1985 low-ozone anomaly, the rare occurrence of seasonally synchronised QBO response amplifications represents the main trigger, together with the ODS-related ozone column decline during the 1980's; the latter makes the intense QBO-related anomaly during 1985 stand out of previous similar events. This finding is in accordance with the study by *Bojkov (1987)* for observed ozone data. SSC-related variability (Figure 3.7b) strengthens the REF 1985 anomaly further, and the volcanic eruption of El Chichon may also contribute (Figure 3.7c), but only very little.

It should be mentioned that *Bodeker et al. (2007)* do not agree on the importance of the ODS-related trend with regard to the 1985 event. The reason may be that *Bodeker et al. (2007)* do not account for ODS-related decadal changes in their analysis. Yet a similar low-ozone event during the year 1997 has been attracting research effort; the present analysis demonstrates that the most relevant stimulation is owing to the QBO and the 11-year solar cycle (Figure 3.7). This finding is in accordance with that by *Bodeker et al. (2007)* for the same year, since trend-like changes during the mid-1990's are weaker than those during the mid-1980's (Figure 3.7d).

It is worth noting that the present MRA is the first to demonstrate a major portion of the year 1985 low-ozone anomaly using regression analysis. But, if the regression analysis does so for measured data sets remains to be demonstrated: the low lid of E39/C implies a one-cell ozone QBO structure, whereas the ozone QBO in both observations and Middle-Atmosphere model runs displays a more complicated two-cell structure.

Last, the ODS-related trend is seasonally dependent, with the strongest trend occurring during southern early summer, likely associated with heterogeneously ozone-depleted air advected from polar latitudes after the wintertime southern polar vortex has broken down. The weakest trend arises during the southern winter, probably because ozone transport dominates column ozone and the effect of heterogeneously ozone-depleted air is largely erased.

(b) NH mid-latitudes

As for the SH mid-latitudes, the NH mid-latitudes display statistically significant ozone effects by the response predictors for QBO, SULF, and ODS. The QBO-related response is seasonally synchronised, but the amplitudes are weaker than that for the SH mid-latitudes. It is interesting that a statistically significant SSC-related ozone modulation is absent; instead, there is a considerably strong ENSO-associated component, where warm ENSO events are associated with positive ozone anomalies, and cold events with negative anomalies.

Both, positive and negative ENSO-related ozone anomalies mainly occur during northern spring, in accordance with well known indications that ENSO modulates the NH mid-latitude Brewer-Dobson circulation, the modulation favouring

the cold months of the year during which tropospheric planetary waves are able to cross the tropopause and to communicate the ENSO signal to the stratosphere. The preference of northern spring may also relate to the well known annual phase-locking of ENSO-related tropical SST anomalies, the anomalies usually occurring during northern winter. Additionally, the phase locking represents a simple explanation why the modelled SH mid-latitude ENSO signal is not significant; during northern winter, the ENSO-signal-transporting tropospheric planetary waves cannot enter the SH extratropical stratosphere.

The stratospheric wave activity modulation mentioned above is usually considered to result from the ENSO-related tropical SST variability altering the pattern of tropical deep convective latent heat release, in turn changing the excitation and propagation characteristics of poleward-proceeding tropospheric planetary waves. Note that this mechanism differs from that proposed in Chapter 2, as here external, and not internal, planetary waves are considered to travel poleward within the troposphere entering the extra-tropics.

Enhanced deep-convective latent-heat release via a realistic increase as well as artificial changes in tropical SSTs may result in analogous external wave activity changes on a decadal scale. This would make the NH mid-latitude Brewer-Dobson circulation more downward-directed, and might hence contribute to the weak increase in scenario REF total column ozone at NH mid-latitudes during northern autumn. The regression analysis does not detect an accompanying depression of tropical column ozone, but anomalously low tropical column ozone during the 1960's seems to obscure the signal of the ODS-related trend predictor.

The opposing negative trend during northern spring, on the other hand, could relate to the time evolution of northern polar heterogeneous ozone depletion affecting NH mid-latitude column ozone. This mid-latitude negative trend is significantly less intense than its SH counterpart, probably because the stronger southern polar vortex allows for a more intense ODS-related evolution of polar heterogeneous ozone depletion.

The regression model appears to underestimate the scenario REF column ozone ENSO signal at NH mid-latitudes, probably due to a nonlinear ENSO-ODS feedback which the current regression model does not account for. A possible feedback mechanism may involve ENSO-related tropical SST anomalies both affecting the NH mid-latitude Brewer-Dobson circulation and northern polar heterogeneous ozone depletion. This would amplify the column ozone ENSO signal the more the higher the ODS concentrations are. Additionally, the impact of ENSO-modulated planetary wave activity on NH mid-latitude column ozone may itself display significant nonlinearity, since a wave-induced ENSO modulation of NH polar stratospheric warmings would cause large modifications of the background flow, in turn altering the propagation conditions for polar- and mid-latitude planetary waves.

(c) Tropics

The tropics reveal statistically significant contributions by the response predictors for QBO, SSC, SULF, and ENSO. In contrast to the mid-latitudes, the regression analysis does not support an ODS-related trend for the tropics (see above).

As expected, the tropical QBO-related ozone response in the REF scenario only contains a minor contribution by seasonal synchronisation, facilitating a comparison with observational data presented by other studies with which it is in excellent agreement. Also, the findings presented here confirm that for REF the QBO-related ozone response causes the main portion of tropical column ozone interannual variability, a well established result for both observational and modelled data. Last, tropical and SH mid-latitude QBO-related response peaks clearly oppose, which accords with the underlying ozone transport mechanism inversely linking the tropics and mid-latitudes. Interestingly, the opposition is less clear for the tropics and the NH mid-latitudes.

The tropical ENSO column ozone response displays slightly weaker amplitudes than that for the NH mid-latitudes. The main difference is that the tropical and NH mid-latitude ENSO response peaks oppose, warm (cold) ENSO events being associated with a negative (positive) column ozone response for the tropics, and vice versa for the NH mid-latitudes. The tropical/NH mid-latitude opposition corresponds with the well known finding that the boreal-winter column ozone variability in the tropics and the NH mid-latitudes is largely reverse, as a result of hemispheric-scale interannual variability in the Brewer-Dobson circulation. Thus, this analysis supports the theory that the ENSO-related column ozone response results from an ENSO-related modification of the Brewer-Dobson circulation. Further support for this theory is associated with the different optimum lags for the ENSO response predictors, a one-month delay in case of tropics, but an eight-month delay for the NH mid-latitudes. One might expect different lags, as the column ozone signal to a change in the Brewer-Dobson circulation establishes more quickly in the tropics than at mid-latitudes.

The tropical SSC-related column ozone response is significantly weaker than that for the SH mid-latitudes, even though the associated UV-induced ozone production 11-year variability maximises in the tropics. However, other studies confirm this result for both measurements and modelled data; the Brewer-Dobson circulation might amplify the signal at SH mid-latitudes via a compressive accumulation of air parcels that carry a SSC-modulated ozone signature from the tropics into the SH mid-latitudes.

3.7.4 Recommendations for future work

In brief, future work may improve the present MRA technically by

- an implementation of initial value routines for full ARMA(n, m) ($n, m > 0$) stochastic models and an adequate application;
- an assessment of how strongly the nonlinear least-squares surface curvature depends on the data set length;
- an implementation of more sophisticated regression assumptions compliance tests;
- a multivariate regression approach which accounts for the loss of information associated with the ensemble-averaging.

Additionally, an extended attribution and quantification of column ozone variability may involve

- nonlinear interactions among deterministic predictors, particularly in case of ENSO and ODS at NH mid-latitudes;
- more sophisticated trend predictors, especially for the NH mid-latitudes and the tropics, while considering predictor collinearity;
- a similar regression analysis of modelled NH and SH polar column ozone;
- a similar regression analysis of observed column ozone data.

Finally, future work might also aim at unraveling short- and long-term SST-related dynamical modifications. On the one hand, the work should investigate changes in the low-latitude stratospheric dynamics as proposed by Chapter 2, and, on the other hand, it should investigate changes in the higher-latitude stratospheric dynamics. The assessment may include

- a regression analysis of dynamical variables such as Eliassen-Palm divergence and the transformed Eulerian-mean stream function;
- a regression analysis of subtropical column ozone to better indicate the latitudinal distribution of the ozone modifications and how it relates to the dynamical changes.

Chapter 4

Wintertime northern polar stratospheric dynamics

Among a variety of realistic boundary conditions, the E39/C scenario PAST (see Appendix A.2 and Figures 3.1, 2.1) accounts for a historically evolving quasi-biennial oscillation (QBO), and incorporates the observed time evolution of the 11-year solar cycle (SSC).

The model assimilates the QBO via a relaxation of its tropical stratospheric winds towards a time series of measured tropical zonal wind profiles, the latter comprising radiosonde data from Canton Island (1953–1967), Gan/Maledives (1967–1975) and Singapore (1976–2000) (*Labitzke et al.*, 2002; *Naujokat*, 1986). The relaxation includes the model levels between 60 hPa and 10 hPa (*Dameris et al.*, 2005, Figure 1).

The evolution of the SSC is parameterised by the 10.7 cm radiation of the sun (*ICARUS*, 2005) because the latter is well observable and co-varies with the 11-year vacillation of the sun’s ultraviolet (UV) radiation (*Haigh*, 1996). There is both an online SSC component within the model domain and an offline component introduced at the uppermost model level to incorporate exchange processes from the upper stratosphere outside the model domain. The former component considers photolysis and radiative heating rates, the latter component considers the ozone-modifying NO_y content taken from a separate transient run of a two-dimensional chemistry climate model (CCM) (*Brühl and Crutzen*, 1993).

Chapter 3 demonstrates that E39/C produces realistic direct SSC and QBO effects on temperature and total ozone outside the wintertime polar regions. Here, the focus is on an inspection of the model’s ability to reproduce indirect SSC and QBO effects in the northern hemisphere (NH) during wintertime at polar latitudes. Since these effects involve rather elusive dynamical mechanisms, the inspection may also help to clarify the physics behind these. Section 4.1 gives background information on the physical mechanisms, Section 4.2 discusses the

model results, Section 4.3 provides both conclusions and suggestions for future work.

4.1 Quasi-biennial oscillation (QBO) and 11-year solar cycle (SSC)

The background information given considers both separate (Sections 4.1.1 and 4.1.2) and entangled physical mechanisms (Section 4.1.3) by which QBO and SSC may affect the stratospheric dynamics. Section 4.1.3 also clarifies if the ER40 re-analyses (*Uppala et al.*, 2005) conform with the concept of entanglement and thereby validates the method of analysis.

4.1.1 QBO-related modulation of the northern polar vortex

The studies by *Holton and Tan* (1982, 1980) demonstrate an apparent modulation of the NH wintertime polar stratospheric dynamics by the equatorial QBO. The NH polar vortex tends to be cold and undisturbed when the QBO at a height of 50 hPa is in its westerly phase (QBO/W), but tends to be warm and disturbed during the easterly phase (QBO/E). A widely accepted explanation for this Holton-Tan (H-T) effect is that the QBO winds in the tropical lower stratosphere modify the background mean flow, affecting the propagation characteristics of planetary-scale waves (*Baldwin et al.*, 2001).

More precisely, for any given level in the lower stratosphere, the QBO determines the position of the zero line in zonal wind. That zero line separates the winter/summer hemispheres and is often referred to as a critical line, as it borders the equatorial wave-guide for the planetary-wave propagation (i.a. *Dickinson*, 1968; *Charney and Drazin*, 1961). During QBO/W the critical line lies close to equator, during QBO/E it moves towards the winter pole which effectively narrows the equatorial wave-guide, keeping upward propagating planetary waves more poleward. The result is weak poleward heat transfer (undisturbed polar vortex) during QBO/W and enhanced transfer (disturbed polar vortex) during QBO/E (*Gray et al.*, 2001b).

Note that the effect of critical lines on planetary wave propagation is not as simple. The reason is that planetary waves propagate both vertically and horizontally, and the concept of a critical surface rather than a single critical line is more appropriate (*Baldwin et al.*, 2001). Also, wave mean-flow interaction is a complex nonlinear process (*Andrews and McIntyre*, 1976) which involves both, wave absorption and reflection (*Harnik and Lindzen*, 2001; *Tung*, 1979; *Dickinson*, 1968).

In *Labitzke* (1987) and *Labitzke et al.* (2006) it has been demonstrated that the H-T relationship appears to be sensitive to the phase of the 11-year solar cycle (SSC). A positive H-T relationship exists only during solar minimum conditions (SSC/min), whereas during solar maximum conditions (SSC/max) there is an inverse connection instead, a negative H-T relationship. In fact, the data basis upon which the studies by *Holton and Tan* (1982, 1980) rely is essentially confined to SSC/min conditions. Nevertheless, *Baldwin et al.* (2001) conclude from various published model studies that the physical basis for the positive H-T effect seems to be sound.

Employing 3-D mechanistic models *Dameris and Ebel* (1990) and *Holton and Austin* (1991) have shown that the strength of the positive H-T effect depends on the amplitude of the wave forcing imposed. More recent model studies conclude that sign, strength and timing of the H-T relationship depend on the altitude range throughout which there is a realistic equatorial wind profile (*Pascoe et al.*, 2006; *Gray*, 2003; *Gray et al.*, 2001a). For instance, the idealised mechanistic model by *Gray et al.* (2001a) only produces a positive H-T effect when the stratospheric equatorial winds are relaxed towards observed values at least up to a height of 3 hPa. When the relaxation is restricted to altitudes below 10 hPa a negative H-T relationship results. In this context it is important to be aware that the QBO signal in the real atmosphere vertically extends to altitudes as high as 1 hPa, and might hence contribute to the effect mentioned above (*Pascoe et al.*, 2005; *Gray et al.*, 2001b).

The H-T relationship depends on the exact QBO phase definition because the latter determines the latitude height positioning of the critical lines (*Baldwin et al.*, 2001). Usually, the motivation for picking the equatorial zonal wind speed at a particular altitude level is to optimise the extratropical QBO signal. A more sophisticated approach involves empirical orthogonal functions analysis, but the resulting definition of the QBO phase for the NH is very similar to the equatorial winds near 40 hPa (*Baldwin et al.*, 2001).

4.1.2 SSC-related modulation of the stratosphere

As already mentioned, there is evidence that the SSC influence reaches down into the lower stratosphere and acts to modify the H-T relationship (*Labitzke et al.*, 2006). That is an intriguing aspect of stratospheric research, as any immediate SSC-related influence is thought to primarily occur above the lower stratosphere, with a maximum influence at the stratopause near 1 hPa (*McCormack*, 2003; *Gray et al.*, 2001b).

During a complete SSC period the solar constant varies by less than 0.1%, too weakly to cause the apparent atmospheric oscillation. The main variation is allocated in the ultraviolet (UV) part of the solar spectrum and exhibits an

amplitude of 6–8% between SSC/max and SSC/min (*Lean and Rind, 1998; Lean et al., 1997; Haigh, 1996; Chandra and McPeters, 1994*).

UV radiation is strongly attenuated before it reaches down to the lower stratosphere and so is its SSC-related variation. During SSC/max, increased UV radiation heats the sunlit areas of the upper stratosphere by both, elevated UV irradiance levels available for absorption and enhanced ozone concentrations. The latter enhancement mainly results from stronger photochemical net ozone production owing to the stronger UV irradiance. During SSC/min the opposite effect occurs, a cooling and low ozone concentrations (*Fadnavis and Beig, 2006; Labitzke and Matthes, 2003*). Both, observational and modelling studies suggest a temperature change of about 1–2 K (*Keckhut et al., 2005; Crooks and Gray, 2005*) and an ozone concentration change of about 3–5% in the tropical middle and upper stratosphere during a solar cycle (*SPARC, 1998*).

The immediate SSC influence is latitude dependent, as daytime insolation decreases away from the tropics. That implies, via the thermal wind relation, a direct impact on the upper-stratospheric zonal winds during the whole annual cycle, with the strongest impact on the winter hemisphere (*Tourpali et al., 2005; Lean and Rind, 1998; Haigh, 1996*).

The SSC hence modulates the upper-stratospheric mean state of temperature, chemistry, and momentum. This SSC-dependent mean state is then thought to alter the propagation characteristics of planetary-scale waves by changing the index of refraction, in turn modifying the planetary wave guides in the winter hemisphere (*Labitzke, 2005*). In this context, the limitation of observational data makes it difficult to follow the large initial solar signal downwards from the upper stratosphere (*Matthes et al., 2006*), and models are thus important to clarify the underlying physical mechanism.

The impact at lower-stratospheric levels might occur in terms of a change in the Brewer-Dobson circulation via the downward-control principle (*Shindell et al., 1999*). However, at middle and high latitudes a different mechanism is potentially more significant. Since breaking planetary waves feed back on the SSC-modulated mean state in the upper stratosphere, the SSC signal might propagate poleward and downward owing to critical layer interaction (*Kodera and Kuroda, 2002*). Critical layer interaction is usually associated with the polar night jet and wintertime stratospheric warmings, which makes this process highly influential.

Another pathway for communicating the SSC signal down to the lower stratosphere involves an SSC-related modulation of the QBO (*Salby and Callaghan, 2006b; Pascoe et al., 2005; Salby and Callaghan, 2000*). This modulation might result from a coupling of the upper-stratospheric semi-annual oscillation (SAO) and the QBO (*Mayr et al., 2006; McCormack, 2003*) and wave ozone feedbacks (*Cordero and Nathan, 2005*).

4.1.3 QBO-SSC entangled impact on the northern polar vortex

The ERA40 data record analysed here (Figures 4.1a,d,g) comprises the 42 winters from 1958 until 1999. The SSC index is identified with the 10.7 cm radiowave time series (*ICARUS*, 2005). The QBO wind is identified with the observed zonal mean wind at 40 hPa and 50 hPa a January/February average (*Labitzke et al.*, 2002). A value of less than -2 m/s signifies QBO/E, a value of more than $+2$ m/s signifies QBO/W. All of the 42 winters contribute to Figure 4.1a, a number of 17 QBO/E winters to Figure 4.1d, and 22 QBO/W winters to Figure 4.1g.

The above definitions are chosen to agree with those in *Labitzke and van Loon* (1992, Figure 5). Only the classification into QBO/E and QBO/W winters might slightly differ as the authors do not tell on which exact wind speeds their discrimination into QBO/W and QBO/E bases. Finally, *Labitzke and van Loon* (1992) use stratospheric data from 1958 until 1991 of the Freie Universität Berlin (FU Berlin) (*Labitzke et al.*, 2002).

The correlation coefficient ρ in the ungrouped case is weak and does not exceed 0.2 in absolute value at polar and middle latitudes. Some regions in the subtropics and the tropics show slightly stronger absolute values of ρ , with a maximum of about 0.3 next to the African west coast. A marked difference becomes apparent when the data are grouped according to QBO/E and QBO/W. In the QBO/E case ρ clearly features negative values at polar latitudes with a minimum of somewhere between -0.5 and -0.6 around the north pole. The correlation becomes positive at extra-polar latitudes and exhibits about the same absolute values as the correlations at polar latitudes. In the QBO/W case basically the opposite effect occurs; although the absolute values of ρ at extra-polar latitudes are markedly smaller than those at polar latitudes.

A comparison with Figure 5 in *Labitzke and van Loon* (1992) validates the calculation method applied here. Minor differences arise in the QBO/E case, where the ERA40 polar peak correlation is weaker, and in the QBO/W case, where the ERA40 extra-polar correlations are less variable. In the ERA40 un-grouped case, the absolute values of ρ are weaker throughout the NH. The most prominent reason for above differences lies in the time span considered, 42 years in case of the ERA40 results presented here, but 34 years in case of the FU Berlin results in *Labitzke and van Loon* (1992). In case the ERA40 data analysed only comprise the 34 years from 1958 to 1991 (not shown here), then the above-mentioned differences reduce strongly.

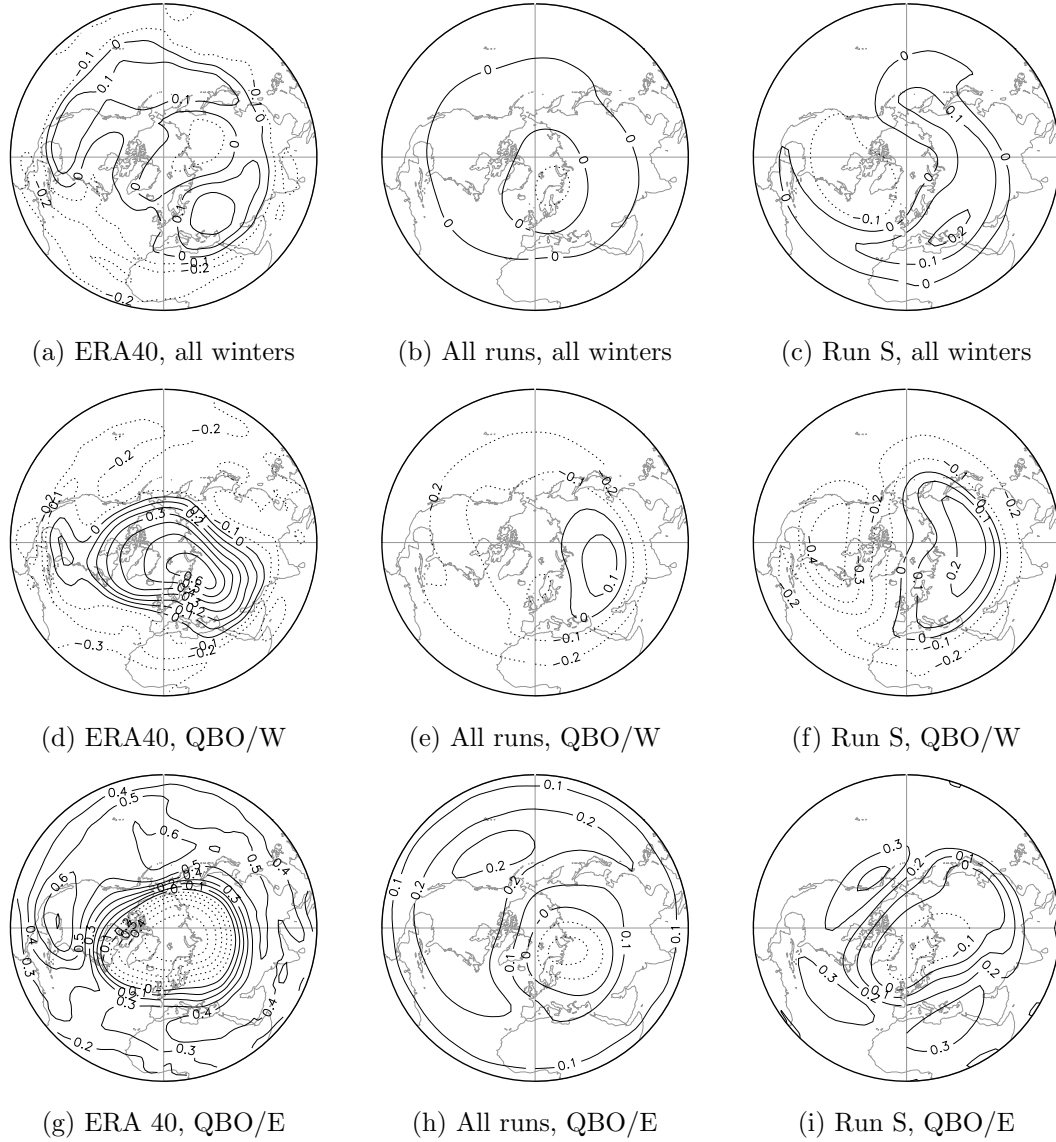


Figure 4.1: Pearson's correlation coefficient (ρ) between the 11-year solar cycle (SSC) and January/February (JF) geopotential heights at 30 hPa. QBO/W stands for the westerly QBO phase, QBO/E for the easterly phase. The QBO index itself is defined as the JF, $(40 \text{ hPa} + 50 \text{ hPa})/2$, $10^\circ\text{N} - 10^\circ\text{S}$ area-weighted average zonal mean wind. "ERA40" (1958 to 1999) roughly comprises 4 SSCs, "all runs" 14 SSCs, "run S" 4 SSCs.

It must be kept in mind that the 30 hPa geopotential represents lower-stratospheric temperature. This follows from the fact that geopotential heights at any particular pressure surface integrate the temperature distribution between that surface and the ground level plus a contribution from surface pressure. Therefore, if the temperature changes below that pressure level tend to act in the same direction, then geopotential height changes at the level may represent a large portion of the atmosphere (*Balachandran et al.*, 1999). In fact, the 30 hPa surface at wintertime polar latitudes usually stands for the whole stratospheric column below. The reason is that temperature changes work in the same direction throughout the wintertime polar lower stratosphere (*Labitzke*, 2005; *Baldwin and Dunkerton*, 1999). *Dameris et al.* (2005, Figure 7a) displays such behaviour in case of E39/C. Finally, monthly scale tropospheric temperature variations and surface pressure vacillations exert a minor influence on the 30 hPa geopotential (*Labitzke*, 2005; *Balachandran et al.*, 1999; *Holton and Tan*, 1980).

Considering the above-mentioned interpretation, the Figures 4.1a, d, and g show that for SSC/min, stratospheric warmings preferentially take place during QBO/E, but for SSC/max during QBO/W. Or, expressed in terms of the H-T relationship, for SSC/min the traditional positive H-T relationship holds, for solar maximum a negative H-T relationship occurs (*Labitzke et al.*, 2006; *Labitzke*, 1987).

The situation at extra-polar latitudes appears to be less straightforward, namely the comparatively strong correlations during QBO/E contrasting the weak correlations during QBO/W. A possible explanation involves the northern annular mode (NAM) which inversely teleconnects the stratospheric heights in the Arctic to those at lower latitudes (*Labitzke*, 2004). Stratospheric warmings initially raise polar geopotential heights, and, owing to the teleconnection, depress those at extra-polar latitudes. This teleconnection pattern is obvious in the QBO/E years, yet much less so in the QBO/W years. A likely explanation is that the two mechanisms, teleconnection and SSC influence at extra-polar latitudes, cooperate in the former case but oppose each other in the latter (*Labitzke and van Loon*, 2000; *Yang and Tung*, 1995).

The QBO-SSC interaction on polar stratospheric warmings as discovered by *Labitzke* (1987) has been subject to a lot of scientific discussions. Among the main points risen have been the short data record which contains only a few solar cycles, aliasing effects from dividing the data into QBO/E and QBO/W, and the lack of a plausible physical mechanism for the negative H-T effect (i.a. *Salby and Callaghan*, 2006b; *Salby and Shea*, 1991; *Teitelbaum and Bauer*, 1990). Today, the statistical significance is more definite and aliasing effects can be excluded, but the observations are still not adequate to definitely pinpoint the underlying physical mechanism (*Labitzke et al.*, 2006; *Salby and Callaghan*, 2006b; *Gray et al.*, 2001b; *Salby and Callaghan*, 2000; *Kodera*, 1993). *Salby and Callaghan* (2006b, 2004b) have presented evidence that the SSC-modulated QBO interacting

with the annual cycle might produce a stratospheric response similar to that shown in *Labitzke* (1987).

Recently, 3D-models have reproduced some of the observed QBO-SSC interaction on polar stratospheric warmings (*Matthes et al.*, 2006; *Palmer and Gray*, 2005; *Gray et al.*, 2004; *Matthes et al.*, 2004). The models did not account for interactive chemistry and the model runs were idealised in order to capture the above SSC-QBO interaction. As for the traditional positive H-T relationship without SSC consideration, the interaction only occurs when the models account for a realistic wind profile throughout the tropical stratosphere; either by relaxation (*Matthes et al.*, 2006; *Gray et al.*, 2004; *Matthes et al.*, 2004) or by self-generation without any relaxation (*Palmer and Gray*, 2005). It has been suggested that part of the interaction between SSC and QBO might occur in the upper stratosphere, involving both, the semi-annual oscillation and the upper-stratospheric QBO (*Pascoe et al.*, 2005).

4.2 Model results

The previous Section has shown that the ERA40 re-analysis data contain a signal suggesting a QBO-SSC entangled mechanism. The longitude-latitude signature of this mechanism is similar to that presented in *Labitzke and van Loon* (1992), validating the analysis method. In the following, the same analysis method is applied to the E39/C model data.

4.2.1 SSC-related influence and QBO-SSC entangled mechanism

For the modelled correlation coefficients (Figures 4.1b,e,h) all definitions, i.a. QBO phases and SSC time series, are identically chosen to those underlying the ERA40 results (Figures 4.1a,d,g). The difference is that the model data comprises more degrees of freedom as it consists of three independent realisations of the 1960–1999 PAST scenario (*Dameris et al.*, 2005) plus three times five years of spin-up. Additionally, a single realisation of a 1981–1999 scenario (*Dameris et al.*, 2006) is considered. It has got the same boundary conditions as the control scenario except that it does not account for volcanic eruptions.

The realisations mentioned above have not been ensemble averaged prior to the correlation calculations, but stuck together at their ends, hence forming an 154-year time series. The whole series roughly embraces 14 solar cycles. The QBO/E case comprises 64 samples, the QBO/W case 80 samples.

Not the length of record governs the statistical inference here, but rather the number of solar cycles the record contains (*Salby and Shea*, 1991). As an

approximate guide, *Salby and Callaghan (2006b)* argue that in case of three solar cycles statistical significance at the 95% level necessitates correlations in excess of ± 0.70 . In case of 6.5 solar cycles, more than twice as many, the same concept indicates correlations in excess of ± 0.5 (*Labitzke et al., 2006*). Therefore, a further doubling into 13 or 14 solar cycles assuredly denotes a 95% critical correlation of beyond ± 0.3 .

Following this concept, the modelled correlation coefficients are not statistically significant, and any hypothetical aliasing effects owing to the QBO/E-QBO/W sampling (*Salby and Shea, 1991*) or any form of auto-correlation actually supported that conclusion (*von Storch and Zwiers, 1999*).

Containing 3.8 solar cycles the ERA40 correlation coefficients are not statistically significant at the 95% level either, apart from the QBO/W polar region of maximum correlation which might approach that level. Note however, that in Figure 5 of *Labitzke et al. (2006)* the maximum correlation is about the same, but even approaches the 99% significance level. There, the observational time series compiled contains 6.5 solar cycles.

It is interesting that the modelled pattern of positive/negative correlations resembles the ERA40 pattern, and a likely reason is that the NAM teleconnection pattern exists in both, modelled and observed data.

Steinbrecht et al. (2006a) present results from a multiple regression analysis in case of a realisation of the 1960 to 1999 PAST scenario (“run S”) (*Dameris et al., 2005*). They do not analyse 30 hPa geopotential height during January/February (JF), but total ozone column and 50 hPa temperature throughout December-February (DJF). Nevertheless, these quantities are intimately related to 30 hPa geopotential heights during the NH polar winter (Section 4.1.3). The relation to ozone results from the anomalous mean meridional transport associated with polar stratospheric warmings. During a warm winter the anomalous meridional residual circulation conveys more ozone from mid-latitudes to polar latitudes than during a cold winter. Stratospheric ozone is considered as inert at winter-time middle- and high latitudes. As a consequence, in a warm winter a positive anomaly occurs at polar- and synchronously a negative anomaly at mid-latitudes (*Yang and Tung, 1995*). Anomalous isentropic mixing may also contribute to this behaviour (*Salby and Callaghan, 2007*).

In their Figure 12, *Steinbrecht et al. (2006a)* show a large dipole-like SSC contribution at NH polar latitudes during DJF which contrasts the results presented here. Note that their results exclusively rely on a single 40-year realisation. For a comparison, the Figures 4.1c, f, and i depict correlation coefficients for that run S only, including five spin-up years.

Again, the results are not statistically significant. Even in case of 65 years of data, that is 6.5 solar cycles, statistical significance at the 95% level demands correlations in excess of ± 0.5 (*Labitzke et al., 2006*). Here, only 4.1 solar cycles

yield a maximum absolute correlation of below 0.5. Note however, that due to statistical fluctuations the correlations in the Figures 4.1c, f, and i become larger than those in the Figure 4.1b, e, and h. Similarly to *Steinbrecht et al.* (2006a) a dipole-like structure appears. Thus, the strong wintertime polar stratospheric SSC dependence in *Steinbrecht et al.* (2006a) is owing to a false usage of regression analysis and vanishes when analysing several model runs simultaneously.

In conclusion, E39/C indicates that the SSC does not significantly impact on NH polar stratospheric warmings, for both the amount of model data available and the method of analysis applied in this Chapter. Or, if there yet existed a relationship, it was weak and required further model runs to be detected.

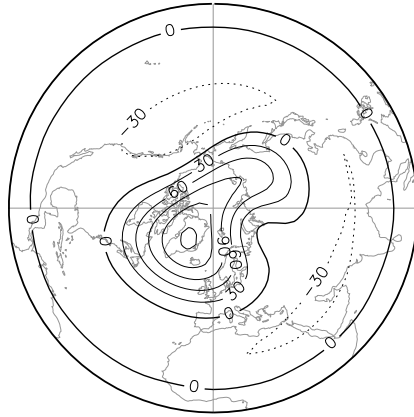
4.2.2 QBO-related modulation without SSC influence

The previous section has shown that E39/C does not produce a statistically significant relation between the SSC and NH wintertime polar stratospheric temperature. Also, the temperature does not display QBO-SSC entangled effects, and thus a H-T relationship may now be sought without simultaneously considering the SSC.

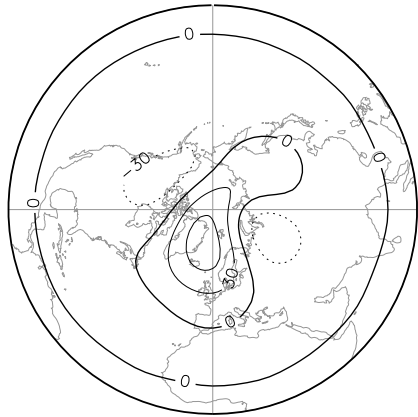
The January/February geopotential height differences in Figure 4.2a base on the same model data that contribute to Figure 4.1b. The QBO phase definition is the same as in Figure 4.1, with a number of 80 QBO/W winters and 64 QBO/E winters. However, not any explicit reference to the SSC is made.

In Figure 4.2a, positive values of $\Delta\Phi$ at polar latitudes indicate NH stratospheric warmings to occur more frequently during QBO/W than during QBO/E, signifying a negative H-T relationship. Negative values of $\Delta\Phi$ at mid-latitudes are consistent with the NAM teleconnectin pattern (*Labitzke, 2004*). Positive values in the tropics directly result from the equatorial wind relaxation, as do the negative values in the sub-tropics (*Yang and Tung, 1995*).

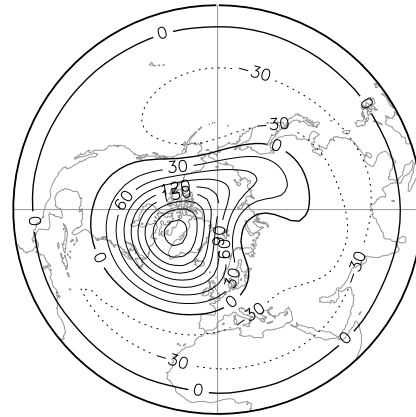
The above negative H-T relationship appears to be a robust feature. Figures 4.2b–e show the same QBO/W–QBO/E geopotential height differences as in Figure 4.2a, but separately for the four model runs. Thus, combining the latter four plots results in Figure 4.2a. Obviously, the negative H-T relationship consistently occurs among each of the four model runs.



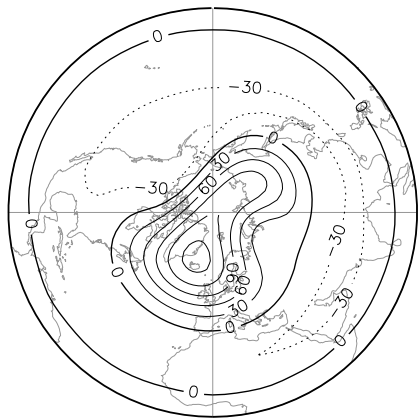
(a) Mean of all runs below, 153 winters



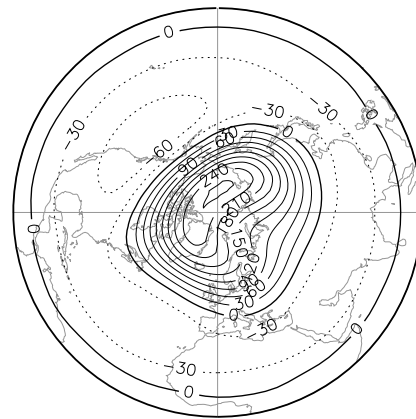
(b) PAST run S, 45 winters



(c) Independent PAST run, 45 winters



(d) Independent PAST run, 45 winters



(e) Run no volcanoes, 18 winters

Figure 4.2: January/February (JF) mean 30 hPa geopotential height difference ($\Delta\Phi$) in gpm. The differences are defined as JF QBO/W minus JF QBO/E. The QBO phases equal those in Figure 4.1.

Also, the relationship is robust with regard to the height at which the QBO phase is defined. The strongest negative relationship results in case of the QBO phase defined at the 60 hPa level (not shown here), which represents the lowermost level at which E39/C assimilates the tropical zonal winds. The negative H-T relationship successively weakens with increasing QBO definition height until the relationship becomes positive for the 20 hPa QBO level (not shown here). The reason is that the QBO phase is height-dependent with the phase at 20 hPa tending to oppose the phase at 60 hPa, and a transition between these two levels (*Dameris et al.*, 2005, Figure 1)

The negative H-T relationship responds robustly to a forward translation in time but not to a backward translation: a relationship is clearly evident for the March/April average, but not for the November/December average (not shown here). The reason may be that, compared to observations, E39/C produces a reduced interannual variability in early winter (*Dameris et al.*, 2005, Figures 9a and 9b).

Figure 10 in *Steinbrecht et al.* (2006a) also displays a negative H-T relationship as it shows an in-phase relationship between the 30 hPa QBO phase and polar stratospheric temperature, similarly to the relationship in Figure 4.2b displayed here. Yet the authors do not infer a robust negative H-T relationship as their multiple regression analysis covers the statistically shorter period of 40 model years, compared to the 153 years here.

4.3 Summary and conclusion

Using E39/C model results the impact of both SSC and QBO on NH stratospheric geopotential heights, and therefore temperatures, has been investigated. In E39/C, these boundary conditions modulate the NH wintertime polar lower-stratospheric dynamical conditions as follows:

1. most likely, the SSC does not modulate the dynamics; if it does the modulation is weak. Consistently, Chapter 3 of the present study fails to verify a statistically significant SSC-influence on NH mid-latitude total column ozone. *Steinbrecht et al.* (2006a) demonstrate a SSC-related modulation of wintertime NH polar stratospheric temperature, but their result is not statistically significant;
2. there is no indication for an entangled action of SSC and QBO on the dynamics;
3. the QBO implicates a negative Holton-Tan (H-T) effect. That is, zonal mean QBO winds at heights around 50 hPa are in phase with modelled wintertime 30 hPa NH polar geopotential heights.

Finding number 2 has the following consequences: first, the model results do not bring further physical plausability to the entangled QBO-SSC action evident in observational data; second, the model does not support a relationship as proposed by *Salby and Callaghan* (2000) even though it contains a realistic SSC-modulated QBO.

It has to be kept in mind that the model results presented above need to be interpreted with caution. It may well be that the low positioning of the E39/C upper lid prevents a realistic coherence between QBO, SSC, and the characteristics of NH polar lower-stratospheric warmings. In fact, finding number 3 is in line with other modelling studies. There, a positive H-T effect is associated with a realistic tropical wind profile throughout the stratosphere, a negative H-T effect with a realistic tropical wind profile restricted to the lower stratosphere. A positive rather than a negative H-T effect is probably more realistic, as the former better corresponds with the concept of planetary wave-guides. Similarly, modelling studies suggest that the existence of an entangled QBO-SSC relationship might require a realistic equatorial wind profile.

Future analyses should specify how the negative H-T effect connects with the propagation characteristics of planetary waves, and how it relates to the position of critical surfaces, the latter associated with a particular QBO phase. The analyses should include Eliassen-Palm fluxes, their divergence, and refractive indices.

Chapter 5

Summary and conclusion

The final Chapter summarises to what extent the objectives of this study were met and gives conclusions as well as suggestions for future work. The objectives were to analyse E39/C output data and to

1. find the reason for climate change accelerating the upward transport across the tropical tropopause;
2. upgrade a statistical procedure used to account for the interannual variability of the ozone layer; gain insight into the causal relationships governing the interannual variability;
3. assess both general characteristics and climate-change-related modifications of the northern polar stratospheric dynamics during winter and spring.

5.1 Objective 1

The reason for climate change accelerating the upward transport across the tropical tropopause involves a cascade of physical effects, but ultimately relates to the tropical sea surface temperatures (SSTs): in a warmer climate, higher tropical SSTs amplify the amounts of rain related to intense tropical thunderstorms; the associated enhancement of latent-heat release in the tropical upper troposphere intensifies the generation of atmospheric global-scale waves; these waves travel mostly upward, cross the tropopause and modify the lower-stratospheric background winds, ultimately strengthening the upward mass transport across the tropical tropopause. The transport enhancement in turn strengthens the input into the tropical lower stratosphere of ozone-poor tropospheric air.

Regarding tropical total column ozone, repercussions of climate-change-induced higher tropical SSTs hence oppose the benefits of climate-change-related

slower ozone-destructing chemical reactions. The low lid of E39/C obscures the influence of climate-change-induced decelerating ozone destruction in fact; but Middle Atmosphere models suggest that the tropical ozone layer is not going to grow significantly beyond the values modelled for the late 1970's. It is likely that the lack of increase in these models refers to the mechanism presented above.

That the transport modification is restricted to the lower stratosphere has a consequence: climate change will probably not speed-up the removal of stratospheric ozone-depleting substances as strongly as has been suggested in previous modelling studies. These studies are not aware that a large portion of their modelled upwelling amplification does probably not reach into the middle and upper stratosphere. Note in this context that the removal of ozone-depleting compounds occurs via intense ultraviolet radiation mostly at altitudes higher than the lower stratosphere.

Also, the intensified tropical absolute upward transport is balanced by reduced absolute upward motions in the respective summer hemisphere subtropics. The summer-hemispheric transport modification does hence not thicken the mid-latitude ozone layer by an amplified delivery of ozone-enriched air masses.

A convincing quantification of the transport-related impact of climate change on the tropical ozone layer is difficult, mainly since thunderstorms represent a small-scale atmospheric process the representation of which in global-scale atmospheric models deserves to be improved. Also, E39/C and most of the other chemistry-climate models do not account for feedbacks between atmosphere and ocean. Nevertheless, E39/C is highly efficient in calculating the tropical-SST-related transport modification, compared to Middle Atmosphere models: E39/C provides high vertical resolution at the essential altitudes near the tropopause while its comparatively low upper lid does not interfere.

Yet the upper lid needs consideration during northern winter: for the warmer climate, E39/C yields a stronger mid-winter activity at northern mid-latitudes of global-scale waves throughout the modelled part of the stratosphere. However, the mass transport does not respond significantly. This wave activity intensification may relate to the higher tropical SSTs intensifying the rain-induced generation of poleward-propagating global-scale waves (see Objective 2), but other mechanisms are also possible.

5.2 Objective 2

A software package for solving nonlinear least-squares problems has been successfully upgraded by routines that permit an efficient use of nonlinear seasonal deterministic/stochastic combined regression models in connection with iterative weighting and a validity assessment of asymptotic linearity. It is this particular

combination of characteristics that has probably not yet been used in stratospheric ozone research, and to which the statistics literature seems to not pay much attention. Additional routines allow for a calculation of both linearly approximated response confidence bands and nonlinear parameter confidence intervals. The usage of these statistical inference features, too, appears to be new to stratospheric ozone research. It is unfortunate that a lack of resources prevented an implementation of initial value algorithms for autoregressive moving-average stochastic models, at present restricting the stochastic analysis to autoregressive decomposition. Yet the present stage of development already represents a significant advancement (see below) and may promote the future use of nonlinear multiple-regression analysis in stratospheric ozone research.

The present regression analysis investigates monthly zonal mean total-column ozone data for the latitudinal averages southern/northern mid-latitudes and tropics of an E39/C 60-year scenario threefold ensemble mean. Regression analyses for the polar regions are subject to future studies.

A simultaneous usage of thorough regression requirement compliance checks together with the upgrades mentioned above has permitted the following achievements:

- this regression analysis is the first in ozone research to address the problem of distorted least-squares surfaces in the context of correlated regression residuals. Only if the distortion is weak, the usage of iterative linear regression methods is possible without the drawback of severe errors in statistical tests, confidence intervals and confidence bands. The present nonlinear regression method demonstrates fortunately that the distortion owing to auto-regression is less than 10%, at least for the ozone time series analysed here. Note that a more disadvantageous result would have cast into doubt most of the regression analyses in stratospheric ozone research published/done so far. Still, checks of least-squares surface contortion need to be carried out whenever nonlinearity arises from deterministic or moving-average regression parameters.
- the present regression analysis is the first such analysis to explain the year 1985 southern mid-latitudes low-ozone event, here reproduced by E39/C. It shows, in accordance with results by *Bojkov (1987)*, that the rare occurrence of seasonally synchronised amplifications in the QBO-related ozone response represents the main trigger. A similarly important trigger is the ozone column decline during the 1980's which relates to a growing burden of ozone-depleting substances; the decline makes the QBO-related low-ozone anomaly during 1985 stand out of previous similar events. *Bodeker et al. (2007)* do not infer an ODS-related contribution to the year 1985 anomaly, probably because their analysis does not account for decadal changes. Apart from the 1985 anomaly, a similar low-ozone event during the year 1997 has

been attracting research effort; the present analysis demonstrates that the most relevant stimulation is owing to the QBO and the 11-year solar cycle. This result is in accordance with that by *Bodeker et al.* (2007) for the same year, since trend-like changes during the mid-1990's are weaker than those during the mid-1980's.

- for the first time in ozone research, the present regression analysis provides evidence for a coupled nonlinear deterministic response in the northern mid-latitude ozone layer during spring: the modulation by intense anomalies in tropical SSTs (ENSO), associated with the El Niño-southern oscillation, may be the larger the more likely ozone depletion on particles in Arctic polar stratospheric clouds becomes, associated with a long-term trend.

Additionally, the present regression analysis demonstrates statistical significance for the well known responses to the 11-year solar cycle (SSC), to sulfate aerosols, and to concentrations of ozone-depleting substances.

The response to the mass-transport-modulating model boundary conditions QBO and ENSO has the following realistic characteristics: the QBO causes a seasonally synchronised ozone response at southern mid-latitudes, more weakly at northern mid-latitudes, but not in the tropics. ENSO affects the tropics and northern mid-latitudes, but not the southern mid-latitudes. In principle, these results confirm those by *Steinbrecht et al.* (2006b); yet the latter rely on a substantially weaker amount of E39/C data and do neither consider the effect of autocorrelation nor check the regression assumptions compliance thoroughly. Their error bounds and statistical tests are hence not reliable; indeed, their regression results regarding a SSC-related modulation of wintertime Arctic temperature are wrong. Also, due to their three-monthly resolution they might underestimate or even miss responses that vary with the annual cycle. Such deficiencies are not crucial for *Steinbrecht et al.* (2006b) as they rather focus on an inter-comparison of E39/C and other data sources than on a thorough quantification of interannual variability. In this context, *Steinbrecht et al.* (2006b, 2003) do not suggest a physical explanation for the ENSO-related stratospheric signal occurring in the northern mid-latitudes but not in the southern mid-latitudes.

In E39/C, the response of the ozone layer to ENSO displays characteristics that strongly argue for the well known involvement of modifications in stratospheric meridional mass transport: The tropical and northern mid-latitude response is inverse, probably due the antagonism inherent in hemispheric-scale mass transport modifications. Enhanced transport increases the rate of ozone-poor tropospheric air penetrating into the tropical stratosphere (see Objective 1), but at the same time increases the transport of ozone-rich air to the mid-latitudes, and vice versa.

The lack of any statistically significant response at southern mid-latitudes points to the matter of fact that intense ENSO events mostly occur during north-

ern winter. This fundamental property of ENSO is commonly associated with an interaction of ocean Rossby waves with the seasonal variation of the tropical convergence zone; E39/C accounts for this effect via its prescribed SSTs. Note that the intense ENSO events during northern winter can hardly modulate the stratospheric meridional mass transport in the southern hemisphere: during northern winter, the mass transport in the extratropical southern hemispheric summer stratosphere is weak and is hence barely susceptible to the ENSO events.

For E39/C, the above-mentioned features make it likely that global-scale poleward-propagating atmospheric waves transfer the ENSO signal to the ozone layer by affecting stratospheric meridional mass transport; this mechanism has already been documented for both measurements and other models: global-scale waves can enter the winter stratosphere and change the meridional mass transport there, but are unable to invade the respective summer stratosphere. In particular, ENSO might affect the generation of global-scale waves by modulating the precipitation patterns associated with intense tropical thunderstorms, also referred to as deep convection; there may hence exist a connection to the mechanism of deep-convective wave generation reported in Objective 1.

In contrast to the climate-change-related response, ENSO appears to affect the northern winter mid-latitudes strongly; this could relate to a different and more intense modulation of the tropical precipitation patterns, affecting the generation of poleward-propagating global-scale waves significantly. Note in this context that, for the present study, strong ENSO events have an amplitude of nearly 4 K (Figure 3.1a), a large amplitude compared to the climate-change-related difference of about 1 K in tropical SSTs (Figures 2.9e and 2.9f).

There is a wintertime wave signal in the northern mid-latitude stratosphere for Objective 1, but the mean meridional mass transport does not respond significantly, and it is unclear whether the signal refers to the deep-convective generation of poleward-propagating global-scale waves. Note that E39/C appears to calculate a relatively weak northern polar vortex in case of intensely high ENSO events. Whether a future intense global warming might weaken the northern vortex in a similar fashion is unclear, as the stabilising effect by higher concentrations of well mixed greenhouse gases (Objective 3) needs to be considered.

5.3 Objective 3

A property of the E39/C wintertime northern polar vortex is that its response to the tropical QBO is unrealistically robust (see below), and implies a negative Holton-Tan (H-T) relationship. That is, westerly zonal winds in the tropics at a height of 50 hPa correlate with a relatively weak polar vortex, easterly winds with a relatively strong vortex. According to other modelling studies with a too

robust response, the presence of a negative H-T relationship instead of a positive H-T relationship is likely to involve the E39/C low upper lid.

In measured data, the QBO-related response of the northern polar vortex is less robust than calculated by most models, possibly due to a modulation of the H-T relationship by the SSC. The E39/C data do not support such a SSC-related modulation, and, according to some modelling studies, the E39/C low upper lid might again be the reason. The absence of SSC-QBO entangled effects on the E39/C northern polar vortex has the following consequences: first, the E39/C results do not bring further physical plausibility to the entangled QBO-SSC action probably existing in observational data; second, the model results do not support a mechanism as proposed by *Salby and Callaghan* (2000) because E39/C accounts for a realistic SSC-modulated QBO, but still does not yield SSC-QBO entangled effects.

It is today accepted that the Arctic polar vortex strength during late winter and spring is correlated with the extent of Arctic springtime ozone depletion occurring on particles in polar stratospheric clouds; this kind of ozone depletion can be intense and causes the almost yearly occurring Antarctic ozone hole. In this respect, there is uncertainty about how much the low upper lid of E39/C impacts on estimates of future Arctic ozone layer thickness, and according results should be interpreted with caution.

Neglecting the drawbacks mentioned above, E39/C supports the following view for the near future: higher concentrations of well mixed greenhouse gases strengthen the polar vortex via radiative effects; this strengthening over-compensates or even provokes the stronger activity of global-scale stratospheric waves at middle and higher latitudes (see Objective 1).

5.4 Conclusions and recommendations for future work

In conclusion, the E39/C boundary conditions modulate the ozone layer as well as stratospheric mean meridional transport on long and short time scales. In this respect, the most important result is the significance of tropical SSTs controlling the tropical/subtropical stratospheric transport on a multi-decadal scale; the control is exerted via a SST-dependent generation of tropical/subtropical upward-propagating global-scale waves.

An important task is to find out whether increasing tropical SSTs can cause ENSO-like changes in the wintertime mid- and polar-latitude stratospheric dynamics; such changes could disturb the northern polar vortex against the effect of radiatively induced stabilisation by higher concentrations of well mixed greenhouse gases. The physical mechanism could involve the generation of poleward-

propagating global-scale waves, similarly to the generation of the upward-propagating waves mentioned above. A related research task is to find out whether ENSO causes in E39/C indeed a response of global-scale waves on monthly and interannual time scales, and whether the response includes upward and poleward propagating global-scale waves.

Regarding regression analyses of the ozone layer variability, future work may account for moving-average regression parameters that are likely to improve the compliance with the regression requirements even further. Also, an inclusion of nonlinear deterministic terms in the regression could aim at testing for a coupled nonlinear deterministic response at northern mid-latitudes. For both suggestions, the amount of nonlinearity in the regression may be considerable, necessitating inspections of the least-squares surface for nonlinear distortions.

Last but not least, the conclusions to Chapters 2, 3, and 4 provide more specific suggestions for future work.

Appendix A

Model and scenario description

A.1 Model description

This study uses the chemistry-climate model ECHAM4.L39(DLR)/CHEM, hereafter referred to as E39/C. In the model, radiation couples the dynamical module (ECHAM4.L39) and the chemical module (CHEM) via both heating rates and photolysis rates, allowing for feedbacks between chemistry and dynamics. The integration time step is 30 min, and chemical species are transported by a semi-Lagrangian advection scheme (*Williamson and Rasch, 1994*).

The following studies provide information on E39/C: *Steil et al. (2003, 1998)* describe the chemistry module CHEM, *Roeckner et al. (1996, 1992)* specify the spectral global climate model ECHAM4, *Land et al. (1999)* describe the DLR 39 layer version of ECHAM4, and *Dameris et al. (2006, 2005)*; *Schnadt et al. (2002)*; *Kurz and Grewe (2002)*; *Grewe et al. (2001)*; *Hein et al. (2001)* describe the coupled model system E39/C.

In brief, the horizontal resolution of E39/C is spectral T30, associated with dynamical processes having an isotropic resolution of about 670 km. The corresponding Gaussian transform latitude/longitude grid, on which the model physics, chemistry, and tracer transport are calculated, has a mesh size of $3.75^\circ \times 3.75^\circ$. In the vertical, E39/C has 39 layers from the surface up to the top layer centered at 10 hPa, allowing for the high resolution of about 700 m in the upper troposphere/lower stratosphere. Convection follows the scheme by *Tiedtke (1989)*.

CHEM is based on a generalised family concept, making the chemical calculations efficient. The module accounts for the relevant stratospheric and tropospheric ozone-related homogeneous chemical reactions, as well as for heterogeneous chemistry on polar stratospheric clouds and sulphate aerosols. It does not include bromine chemistry, which may impact on the calculated ozone depletion rates, especially in the Northern Hemisphere. There, ozone is less efficiently destroyed by chlorine than in the Southern Hemisphere.

The net heating rates and photolysis rates in E39/C are calculated from the modelled three-dimensional distributions of the radiatively active gases and clouds, and account for twilight stratospheric ozone chemistry (*Lamago et al.*, 2003).

A.2 Scenario description

Table A.1 specifies important assumptions with regard to the boundary conditions for the E39/C scenarios PAST, WARM, and COLD. Note that Chapter 3 of the present study refers to the combined scenarios PAST and WARM as “REF”. Further background about the boundary conditions is available in Section 2.0.1 and in the first few paragraphs of the Chapters 3 and 4. Additionally, Figures 2.1 and 3.1 illustrate the time evolution of those boundary conditions which are the most relevant to this study. Finally, *Dameris et al.* (2006, 2005) and Section 5.3.7 in *WMO* (2007) provide further information.

Rayner et al. (2003) specify the data set of observed SSTs. *Stott et al.* (2006); *Johns et al.* (2006) inform about the SSTs taken from a run of the HADGEM1 atmosphere ocean general circulation model (AOGCM). The ODS data come from *Brühl and Crutzen* (1993). The SSC data base on *ICARUS* (2005); *Brühl and Crutzen* (1993). *Labitzke et al.* (2002) and *Naujokat* (1986) describe the QBO data set. *Dameris et al.* (2006, 2005) specify the evolution of SULF and NO_x.

Technically, E39/C adopts the SST data sets while not accounting for any atmosphere/ocean feedbacks. Regarding GHG, the gases CH₄ and N₂O represent a condition of the lower boundary, whereas CO₂ is prescribed throughout the model domain. In case of ODS, the chlorine-containing family CIX = HCl + ClONO₂ + Cl + ClO + ClOH + 2 · Cl₂O₂ + 2 · Cl₂, is introduced at the two uppermost model levels, 10 and 20 hPa, and serves as a source for total chlorine by photolysis within the model domain. The CIX data are taken from a separate transient run of the two-dimensional MPIC model (*Brühl and Crutzen*, 1993).

In case of SSC, the evolution of the 11-year cycle in the ultraviolet part of the solar spectrum is parameterised by the 10.7 cm radiation of the sun. There is both an online SSC component within the E39/C model domain and an offline component introduced at the two uppermost model levels to incorporate exchange processes from the upper stratosphere outside the model domain. The former component considers photolysis and radiative heating rates, the latter component considers the ozone-destroying family NO_y = N + NO + NO₂ + NO₃ + 2 · N₂O₅ + HNO₄ + HNO₃. The NO_y data are taken from the MPIC transient model run mentioned above.

The model assimilates the QBO via a relaxation of its tropical stratospheric winds towards the time series of measured tropical zonal wind profiles. The relaxation includes the model levels between 60 hPa and 10 hPa.

With regards to SULF, the separate prescription of sulphate aerosol surface area densities and heating rates accounts for the impact of volcanic eruptions.

Table A.1: E39/C scenario assumptions for the boundary conditions SST (sea surface temperature including sea ice coverage), GHG (well mixed greenhouse gases), ODS (ozone-depleting substances), QBO (quasi-biennial oscillation), SSC (11-year solar cycle), SULF (sulfate aerosol surfaces). *Dameris et al.* (2006, 2005) describe the evolution adopted in case of NO_x (same evolution for WARM and COLD from the year 2000 onwards).

	<i>PAST (1960–1999): three realisations</i>
<i>SST:</i>	observed
<i>GHG:</i>	observed
<i>ODS:</i>	observed
<i>SSC:</i>	observed
<i>QBO:</i>	observed
<i>SULF:</i>	observed
	<i>WARM (2000–2019): three realisations</i>
<i>SST:</i>	AOGCM results following the A1b “medium” scenario in <i>IPCC</i> (2001)
<i>GHG:</i>	A1b “medium” scenario in <i>IPCC</i> (2001)
<i>ODS:</i>	Ab scenario in <i>WMO</i> (2003)
<i>SSC:</i>	1956–1976 observed
<i>QBO:</i>	1960–1979 observed
<i>SULF:</i>	atmospheric background
	<i>COLD (1980–2019): two realisations</i>
<i>SST:</i>	1970–1979 observed, adopted for each decade in 1980–2019
<i>GHG:</i>	1980 observed
<i>ODS:</i>	Ab scenario in <i>WMO</i> (2003)
<i>SSC:</i>	1980–1999: observed, 2000–2019: 1956–1976 observed
<i>QBO:</i>	1980–1999: observed, 2000–2019: 1960–1979 observed
<i>SULF:</i>	1980–1999: observed, 2000–2019: atmospheric background

Bibliography

- An, S.-I., and B. Wang (2001), Mechanisms of locking of the El Niño and La Niña mature phases to boreal winter*, *J. Climate*, *14*, 2164–2176.
- Anderson, J. L., V. Balaji, A. J. Broccoli, W. F. Cooke, T. L. Delworth, K. W. Dixon, L. J. Donner, K. A. Dunne, S. M. Freidenreich, S. T. Garner, R. G. Gudgel, C. T. Gordon, I. M. Held, R. S. Hemler, L. W. Horowitz, S. A. Klein, T. R. Knutson, P. J. Kushner, A. R. Langenhost, N. . Lau, Z. Liang, S. L. Malyshev, P. C. D. Milly, M. J. Nath, J. J. Ploshay, V. Ramaswamy, M. D. Schwarzkopf, E. Shevliakova, J. J. Sirutis, B. J. Soden, W. F. Stern, L. A. Thompson, R. J. Wilson, A. T. Wittenberg, and B. L. Wyman (2004), The new GFDL global atmosphere and land model AM2-LM2: evaluation with prescribed SST simulations, *J. Climate*, *17*(24), 4641–4673.
- Andrews, D. G., and M. E. McIntyre (1976), Planetary waves in horizontal and vertical shear: the generalized Eliassen-Palm relation and the mean zonal acceleration, *J. Atmos. Sci.*, *33*, 2031–2048.
- Andrews, D. G., and M. E. McIntyre (1978), Generalized Eliassen-Palm and Charney-Drazin theorems for waves on axisymmetric mean flows in compressible atmospheres, *J. Atmos. Sci.*, *35*, 175–185.
- Andrews, D. G., J. R. Holton, and C. B. Leovy (1987), *Middle atmosphere dynamics*, 489 pp., Academic Press, Inc., Orlando.
- Aschheim, J., and G. S. Tavlas (1987), Inconsistency in correcting for serial correlation in money-demand models, *Atlantic Econ. J.*, *15*(4), 16–21.
- Aucamp, P. J. (2007), Questions and answers about the effects of the depletion of the ozone layer on humans and the environment, *Photochem. Photobiol. Sci.*, *6*(3), 319–330.
- Austin, J., and F. Li (2006), On the relationship between the strength of the Brewer-Dobson circulation and the age of stratospheric air, *Geophys. Res. Lett.*, *33*, L17807, doi:10.1029/2006GL026867.

- Austin, J., and R. J. Wilson (2006), Ensemble simulations of the decline and recovery of stratospheric ozone, *J. Geophys. Res.*, *111*, D16314, doi:10.1029/2005JD006907.
- Austin, J., D. Shindell, S. R. Beagley, C. Brühl, M. Dameris, E. Manzini, T. Nagashima, P. Newman, S. Pawson, G. Pitari, E. Rozanov, C. Schnadt, and T. G. Shepherd (2003), Uncertainties and assessments of chemistry-climate models of the stratosphere, *Atmos. Chem. Phys.*, *3*, 1–27.
- Austin, J., J. Wilson, F. Li, and H. Vömel (2007), Evolution of water vapor concentrations and stratospheric age of air in coupled chemistry-climate model simulations, *J. Atmos. Sci.*, *64*(3), 905–921.
- Balachandran, N. K., D. Rind, P. Lonergan, and D. T. Shindell (1999), Effects of solar cycle variability on the lower stratosphere and the troposphere, *J. Geophys. Res.*, *104*, 27321–27340, doi:10.1029/1999JD900924.
- Baldwin, M. P., and T. J. Dunkerton (1999), Propagation of the arctic oscillation from the stratosphere to the troposphere, *J. Geophys. Res.*, *104*, 30937–30946, doi:10.1029/1999JD900445.
- Baldwin, M. P., and T. J. Dunkerton (2001), Stratospheric harbingers of anomalous weather regimes, *Science*, *294*, 581–584, doi:10.1126/science.1063315.
- Baldwin, M. P., and D. O’Sullivan (1995), Stratospheric effects of ENSO-related tropospheric circulation anomalies, *J. Climate*, *8*, 649–667.
- Baldwin, M. P., L. J. Gray, T. J. Dunkerton, K. Hamilton, P. H. Haynes, W. J. Randel, J. R. Holton, M. J. Alexander, I. Hirota, T. Horinouchi, D. B. A. Jones, J. S. Kinnersley, C. Marquardt, K. Sato, and M. Takahashi (2001), The quasi-biennial oscillation, *Rev. Geophys.*, *39*, 179–230, doi:10.1029/1999RG000073.
- Baldwin, M. P., D. B. Stephenson, D. W. J. Thompson, T. J. Dunkerton, A. J. Charlton, and A. O’Neill (2003), Stratospheric memory and skill of extended-range weather forecasts, *Science*, *301*, 636–640, doi:10.1126/science.1087143.
- Baldwin, M. P., M. Dameris, and T. G. Shepherd (2007), How will the stratosphere affect climate change?, *Science*, *316*(5831), 1576–1577.
- Barsugli, J., S.-I. Shin, and P. D. Sardeshmukh (2005), Tropical climate regimes and global climate sensitivity in a simple setting, *J. Atmos. Sci.*, *62*, 1226–1240.
- Barsugli, J. J., S.-I. Shin, and P. D. Sardeshmukh (2006), Sensitivity of global warming to the pattern of tropical ocean warming, *Clim. Dynam.*, *27*, 483–492, doi:10.1007/s00382-006-0143-7.
- Bates, D. M., and D. G. Watts (1988), *Nonlinear regression analysis and its applications*, 364 pp., John Wiley & Sons, Inc., New York.

- Benabbas, L., S. P. Asprey, and S. Macchietto (2005), Curvature-based methods for designing optimally informative experiments in multiresponse nonlinear dynamic situations, *Ind. Eng. Chem.*, *44*(18), 7120–7131.
- Black, E., and R. Sutton (2007), The influence of oceanic conditions on the hot European summer of 2003, *Clim. Dynam.*, *28*, 53–66, doi:10.1007/s00382-006-0179-8.
- Blackmon, M. L., and G. H. White (1982), Zonal wavenumber characteristics of northern hemisphere transient eddies, *J. Atmos. Sci.*, *39*, 1985–1998.
- Blackmon, M. L., G. W. Branstator, G. T. Bates, and J. E. Geisler (1987), An analysis of equatorial pacific sea surface temperature anomaly experiments in general circulation models with and without mountains, *J. Atmos. Sci.*, *44*, 1828–1844.
- Bodeker, G. E., I. S. Boyd, and W. A. Matthews (1998), Trends and variability in vertical ozone and temperature profiles measured by ozonesondes at Lauder, New Zealand: 1986-1996, *J. Geophys. Res.*, *103*, 28661–28682, doi:10.1029/98JD02581.
- Bodeker, G. E., H. Garny, D. Smale, M. Dameris, and R. Deckert (2007), The 1985 southern hemisphere mid-latitude total column ozone anomaly, *Atmos. Chem. Phys.*, *7*(3), 5625–5637.
- Boehm, M. T., and S. Lee (2003), The implications of tropical rossby waves for tropical tropopause cirrus formation and for the equatorial upwelling of the Brewer-Dobson circulation, *J. Atmos. Sci.*, *60*, 247–261.
- Bojkov, R., L. Bishop, W. J. Hill, G. C. Reinsel, and G. C. Tiao (1990), A statistical trend analysis of revised Dobson total ozone data over the northern hemisphere, *J. Geophys. Res.*, *95*, 9785–9807.
- Bojkov, R. D. (1987), The 1983 and 1985 anomalies in ozone distribution in perspective, *Mon. Weather Rev.*, *115*, 2187–2201.
- Bojkov, R. D., and V. E. Fioletov (1995), Estimating the global ozone characteristics during the last 30 years, *J. Geophys. Res.*, *100*, 16537–16552, doi:10.1029/95JD00692.
- Box, G. E., G. M. Jenkins, and G. C. Reinsel (1994), *Time series analysis: forecasting and control*, 3d ed., 592 pp., Prentice Hall, New York.
- Branstator, G. (1985), Analysis of general circulation model sea-surface temperature anomaly simulations using a linear model. Part I: forced solutions, *J. Atmos. Sci.*, *42*, 2225–2241.

- Brasseur, G., and S. Solomon (1986), *Aeronomy of the middle atmosphere*, 452 pp., D. Reidel Publishing Company, Dordrecht.
- Brönnimann, S., M. Schraner, B. Müller, A. Fischer, D. Brunner, E. Rozanov, and T. Egorova (2006), The 1986-1989 ENSO cycle in a chemical climate model, *Atmos. Chem. Phys.*, *6*, 4669–4685.
- Brühl, C., and P. J. Crutzen (1993), MPIC two-dimensional model, *NASA Ref. Publ. 1292*, NASA, 103-104.
- Brunner, D., J. Staehelin, J. A. Maeder, I. Wohltmann, and G. E. Bodeker (2006), Variability and trends in total and vertically resolved stratospheric ozone based on the CATO ozone data set, *Atmos. Chem. Phys.*, *6*, 4985–5008.
- Butchart, N., and A. A. Scaife (2001), Removal of chlorofluorocarbons by increased mass exchange between the stratosphere and troposphere in a changing climate, *Nature*, *410*, 799–802.
- Butchart, N., J. Austin, J. R. Knight, A. A. Scaife, and M. L. Gallani (2000), The response of the stratospheric climate to projected changes in the concentrations of well-mixed greenhouse gases from 1992 to 2051, *J. Climate*, *13*, 2142–2159.
- Butchart, N., A. A. Scaife, M. Bourqui, J. de Grandpré, S. H. E. Hare, J. Kettleborough, U. Langematz, E. Manzini, F. Sassi, K. Shibata, D. Shindell, and M. Sigmond (2006), Simulations of anthropogenic change in the strength of the Brewer Dobson circulation, *Clim. Dynam.*, *27*, 727–741, doi:10.1007/s00382-006-0162-4.
- Calvo Fernández, N., R. R. García, R. García Herrera, D. Gallego Puyol, L. Gimeno Presa, E. Hernández Martín, and P. Ribera Rodríguez (2004), Analysis of the ENSO signal in tropospheric and stratospheric temperatures observed by MSU, 1979-2000, *J. Climate*, *17*(20), 3934–3946.
- Canjels, E., and M. W. Watson (1997), Estimating deterministic trends in the presence of serially correlated errors, *Rev. Econ. Statist.*, *79*(2), 184–197.
- Carroll, R. J., and D. Ruppert (1988), *Transformation and weighting in Regression*, 264 pp., John Wiley & Sons, Inc., New York.
- Chandra, S., and R. D. McPeters (1994), The solar cycle variation of ozone in the stratosphere inferred from Nimbus 7 and NOAA 11 satellites, *J. Geophys. Res.*, *99*, 20665–20671.
- Charney, J. G., and P. G. Drazin (1961), Propagation of planetary-scale disturbances from the lower into the upper atmosphere, *J. Geophys. Res.*, *66*, 83–109.

- Charney, J. G., and A. Eliassen (1949), A numerical method for predicting the perturbations of the middle latitude westerlies, *Tellus*, *1*, 38–54.
- Chen, C. T., and E. Roeckner (1997), Cloud simulations with the Max Planck Institute for Meteorology general circulation model ECHAM4 and comparison with observations, *J. Geophys. Res.*, *102*(8), 9335–9350.
- Chen, P. (2001), Thermally forced stationary waves in a quasigeostrophic system, *J. Atmos. Sci.*, *58*, 1585–1594.
- Chen, P., and W. A. Robinson (1992), Propagation of planetary waves between the troposphere and stratosphere, *J. Atmos. Sci.*, *49*, 2533–2545.
- Chen, P., M. P. Hoerling, and R. M. Dole (2001), The origin of the subtropical anticyclones, *J. Atmos. Sci.*, *58*, 1827–1835.
- Chen, T. C., and M. C. Yen (1993), Interannual variation of summertime stationary eddies, *J. Climate*, *6*, 2263–2277.
- Chen, W., M. Takahashi, and H.-F. Graf (2003), Interannual variations of stationary planetary wave activity in the northern winter troposphere and stratosphere and their relations to NAM and SST, *J. Geophys. Res.*, *108*, 4797, doi:10.1029/2003JD003834.
- Chipperfield, M. P. (1999), Multiannual simulations with a three-dimensional chemical transport model, *J. Geophys. Res.*, *104*, 1781–1806, doi:10.1029/98JD02597.
- Chipperfield, M. P. (2003), A three-dimensional model study of long-term mid-high latitude lower stratosphere ozone changes, *Atmos. Chem. Phys.*, *3*, 1253–1265.
- Clarke, A. J., and K.-Y. Kim (2005), On weak zonally symmetric ENSO atmospheric heating and the strong zonally symmetric ENSO air temperature response, *J. Atmos. Sci.*, *62*, 2012–2022.
- Cochrane, D., and G. H. Orcutt (1949), Application of least squares regression to relationships containing autocorrelated error terms, *J. Amer. Statistical Assoc.*, *44*, 32–61.
- Connor, B. J., G. E. Bodeker, R. L. McKenzie, and I. S. Boyd (1999), The total ozone anomaly at Lauder, NZ in 1997, *Geophys. Res. Lett.*, *26*, 189–192, doi:10.1029/1998GL900250.
- Cordero, E. C., and S. R. Kawa (2001), Ozone and tracer transport variations in the summer Northern Hemisphere stratosphere, *J. Geophys. Res.*, *106*, 12227–12240, doi:10.1029/2001JD900004.

- Cordero, E. C., and T. R. Nathan (2002), An examination of anomalously low column ozone in the Southern Hemisphere midlatitudes during 1997, *Geophys. Res. Lett.*, *29*, 27–1.
- Cordero, E. C., and T. R. Nathan (2005), A new pathway for communicating the 11-year solar cycle signal to the QBO, *Geophys. Res. Lett.*, *32*, L18805, doi:10.1029/2005GL023696.
- Crooks, S. A., and L. J. Gray (2005), Characterization of the 11-year solar signal using a multiple regression analysis of the ERA-40 dataset, *J. Climate*, *18*, 996–1015.
- Crutcher, H. L., and J. M. Meserve (1970), *Selected level heights, temperatures and dew points for the northern hemisphere, NAVAIR-50-1C-52, revised.*, Chief of Nav. Operat., Washington, D.C.
- Dameris, M. (Ed.) (2007), *Impact of climate change on ozone recovery*, chap. 5.3.7, Scientific assessment of ozone depletion: 2006, World Meteorological Organization, Geneva, Switzerland.
- Dameris, M., and R. Deckert (2008), *Simulation of long-term evolution of stratospheric dynamics and chemistry: role of natural and anthropogenic forcings*, chap. 18, pp. 283–291, Climate variability and extremes during the past 100 years, Springer.
- Dameris, M., and A. Ebel (1990), The quasi-biennial oscillation and major stratospheric warmings - a three-dimensional model study, *Ann. Geophys.*, *8*, 79–85.
- Dameris, M., V. Grewe, M. Ponater, R. Deckert, V. Eyring, F. Mager, S. Matthes, C. Schnadt, A. Stenke, B. Steil, C. Brühl, and M. A. Giorgetta (2005), Long-term changes and variability in a transient simulation with a chemistry-climate model employing realistic forcing, *Atmos. Chem. Phys.*, *5*, 2121–2145.
- Dameris, M., S. Matthes, R. Deckert, V. Grewe, and M. Ponater (2006), Solar cycle effect delays onset of ozone recovery, *Geophys. Res. Lett.*, *33*, L03806, doi:10.1029/2005GL024741.
- Dhomse, S., M. Weber, I. Wohltmann, M. Rex, and J. P. Burrows (2006), On the possible causes of recent increases in northern hemispheric total ozone from a statistical analysis of satellite data from 1979 to 2003, *Atmos. Chem. Phys.*, *6*, 1165–1180.
- Diaz, H. F., M. P. Hoerling, and J. K. Eischeid (2001), ENSO variability, teleconnections and climate change, *Int. J. Climatol.*, *21*, 1845–1862.
- Dickinson, R. E. (1968), Planetary rossby waves propagating vertically through weak westerly wind wave guides, *J. Atmos. Sci.*, *25*, 984–1002.

- Dolan, K. D., L. Yang, and C. P. Trampel (2007), Nonlinear regression technique to estimate kinetic parameters and confidence intervals in unsteady-state conduction-heated foods, *J. Food Eng.*, *80*(2), 581–593.
- Douville, H. (2005), Limitations of time-slice experiments for predicting regional climate change over South Asia, *Clim. Dynam.*, *24*, 373–391, doi:10.1007/s00382-004-0509-7.
- Draper, N. R., and H. Smith (1998), *Applied regression analysis*, 3d ed., 602 pp., John Wiley & Sons, Inc., New York.
- Dufour, J. ., M. J. I. Gaudry, and R. W. Hafer (1983), A warning on the use of the Cochrane-Orcutt procedure based on a money demand equation, *Empirical Econ.*, *8*(2), 111–117.
- Dunkerton, T. (1978), On the mean meridional mass motions of the stratosphere and mesosphere, *J. Atmos. Sci.*, *35*, 2325–2333.
- Dutton, J. A. (1976), *The ceaseless wind*, 579 pp., McGraw-Hill, New York.
- Edmon, H. J., B. J. Hoskins, and M. E. McIntyre (1980), Eliassen-Palm cross sections for the troposphere, *J. Atmos. Sci.*, *37*, 2600–2616.
- Eliassen, A., and E. Palm (1961), On the transfer of energy in stationary mountain waves, *Geophys. Publ.*, *22*, 1–23.
- Eyring, V., N. Butchart, D. W. Waugh, H. Akiyoshi, J. Austin, S. Bekki, G. E. Bodeker, B. A. Boville, C. Brühl, M. P. Chipperfield, E. Cordero, M. Dameris, M. Deushi, V. E. Fioletov, S. M. Frith, R. R. Garcia, A. Gettelman, M. A. Giorgetta, V. Grewe, L. Jourdain, D. E. Kinnison, E. Mancini, E. Manzini, M. Marchand, D. R. Marsh, T. Nagashima, P. A. Newman, J. E. Nielsen, S. Pawson, G. Pitari, D. A. Plummer, E. Rozanov, M. Schraner, T. G. Shepherd, K. Shibata, R. S. Stolarski, H. Struthers, W. Tian, and M. Yoshiki (2006), Assessment of temperature, trace species, and ozone in chemistry-climate model simulations of the recent past, *J. Geophys. Res.*, *111*, D22308, doi:10.1029/2006JD007327.
- Eyring, V., D. W. Waugh, G. E. Bodeker, E. Cordero, H. Akiyoshi, J. Austin, S. R. Beagley, B. A. Boville, P. Braesicke, C. Brühl, N. Butchart, M. P. Chipperfield, M. Dameris, R. Deckert, M. Deushi, S. M. Frith, R. R. Garcia, A. Gettelman, M. A. Giorgetta, D. E. Kinnison, E. Mancini, E. Manzini, D. R. Marsh, S. Matthes, T. Nagashima, P. A. Newman, J. E. Nielsen, S. Pawson, G. Pitari, D. A. Plummer, E. Rozanov, M. Schraner, J. F. Scinocca, K. Semeniuk, T. G. Shepherd, K. Shibata, B. Steil, R. S. Stolarski, W. Tian, and M. Yoshiki (2007), Multimodel projections of stratospheric ozone in the 21st century, *J. Geophys. Res.*, *112*, D16303, doi:10.1029/2006JD008332.

- Fadnavis, S., and G. Beig (2006), Decadal solar effects on temperature and ozone in the tropical stratosphere, *Ann. Geophys.*, *24*, 2091–2103.
- Feldstein, S. B. (2003), The dynamics associated with equatorial atmospheric angular momentum in an aquaplanet GCM, *J. Atmos. Sci.*, *60*, 1822–1834.
- Feldstein, S. B. (2006), Dynamical processes of equatorial atmospheric angular momentum, *J. Atmos. Sci.*, *63*, 565–581.
- Fels, S. B., J. D. Mahlman, M. D. Schwarzkopf, and R. W. Sinclair (1980), Stratospheric sensitivity to perturbations in ozone and carbon dioxide: radiative and dynamical response, *J. Atmos. Sci.*, *37*, 2265–2297.
- Fioletov, V. E., and T. G. Shepherd (2005), Summertime total ozone variations over middle and polar latitudes, *Geophys. Res. Lett.*, *32*, L04807, doi:10.1029/2004GL022080.
- Fioletov, V. E., G. E. Bodeker, A. J. Miller, R. D. McPeters, and R. Stolarski (2002), Global and zonal total ozone variations estimated from ground-based and satellite measurements: 1964–2000, *J. Geophys. Res.*, *107*, 4647, doi:10.1029/2001JD001350.
- Fleming, E. L., C. H. Jackman, D. K. Weisenstein, and M. K. W. Ko (2007), The impact of interannual variability on multidecadal total ozone simulations, *J. Geophys. Res.*, *112*, D10310, doi:10.1029/2006JD007953.
- Fomichev, V. I., A. I. Jonsson, J. de Grandpré, S. R. Beagley, C. McLandress, K. Semeniuk, and T. G. Shepherd (2007), Response of the middle atmosphere to CO₂ doubling: results from the canadian middle atmosphere model, *J. Climate*, *20*(7), 1121–1144.
- Forster, P. M. d. F., and K. P. Shine (1999), Stratospheric water vapor changes as a possible contributor to observed stratospheric cooling, *Geophys. Res. Lett.*, *26*, 3309–3312, doi:10.1029/1999GL010487.
- Fusco, A. C., and M. L. Salby (1999), Interannual variations of total ozone and their relationship to variations of planetary wave activity, *J. Climate*, *12*, 1619–1629.
- Garbow, B. S., K. E. Hillstrom, and J. J. Moré (1980), *Documentation for MINPACK*, Argonne National Laboratory, 9700 South Class Avenue, Argonne, Illinois 60439, USA.
- Garcia, R. R., and M. L. Salby (1987), Transient response to localized episodic heating in the tropics. Part II: far-field behavior, *J. Atmos. Sci.*, *44*, 499–532.

- García-Herrera, R., N. Calvo, R. R. Garcia, and M. A. Giorgetta (2006), Propagation of ENSO temperature signals into the middle atmosphere: a comparison of two general circulation models and ERA-40 reanalysis data, *J. Geophys. Res.*, *111*, D06101, doi:10.1029/2005JD006061.
- Garny, H., G. E. Bodeker, and M. Dameris (2007), Trends and variability in stratospheric mixing: 1979-2005, *Atmos. Chem. Phys.*, *7*, 5611–5624.
- Geisler, J. E., M. L. Blackmon, G. T. Bates, and S. Muñoz (1985), Sensitivity of january climate response to the magnitude and position of equatorial pacific sea surface temperature anomalies, *J. Atmos. Sci.*, *42*, 1037–1049.
- Gettelman, A., J. R. Holton, and K. H. Rosenlof (1997), Mass fluxes of O₃, CH₄, N₂O and CF₂Cl₂ in the lower stratosphere calculated from observational data, *J. Geophys. Res.*, *102*, 19149–19160, doi:10.1029/97JD01014.
- Gettelman, A., W. J. Randel, S. Massie, F. Wu, W. G. Read, and J. M. Russell, III (2001), El Niño as a natural experiment for studying the tropical tropopause region, *Journal of Climate*, *14*, 3375–3392.
- Giannini, A., R. Saravanan, and P. Chang (2003), Oceanic forcing of sahel rainfall on interannual to interdecadal time scales, *Science*, *302*, 1027–1030, doi:10.1126/science.1089357.
- Gill, A. E. (1980), Some simple solutions for heat-induced tropical circulation, *Quart. J. Roy. Meteorol. Soc.*, *106*, 447–462.
- Gillett, N. P., M. R. Allen, and K. D. Williams (2003), Modelling the atmospheric response to doubled CO₂ and depleted stratospheric ozone using a stratosphere-resolving coupled GCM, *Quart. J. Roy. Meteorol. Soc.*, *129*, 947–966.
- Gray, L. J. (2003), The influence of the equatorial upper stratosphere on stratospheric sudden warmings, *Geophys. Res. Lett.*, *30*, 1–15.
- Gray, L. J., E. F. Drysdale, T. J. Dunkerton, and B. N. Lawrence (2001a), Model studies of the interannual variability of the northern-hemisphere stratospheric winter circulation: the role of the quasi-biennial oscillation, *Quart. J. Roy. Meteorol. Soc.*, *127*, 1413–1432.
- Gray, L. J., S. J. Phipps, T. J. Dunkerton, M. P. Baldwin, E. F. Drysdale, and M. R. Allen (2001b), A data study of the influence of the equatorial upper stratosphere on northern-hemisphere stratospheric sudden warmings, *Quart. J. Roy. Meteorol. Soc.*, *127*, 1985–2004.
- Gray, L. J., S. Sparrow, M. Juckes, A. O’Neill, and D. G. Andrews (2003), Flow regimes in the winter stratosphere of the northern hemisphere, *Quart. J. Roy. Meteorol. Soc.*, *129*, 925–945.

- Gray, L. J., S. Crooks, C. Pascoe, S. Sparrow, and M. Palmer (2004), Solar and QBO influences on the timing of stratospheric sudden warmings, *J. Atmos. Sci.*, *61*, 2777–2796.
- Grewe, V. (2006), The origin of ozone, *Atmos. Chem. Phys.*, *6*, 1495–1511.
- Grewe, V. (2007), Institut für Physik der Atmosphäre, DLR-Oberpfaffenhofen, Wessling, Germany, Personal communication.
- Grewe, V., D. Brunner, M. Dameris, J. L. Grenfell, R. Hein, D. Shindell, and J. Staehelin (2001), Origin and variability of upper tropospheric nitrogen oxides and ozone at northern mid-latitudes, *Atmos. Environ.*, *35*(20), 3421–3433.
- Haigh, J. D. (1996), The impact of solar variability on climate, *Science*, *272*, 981–984.
- Hall, N. M. J., and J. Derome (2000), Transience, nonlinearity, and eddy feedback in the remote response to El Niño, *J. Atmos. Sci.*, *57*, 3992–4007.
- Hall, N. M. J., J. Derome, and H. Lin (2001a), The extratropical signal generated by a midlatitude SST anomaly. Part I: sensitivity at equilibrium, *J. Climate*, *14*, 2035–2053.
- Hall, N. M. J., H. Lin, and J. Derome (2001b), The extratropical signal generated by a midlatitude SST anomaly. Part II: influence on seasonal forecasts, *J. Climate*, *14*, 2696–2709.
- Harnik, N., and R. S. Lindzen (2001), The effect of reflecting surfaces on the vertical structure and variability of stratospheric planetary waves, *J. Atmos. Sci.*, *58*, 2872–2894.
- Hartmann, D. L., J. M. Wallace, V. Limpasuvan, D. W. J. Thompson, and J. R. Holton (2000), Can ozone depletion and global warming interact to produce rapid climate change?, *P. Nat. Ac. Sc. Am.*, *97*(4), 1412–1417.
- Haynes, P. (2005), Stratospheric dynamics, *Annu. Rev. Fluid. Mech.*, *37*, 263–293.
- Haynes, P. H., M. E. McIntyre, T. G. Shepherd, C. J. Marks, and K. P. Shine (1991), On the ‘downward control’ of extratropical diabatic circulations by eddy-induced mean zonal forces, *J. Atmos. Sci.*, *48*, 651–680.
- Hein, R., M. Dameris, C. Schnadt, C. Land, V. Grewe, I. Köhler, M. Ponater, R. Sausen, B. Steil, J. Landgraf, and C. Brühl (2001), Results of an interactively coupled atmospheric chemistry – general circulation model: comparison with observations, *Ann. Geophys.*, *19*, 435–457.
- Held, I. M. (1985), Pseudomomentum and the orthogonality of modes in shear flows, *J. Atmos. Sci.*, *42*(21), 2280–2288.

- Hines, C. O. (1960), Internal atmospheric gravity waves at ionospheric heights, *Can. J. Phys.*, *38*, 1441–1481.
- Hitchman, M. H., and A. S. Huesmann (2007), A seasonal climatology of Rossby wave breaking in the 320–2000-K layer, *J. Atmos. Sci.*, *64*, 1922–1940, doi: 10.1175/JAS3927.1.
- Holton, J. R., and J. Austin (1991), The influence of the equatorial QBO on sudden stratospheric warmings, *J. Atmos. Sci.*, *48*, 607–618.
- Holton, J. R., and H.-C. Tan (1980), The influence of the equatorial quasibiennial oscillation on the global circulation at 50 MB, *J. Atmos. Sci.*, *37*, 2200–2208.
- Holton, J. R., and H.-C. Tan (1982), The influence of the equatorial quasibiennial oscillation on the global circulation at 50 MB, *J. Phys. Soc. Japan*, *60*, 140–148.
- Holton, J. R., P. H. Haynes, M. E. McIntyre, A. R. Douglass, R. B. Rood, and L. Pfister (1995), Stratosphere-troposphere exchange, *Rev. Geophys.*, *33*, 403–439.
- Hood, L. L., and B. E. Soukharev (2005), Interannual variations of total ozone at northern midlatitudes correlated with stratospheric EP flux and potential vorticity, *J. Atmos. Sci.*, *62*, 3724–3740.
- Horinouchi, T., S. Pawson, K. Shibata, U. Langematz, E. Manzini, M. A. Giorgetta, F. Sassi, R. J. Wilson, K. Hamilton, J. de Grandpré, and A. A. Scaife (2003), Tropical cumulus convection and upward-propagating waves in middle-atmospheric GCMs, *J. Atmos. Sci.*, *60*, 2765–2782.
- Hoskins, B. J., I. N. James, and G. H. White (1983), The shape, propagation and mean-flow interaction of large-scale weather systems, *J. Atmos. Sci.*, *40*, 1595–1612.
- Hu, Y., and K. K. Tung (2002), Interannual and decadal variations of planetary wave activity, stratospheric cooling, and northern hemisphere annular mode, *J. Climate*, *15*(13), 1659–1673.
- ICARUS (2005), Data taken from <http://www.drao.nrc.ca/icarus/www/daily.html>, Herzberg Institute of Astrophysics, Penticton, Canada.
- Inatsu, M., H. Mukougawa, and S.-P. Xie (2002), Stationary eddy response to surface boundary forcing: idealized GCM experiments*, *J. Atmos. Sci.*, *59*, 1898–1915.
- IPCC (2001), *Climate Change 2001 – The scientific basis*, Intergovernmental Panel on Climate Change, New York, USA.

- IPCC (2007), *Climate change 2007 – the scientific basis*, Intergovernmental Panel on Climate Change, New York, USA.
- Itoh, H. (1985), The role of transient motions in the formation of quasi-stationary planetary waves, *J. Atmos. Sci.*, *42*, 917–932.
- Jiang, X., S. J. Eichelberger, D. L. Hartmann, R. Shia, and Y. L. Yung (2007), Influence of doubled CO₂ on ozone via changes in the Brewer-Dobson circulation, *J. Atmos. Sci.*, *64*(7), 2751–2755.
- Johns, T. C., C. F. Durman, H. T. Banks, M. J. Roberts, A. J. McLaren, J. K. Ridley, C. A. Senior, K. D. Williams, A. Jones, G. J. Rickard, S. Cusack, W. J. Ingram, M. Crucifix, D. M. H. Sexton, M. M. Joshi, B. . Dong, H. Spencer, R. S. R. Hill, J. M. Gregory, A. B. Keen, A. K. Pardaens, J. A. Lowe, A. Bodas-Salcedo, S. Stark, and Y. Searl (2006), The new Hadley Centre Climate Model (HadGEM1): evaluation of coupled simulations, *J. Climate*, *19*(7), 1327–1353.
- Kalnay, E., M. Kanamitsu, R. Kistler, W. Collins, D. Deaven, L. Gandin, M. Iredell, S. Saha, G. White, J. Woollen, Y. Zhu, A. Leetmaa, B. Reynolds, M. Chelliah, W. Ebisuzaki, W. Higgins, J. Janowiak, K. C. Mo, C. Ropelewski, J. Wang, R. Jenne, and D. Joseph (1996), The NCEP/NCAR 40-year reanalysis project, *Bull. Amer. Astron. Soc.*, *77*, 437–472.
- Keckhut, P., C. Cagnazzo, M.-L. Chanin, C. Claud, and A. Hauchecorne (2005), The 11-year solar-cycle effects on the temperature in the upper-stratosphere and mesosphere: part I assessment of observations, *J. Atmos. Terr. Phys.*, *67*, 940–947, doi:10.1016/j.jastp.2005.01.008.
- Kim, S. E., and A. Kumar (2005), Accounting seasonal nonstationarity in time series models for short-term ozone level forecast, *Stoch. Env. Res. Risk. A.*, *19*, 241–248.
- Kinnersley, J. S., and K. K. Tung (1998), Modeling the global interannual variability of ozone due to the equatorial QBO and to extratropical planetary wave variability, *J. Atmos. Sci.*, *55*, 1417–1428.
- Kinnersley, J. S., and K. K. Tung (1999), Mechanisms for the extratropical QBO in circulation and ozone, *J. Atmos. Sci.*, *56*, 1942–1962.
- Kirchner, I., G. L. Stenchikov, H.-F. Graf, A. Robock, and J. C. Antuña (1999), Climate model simulation of winter warming and summer cooling following the 1991 Mount Pinatubo volcanic eruption, *J. Geophys. Res.*, *104*, 19039–19056, doi:10.1029/1999JD900213.
- Kodera, K. (1993), Quasi-decadal modulation of the influence of the equatorial quasi-biennial oscillation of the north polar stratospheric temperatures, *J. Geophys. Res.*, *98*, 7245–7250.

- Kodera, K., and Y. Kuroda (2002), Dynamical response to the solar cycle, *J. Geophys. Res.*, *107*, 5–1, doi:10.1029/2002JD002224.
- Kodera, K., and K. Yamazaki (1994), A possible influence of recent polar stratospheric coolings on the troposphere in the northern hemisphere winter, *Geophys. Res. Lett.*, *21*, 809–812.
- Koshyk, J. N., and K. Hamilton (2001), The horizontal kinetic energy spectrum and spectral budget simulated by a high-resolution troposphere-stratosphere-mesosphere GCM, *J. Atmos. Sci.*, *58*, 329–348.
- Krishnamurti, T. N., and D. R. Chakraborty (2005), The dynamics of phase locking, *J. Atmos. Sci.*, *62*, 2952–2964.
- Krzyszcin, J., K. Eerme, and M. Janouch (2004), Long-term variations of the UV-B radiation over Central Europe as derived from the reconstructed UV time series, *Ann. Geophys.*, *22*, 1473–1485.
- Krzyścin, J. W. (1994), On the interannual oscillations in the northern temperature total ozone, *J. Geophys. Res.*, *99*, 14527–14534, doi:10.1029/94JD01022.
- Kurz, C., and V. Grewe (2002), Lightning and thunderstorms, part 1: observational data and model results, *Meteor. Z.*, *11*, 379–393.
- Kushnir, Y., W. A. Robinson, I. Bladé, N. M. J. Hall, S. Peng, and R. Sutton (2002), Atmospheric GCM response to extratropical SST anomalies: synthesis and evaluation, *J. Climate*, *15*, 2233–2256.
- Labitzke, K. (1972), Climatology of the stratosphere in the northern hemisphere, 1, heights, temperatures, and geostrophic resultant wind speeds at 100, 50, 30, and 10 mb, *Bonn. Meteorol. Abh.*, *100*, 4.
- Labitzke, K. (1987), Sunspots, the QBO, and the stratospheric temperature in the north polar region, *Geophys. Res. Lett.*, *14*, 535–537.
- Labitzke, K. (2004), On the signal of the 11-year sunspot cycle in the stratosphere and its modulation by the quasi-biennial oscillation, *J. Atmos. Terr. Phys.*, *66*, 1151–1157, doi:10.1016/j.jastp.2004.05.011.
- Labitzke, K. (2005), On the solar cycle QBO relationship: a summary, *J. Atmos. Terr. Phys.*, *67*, 45–54, doi:10.1016/j.jastp.2004.07.016.
- Labitzke, K., and K. Matthes (2003), 11-year solar cycle variations in the atmosphere: observations, mechanisms, and models, *Holocene*, *13*, 311–317.
- Labitzke, K., and H. van Loon (1992), Die 10-12jährige Schwingung in der Stratosphäre, in *Meteorologische Fortbildung*, *22. Jahrgang*, pp. 58–61, Deutscher Wetterdienst, Offenbach (Main), Germany.

- Labitzke, K., and H. van Loon (2000), The QBO effect on the solar signal in the global stratosphere in the winter of the northern hemisphere, *J. Atmos. Terr. Phys.*, *62*, 621–628.
- Labitzke, K., D. Lamago, M. Dameris, C. Schnadt, V. Eyring, and C. Brühl (2002), The Berlin stratospheric data set, CD from the Meteorological Institute of the Free University Berlin.
- Labitzke, K., M. Kunze, and S. Brönnimann (2006), Sunspots, the QBO and the stratosphere in the north polar region – 20 years later, *Meteor. Z.*, *15*, 355–363.
- Lamago, D., M. Dameris, C. Schnadt, V. Eyring, and C. Brühl (2003), Impact of large solar zenith angles on lower stratospheric dynamical and chemical processes in a coupled chemistry-climate model, *Atmos. Chem. Phys.*, *3*, 1981–1990.
- Land, C., M. Ponater, S. R., and R. E. (1999), The ECHAM4.L39(DLR) atmosphere GCM – technical description and model climatology, *Report 1999-32*, DLR Oberpfaffenhofen, Wessling, Germany.
- Lean, J., and D. Rind (1998), Climate forcing by changing solar radiation, *J. Climate*, *11*, 3069–3094.
- Lean, J. L., G. J. Rottman, H. L. Kyle, T. N. Woods, J. R. Hickey, and L. C. Puga (1997), Detection and parameterization of variations in solar mid- and near-ultraviolet radiation (200–400 nm), *J. Geophys. Res.*, *102*, 29939–29956, doi:10.1029/97JD02092.
- Lee, H., and A. K. Smith (2003), Simulation of the combined effects of solar cycle, quasi-biennial oscillation, and volcanic forcing on stratospheric ozone changes in recent decades, *J. Geophys. Res.*, *108*, 4049, doi:10.1029/2001JD001503.
- Lee, S. (1999), Why are the climatological zonal winds easterly in the equatorial upper troposphere?, *J. Atmos. Sci.*, *56*, 1353–1363.
- Li, Q., H.-F. Graf, and M. A. Giorgetta (2007), Stationary planetary wave propagation in northern hemisphere winter - climatological analysis of the refractive index, *Atmos. Chem. Phys.*, *7*, 183–200.
- Lighthill, J. (1978), *Waves in fluids*, Cambridge, Cambridge University Press, 1978. 516 p.
- Limpasuvan, V., and D. L. Hartmann (2000), Wave-maintained annular modes of climate variability*, *J. Climate*, *13*, 4414–4429.
- Logan, J. A. (1994), Trends in the vertical distribution of ozone: an analysis of ozonesonde data, *J. Geophys. Res.*, *99*, 25553–25586, doi:10.1029/94JD02333.

- Longuet-Higgins, M. S. (1968), The eigenfunctions of Laplace's tidal equations over a sphere, *Philos. Trans. Roy. Soc. London Ser. A*, *262*, 511–607.
- Lu, J., and T. L. Delworth (2005), Oceanic forcing of the late 20th century Sahel drought, *Geophys. Res. Lett.*, *32*, L22706, doi:10.1029/2005GL023316.
- Mäder, J. A., J. Staehelin, D. Brunner, W. A. Stahel, I. Wohltmann, and T. Peter (2007), Statistical modeling of total ozone: selection of appropriate explanatory variables, *J. Geophys. Res.*, *112*, D11108, doi:10.1029/2006JD007694.
- Mahfouf, J., D. Cariolle, J.-F. Royer, J.-F. Geleyn, and B. Timbal (1994), Response of the Météo-France climate model to changes in CO₂ and sea surface temperature, *Clim. Dynam.*, *9*, 345–362.
- Malone, R. C., E. J. Pitcher, M. L. Blackmon, K. Puri, and W. Bourke (1984), The simulation of stationary and transient geopotential-height eddies in January and July with a spectral general circulation model, *J. Atmos. Sci.*, *41*, 1394–1419.
- Manzini, E., M. A. Giorgetta, M. Esch, L. Kornblueh, and E. Roeckner (2006), The influence of sea surface temperatures on the northern winter stratosphere: ensemble simulations with the MAECHAM5 model, *J. Climate*, *19*(16), 3863–3881.
- Matsuno, T. (1970), Vertical propagation of stationary planetary waves in the winter northern hemisphere, *J. Atmos. Sci.*, *27*, 871–883.
- Matthes, K., U. Langematz, L. L. Gray, K. Kodera, and K. Labitzke (2004), Improved 11-year solar signal in the Freie Universität Berlin climate middle atmosphere model (FUB-CMAM), *J. Geophys. Res.*, *109*, D06101, doi:10.1029/2003JD004012.
- Matthes, K., Y. Kuroda, K. Kodera, and U. Langematz (2006), Transfer of the solar signal from the stratosphere to the troposphere: northern winter, *J. Geophys. Res.*, *111*, D06108, doi:10.1029/2005JD006283.
- May, W. (2004a), Potential future changes in the Indian summer monsoon due to greenhouse warming: analysis of mechanisms in a global time-slice experiment, *Clim. Dynam.*, *22*, 389–414, doi:10.1007/s00382-003-0389-2.
- May, W. (2004b), Simulation of the variability and extremes of daily rainfall during the Indian summer monsoon for present and future times in a global time-slice experiment, *Clim. Dynam.*, *22*, 183–204, doi:10.1007/s00382-003-0373-x.
- Mayr, H. G., J. G. Mengel, C. L. Wolff, and H. S. Porter (2006), QBO as potential amplifier of solar cycle influence, *Geophys. Res. Lett.*, *33*, L05812, doi:10.1029/2005GL025650.

- McCormack, J. P. (2003), The influence of the 11-year solar cycle on the quasi-biennial oscillation, *Geophys. Res. Lett.*, *30*, 6–1.
- McCormick, M. P., L. W. Thomason, and C. R. Trepte (1995), Atmospheric effects of the Mt Pinatubo eruption, *Science*, *373*, 399–404.
- McIntyre, M. E. (1998), Breaking waves and global-scale chemical transport in the earth’s atmosphere, with spinoffs for the sun’s interior, *Progr. Theoret. Phys. Suppl.*, *130*, 137–166.
- Milionis, A. E., and T. D. Davies (1994), Regression and stochastic models for air pollution-I. Review, comments and suggestions, *Atmos. Environ.*, *28*(17), 2801–2810.
- Moré, J. J., B. S. Garbow, and K. E. Hillstom (1980), *User guide for MINPACK-1*, Argonne National Laboratory, 9700 South Class Avenue, Argonne, Illinois 60439, USA.
- Naiman, D. Q. (1987), Minmax regret simultaneous confidence bands for multiple regression functions, *J. Amer. Statistical Assoc.*, *82*(399), 894–901.
- Nathan, T. R., and E. C. Cordero (2007), An ozone-modified refractive index for vertically propagating planetary waves, *J. Geophys. Res.*, *112*(2).
- Naujokat, B. (1986), An update of the observed quasi-biennial oscillation of the stratospheric winds over the tropics, *J. Atmos. Sci.*, *43*(17), 1873–1877.
- Newchurch, M. J., E.-S. Yang, D. M. Cunnold, G. C. Reinsel, J. M. Zawodny, and J. M. Russell (2003), Evidence for slowdown in stratospheric ozone loss: first stage of ozone recovery, *J. Geophys. Res.*, *108*, 4507, doi:10.1029/2003JD003471.
- Newman, P. A., and E. R. Nash (2000), Quantifying the wave driving of the stratosphere, *J. Geophys. Res.*, *105*, 12485–12498, doi:10.1029/1999JD901191.
- Newman, P. A., E. R. Nash, and J. E. Rosenfield (2001), What controls the temperature of the arctic stratosphere during the spring?, *J. Geophys. Res.*, *106*, 19999–20010, doi:10.1029/2000JD000061.
- Nigam, S., and R. S. Lindzen (1989), The sensitivity of stationary waves to variations in the basic state zonal flow, *J. Atmos. Sci.*, *46*, 1746–1768.
- Norval, M., A. P. Cullen, F. R. DeGruijl, J. Longstreth, Y. Takizawa, R. M. Lucas, F. P. Noonan, and J. C. VanDerLeun (2007), The effects on human health from stratospheric ozone depletion and its interactions with climate change, *Photochem. Photobiol. Sci.*, *6*(3), 232–251.

- Palmer, M. A., and L. J. Gray (2005), Modeling the atmospheric response to solar irradiance changes using a GCM with a realistic QBO, *Geophys. Res. Lett.*, *32*, L24701, doi:10.1029/2005GL023809.
- Pandit, S. M., and S. M. Wu (1983), *Time series and system analysis with applications*, 586 pp., John Wiley & Sons, Inc., New York.
- Pascoe, C. L., L. J. Gray, S. A. Crooks, M. N. Juckes, and M. P. Baldwin (2005), The quasi-biennial oscillation: analysis using ERA-40 data, *J. Geophys. Res.*, *110*(D9), D08105, doi:10.1029/2004JD004941.
- Pascoe, C. L., L. J. Gray, and A. A. Scaife (2006), A GCM study of the influence of equatorial winds on the timing of sudden stratospheric warmings, *Geophys. Res. Lett.*, *33*, L06825, doi:10.1029/2005GL024715.
- Pawson, S., K. Kodera, K. Hamilton, T. G. Shepherd, S. R. Beagley, B. A. Boville, J. D. Farrara, T. D. A. Fairlie, A. Kitoh, W. A. Lahoz, U. Langematz, E. Manzini, D. H. Rind, A. A. Scaife, K. Shibata, P. Simon, R. Swinbank, L. Takacs, R. J. Wilson, J. A. Al-Saadi, M. Amodei, M. Chiba, L. Coy, J. D. de Grandpré, R. S. Eckman, M. Fiorino, W. L. Grose, H. Koide, J. N. Koshyk, D. Li, J. Lerner, J. D. Mahlman, N. A. McFarlane, C. R. Mechoso, A. Molod, A. O'Neill, R. B. Pierce, W. J. Randel, R. B. Rood, and F. Wu (2000), The GCM-reality intercomparison project for SPARC (GRIPS): scientific issues and initial results, *Bull. Amer. Astron. Soc.*, *81*, 781–796.
- Perlwitz, J., and H.-F. Graf (1995), The statistical connection between tropospheric and stratospheric circulation of the northern hemisphere in winter, *J. Climate*, *8*, 2281–2295.
- Perlwitz, J., and N. Harnik (2003), Observational evidence of a stratospheric influence on the troposphere by planetary wave reflection, *J. Climate*, *16*, 3011–3026.
- Phillips, P. C. B. (2007), Regression with slowly varying regressors and nonlinear trends, *Economet. Theor.*, *23*(4), 557–614.
- Pitari, G., E. Mancini, V. Rizi, and D. T. Shindell (2002), Impact of future climate and emission changes on stratospheric aerosols and ozone, *J. Atmos. Sci.*, *59*, 414–440.
- Plumb, R. A. (1985), On the three-dimensional propagation of stationary waves, *J. Atmos. Sci.*, *42*, 217–229.
- Plumb, R. A., and J. Eluszkiewicz (1999), The Brewer-Dobson circulation: dynamics of the tropical upwelling, *J. Atmos. Sci.*, *56*, 868–890.

- Randel, W. J. (1987), A study of planetary waves in the southern winter troposphere and stratosphere. Part I: wave structure and vertical propagation, *J. Atmos. Sci.*, *44*, 917–935.
- Randel, W. J. (1992), Global atmospheric circulation statistics, 1000-1mb, *NCAR Technical Note TN-366+STR*, NCAR.
- Randel, W. J. (1993), Global variations of zonal mean ozone during stratospheric warming events, *J. Atmos. Sci.*, *50*, 3308–3321.
- Randel, W. J., and J. B. Cobb (1994), Coherent variations of monthly mean total ozone and lower stratospheric temperature, *J. Geophys. Res.*, *99*, 5433–5448, doi:10.1029/93JD03454.
- Randel, W. J., and F. Wu (1996), Isolation of the ozone QBO in SAGE II data by singular-value decomposition, *J. Atmos. Sci.*, *53*, 2546–2560.
- Randel, W. J., F. Wu, J. M. Russell, J. W. Waters, and L. Froidevaux (1995), Ozone and temperature changes in the stratosphere following the eruption of Mount Pinatubo, *J. Geophys. Res.*, *100*, 16753–16764, doi:10.1029/95JD01001.
- Randel, W. J., R. S. Stolarski, D. M. Cunnold, J. A. Logan, M. J. Newchurch, and J. M. Zawodny (1999), Trends in the vertical distribution of ozone, *Science*, *285*, 1689–1692, doi:10.1126/science.285.5434.1689.
- Rayner, N. A., D. E. Parker, E. B. Horton, C. K. Folland, L. V. Alexander, D. P. Rowell, E. C. Kent, and A. Kaplan (2003), Global analyses of sea surface temperature, sea ice, and night marine air temperature since the late nineteenth century, *J. Geophys. Res.*, *108*, 4407, doi:10.1029/2002JD002670.
- Reinsel, G. C., G. C. Tiao, A. J. Miller, D. J. Wuebbles, and P. S. Connell (1987), Statistical analysis of total ozone and stratospheric umkehr data for trends and solar cycle relationship, *J. Geophys. Res.*, *92*, 2201–2209.
- Reinsel, G. C., G. C. Tiao, D. J. Wuebbles, J. B. Kerr, A. J. Miller, R. M. Nagatani, L. Bishop, and L. H. Ying (1994), Seasonal trend analysis of published ground-based and TOMS total ozone data through 1991, *J. Geophys. Res.*, *99*, 5449–5464, doi:10.1029/93JD03517.
- Reinsel, G. C., A. J. Miller, E. C. Weatherhead, L. E. Flynn, R. M. Nagatani, G. C. Tiao, and D. J. Wuebbles (2005), Trend analysis of total ozone data for turnaround and dynamical contributions, *J. Geophys. Res.*, *110*, D16306, doi:10.1029/2004JD004662.
- Ricciardulli, L., and R. R. Garcia (2000), The excitation of equatorial waves by deep convection in the NCAR community climate model (CCM3), *J. Atmos. Sci.*, *57*, 3461–3487.

- Rind, D. (1998), Latitudinal temperature gradients and climate change, *J. Geophys. Res.*, *103*, 5943–5972, doi:10.1029/97JD03649.
- Rind, D., R. Suozzo, N. K. Balachandran, and M. J. Prather (1990), Climate change and the middle atmosphere. Part I: the doubled CO₂ climate, *J. Atmos. Sci.*, *47*, 475–494.
- Rind, D., D. Shindell, P. Lonergan, and N. K. Balachandran (1998), Climate change and the middle atmosphere. Part III: the doubled CO₂ climate revisited, *J. Climate*, *11*, 876–894.
- Rind, D., J. Lerner, and C. McLinden (2001), Changes of tracer distributions in the doubled CO₂ climate, *J. Geophys. Res.*, *106*, 28061–28080, doi:10.1029/2001JD000439.
- Rind, D., J. Lerner, J. Perlwitz, C. McLinden, and M. Prather (2002), Sensitivity of tracer transports and stratospheric ozone to sea surface temperature patterns in the doubled CO₂ climate, *J. Geophys. Res.*, *107*, 4800, doi:10.1029/2002JD002483.
- Rind, D., P. Lonergan, N. K. Balachandran, and D. Shindell (2002), 2×CO₂ and solar variability influences on the troposphere through wave-mean flow interactions, *J. Phys. Soc. Japan*, *80*(4 B), 863–876.
- Rind, D., J. Perlwitz, and P. Lonergan (2005a), AO/NAO response to climate change: 1. Respective influences of stratospheric and tropospheric climate changes, *J. Geophys. Res.*, *110*, D12107, doi:10.1029/2004JD005103.
- Rind, D., J. Perlwitz, P. Lonergan, and J. Lerner (2005b), AO/NAO response to climate change: 2. Relative importance of low- and high-latitude temperature changes, *J. Geophys. Res.*, *110*, D12108, doi:10.1029/2004JD005686.
- Rodwell, M. J., and B. J. Hoskins (1996), Monsoons and the dynamics of deserts, *Quart. J. Roy. Meteorol. Soc.*, *122*, 1385–1404.
- Roeckner, E., K. Arpe, L. Bengtsson, S. Brinkop, L. Dümenil, M. Esch, E. Kirk, F. Lunkeit, M. Ponater, B. Rockel, R. Sausen, U. Schlese, S. Schubert, and M. Windelband (1992), Simulation of the present-day climate with the ECHAM model: impact of model physics and resolution, *Report 93*, Max-Planck-Institut für Meteorologie, Hamburg, Germany.
- Roeckner, E., K. Arpe, M. Bengtsson, L. and Christoph, M. Claussen, L. Dümenil, M. Esch, M. Giorgetta, U. Schlese, and U. Schulzweida (1996), The atmospheric general circulation model ECHAM4: model description and simulation of present-day climate, *Report 218*, Max-Planck-Institut für Meteorologie, Hamburg, Germany.

- Rosenfield, J. E., and M. R. Schoeberl (2005), Recovery of the tropical lower stratospheric ozone layer, *Geophys. Res. Lett.*, *32*, L21806, doi:10.1029/2005GL023626.
- Rosenfield, J. E., A. R. Douglass, and D. B. Considine (2002), The impact of increasing carbon dioxide on ozone recovery, *J. Geophys. Res.*, *107*, 4049, doi:10.1029/2001JD000824.
- Rowell, D. P., C. K. Folland, K. Maskell, and N. M. Ward (1995), Variability of summer rainfall over tropical north africa (1906-92): observations and modelling, *Quart. J. Roy. Meteorol. Soc.*, *121*, 669–704.
- Russell, J. M., III, L. L. Gordley, J. H. Park, S. R. Drayson, W. D. Hesketh, R. J. Cicerone, A. F. Tuck, J. E. Frederick, J. E. Harries, and P. J. Crutzen (1993), The halogen occultation experiment, *J. Geophys. Res.*, *98*, 10777–10797.
- Ryan, D. P. (1997), *Modern regression methods*, 515 pp., John Wiley & Sons, Inc., New York.
- Salby, M., and P. Callaghan (2000), Connection between the solar cycle and the QBO: the missing link*, *J. Climate*, *13*, 2652–2662.
- Salby, M. L., and P. F. Callaghan (2004a), Interannual changes of the stratospheric circulation: influence on the tropics and southern hemisphere, *J. Climate*, *17*, 952–964.
- Salby, M. L., and P. F. Callaghan (2004b), Interannual changes of the stratospheric circulation: influence on the tropics and southern hemisphere, *J. Climate*, *17*, 952–964.
- Salby, M. L., and P. F. Callaghan (2006a), Influence of the Brewer-Dobson circulation on stratosphere-troposphere exchange, *J. Geophys. Res.*, *111*, D21106, doi:10.1029/2006JD007051.
- Salby, M. L., and P. F. Callaghan (2006b), Relationship of the quasi-biennial oscillation to the stratospheric signature of the solar cycle, *J. Geophys. Res.*, *111*, D06110, doi:10.1029/2005JD006012.
- Salby, M. L., and P. F. Callaghan (2006c), Residual mean transport in the stratosphere: contributions from wave driving and seasonal transience, *J. Geophys. Res.*, *111*, D22304, doi:10.1029/2005JD006767.
- Salby, M. L., and P. F. Callaghan (2007), On the wintertime increase of arctic ozone: relationship to changes of the polar-night vortex, *J. Geophys. Res.*, *112*(6).

- Salby, M. L., and R. R. Garcia (1987), Transient response to localized episodic heating in the tropics. Part I: excitation and short-time near-field behavior, *J. Atmos. Sci.*, *44*, 458–498.
- Salby, M. L., and D. J. Shea (1991), Correlations between solar activity and the atmosphere - an unphysical explanation, *J. Geophys. Res.*, *96*, 22579–22595.
- Saltzman, B. (1970), Large-scale atmospheric energetics in the wave-number domain, *Rev. Geophys. Space Phys.*, *8*, 289–302.
- Sassi, F., D. Kinnison, B. A. Boville, R. R. Garcia, and R. Roble (2004), Effect of El Niño-Southern oscillation on the dynamical, thermal, and chemical structure of the middle atmosphere, *J. Geophys. Res.*, *109*, D17108, doi:10.1029/2003JD004434.
- Schnadt, C., M. Dameris, M. Ponater, R. Hein, V. Grewe, and B. Steil (2002), Interaction of atmospheric chemistry and climate and its impact on stratospheric ozone, *Clim. Dynam.*, *18*, 501–517.
- Scinocca, J. F., and P. H. Haynes (1998), Dynamical forcing of stratospheric planetary waves by tropospheric baroclinic eddies, *J. Atmos. Sci.*, *55*, 2361–2392.
- Seager, R., N. Harnik, Y. Kushnir, W. Robinson, and J. Miller (2003), Mechanisms of hemispherically symmetric climate variability, *J. Climate*, *16*, 2960–2978.
- Sheinbaum, J. (2003), Current theories on El Niño-Southern oscillation: a review, *Geofis. Int.*, *42*, 291–305.
- Shindell, D., D. Rind, N. Balachandran, J. Lean, and P. Lonergan (1999), Solar cycle variability, ozone, and climate, *Science*, *284*, 305–308.
- Shindell, D. T., and V. Grewe (2002), Separating the influence of halogen and climate changes on ozone recovery in the upper stratosphere, *J. Geophys. Res.*, *107*, 4144, doi:10.1029/2001JD000420.
- Shindell, D. T., D. Rind, and P. Lonergan (1998), Increased polar stratospheric ozone losses and delayed eventual recovery owing to increasing greenhouse-gas concentrations, *Nature*, *392*, 589–592, doi:10.1038/33385.
- Shindell, D. T., G. A. Schmidt, R. L. Miller, and D. Rind (2001), Northern hemisphere winter climate response to greenhouse gas, ozone, solar, and volcanic forcing, *J. Geophys. Res.*, *106*, 7193–7210, doi:10.1029/2000JD900547.
- Shindell, D. T., G. Faluvegi, N. Unger, E. Aguilar, G. A. Schmidt, D. M. Koch, S. E. Bauer, and R. L. Miller (2006), Simulations of preindustrial, present-day, and 2100 conditions in the NASA GISS composition and climate model G-PUCCINI, *Atmos. Chem. Phys.*, *6*, 4427–4459.

- Sigmond, M., P. C. Siegmund, E. Manzini, and H. Kelder (2004), A simulation of the separate climate effects of middle-atmospheric and tropospheric CO₂ doubling, *J. Climate*, *17*, 2352–2367.
- Simmons, A. J., J. M. Wallace, and G. W. Branstator (1983), Barotropic wave propagation and instability, and atmospheric teleconnection patterns, *J. Atmos. Sci.*, *40*, 1363–1392.
- Singh, U. S. (1982), A study of energy conversion in the wave number domain, *Pure Appl. Geophys.*, *120*, 211–217.
- Smagorinsky, J. (1953), The dynamical influence of large-scale heat sources and sinks on the quasi-stationary mean motions of the atmosphere, Ph.D. thesis, New York University.
- Solomon, S. (1999), Stratospheric ozone depletion: a review of concepts and history, *Rev. Geophys.*, *37*, 275–316, doi:10.1029/1999RG900008.
- Son, S. ., S. Lee, and S. B. Feldstein (2007), Intraseasonal variability of the zonal-mean extratropical tropopause height, *J. Atmos. Sci.*, *64*(2), 608–620.
- Soukharev, B. E., and L. L. Hood (2006), Solar cycle variation of stratospheric ozone: multiple regression analysis of long-term satellite data sets and comparisons with models, *J. Geophys. Res.*, *111*, D20314, doi:10.1029/2006JD007107.
- SPARC (1998), Assessment of trends in the vertical distribution of ozone, in *SPARC report, World Climate Research Programme*, vol. 1, edited by N. Harris, R. Hudson, and C. Phillips, chap. 3, p. 289, World Meteorological Organisation, Geneva, Switzerland.
- Staehelin, J., J. Mäder, A. K. Weiss, and C. Appenzeller (2002), Long-term ozone trends in northern mid-latitudes with special emphasis on the contribution of changes in dynamics, *Phys. Chem. Earth*, *27*, 461–469.
- Steil, B., M. Dameris, C. Brühl, P. J. Crutzen, V. Grewe, M. Ponater, and R. Sausen (1998), Development of a chemistry module for GCMs: first results of a multiannual integration, *Ann. Geophys.*, *16*, 205–228.
- Steil, B., C. Brühl, E. Manzini, P. J. Crutzen, J. Lelieveld, P. J. Rasch, E. Roeckner, and K. Krüger (2003), A new interactive chemistry-climate model: 1. Present-day climatology and interannual variability of the middle atmosphere using the model and 9 years of HALOE/UARS data, *J. Geophys. Res.*, *108*, D4290, doi:10.1029/2002JD002971.
- Steinbrecht, W., H. Claude, U. Köhler, and K. P. Hoinka (1998), Correlations between tropopause height and total ozone: implications for long-term changes, *J. Geophys. Res.*, *103*, 19183–19192, doi:10.1029/98JD01929.

- Steinbrecht, W., B. Hassler, H. Claude, P. Winkler, and R. S. Stolarski (2003), Global distribution of total ozone and lower stratospheric temperature variations, *Atmos. Chem. Phys.*, *3*, 1421–1438.
- Steinbrecht, W., H. Claude, and P. Winkler (2004), Enhanced upper stratospheric ozone: sign of recovery or solar cycle effect?, *J. Geophys. Res.*, *109*, D02308, doi:10.1029/2003JD004284.
- Steinbrecht, W., B. Haßler, C. Brühl, M. Dameris, M. A. Giorgetta, V. Grewe, E. Manzini, S. Matthes, C. Schnadt, B. Steil, and P. Winkler (2006a), Interannual variation patterns of total ozone and lower stratospheric temperature in observations and model simulations, *Atmos. Chem. Phys.*, *6*, 349–374.
- Steinbrecht, W., B. Haßler, C. Brühl, M. Dameris, M. A. Giorgetta, V. Grewe, E. Manzini, S. Matthes, C. Schnadt, B. Steil, and P. Winkler (2006b), Interannual variation patterns of total ozone and lower stratospheric temperature in observations and model simulations, *Atmos. Chem. Phys.*, *6*, 349–374.
- Stenke, A., and V. Grewe (2005), Simulation of stratospheric water vapor trends: impact on stratospheric ozone chemistry, *Atmos. Chem. Phys.*, *5*, 1257–1272.
- Stenke, A., V. Grewe, and P. M. (2007), Lagrangian transport of water vapor and cloud water in the ECHAM4 GCM and its impact on the cold bias, *Clim. Dynam.*, doi:10.1007/s00382-007-0347-5.
- Stott, P. A., G. S. Jones, J. A. Lowe, P. Thorne, C. Durman, T. C. Johns, and J. . Thelen (2006), Transient climate simulations with the HadGEM1 climate model: causes of past warming and future climate change, *J. Climate*, *19*(12), 2763–2782.
- Teitelbaum, H., and P. Bauer (1990), Stratospheric temperature eleven years variations - solar cycle influence or stroboscopic effect?, *Ann. Geophys.*, *8*, 239–241.
- Thejll, P., and T. Schmith (2005), Limitations on regression analysis due to serially correlated residuals: application to climate reconstruction from proxies, *J. Geophys. Res.*, *110*, D18103, doi:10.1029/2005JD005895.
- Thompson, D. W. J., and S. Solomon (2005), Recent stratospheric climate trends as evidenced in radiosonde data: global structure and tropospheric linkages, *J. Climate*, *18*, 4785–4795.
- Tiao, G. C., D. Xu, J. H. Pedrick, X. Zhu, and G. C. Reinsel (1990), Effects of autocorrelation and temporal sampling schemes on estimates of trend and spatial correlation, *J. Geophys. Res.*, *95*, 20507–20517.
- Tiedtke, M. (1989), A comprehensive mass flux scheme for cumulus parameterization in large-scale models, *Mon. Weather Rev.*, *117*(8), 1779–1800.

- Timbal, B., J.-F. Mahfouf, J.-F. Royer, U. Cubasch, and J. M. Murphy (1997), Comparison between doubled CO₂ time-slice and coupled experiments, *J. Climate*, *10*, 1463–1469.
- Toth, Z. (1992), Quasi-stationary and transient periods in the northern hemisphere circulation series, *J. Climate*, *5*, 1235–1248.
- Tourpali, K., C. J. E. Schuurmans, R. van Dorland, B. Steil, and C. Brühl (2003), Stratospheric and tropospheric response to enhanced solar UV radiation: a model study, *Geophys. Res. Lett.*, *30*, 35–1.
- Tourpali, K., C. J. E. Schuurmans, R. van Dorland, B. Steil, C. Brühl, and E. Manzini (2005), Solar cycle modulation of the arctic oscillation in a chemistry-climate model, *Geophys. Res. Lett.*, *32*, L17803, doi:10.1029/2005GL023509.
- Tung, K. (1979), A theory of stationary long waves. Part III. quasi-normal modes in a singular wave guide, *Mon. Weather Rev.*, *107*, 751–774.
- Uppala, S. M., P. W. Kållberg, A. J. Simmons, U. Andrae, V. da Costa Bechtold, M. Fiorino, J. K. Gibson, J. Haseler, A. Hernandez, G. A. Kelly, X. Li, K. Onogi, S. Saarinen, N. Sokka, R. P. Allan, E. Andersson, K. Arpe, M. A. Balmaseda, A. C. M. Beljaars, L. van de Berg, J. Bidlot, N. Bormann, S. Caires, F. Chevallier, A. Dethof, M. Dragosavac, M. Fisher, M. Fuentes, S. Hagemann, E. Hólm, B. J. Hoskins, L. Isaksen, P. A. E. M. Janssen, R. Jenne, A. P. McNally, J. F. Mahfouf, J. J. Morcrette, N. A. Rayner, R. W. Saunders, P. Simon, A. Sterl, K. E. Trenberth, A. Untch, D. Vasiljevic, P. Viterbo, and J. Woollen (2005), The ERA-40 re-analysis, *Quart. J. Roy. Meteorol. Soc.*, *131*, 2961–3012.
- Uusipaikka, E. (1996), A new method for construction of profile likelihood based confidence intervals, *ASA Pro. Biom.*, pp. 244–249.
- van Loon, H., R. L. Jenne, and L. K. (1973), Zonal harmonic standing waves, *J. Geophys. Res.*, *78*, 4463–4471.
- von Storch, H., and F. w. Zwiers (1999), *Statistical analysis in climate research*, 484 pp., Cambridge University Press, Cambridge.
- Vyushin, D. I., V. E. Fioletov, and T. G. Shepherd (2007), Impact of long-range correlations on trend detection in total ozone, *J. Geophys. Res.*, *112*, D14307, doi:10.1029/2006JD008168.
- Wang, H., and M. Ting (1999), Seasonal cycle of the climatological stationary waves in the NCEP-NCAR reanalysis, *J. Atmos. Sci.*, *56*, 3892–3919.
- Weatherhead, E. C., G. C. Reinsel, G. C. Tiao, C. H. Jackman, L. Bishop, S. M. H. Firth, J. DeLuisi, T. Keller, S. J. Oltmans, E. L. Fleming, D. J.

- Wuebbles, J. B. Kerr, A. J. Miller, J. Herman, R. McPeters, R. M. Nagatani, and J. E. Frederick (2000), Detecting the recovery of total column ozone, *J. Geophys. Res.*, *105*, 22201–22210, doi:10.1029/2000JD900063.
- White, G. H. (1982), An observational study of the northern hemisphere extratropical summertime general circulation, *J. Atmos. Sci.*, *39*, 24–40.
- Williamson, D. L., and P. J. Rasch (1994), Water vapor transport in the NCAR CCM2, *Tellus (A)*, *46*, 34–51, doi:10.1034/j.1600-0870.1994.00004.
- WMO (2003), *Scientific assessment of ozone depletion: 2002, Global Ozone Res. Monit. Proj. Rep.*, vol. 47, World Meteorological Organization, Geneva, Switzerland.
- WMO (2007), *Scientific assessment of ozone depletion: 2006, Global Ozone Res. Monit. Proj. Rep.*, vol. 50, World Meteorological Organization, Geneva, Switzerland.
- Wohltmann, I., R. Lehmann, M. Rex, D. Brunner, and J. A. Mäder (2007), A process-oriented regression model for column ozone, *J. Geophys. Res.*, *112*, D12304, doi:10.1029/2006JD007573.
- Yang, H., and K. K. Tung (1994), Statistical significance and pattern of extratropical QBO in column ozone, *Geophys. Res. Lett.*, *21*, 2235–2238.
- Yang, H., and K. K. Tung (1995), On the phase propagation of extratropical ozone quasi-biennial oscillation in the observational data, *J. Geophys. Res.*, *100*, 9091–9100, doi:10.1029/95JD00694.
- Zerefos, C. S., A. F. Bais, I. C. Ziomas, and R. D. Bojkov (1992), On the relative importance of quasi-biennial oscillation and El Niño/Southern oscillation in the revised Dobson total ozone records, *J. Geophys. Res.*, *97*, 10135–10144.
- Zerefos, C. S., K. Tourpali, and A. F. Bais (1994), Further studies on possible volcanic signal to the ozone layer, *J. Geophys. Res.*, *99*, 25741–25746, doi:10.1029/94JD02142.
- Zhou, T., M. A. Geller, and K. Hamilton (2006), The roles of the Hadley circulation and downward control in tropical upwelling, *J. Atmos. Sci.*, *63*, 2740–2757, doi:10.1175/JAS3770.1.
- Ziemke, J. R., S. Chandra, R. D. McPeters, and P. A. Newman (1997), Dynamical proxies of column ozone with applications to global trend models, *J. Geophys. Res.*, *102*, 6117–6130, doi:10.1029/96JD03783.

Danksagungen

Der Enthusiasmus meines Doktorvaters Prof. Martin Dameris für die Erforschung der Stratosphäre ist überaus motivierend. Er war bei Fragen und Problemen immer zur Stelle und gab äußerst wertvolle Hinweise und Anregungen, vielen Dank. Außerdem profitierte ich von seiner Erfahrung sehr. Vielen Dank auch dafür, mir bei eigenen Wegen in meiner Arbeit vertraut und mich auf diesen Wegen begleitet zu haben.

Herrn Prof. Olaf Krüger danke ich für die Begutachtung meiner Arbeit.

Herrn Prof. Ulrich Schumann möchte ich für die Möglichkeit danken, am Institut für Physik der Atmosphäre promovieren zu können. Ich möchte ihm auch dafür danken, mich während der letzten Phase meiner Arbeit weiter unterstützt zu haben. Hier geht mein Dank auch an Dr. Volker Grewe, Prof. Martin Dameris, Prof. Robert Sausen, und Dr. Reinhold Busen. Herr Prof. Ulrich Schumann gab mir außerdem wertvolle Hinweise für meine Arbeit.

Ich danke Dr. Sigrun Matthes, Dr. Fabian Mager, Dr. Volker Grewe, Prof. Michael Ponater, Dr. Axel Lauer, Dr. Christian Kurz, Dr. Andrea Stenke, und Dr. Ulrike Burkhardt für wertvolle Hinweise, all die Unterstützung und vielfache Anregungen. Ebenso gilt mein Dank der gesamten Abteilung 1 für eine produktive und angenehme Arbeitsatmosphäre. Für das Korrekturlesen meiner Arbeit danke ich Prof. Martin Dameris, Frau Hella Garny, und Frau Susanne Huber. My special thanks go to Dr. Timothy Callaghan for the proofreading.

Ich danke Dr. Greg Bodeker, Prof. Robert Sausen, Dr. Klaus Gierens, Dr. Wolfgang Steinbrecht, und Frau Birgit Haßler für all die wertvollen Hinweise hinsichtlich der Regressionsanalyse. Thanks to Dr. Greg Bodeker, Prof. Robert Sausen, Dr. Klaus Gierens, Dr. Wolfgang Steinbrecht, Mrs Birgit Haßler for helping me with the regression analysis. I also wish to acknowledge Dr. Barnaby Love for his kind support.

Herrn Winfried Beer und Herrn Karl-Ernst Müller danke ich für die hervorragende technische Unterstützung. Frau Sylvia Wohofsky aus der Bibliothek danke ich für die schnelle Bereitstellung schwer verfügbarer Veröffentlichungen. Herrn Prof. Thomas Hauf danke ich dafür, mich auf diese Promotionsstelle aufmerksam gemacht zu haben.

Thanks to Prof. Vitali Fioletov for providing an update of total ozone anomaly analysis for comparison with the model data. I wish to thank the European Commission for funding the project SCOUT-O3 (within the 6th framework programme).

Last but not least, mein besonderer Dank gilt Susanne Huber für all die Unterstützung.

Lebenslauf

PERSÖNLICHE DATEN

Name: Rudolf Deckert

Geburtsdatum: 26. September 1976

Geburtsort: Wasserburg am Inn, Deutschland

AUSBILDUNG

- 09/1983 – 07/1987 Besuch der Grundschule Traunstein-Haslach
- 09/1987 – 05/1996 Abitur am Chiemgau-Gymnasium Traunstein
Leistungskurse: Französisch, Mathematik
- 07/1996 – 09/1997 Ausbildung zum Rettungshelfer bei den Maltesern in Würzburg, Deutschland (Zivildienst)
- 02/2001 – 11/2001 Graduate Diploma of Science (Antarctic and Southern Ocean Studies) with “first class” Honours an der Universität von Tasmanien, Australien
Honours thesis: *The lensing effect on underwater levels of UV radiation*
- 10/1997 – 09/2003 Diplom “mit Auszeichnung” in Meteorologie an der Universität Hannover
Diplomarbeit: *An experimental study on drying-up paved surfaces*
- 04/2004 – 02/2005 Promotionsstudium der Meteorologie an der Ludwig-Maximilians-Universität München
- seit 03/2004 Wissenschaftlicher Mitarbeiter am Institut für Physik der Atmosphäre, DLR Oberpfaffenhofen
-

AUSZEICHNUNGEN

- 12/1999 Auszeichnung durch die Christian-Kuhleemann-Stiftung der Universität Hannover für hervorragende Leistungen im Rahmen der Diplomvorprüfung

Oberpfaffenhofen, 21. Dezember 2007